NASA Contractor Report 189084

NASA-CR-189084
19920011652

High Strain Rate Properties of Off-Axis Composite Laminates

Final Report—Part II

I.M. Daniel
IIT Research Institute
Chicago, Illinois

December 1991

Prepared for
Lewis Research Center
Under Contract NAS3-21016

NASA
National Aeronautics and
Space Administration

FOREWORD

This is the Final Report on IIT Research Institute Project No. M06026, "High Strain Rate Properties of Off-Axis Composite Laminates," prepared by IITRI for NASA-Lewis Research Center, under Contract No. NAS3-21016. The work described in this report was conducted in the period July 11, 1977 to April 11, 1981. Dr. C. C. Chamis was the NASA-Lewis Project Manager. Dr. I. M. Daniel of IITRI was the Principal Investigator. Additional contributions to the work reported herein were made by Messrs. W. G. Hamilton, G. M. Koller, T. Niiro, and S. W. Schramm of IITRI, Dr. T. Liber of Travenol Laboratories, and Mr. R. H. LaBedz of International Harvester.

Respectfully submitted,
IIT RESEARCH INSTITUTE

I. M. Daniel
Science Advisor
Materials and Manufacturing Technology

APPROVED:

Maurice A. H. Howes, Director
Materials and Manufacturing
Technology Division

HIGH STRAIN RATE PROPERTIES OF OFF-AXIS COMPOSITE LAMINATES

ABSTRACT

Unidirectional off-axis graphite/epoxy and graphite/S-glass/epoxy laminates were characterized in uniaxial tension at strain rates ranging from quasi-static to over $500s^{-1}$. Laminate ring specimens were loaded by internal pressure with the tensile stress at 22.5°, 30°, and 45° with the fiber direction. Results were presented in the form of stress-strain curves to failure. Properties determined included moduli, Poisson's ratios, strength, and ultimate strain. In all three laminates of both materials the modulus and strength increase sharply with strain rate, reaching values roughly 100%, 150%, and 200% higher than corresponding static values for the $[22.5_8]$, $[30_8]$, and $[45_8]$ laminates, respectively. In the case of ultimate strain no definite trends could be established, but the maximum deviation from the average of any value for any strain rate was less than 18%.

TABLE OF CONTENTS

LIST OF TABLES

LIST OF TABLES (Cont.)

LIST OF FIGURES

LIST OF FIGURES (Cont.)

LIST OF FIGURES (Cont.)

LIST OF FIGURES (Cont.)

LIST OF FIGURES (Cont.)

LIST OF FIGURES (Cont.)

LIST OF FIGURES (Cont.)

LIST OF FIGURES (Cont.)

LIST OF FIGURES (Cont.)

LIST OF FIGURES (Cont.)

HIGH STRAIN RATE PROPERTIES OF OFF-AXIS COMPOSITE LAMINATES

1. INTRODUCTION

In Part I of this report methods were described for testing and characterization of composite materials at strain rates ranging from quasi-static to over $500s^{-1}$. Three unidirectional materials were characterized, SP288/T300 graphite/epoxy, SP288/AS graphite/epoxy, and 80AS/20S/PR288 graphite/S-glass/epoxy.

It was found that the longitudinal modulus increases moderately with strain rate by up to 20%, but the longitudinal strength and ultimate strain did not vary much. Transverse modulus and strength increase sharply with strain rate, reaching values up to three times the static value. The in-plane shear modulus and shear strength increase noticeably with strain rate by up to approximately 65%. In all cases, it was found that ultimate strains did not vary with strain rate in any significant manner.

The objective of the task described in this part of the report is to characterize unidirectional composites of two material systems in uniaxial tension at various angles with the fiber direction at three strain rates. The material systems characterized are SP288/AS graphite/epoxy and 80AS/20S/PR288 graphite/S-glass/epoxy (intraply hybrid). The three strain rates selected are quasi-static, intermediate, and high rates ranging from $10^{-4}s^{-1}$ to over $500s^{-1}$. All characterization tests were conducted by testing thin rings 10.16 cm (4 in.) in diameter, 2.54 cm (1 in.) wide, and 8-plies thick under internal pressure. Rings of $[22.5_8]$, $[30_8]$, and $[45_8]$ layups, where the angle indicates the fiber orientation with respect to the circumferential direction, were tested. Three replications per test were used. The data were analyzed according to procedures described in Part I of this report. Results were presented in the form of stress-strain curves to failure. Properties determined included initial, secant, and terminal strain rate; initial, secant, and terminal modulus, and Poisson's ratio; and strength and ultimate strain. The effects of strain rate on the various properties are discussed below.

2. QUASI-STATIC TENSILE PROPERTIES OF OFF-AXIS LAMINATES

Static tensile properties of off-axis laminates were obtained by testing rings under static internal pressure. Three rings were tested of each of the $[22.5_8]$, $[30_8]$, and $[45_8]$ layups for each of two materials, the SP288/AS graphite/epoxy and the 80AS/20S/PR288 graphite/S-glass/epoxy. Each ring was instrumented with a 3-gage rosette with elements in the circumferential, axial, and 45-deg directions.

Stress-strain curves for all specimens tested are shown in Figures 2-1 through 2-18. Values for the modulus, Poisson's ratio, strength, and ultimate strain computed from these curves are indicated in these figures and summarized in Table 2-1. All specimens show nonlinear response. In both the graphite/epoxy and graphite/S-glass/epoxy, modulus, strength and, with one exception, ultimate strain decrease with increasing angle of ply orientation, as expected. With the exception of the $[22.5_8]$ specimens, moduli and strengths were not significantly different between the two material systems, but the ultimate strains in the hybrid material are a little higher than those in the graphite/epoxy material.

TABLE 2-1. STATIC TENSILE PROPERTIES OF $[\theta_8]$ OFF-AXIS LAMINATES

Material	Laminate	Modulus ($E_{\theta\theta}$) GPa (10^6 psi)	Poisson's Ratio ($\nu_{\theta x}$)	Strength ($S_{\theta\theta T}$) MPa (ksi)	Ultimate Strain ($\varepsilon^u_{\theta\theta T}$)
SP288/AS	$[22.5_8]$	34.6 (5.01)	0.31	218 (31.6)	0.0110
Graphite/Epoxy	$[30_8]$	25.4 (3.68)	0.33	149 (21.6)	0.0080
	$[45_8]$	14.7 (2.13)	0.27	90 (13.1)	0.0070
80AS/20S/PR288	$[22.5_8]$	38.6 (5.59)	0.38	204 (29.6)	0.0077
Graphite/S-Glass/ Epoxy	$[30_8]$	24.7 (3.57)	0.35	157 (22.8)	0.0097
	$[45_8]$	15.3 (2.22)	0.20	100 (14.5)	0.0080

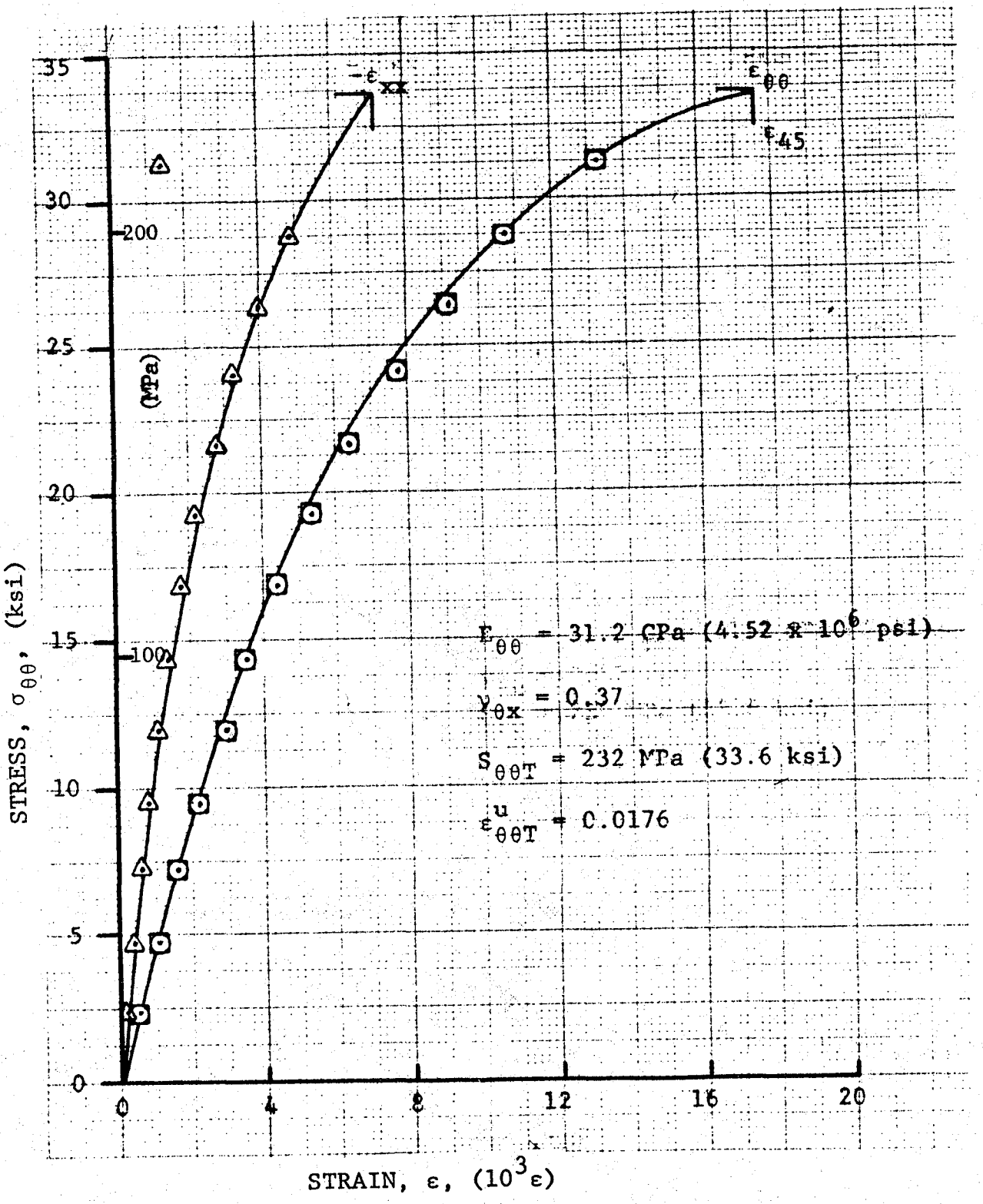

Figure 2-1. Strains in $[22.5_8]$ SP288/AS ring specimen under static tensile loading (Specimen No. 46-1).

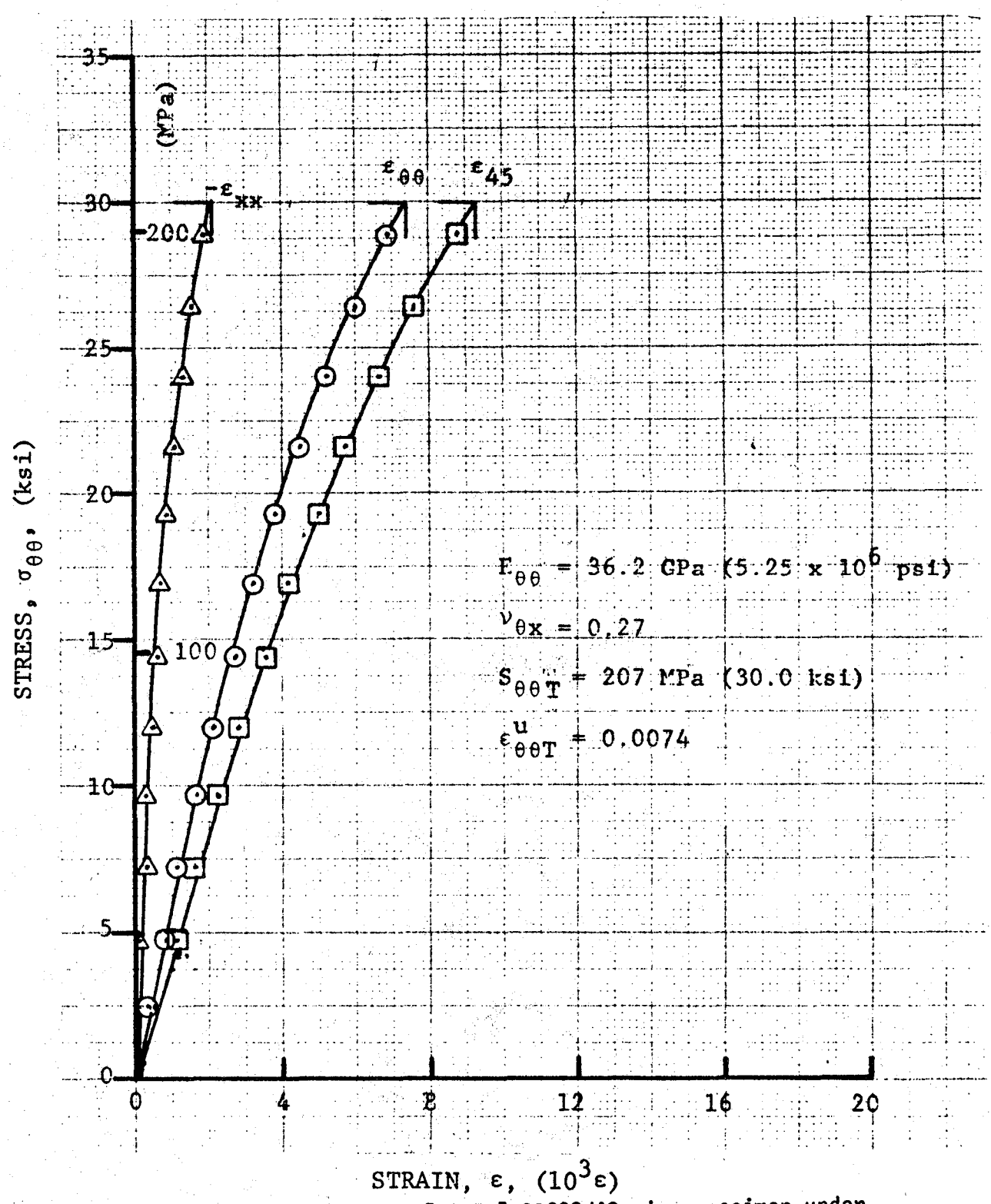

Figure 2-2. Strains in [22.5$_8$] SP288/AS ring specimen under static tensile loading (Specimen No. 46-2).

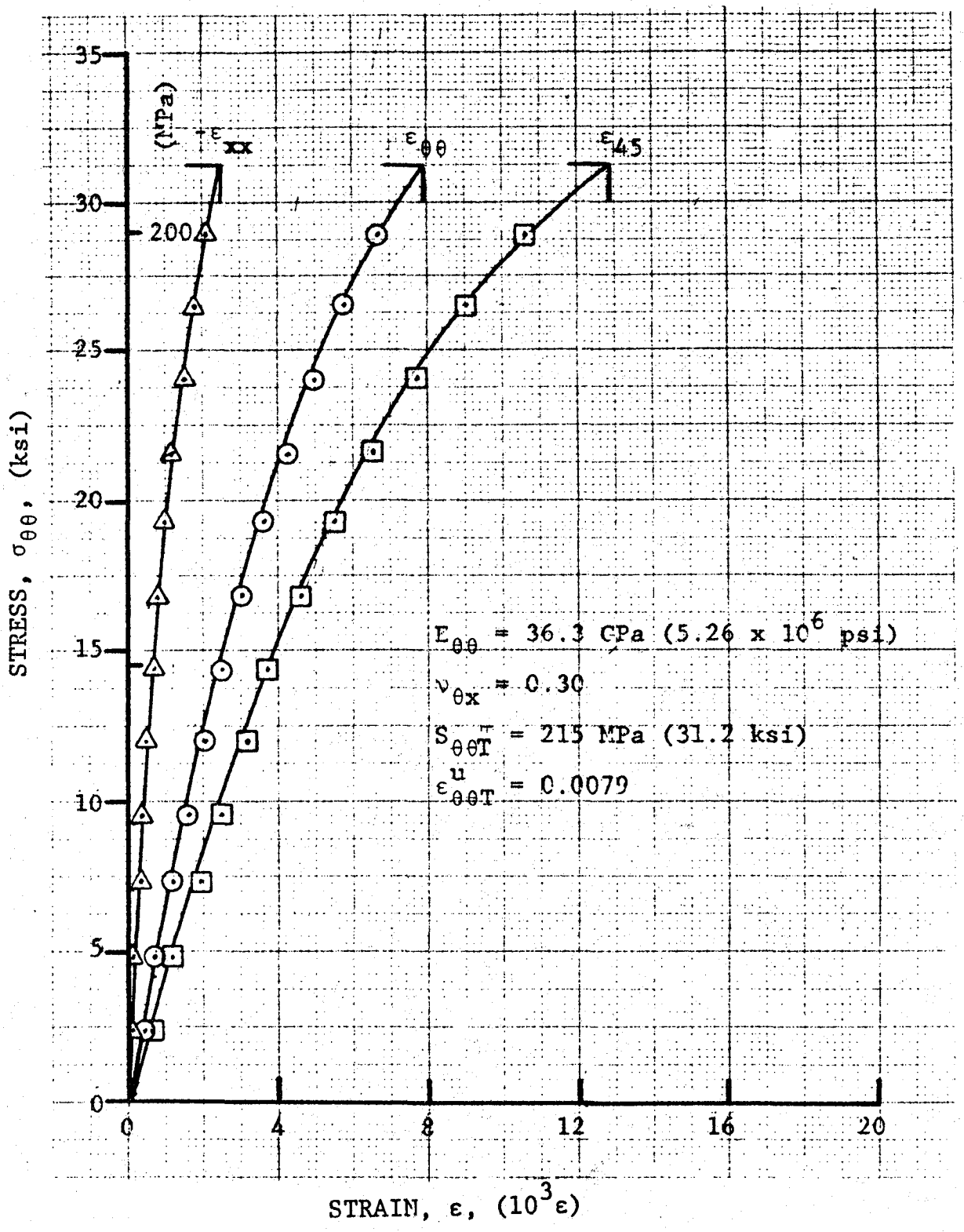

Figure 2-3. Strains in [22.5$_8$] SP288/AS ring specimen under static tensile loading (Specimen No. 46-3).

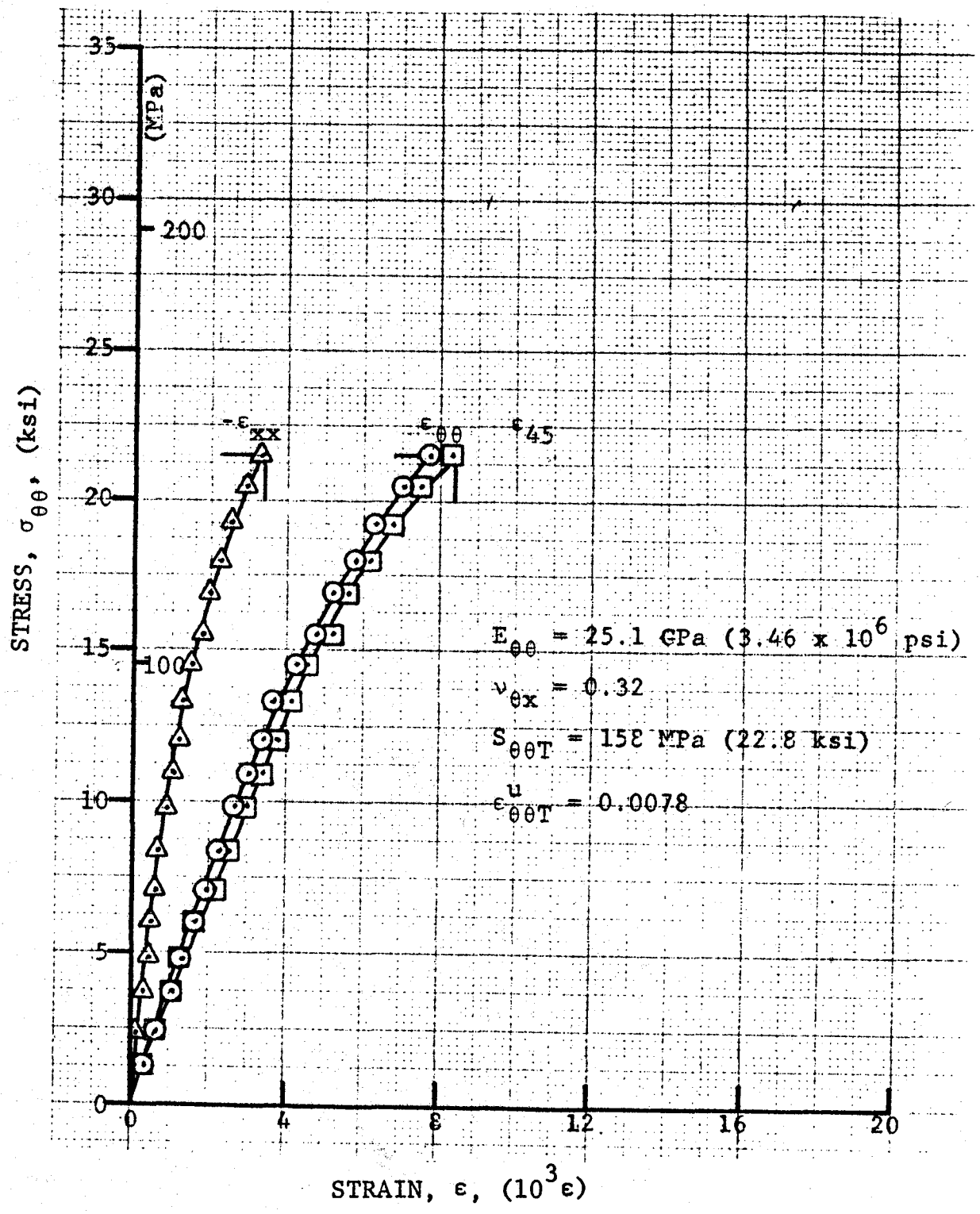

Figure 2-4. Strains in $[30_8]$ SP288/AS ring specimen under static tensile loading (Specimen No. 48-1).

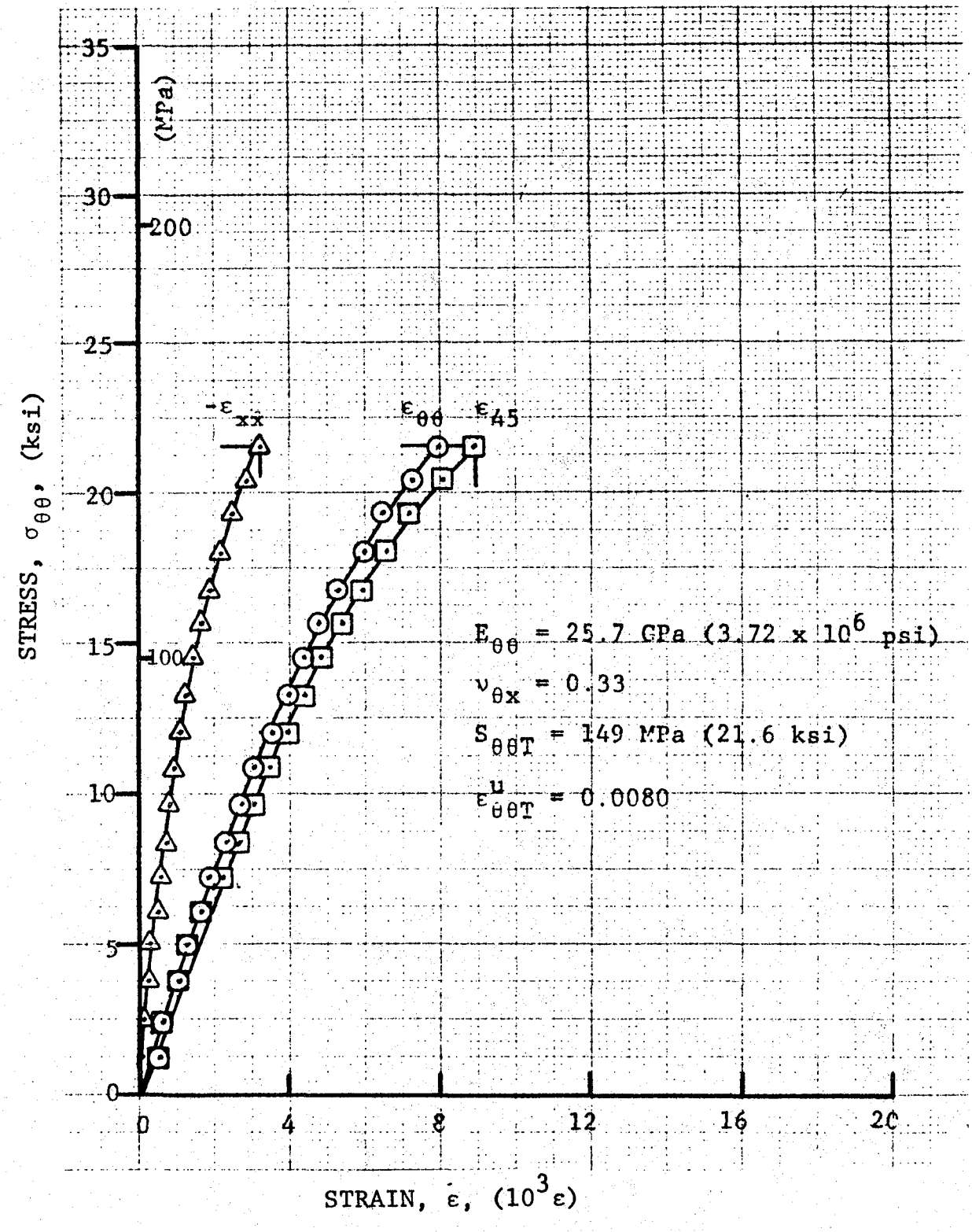

Figure 2-5. Strains in $[30_8]$ SP288/AS ring specimen under static tensile loading (Specimen No. 48-2).

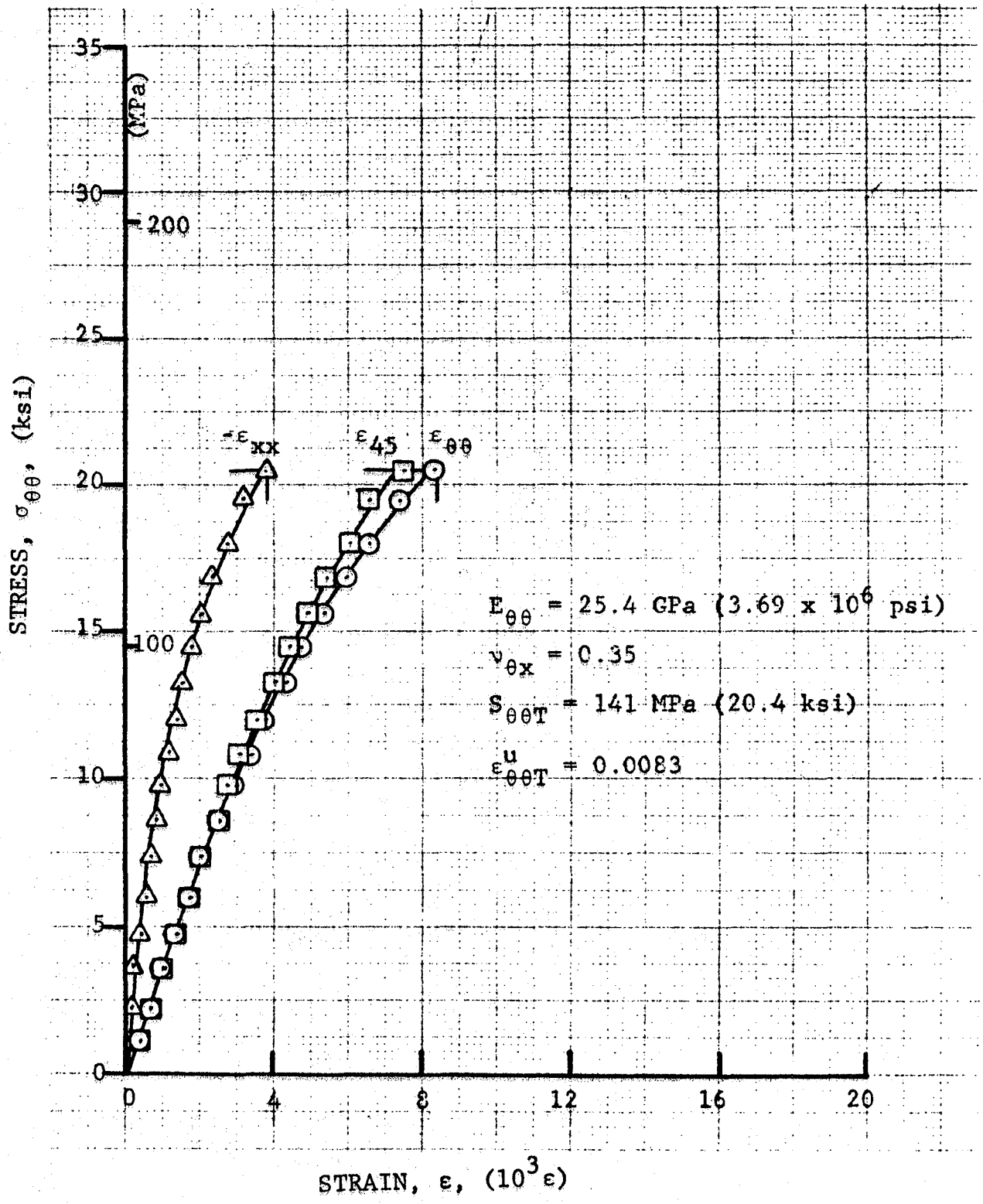

Figure 2-6. Strains in $[30_8]$ SP288/AS ring specimen under static tensile loading (Specimen No. 48-3).

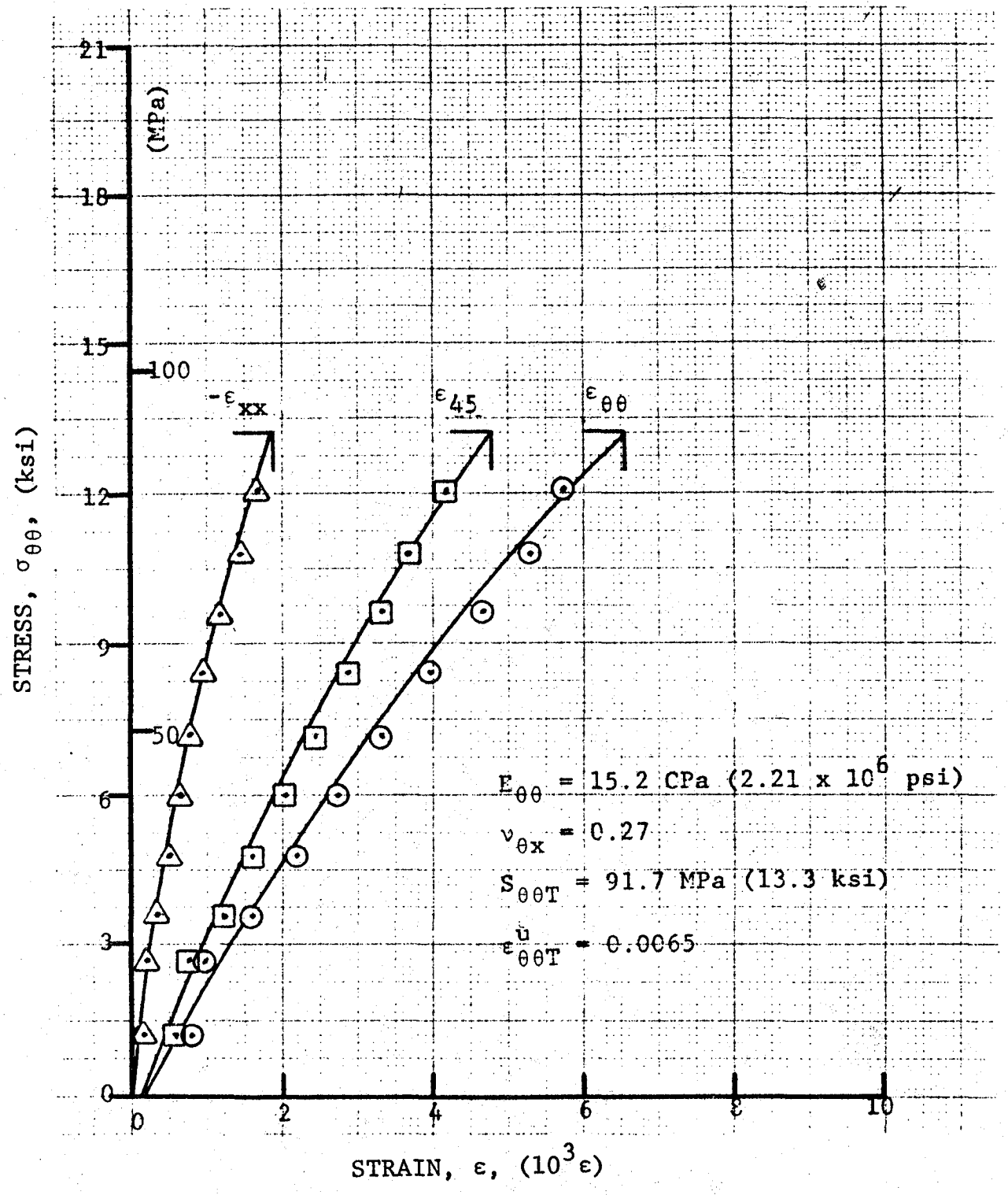

Figure 2-7. Strains in $[45_8]$ SP288/AS ring specimen under static tensile loading (Specimen No. 50-1).

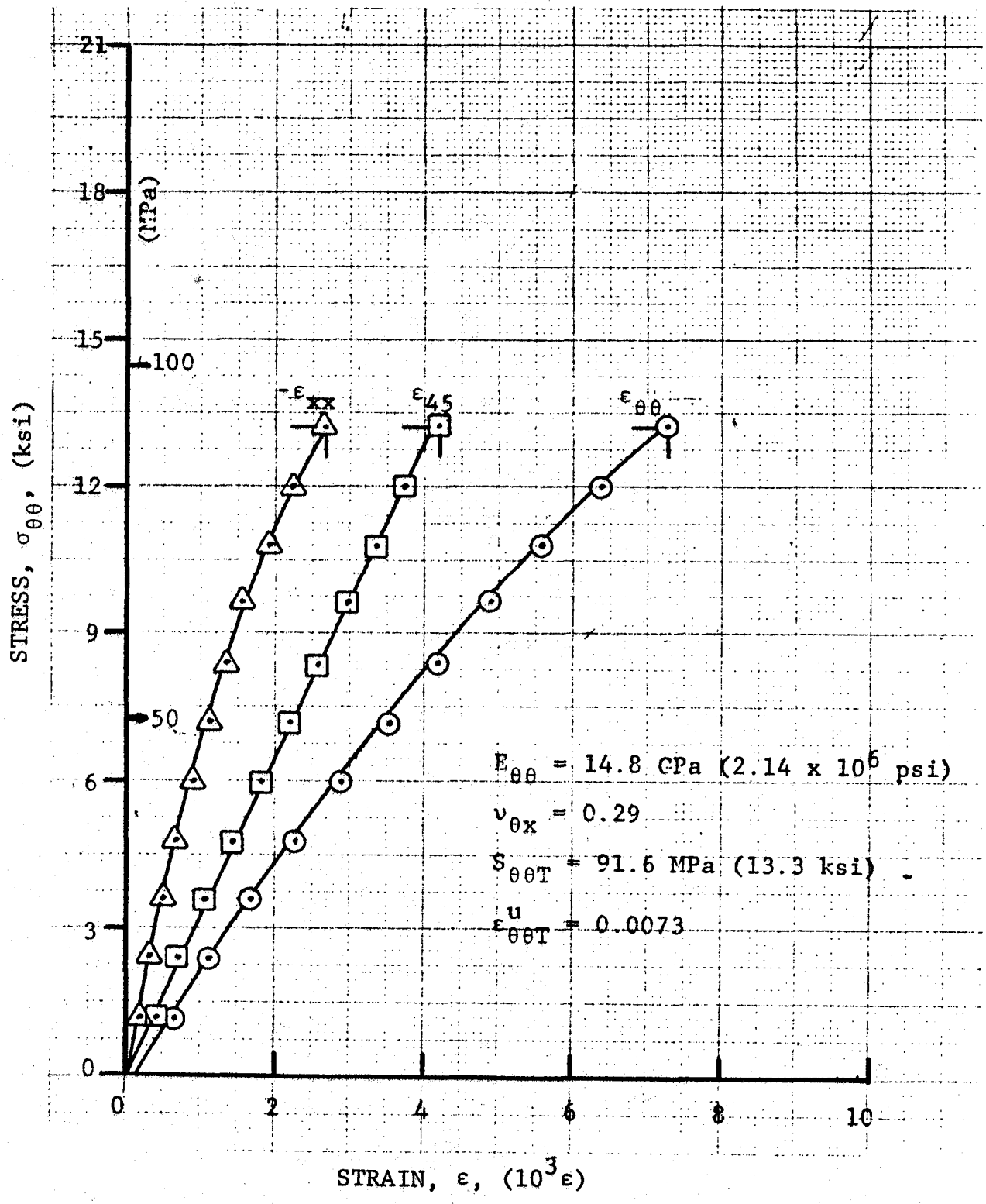

Figure 2-8. Strains in $[45_8]$ SP288/AS ring specimen under static tensile loading (Specimen No. 50-2).

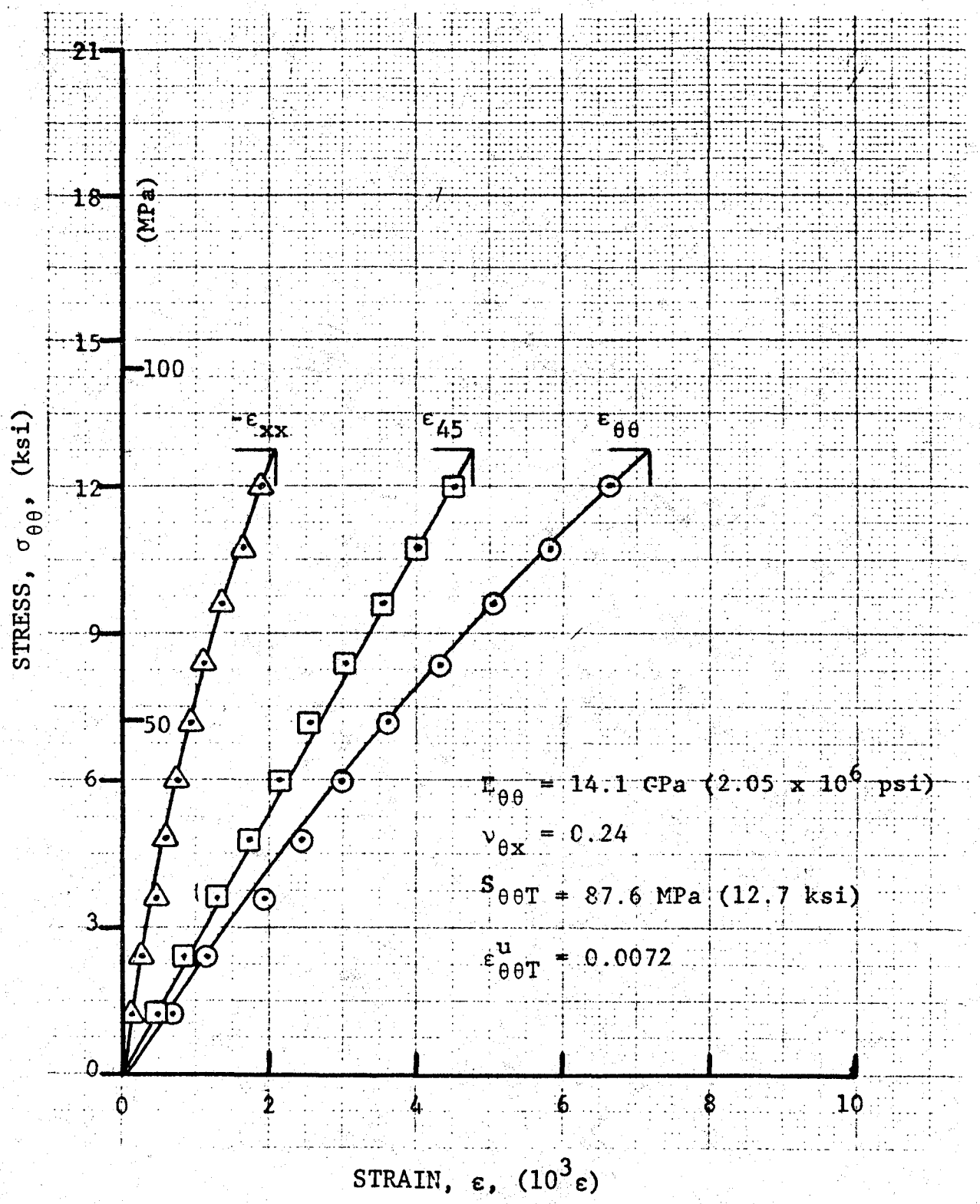

Figure 2-9. Strains in $[45_8]$ SP288/AS ring specimen under static tensile loading (Specimen No. 50-3).

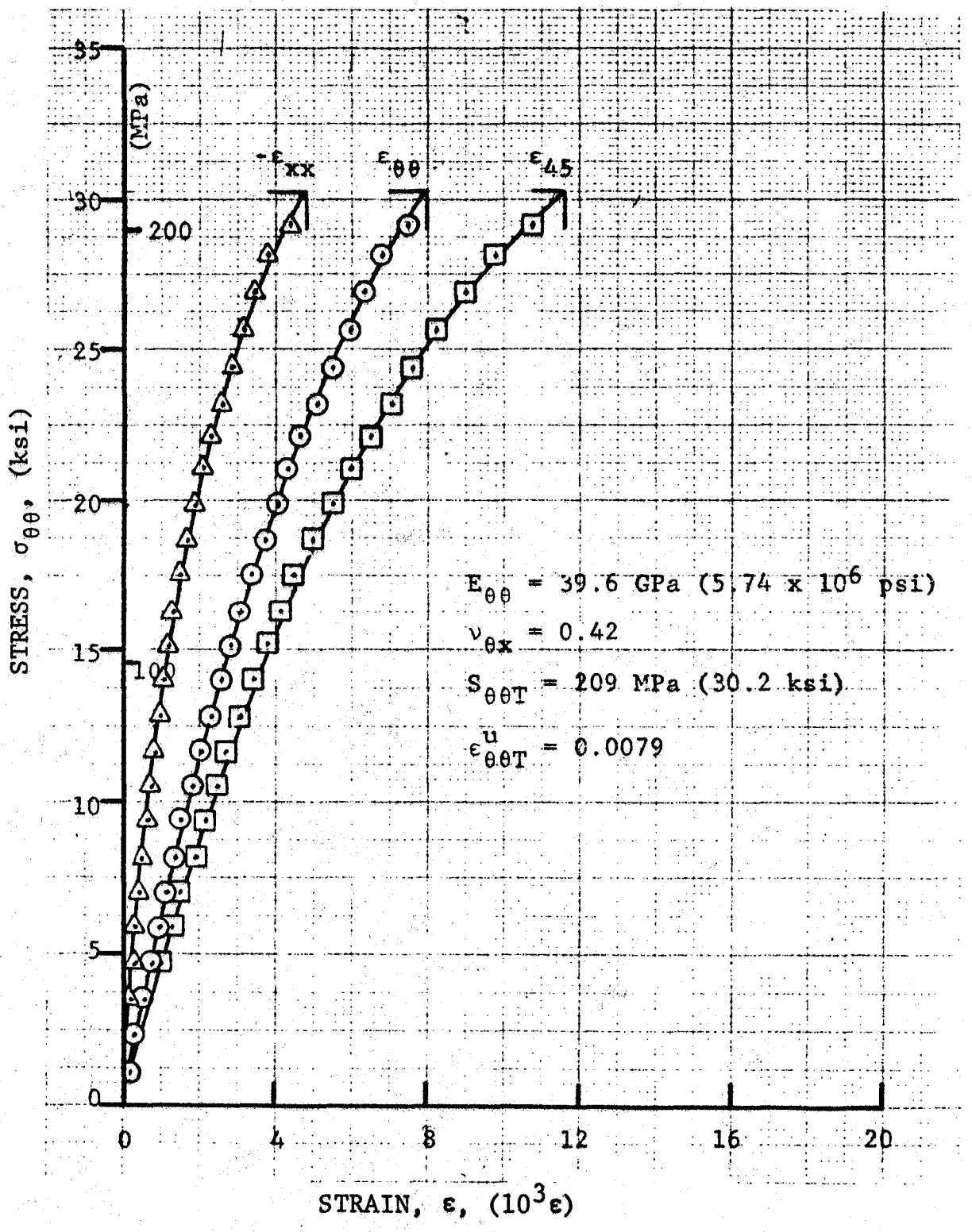

Figure 2-10. Strains in $[22.5_8]$ 80AS/20S/PR288 ring specimen under static tensile loading (Specimen No. 47-1).

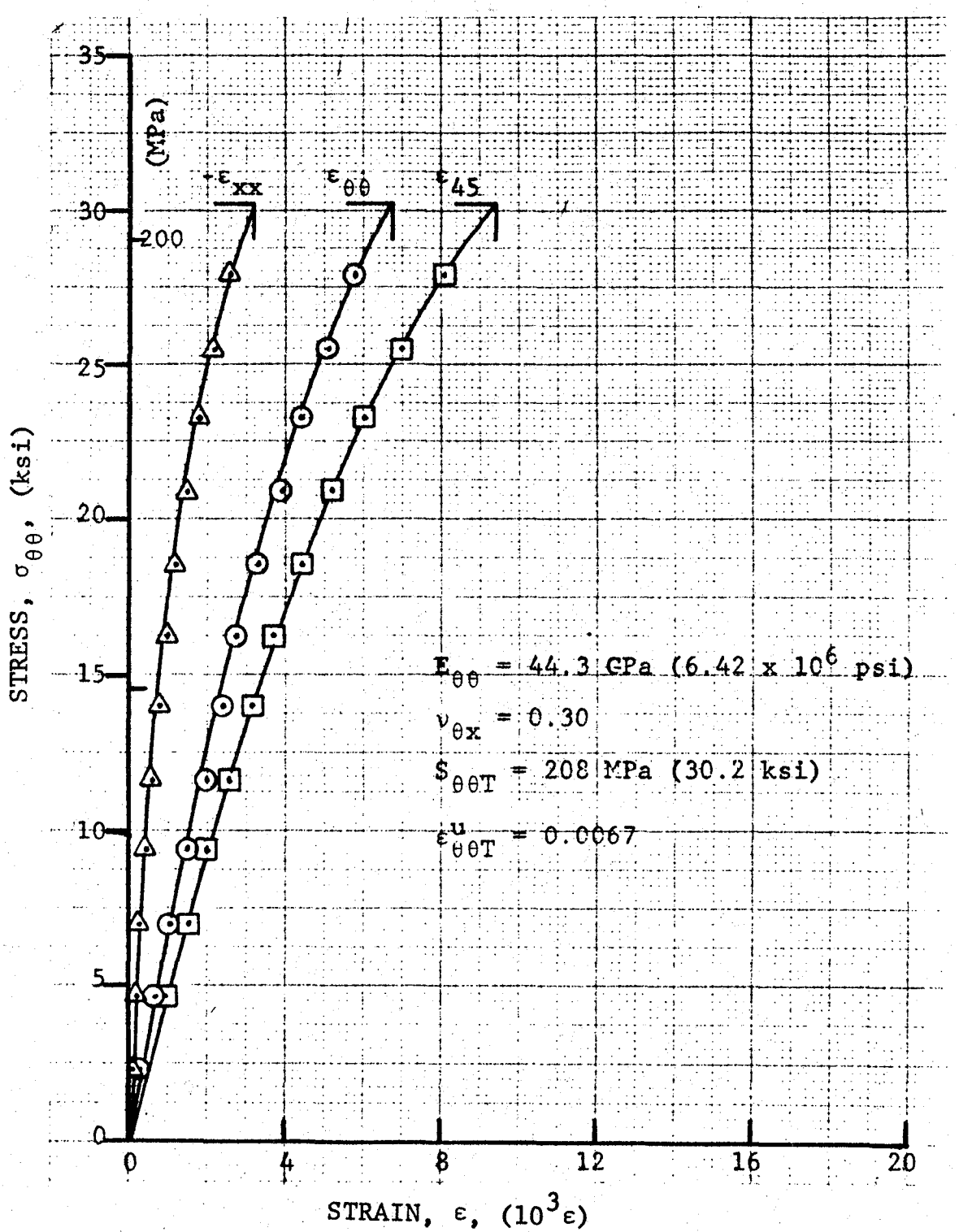

Figure 2-11. Strains in [22.5$_8$] 80AS/20S/PR288 ring specimen under static tensile loading (Specimen No. 47-2).

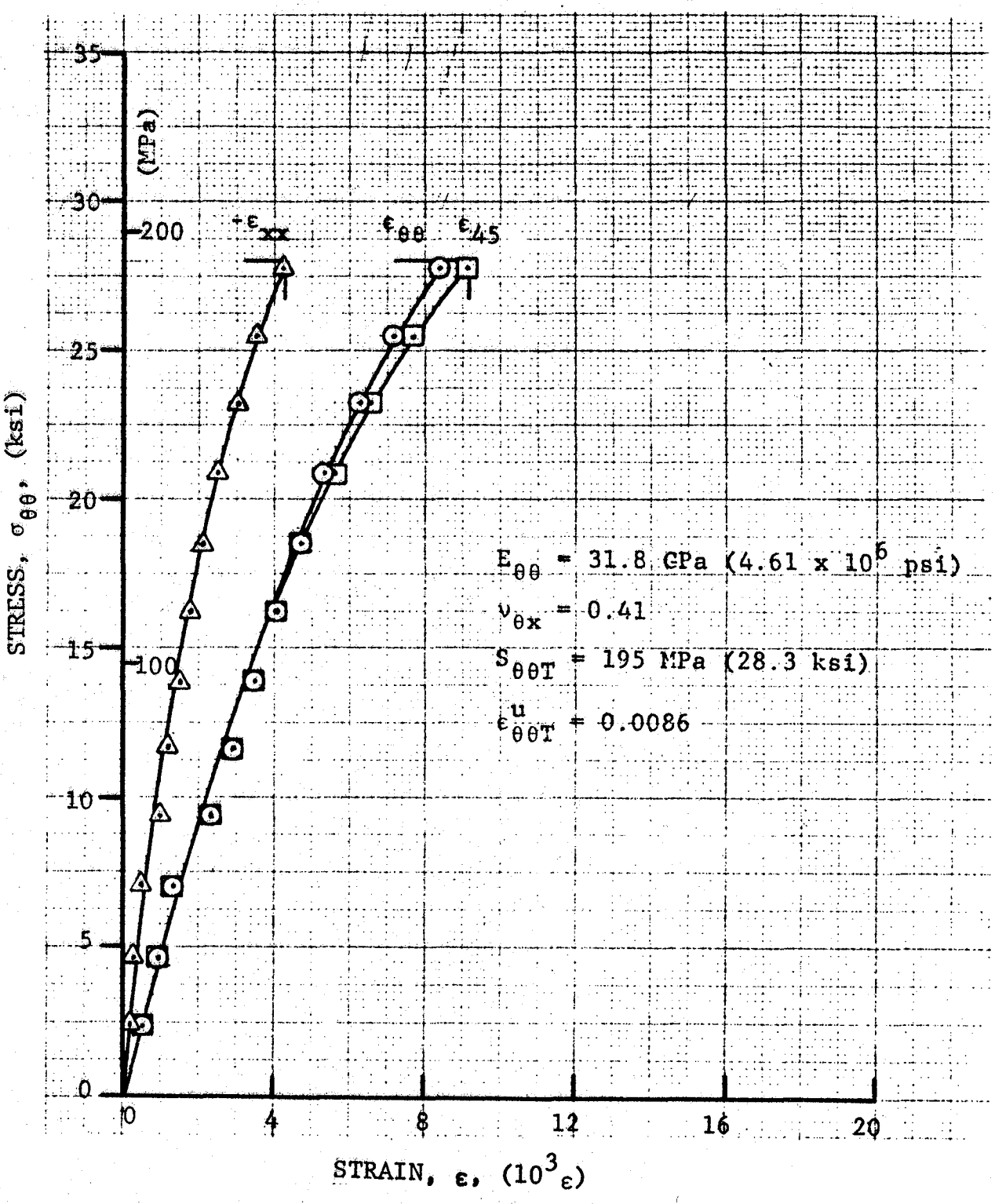

Figure 2-12. Strains in $[22.5_8]$ 80AS/20S/PR288 ring specimen under static tensile loading (Specimen No. 47-3).

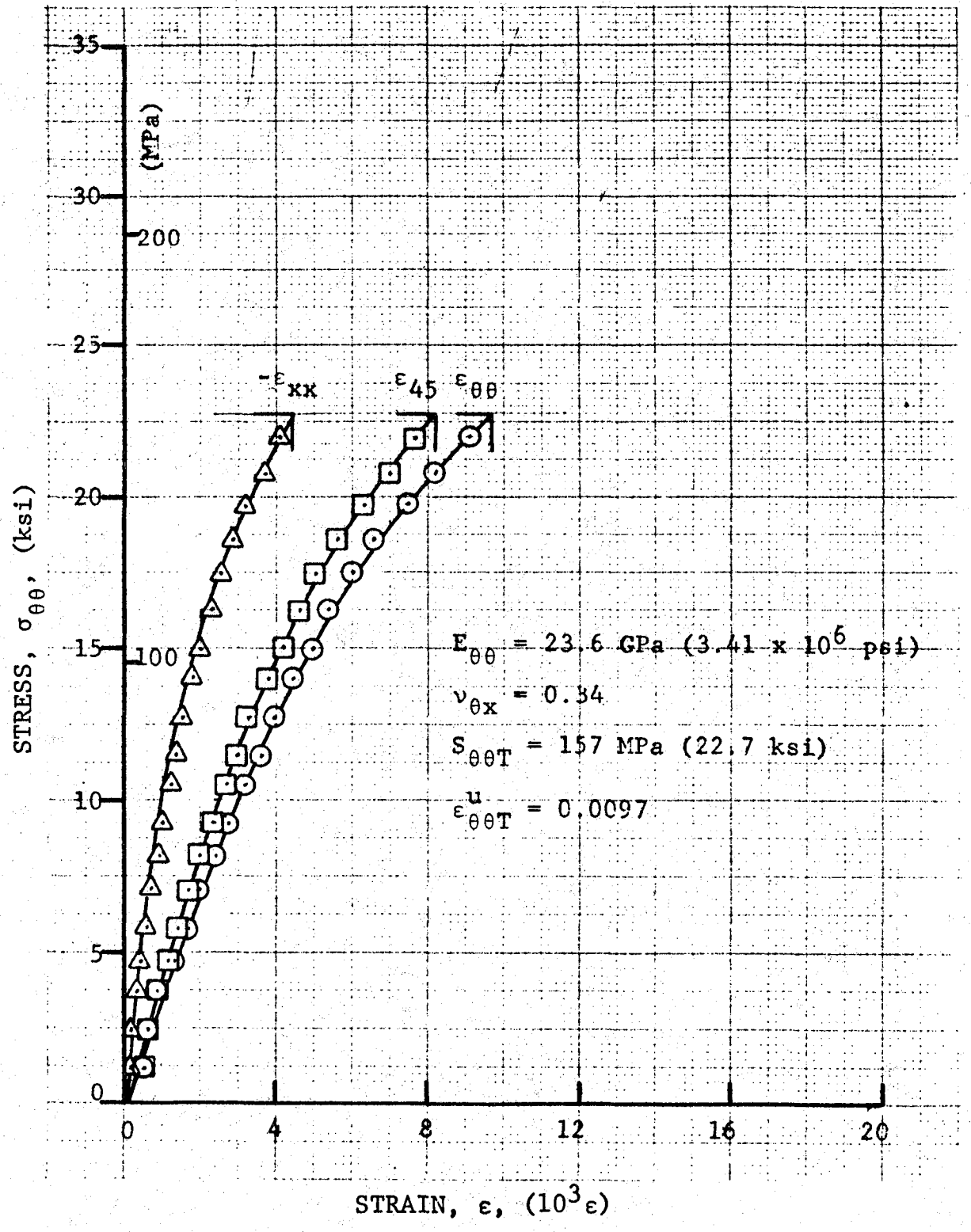

Figure 2-13. Strains in $[30_8]$ 80AS/20S/PR288 ring specimen under static tensile loading (Specimen No. 49-1).

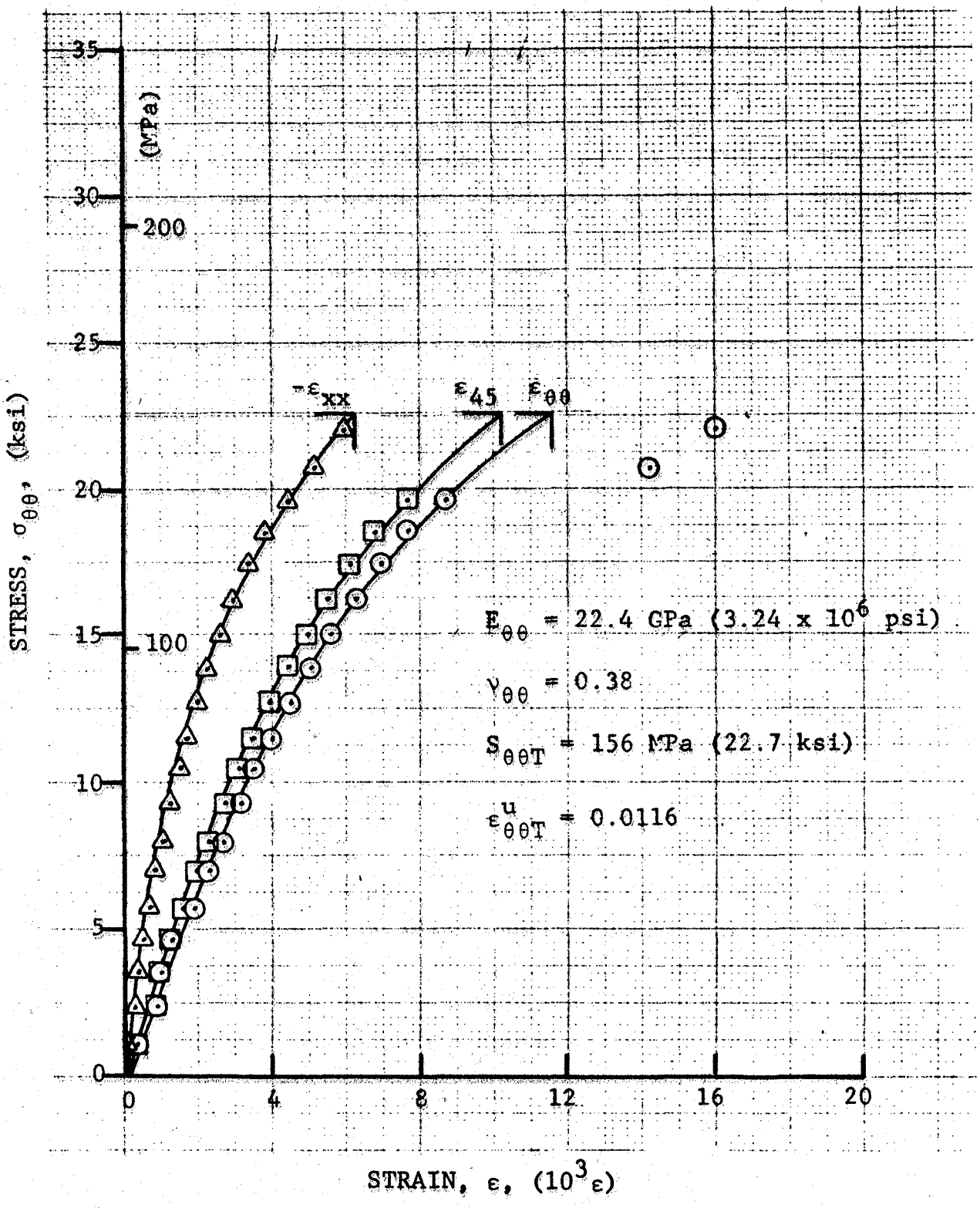

Figure 2-14. Strains in [30$_8$] 80AS/20S/PR288 ring specimen under static tensile loading (Specimen No. 49-2).

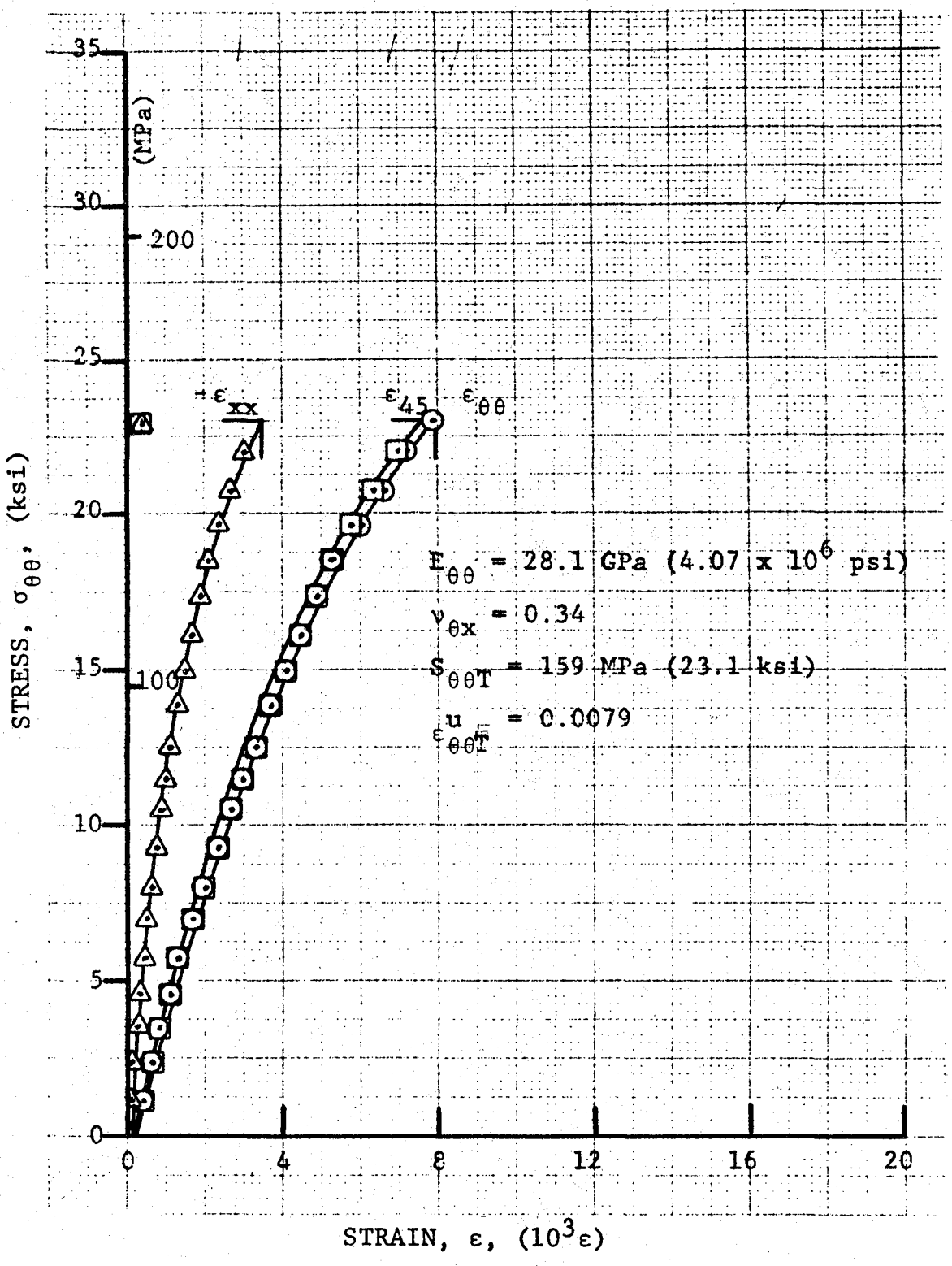

Figure 2-15. Strains in $[30_8]$ 80AS/20S/PR288 ring specimen under static tensile loading (Specimen No. 49-3).

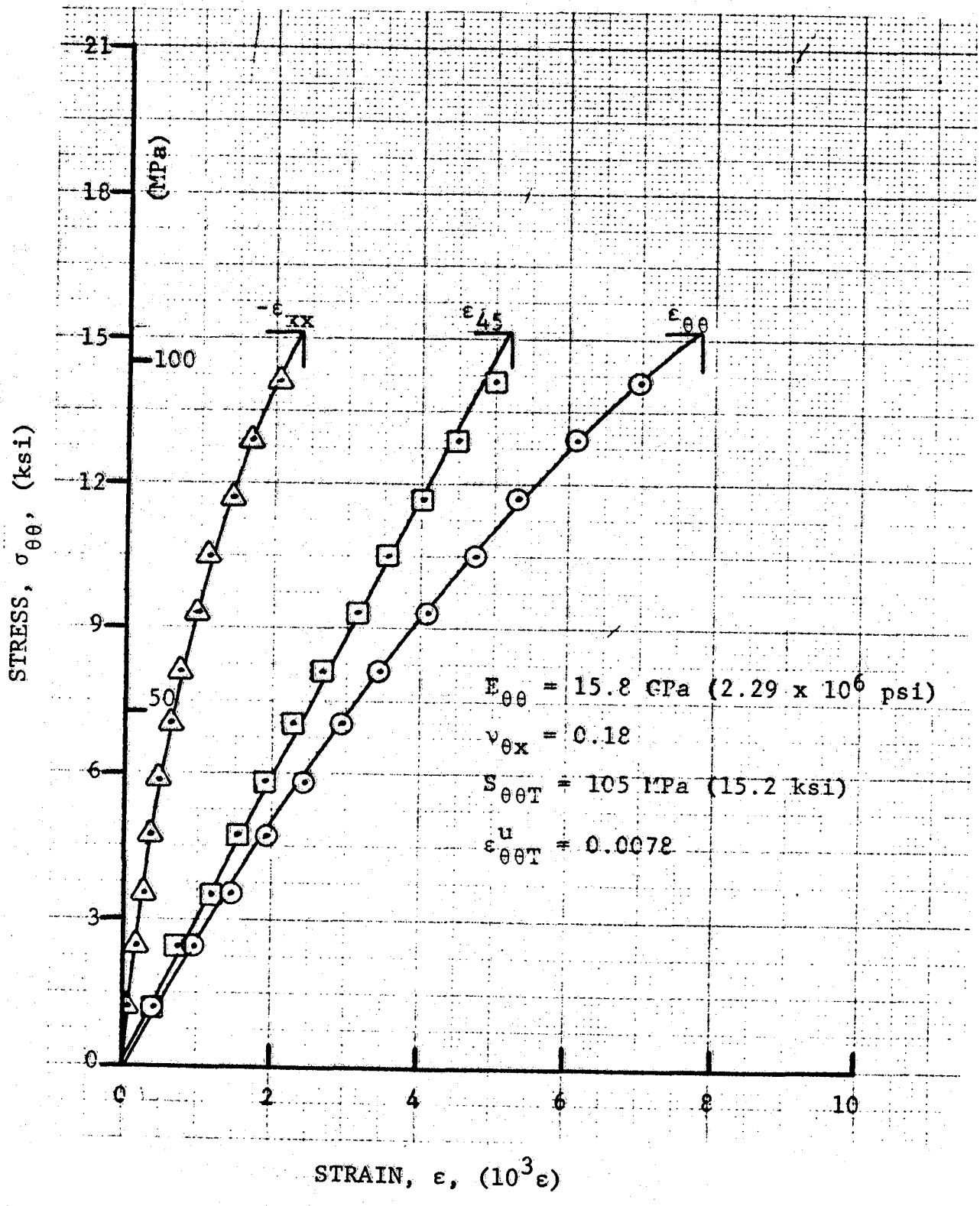

Figure 2-16. Strains in $[45_8]$ 80AS/20S/PR288 ring specimen under static tensile loading (Specimen No. 51-1).

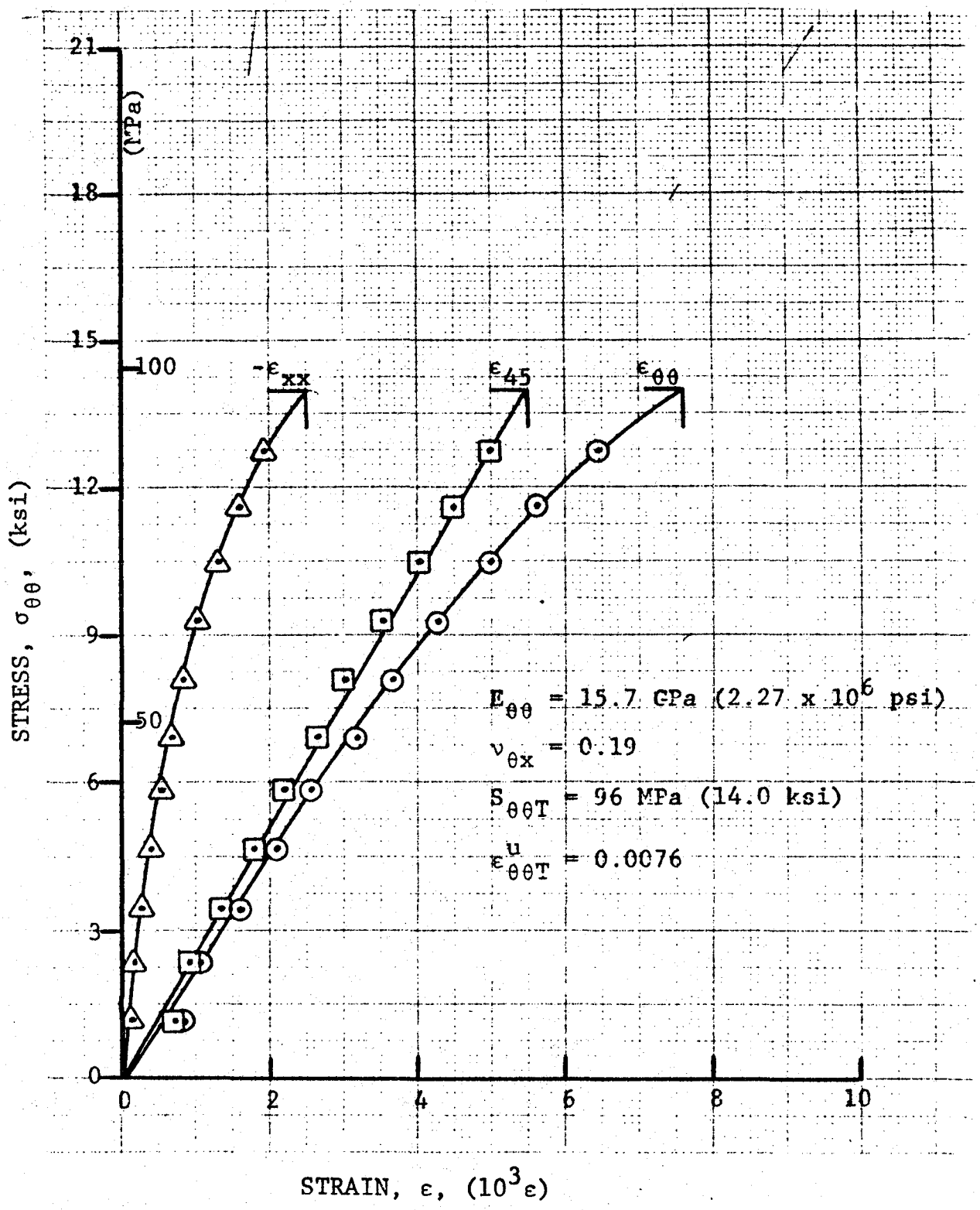

Figure 2-17. Strains in $[45_8]$ 80AS/20S/PR288 ring specimen under static tensile loading (Specimen No. 51-2).

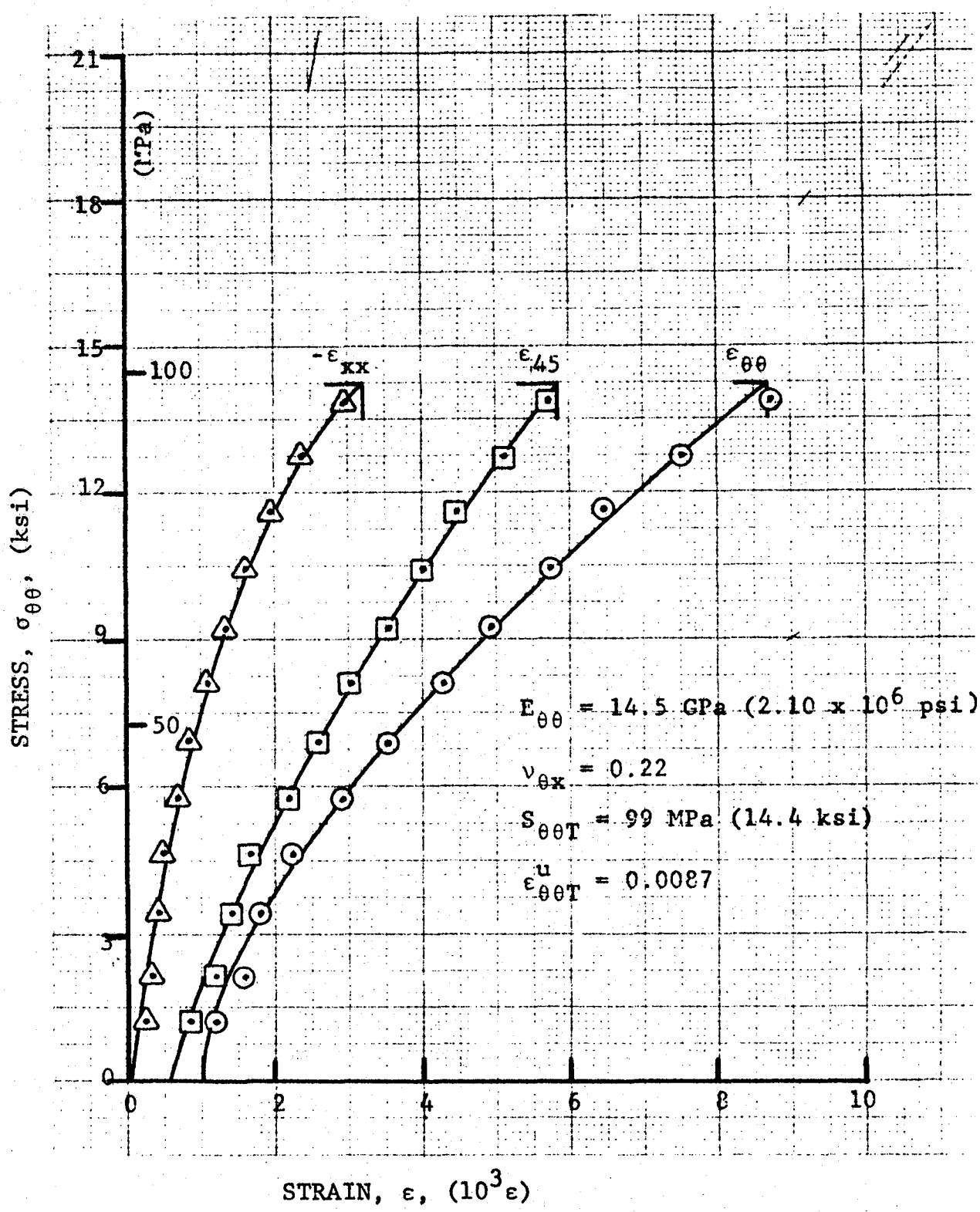

Figure 2-18. Strains in $[45_8]$ 80AS/20S/PR288 ring specimen under static tensile loading (Specimen No. 51-3).

3. INTERMEDIATE STRAIN RATE TENSILE PROPERTIES OF OFF-AXIS LAMINATES

3.1 $[22.5_8]$ LAMINATES

Intermediate rate tensile properties of $[22.5_8]$ SP288/AS graphite/epoxy and 80AS/20S/PR288 graphite/S-glass/epoxy were obtained by testing rings under dynamic internal pressure. Three rings of each material were loaded dynamically using 650 mg of slow burning pistol powder (red dot) in the pressure chamber of the fixture. The circumferential, axial, and 45° strains in the composite rings and the circumferential strain in the steel calibration ring were recorded in every case.

Strain records for the three graphite/epoxy rings are shown in Figures 3-1, 3-2, and 3-3 (Specimen Nos. 46-9, 46-10, and 46-11). These data were analyzed following the procedures described in Part I of this report (Section 3.3.2). Results in the form of dynamic stress-strain curves are shown in Figures 3-4, 3-5, and 3-6. Results for the three rings tested are tabulated in Table 3-1. The initial strain rates range between $14s^{-1}$ and $53s^{-1}$, and the average (secant) rates between $43s^{-1}$ and $70s^{-1}$. The times to failure range between 138 μs and 207 μs. The initial and secant moduli of 45.3 GPa (6.57×10^6 psi) and 37.6 GPa (5.45×10^6 psi), respectively, are higher than the static modulus of 34.6 GPa (5.01×10^6 psi) by 31% and 9%, respectively. The average initial and secant Poisson's ratios of 0.25 and 0.39 are lower and higher, respectively, than the static value of 0.31. The average dynamic strength of 339 MPa (49 ksi) is much higher than the static strength of 218 MPa (31.6 ksi). The increase in dynamic strength is much higher than the increase in dynamic modulus. The average dynamic ultimate strain of 0.0092 is lower than the static value of 0.0110.

Strain records for the three hybrid rings are shown in Figures 3-7, 3-8, and 3-9 (Specimen Nos. 47-7, 47-8, and 47-9). The corresponding dynamic stress-strain curves are shown in Figures 3-10, 3-11, and 3-12. Results are tabulated in Table 3-2. The initial strain rates range between $31s^{-1}$ and $42s^{-1}$, and the average (secant) rates between $51s^{-1}$ and $69s^{-1}$. The time to failure is almost the same for all three specimens, 158 μs and 159 μs. The initial and secant

TABLE 3-1. INTERMEDIATE STRAIN RATE TENSILE PROPERTIES OF $[22.5_8]$ SP288/AS GRAPHITE/EPOXY

Specimen Number	Strain Rate ($\dot{\varepsilon}_{\theta\theta}$), s^{-1}	Modulus ($E_{\theta\theta}$), GPa (10^6 psi)	Poisson's Ratio ($\nu_{\theta x}$)
	Initial Properties		
46-9	53	42.2 (6.12)	0.18
46-10	14	39.6 (5.74)	0.33
46-11	33	54.1 (7.84)	0.23
	Secant Properties		
46-9	70	35.4 (5.14)	0.38
46-10	49	31.4 (4.55)	0.35
46-11	43	45.9 (6.65)	0.43
	Terminal Properties		
46-9	151	16.0 (2.32)	0.42
46-10	126	20.7 (3.00)	0.29
46-11	101	55.2 (8.00)	0.47
	Ultimate Properties		
	Time to Failure (t_f), μs	Strength ($S_{\theta\theta T}$), MPa (ksi)	Strain ($\varepsilon^u_{\theta\theta T}$)
46-9	138	345 (50)	0.0097
46-10	207	320 (46)	0.0102
46-11	180	353 (51)	0.0077

TABLE 3-2. INTERMEDIATE STRAIN RATE TENSILE PROPERTIES OF $[22.5_8]$ 80AS/20S/PR288 GRAPHITE/S-GLASS/EPOXY

Specimen Number	Strain Rate ($\dot{\varepsilon}_{\theta\theta}$), s^{-1}	Modulus ($E_{\theta\theta}$), GPa (10^6 psi)	Poisson's Ratio ($\nu_{\theta x}$)
		Initial Properties	
47-7	31	42.8 (6.20)	0.19
47-8	35	39.6 (5.74)	0.29
47-9	42	48.3 (7.00)	0.21
		Secant Properties	
47-7	69	29.1 (4.22)	0.37
47-8	65	30.2 (4.38)	0.32
47-9	51	35.8 (5.19)	0.33
		Terminal Properties	
47-7	170	25.7 (3.72)	0.45
47-8	139	28.4 (4.12)	0.32
47-9	118	25.9 (3.76)	0.36
		Ultimate Properties	
	Time to Failure (t_f), μs	Strength ($S_{\theta\theta T}$), MPa (ksi)	Strain ($\varepsilon^u_{\theta\theta T}$)
47-7	159	320 (46)	0.0110
47-8	158	312 (45)	0.0103
47-9	159	290 (42)	0.0081

moduli of 43.6 GPa (6.31 x 10^6 psi) and 31.7 GPa (4.60 x 10^6 psi), respectively, are higher and lower, respectively, than the initial static modulus of 38.6 GPa (5.59 x 10^6 psi). The average initial and secant Poisson's ratios of 0.23 and 0.34 are lower than the static value of 0.38. The average dynamic strength of 306 MPa (44 ksi) is much higher than the static strength of 204 MPa (29.6 ksi). The average dynamic ultimate strain of 0.0098 is higher than the static value of 0.0077.

3.2 $[30_8]$ LAMINATES

Intermediate rate tensile properties of $[30_8]$ SP288/AS graphite/epoxy and 80AS/20S/PR288 graphite/S-glass/epoxy were obtained by testing rings under dynamic internal pressure. Three rings of each material were loaded dynamically using 650 mg pistol powder in the pressure chamber of the fixture.

Strain records for the three graphite/epoxy rings tested are shown in Figures 3-13, 3-14, and 3-15 (Specimen Nos. 48-7, 48-8, and 48-9). The corresponding dynamic stress-strain curves are shown in Figures 3-16, 3-17, and 3-18. Results are tabulated in Table 3-3. The initial strain rates range between 41s^{-1} and 72s^{-1} and the average (secant) between 66s^{-1} and 91s^{-1}. The times to failure range between 122 μs and 152 μs. The initial and secant moduli of 27.5 GPa (3.98 x 10^6 psi) and 24.9 GPa (3.61 x 10^6 psi), respectively, are only slightly higher and slightly lower than the static initial modulus of 25.4 GPa (3.68 x 10^6 psi). The average dynamic strength of 254 MPa (36.8 ksi) is much higher than the static strength of 149 MPa (21.6 ksi). This is consistent with the fact that the dynamic ultimate strain of 0.0105 is higher than the static value of 0.0080.

Strain records for the three hybrid rings are shown in Figures 3-19, 3-20, and 3-21 (Specimen Nos. 49-8, 49-9, and 49-10). The corresponding dynamic stress-strain curves are shown in Figures 3-22, 3-23, and 3-24. Results are tabulated in Table 3-4. The initial strain rates range between 40s^{-1} and 74s^{-1} and the average (secant) between 70s^{-1} and 102s^{-1}. The times to failure range between 116 μs and 155 μs. The initial and secant moduli of 28.1 GPa (4.07 x 10^6 psi) and 23.8 GPa (3.45 x 10^6 psi), respectively, straddle the value of the static initial modulus of 24.7 GPa (3.57 x 10^6 psi). The average dynamic strength of 264 MPa (38.3 ksi) is much higher than the static strength of 157 MPa (22.8 ksi). Also, the dynamic ultimate strain of 0.0113 is higher than the static value of 0.0097.

TABLE 3-3. INTERMEDIATE STRAIN RATE TENSILE PROPERTIES OF $[30_8]$ SP288/AS GRAPHITE/EPOXY

Specimen Number	Strain Rate ($\dot{\varepsilon}_{\theta\theta}$), s^{-1}	Modulus ($E_{\theta\theta}$), GPa (10^6 psi)	Poisson's Ratio ($\nu_{\theta x}$)
	Initial Properties		
48-7	72	21.8 (3.16)	-
48-8	68	31.9 (4.62)	0.26
48-9	41	28.7 (4.16)	-
	Secant Properties		
48-7	70	29.7 (4.31)	0.37
48-8	91	22.0 (3.19)	0.37
48-9	66	23.0 (3.33)	0.31
	Terminal Properties		
48-7	94	32.4 (4.70)	0.57
48-8	200	16.7 (2.42)	0.42
48-9	132	13.2 (1.92)	0.36
	Ultimate Properties		
	Time to Failure (t_f), μs	Strength ($S_{\theta\theta T}$), MPa (ksi)	Strain ($\varepsilon^u_{\theta\theta T}$)
48-7	122	253 (36.6)	0.0085
48-8	142	282 (40.8)	0.0129
48-9	152	228 (33.0)	0.0100

TABLE 3-4. INTERMEDIATE STRAIN RATE TENSILE PROPERTIES OF $[30_8]$ 80AS/20S/PR288 GRAPHITE/S-GLASS/EPOXY

Specimen Number	Strain Rate ($\dot{\varepsilon}_{\theta\theta}$), s^{-1}	Modulus ($E_{\theta\theta}$), GPa (10^6 psi)	Poisson's Ratio ($\nu_{\theta x}$)
	Initial Properties		
49-8	40	29.1 (4.22)	-
49-9	74	24.3 (3.52)	0.31
49-10	73	30.9 (4.48)	-
	Secant Properties		
49-8	70	21.8 (3.16)	0.31
49-9	102	20.9 (3.02)	0.43
49-10	87	28.7 (4.16)	0.34
	Terminal Properties		
49-8	149	18.9 (2.74)	0.38
49-9	197	14.5 (2.10)	0.47
49-10	101	34.2 (4.96)	0.66
	Ultimate Properties		
	Time to Failure (t_f), μs	Strength ($S_{\theta\theta T}$), MPa (ksi)	Strain ($\varepsilon^u_{\theta\theta T}$)
49-8	155	233 (33.8)	0.0108
49-9	127	269 (39.0)	0.0129
49-10	116	290 (42.0)	0.0101

3.3 $[45_8]$ LAMINATES

Intermediate rate tensile properties of $[45_8]$ SP288/AS graphite/epoxy and 80AS/20S/PR288 graphite/S-glass/epoxy were obtained by testing three rings of each material under dynamic internal pressure. The pressure was produced by detonating 650 mg pistol powder in the pressure chamber of the fixture.

Strain records for the three graphite/epoxy rings tested are shown in Figures 3-25, 3-26, and 3-27 (Specimen Nos. 50-8, 50-9, and 50-10). The corresponding dynamic stress-strain curves are shown in Figures 3-28, 3-29, and 3-30. Results are tabulated in Table 3-5. The initial strain rates range between $47s^{-1}$ and $64s^{-1}$, and the average (secant) rates between $72s^{-1}$ and $93s^{-1}$. The times to failure range between 114 μs and 121 μs. The initial and secant moduli of 25.5 GPa (3.70×10^6 psi) and 17.0 GPa (2.46×10^6 psi), respectively, are noticeably higher than the static initial modulus of 14.7 GPa (2.13×10^6 psi). The average dynamic strength of 161 MPa (23.4×10^6 psi) is almost twice as high as the static strength of 90 MPa (13.1 ksi). The dynamic ultimate strain of 0.0096 is higher than the static value of 0.0070.

Strain records for the three hybrid rings are shown in Figures 3-31, 3-32, and 3-33 (Specimen Nos. 51-7, 51-8, and 51-9). The corresponding dynamic stress-strain curves are shown in Figures 3-34, 3-35, and 3-36. Results are tabulated in Table 3-6. The initial strain rates range between $61s^{-1}$ and $87s^{-1}$, and the average (secant) rates between $65s^{-1}$ and $83s^{-1}$. The times to failure range between 114 μs and 143 μs. The initial and secant moduli of 24.3 GPa (3.53×10^6 psi) and 19.9 GPa (2.89×10^6 psi), respectively, are higher than the static value of 15.3 GPa (2.22×10^6 psi). The dynamic secant Poisson's ratio of 0.21 is almost the same as the static value of 0.20. The average dynamic strength of 195 MPa (28.2 ksi) is almost twice as high as the static strength of 100 MPa (14.5 ksi). The dynamic ultimate strain of 0.0098 is higher than the static value of 0.0080 as in most cases mentioned before.

TABLE 3-5. INTERMEDIATE STRAIN RATE TENSILE PROPERTIES OF $[45_8]$ SP288/AS GRAPHITE/EPOXY

Specimen Number	Strain Rate ($\dot{\varepsilon}_{\theta\theta}$), s^{-1}	Modulus ($E_{\theta\theta}$), GPa (10^6 psi)	Poisson's Ratio ($\nu_{\theta x}$)
		Initial Properties	
50-8	60	26.4 (3.82)	-
50-9	64	28.4 (4.12)	-
50-10	47	21.8 (3.16)	0.20
		Secant Properties	
50-8	72	16.5 (2.39)	0.18
50-9	93	17.3 (2.51)	0.45
50-10	82	17.0 (2.47)	0.23
		Terminal Properties	
50-8	114	11.9 (1.73)	0.32
50-9	136	30.8 (4.46)	-
50-10	130	17.3 (2.50)	0.32
		Ultimate Properties	
	Time to Failure (t_f), μs	Strength ($S_{\theta\theta T}$), MPa (ksi)	Strain ($\varepsilon^u_{\theta\theta T}$)
50-8	114	135 (19.6)	0.0082
50-9	116	182 (26.4)	0.0108
50-10	121	167 (24.2)	0.0099

TABLE 3-6. INTERMEDIATE STRAIN RATE TENSILE PROPERTIES OF $[45_8]$ 80AS/20S/PR288 GRAPHITE/S-GLASS/EPOXY

Specimen Number	Strain Rate ($\dot{\varepsilon}_{\theta\theta}$), s^{-1}	Modulus ($E_{\theta\theta}$), GPa (10^6 psi)	Poisson's Ratio ($\nu_{\theta x}$)
	Initial Properties		
51-7	87	24.0 (3.48)	-
51-8	67	24.6 (3.56)	-
51-9	61	24.4 (3.54)	-
	Secant Properties		
51-7	83	22.2 (3.22)	0.22
51-8	80	18.5 (2.68)	0.22
51-9	65	19.1 (2.76)	0.18
	Terminal Properties		
51-7	101	30.9 (4.48)	0.45
51-8	153	13.5 (1.96)	0.35
51-9	120	18.8 (2.72)	0.35
	Ultimate Properties		
	Time to Failure (t_f), μs	Strength ($S_{\theta\theta T}$), MPa (ksi)	Strain ($\varepsilon^u_{\theta\theta T}$)
51-7	114	211 (30.6)	0.0095
51-8	132	196 (28.4)	0.0106
51-9	143	177 (25.7)	0.0093

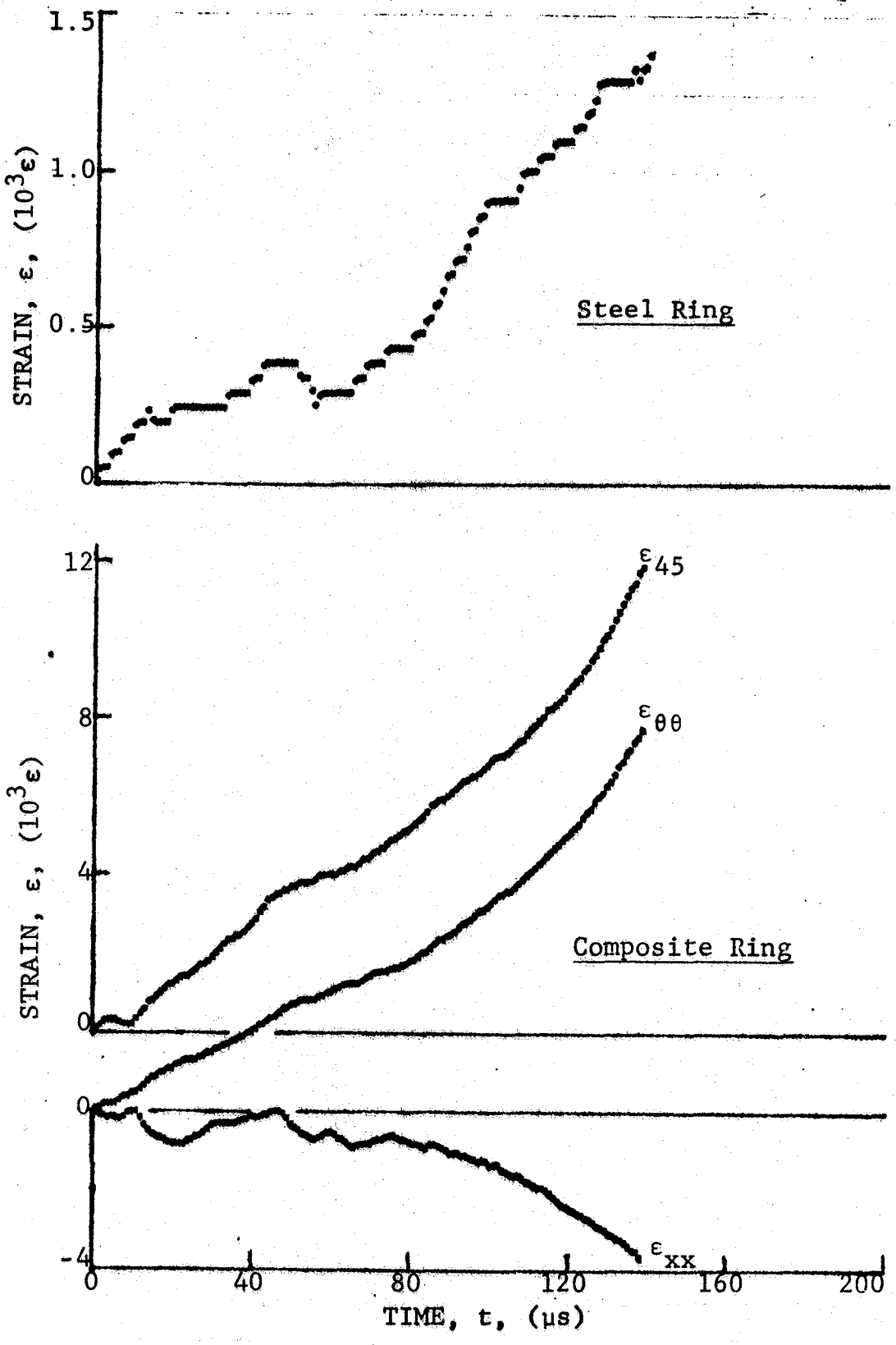

Figure 3-1. Strain records in steel ring and [22.5₈] SP288/AS graphite/epoxy ring under dynamic loading for Specimen No. 46-9 (0.65 g shotgun powder).

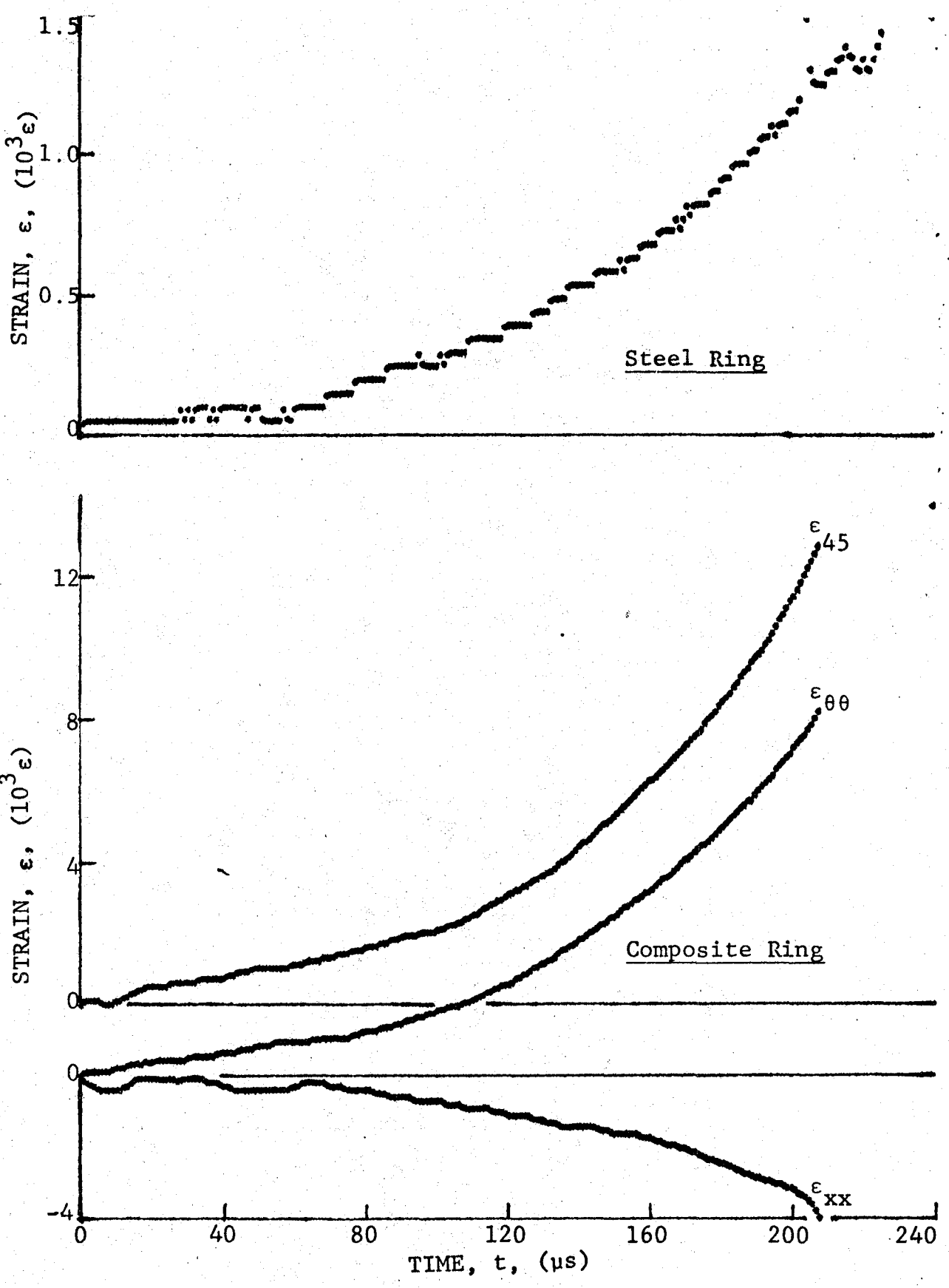

Figure 3-2. Strain records in steel ring and $[22.5_8]$ SP288/AS graphite/epoxy ring under dynamic loading for Specimen No. 46-10 (0.65 g shotgun powder).

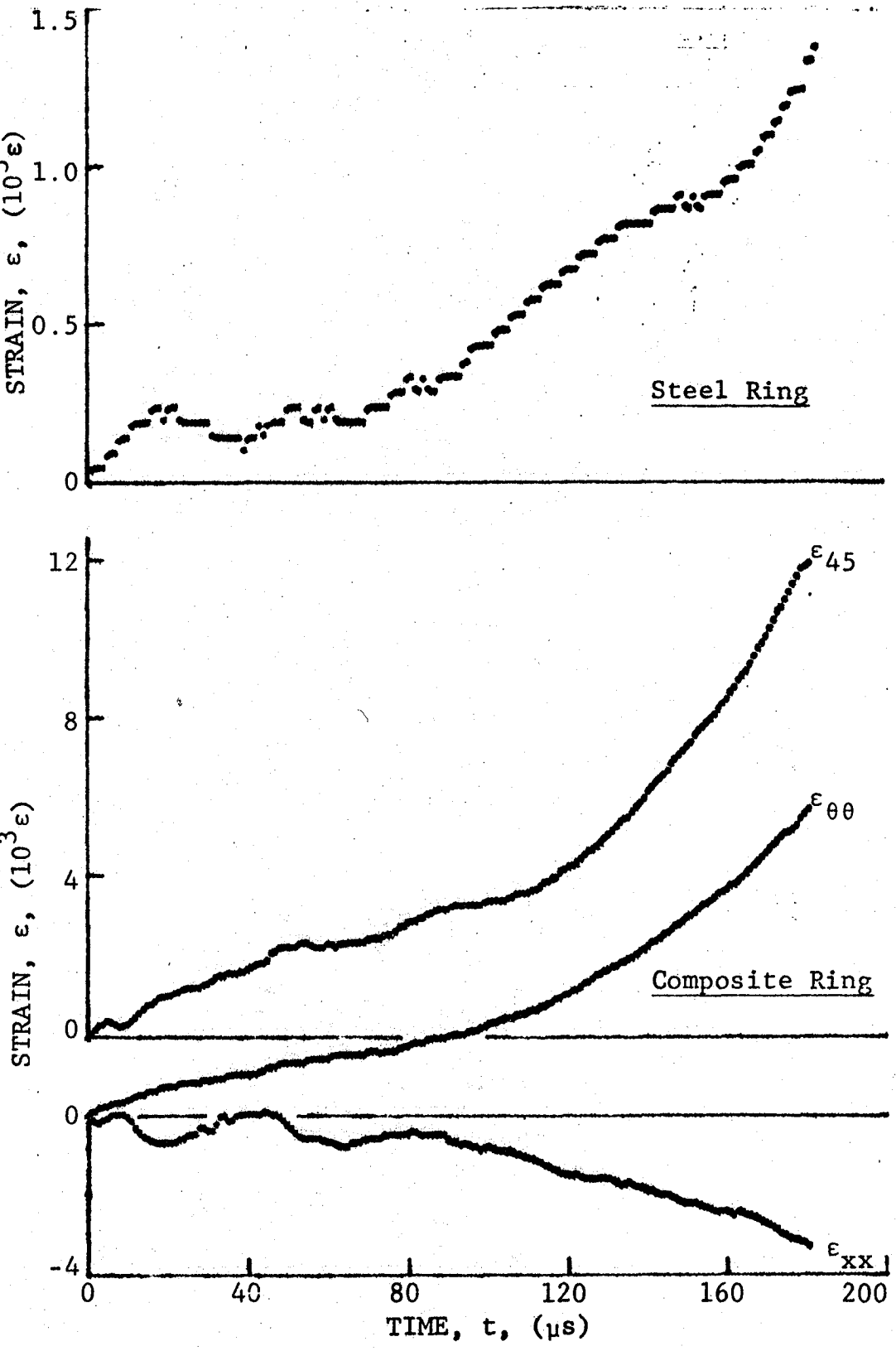

Figure 3-3. Strain records in steel ring and $[22.5_8]$ SP288/AS graphite/epoxy ring under dynamic loading for Specimen No. 46-11 (0.65 g shotgun powder).

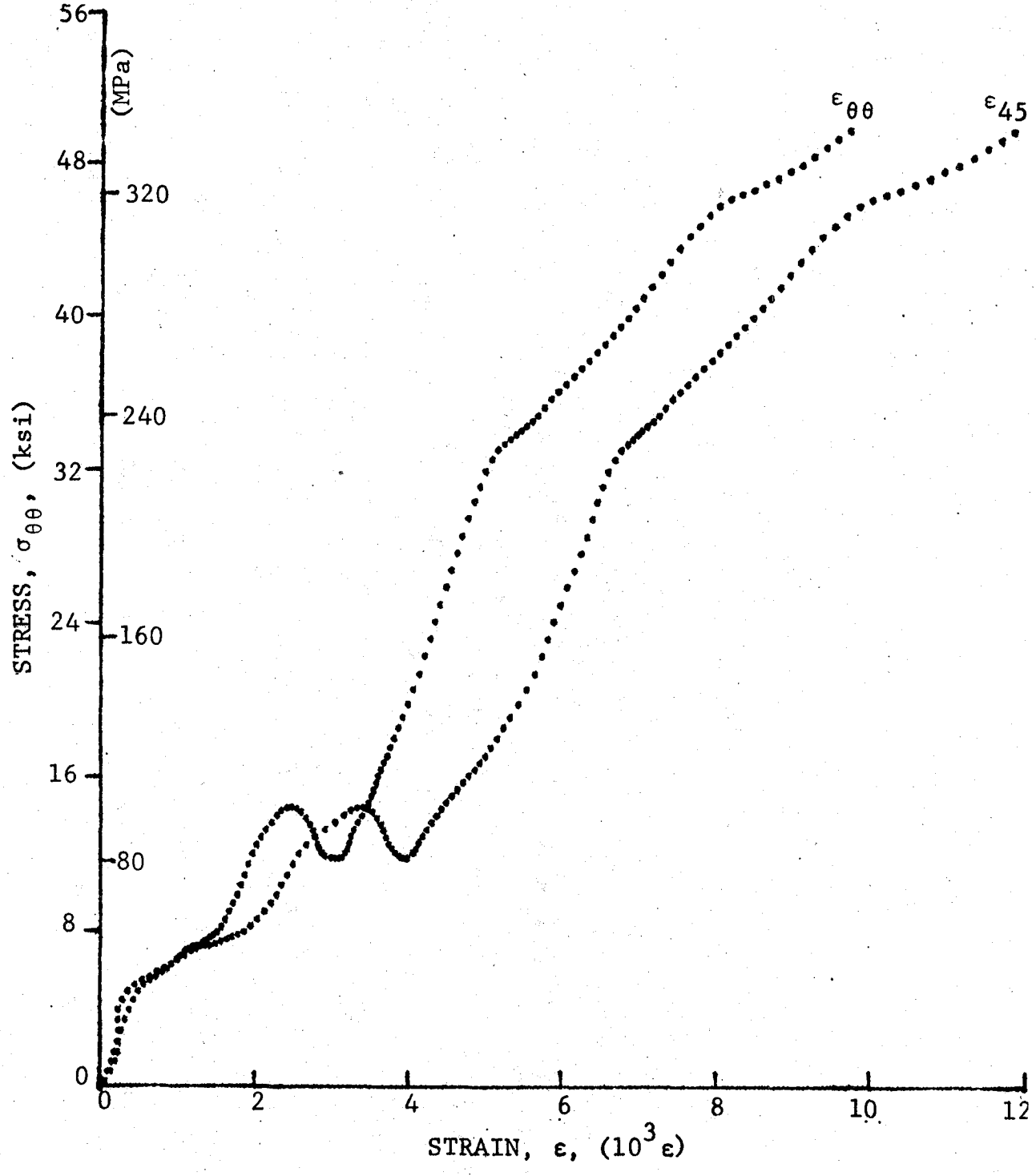

Figure 3-4. Stress-strain curves for dynamically loaded $[22.5_8]$ SP288/AS graphite/epoxy ring, Specimen No. 46-9.

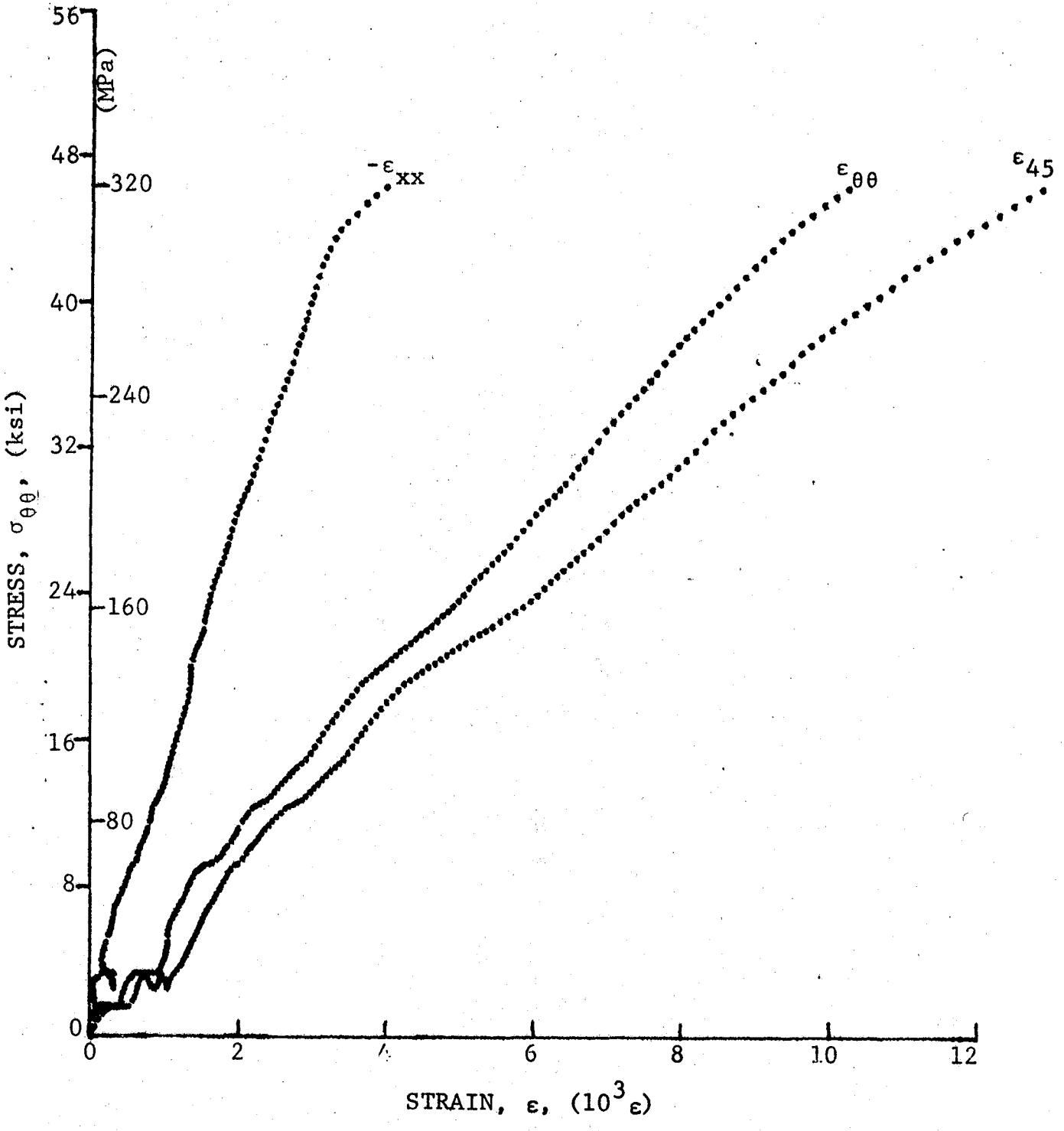

Figure 3-5. Stress-strain curves for dynamically loaded $[22.5_8]$ SP288/AS graphite/epoxy ring, Specimen No. 46-10.

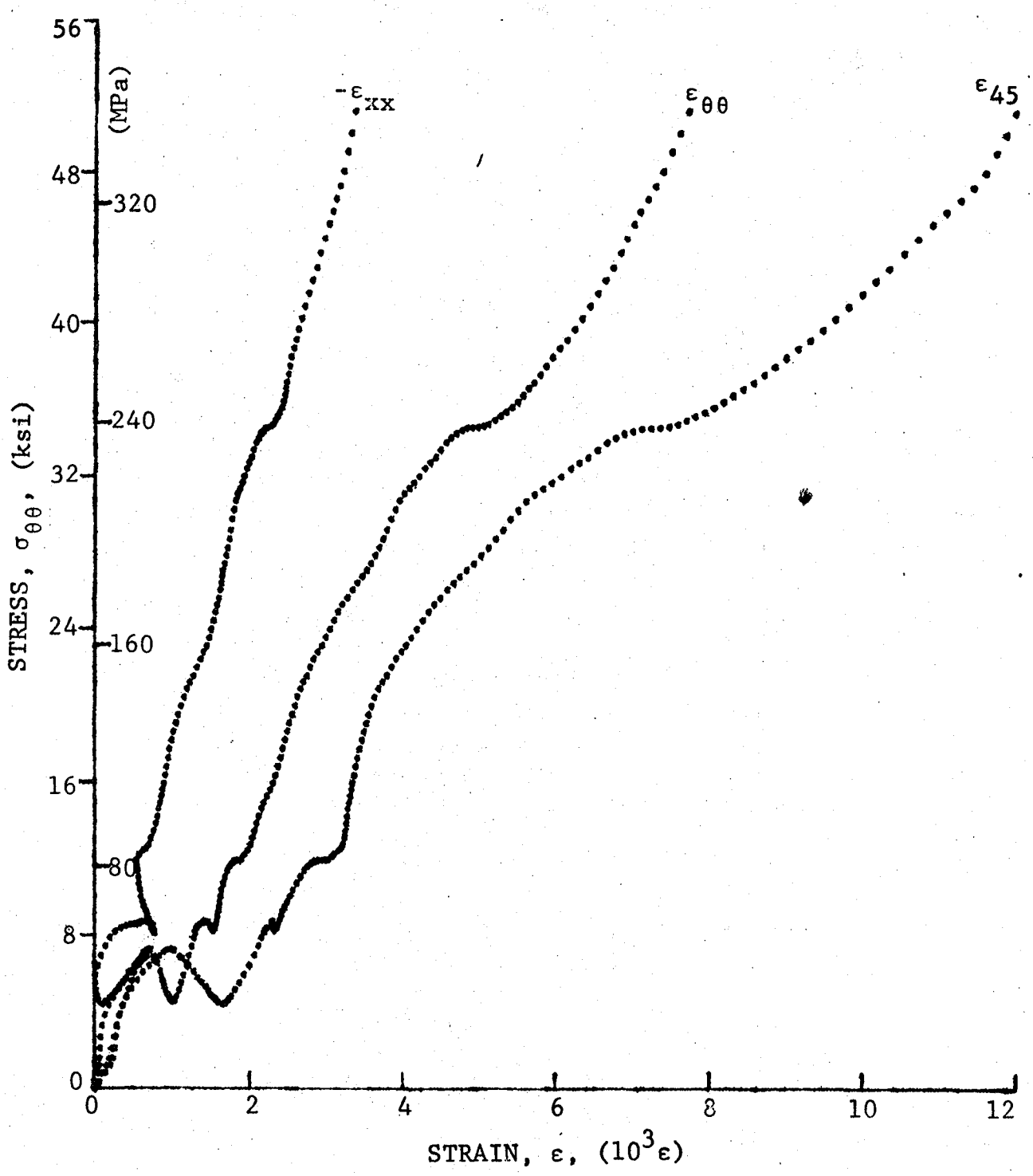

Figure 3-6. Stress-strain curves for dynamically loaded $[22.5_8]$ SP288/AS graphite/epoxy ring, Specimen No. 46-11.

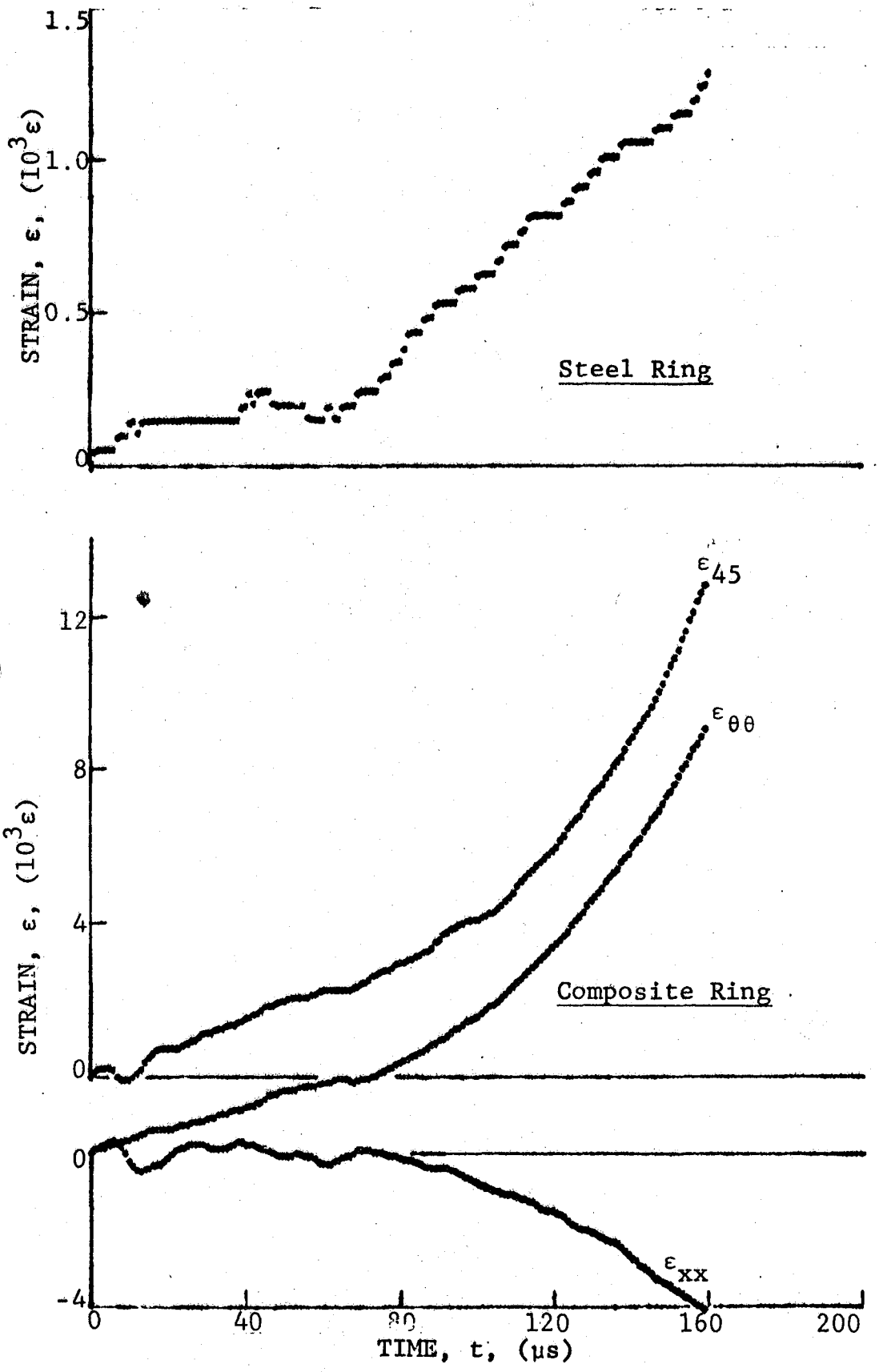

Figure 3-7. Strain records in steel ring and 80AS/20S/PR288 [22.5$_8$] graphite/S-glass/epoxy ring under dynamic loading for Specimen No. 47-7 (0.65 g shotgun powder).

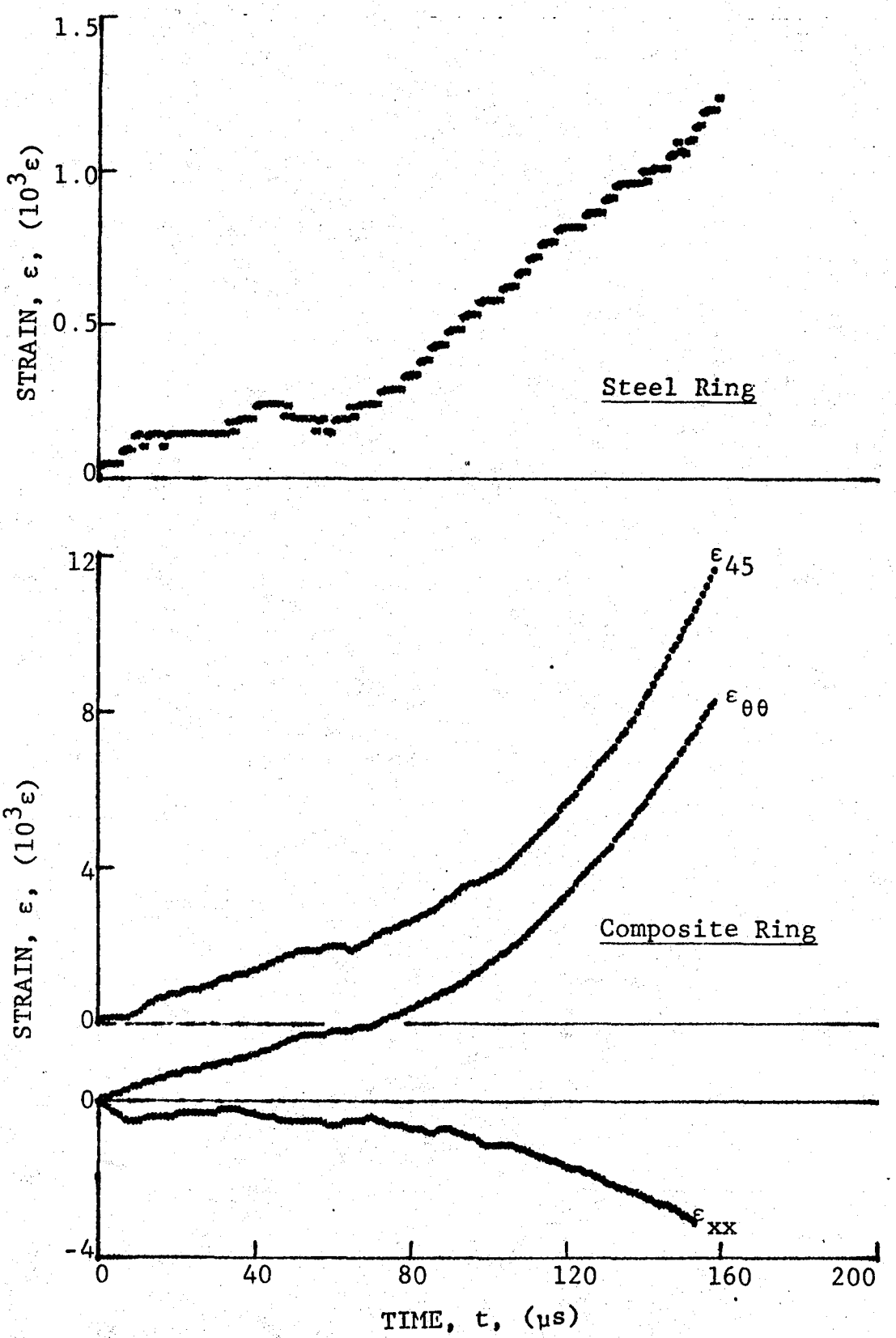

Figure 3-8. Strain records in steel ring and 80AS/20S/PR288 [22.5$_8$] graphite/S-glass/epoxy ring under dynamic loading for Specimen No. 47-8 (0.65 g shotgun powder).

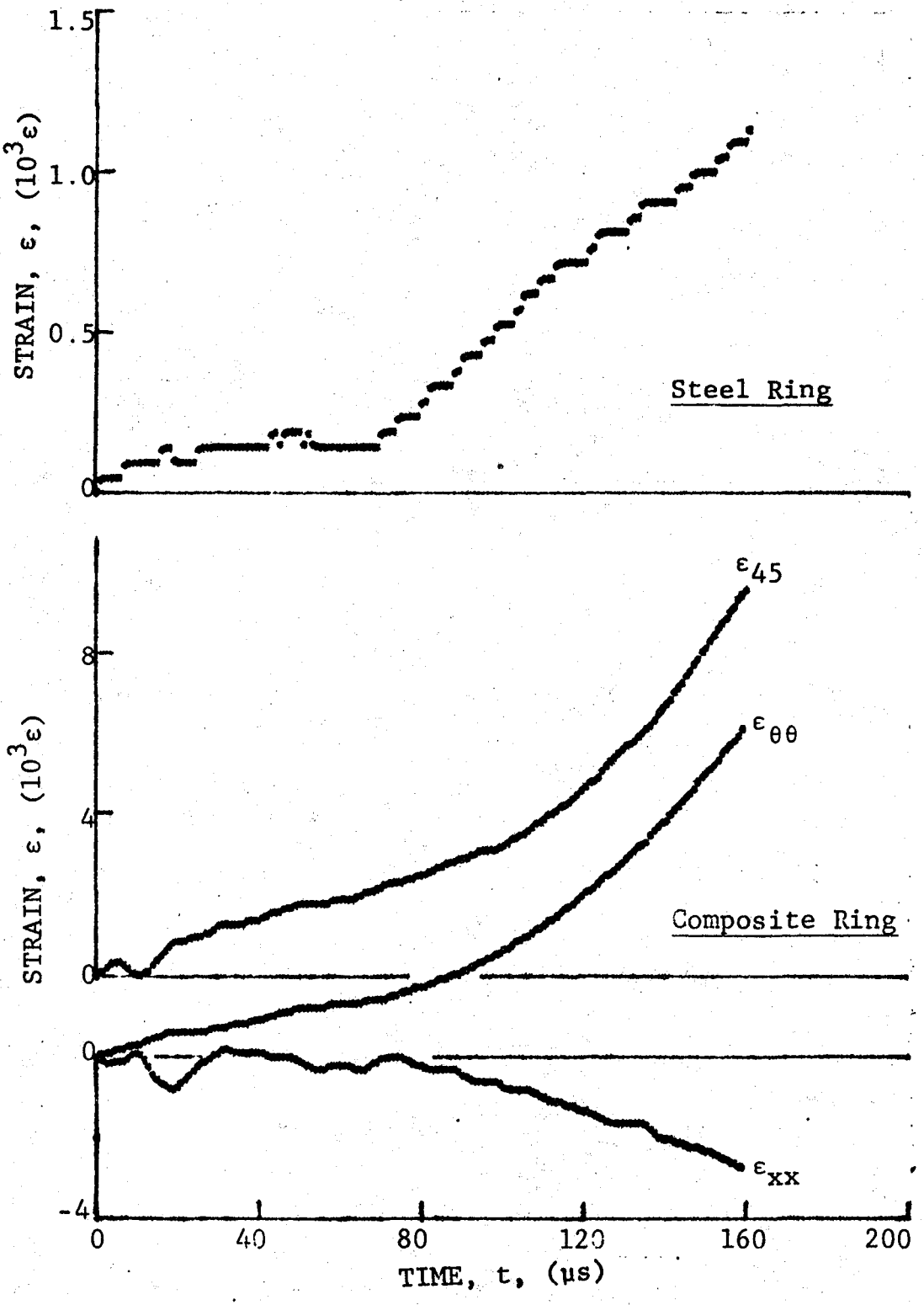

Figure 3-9. Strain records in steel ring and 80AS/20S/PR288 [22.5$_8$] graphite/S-glass/epoxy ring under dynamic loading for Specimen No. 47-9 (0.65 g shotgun powder).

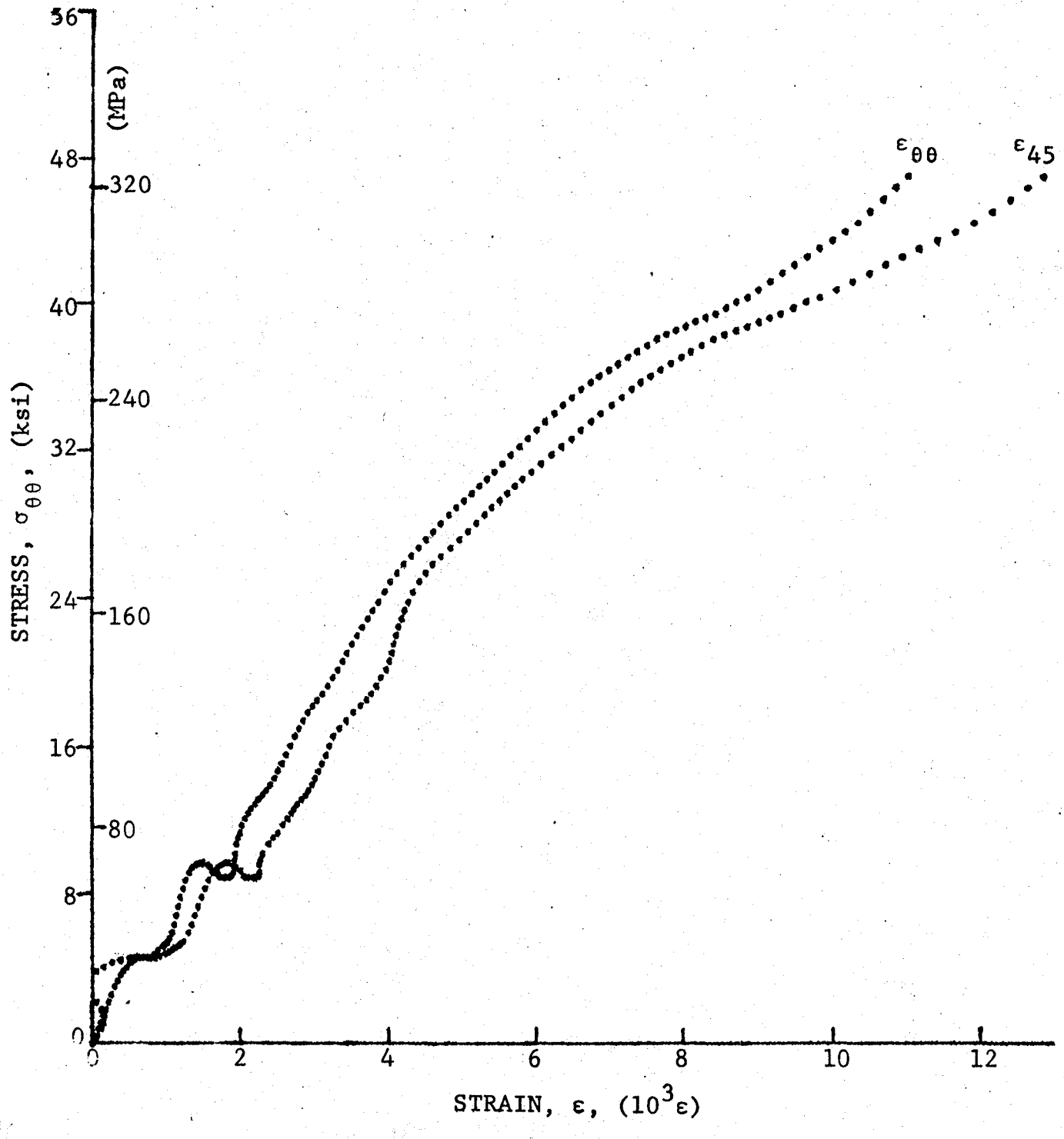

Figure 3-10. Stress-strain curves for dynamically loaded $[22.5_8]$ 80AS/20S/PR288 graphite/S-glass/epoxy ring, Specimen No. 47-7.

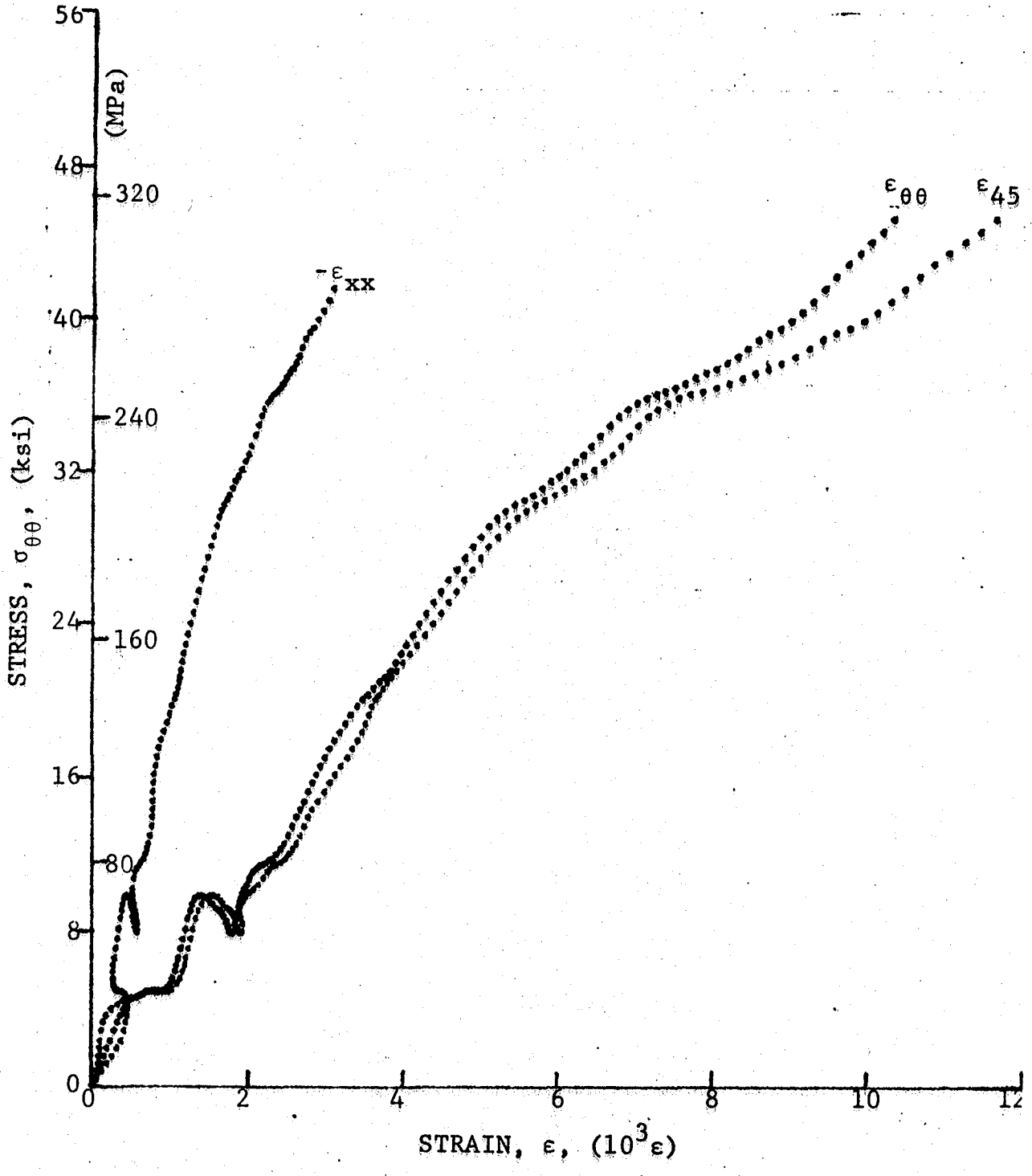

Figure 3-11. Stress-strain curves for dynamically loaded $[22.5_8]$ 80AS/20S/PR288 graphite/S-glass/epoxy ring, Specimen No. 47-8.

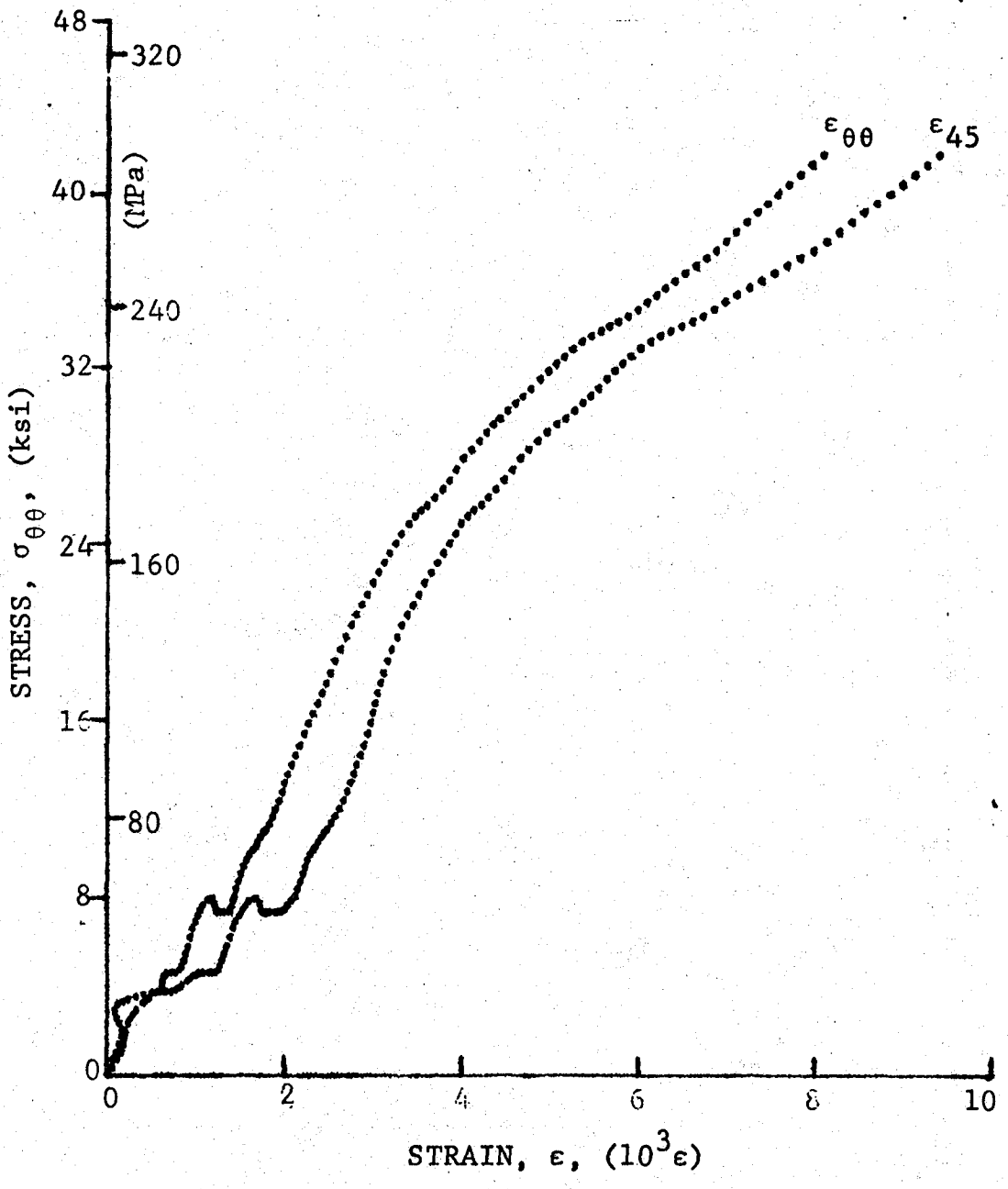

Figure 3-12. Stress-strain curves for dynamically loaded $[22.5_8]$ 80AS/20S/PR288 graphite/S-glass/epoxy ring, Specimen No. 47-9.

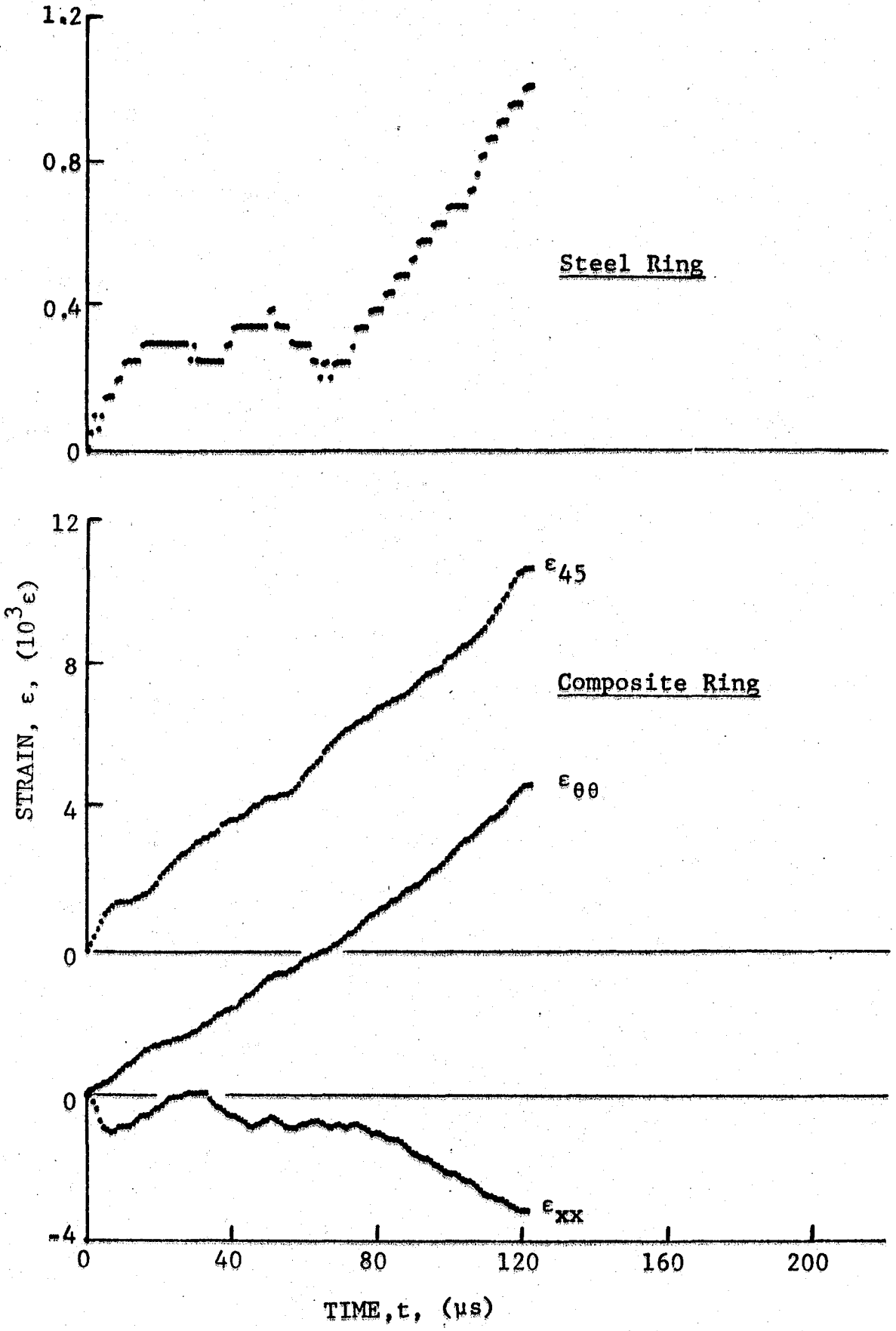

Figure 3-13. Strain records in steel ring and [30_8] SP288/AS graphite/epoxy ring under dynamic loading for Specimen No. 48-7 (650 mg pistol powder).

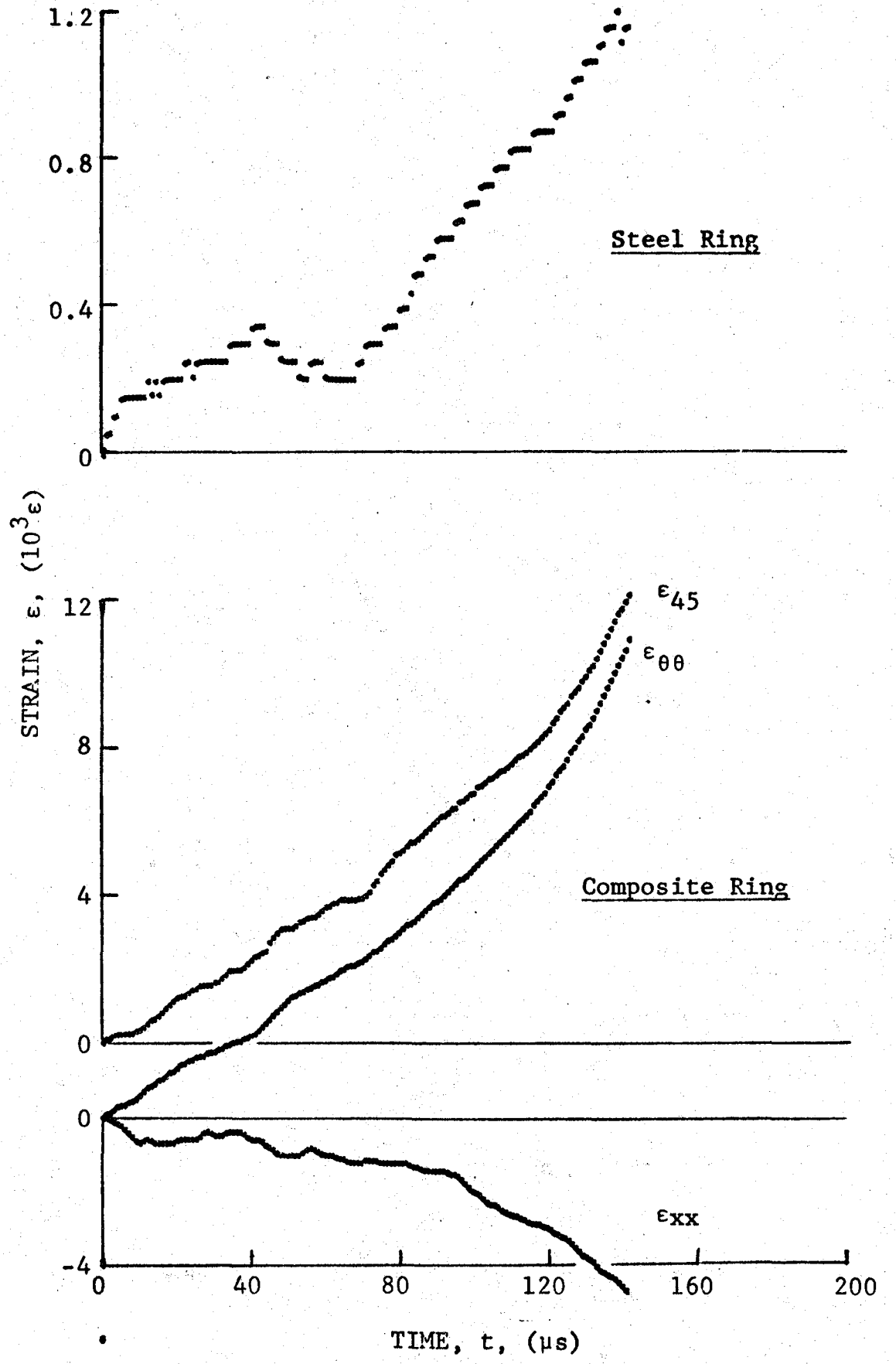

Figure 3-14. Strain records in steel ring and [30_8] SP288/AS graphite/epoxy ring under dynamic loading for Specimen No. 48-8 (650 mg pistol powder).

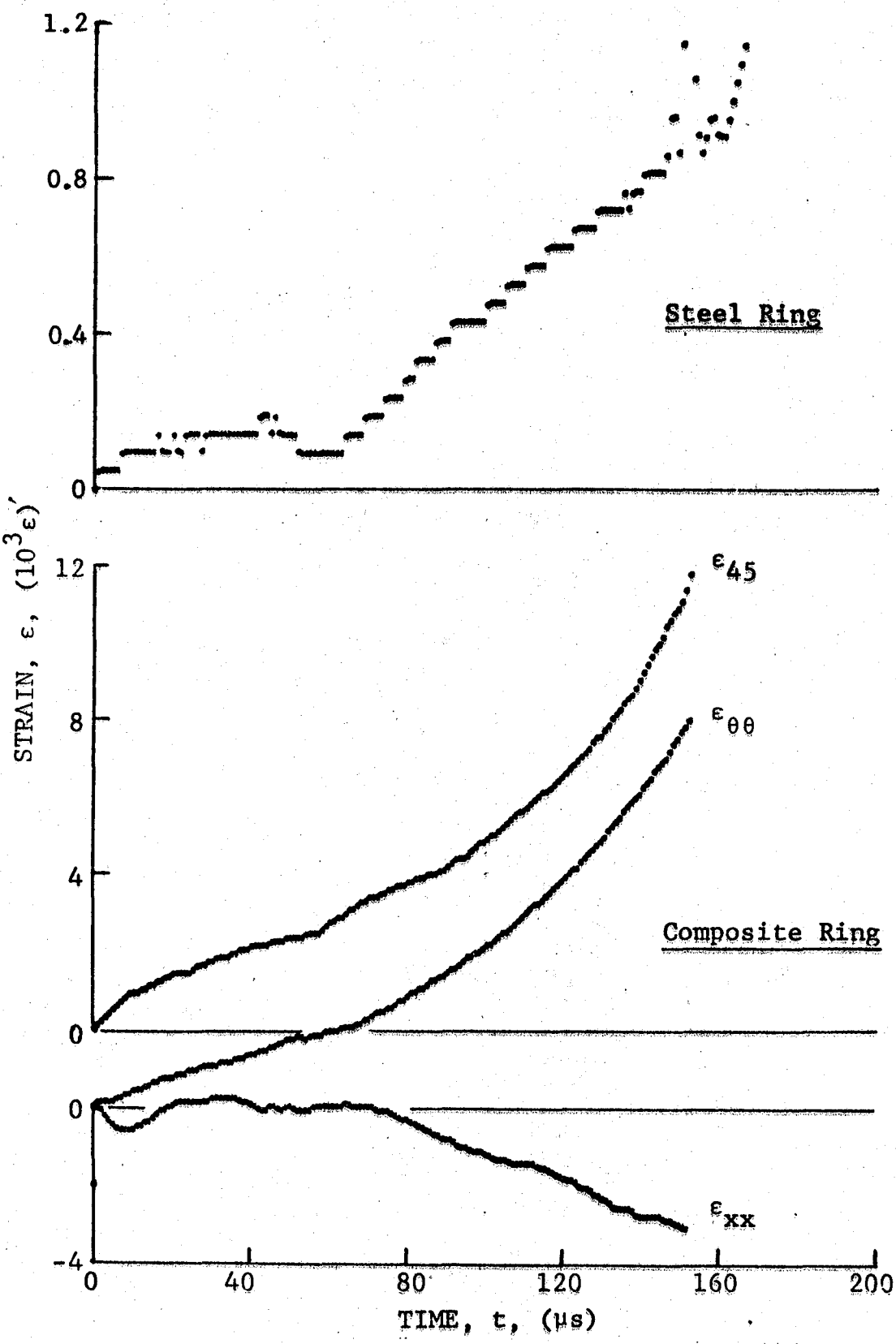

Figure 3-15. Strain records in steel ring and $[30_8]$ SP288/AS graphite/epoxy ring under dynamic loading for Specimen No. 48-9 (650 mg pistol powder).

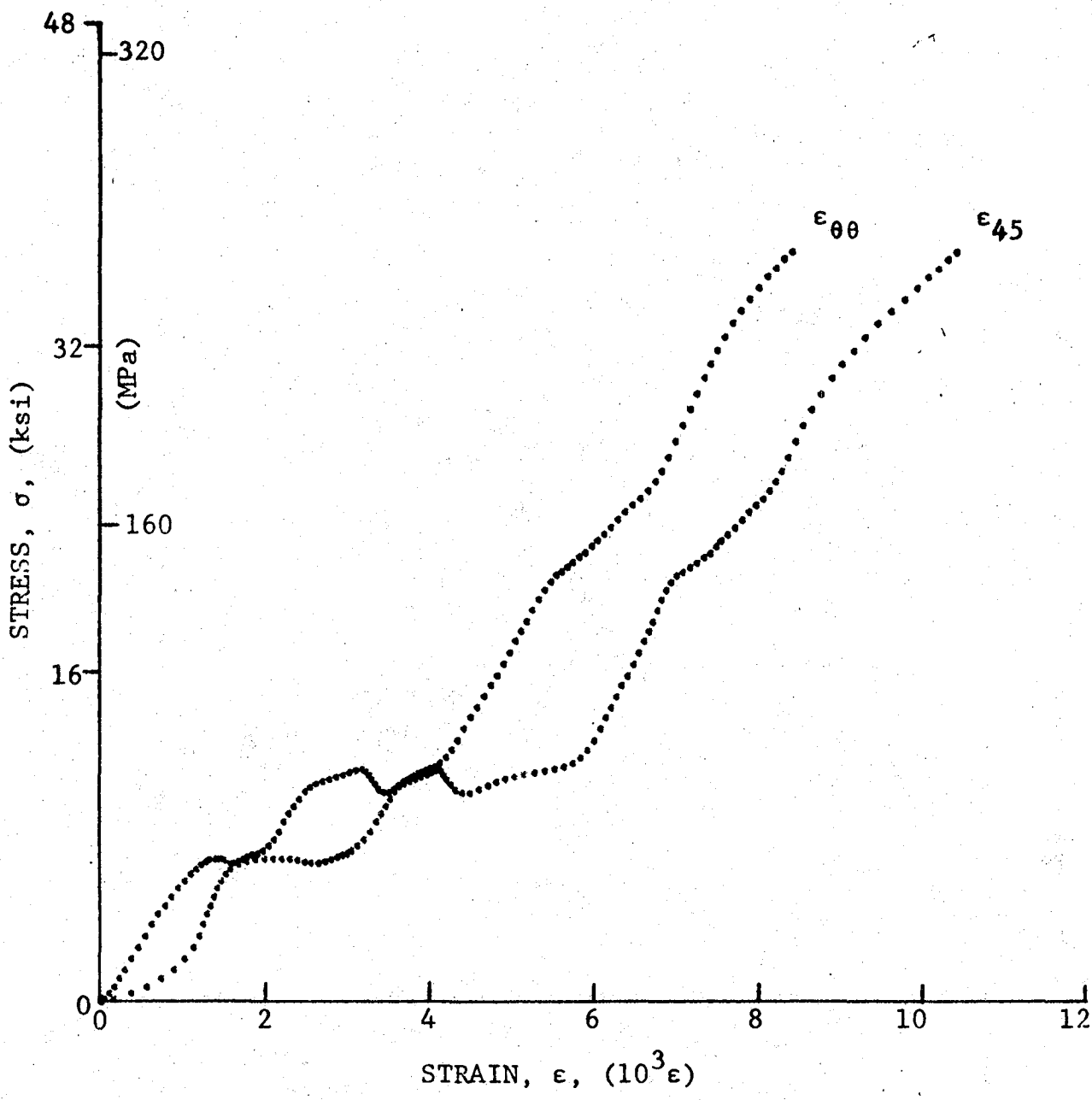

Figure 3-16. Stress-strain curves for dynamically loaded $[30_8]$ SP288/AS graphite/epoxy ring, Specimen No. 48-7.

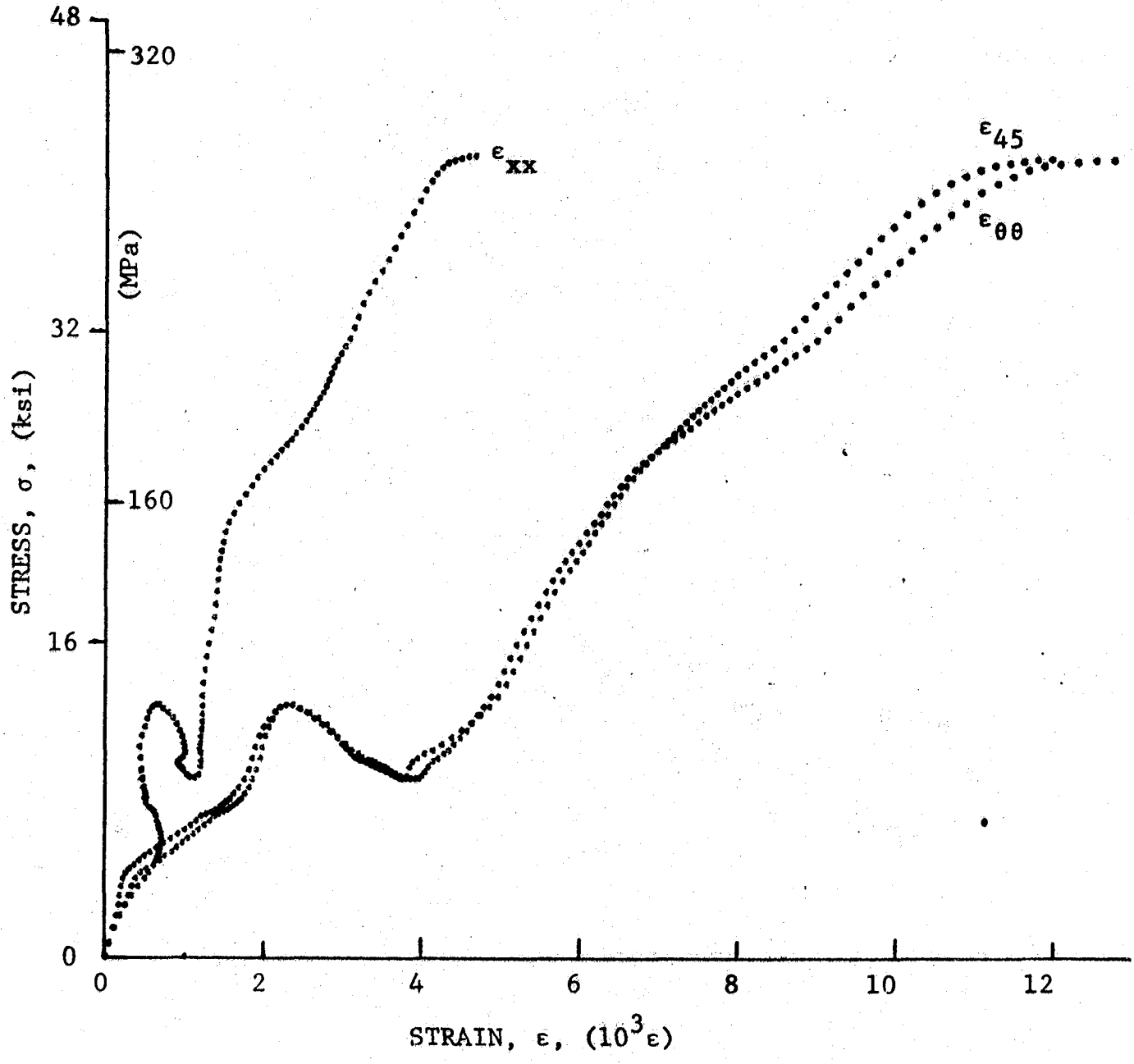

Figure 3-17. Stress-strain curves for dynamically loaded $[30_8]$ SP288/AS graphite/epoxy ring, Specimen No. 48-8.

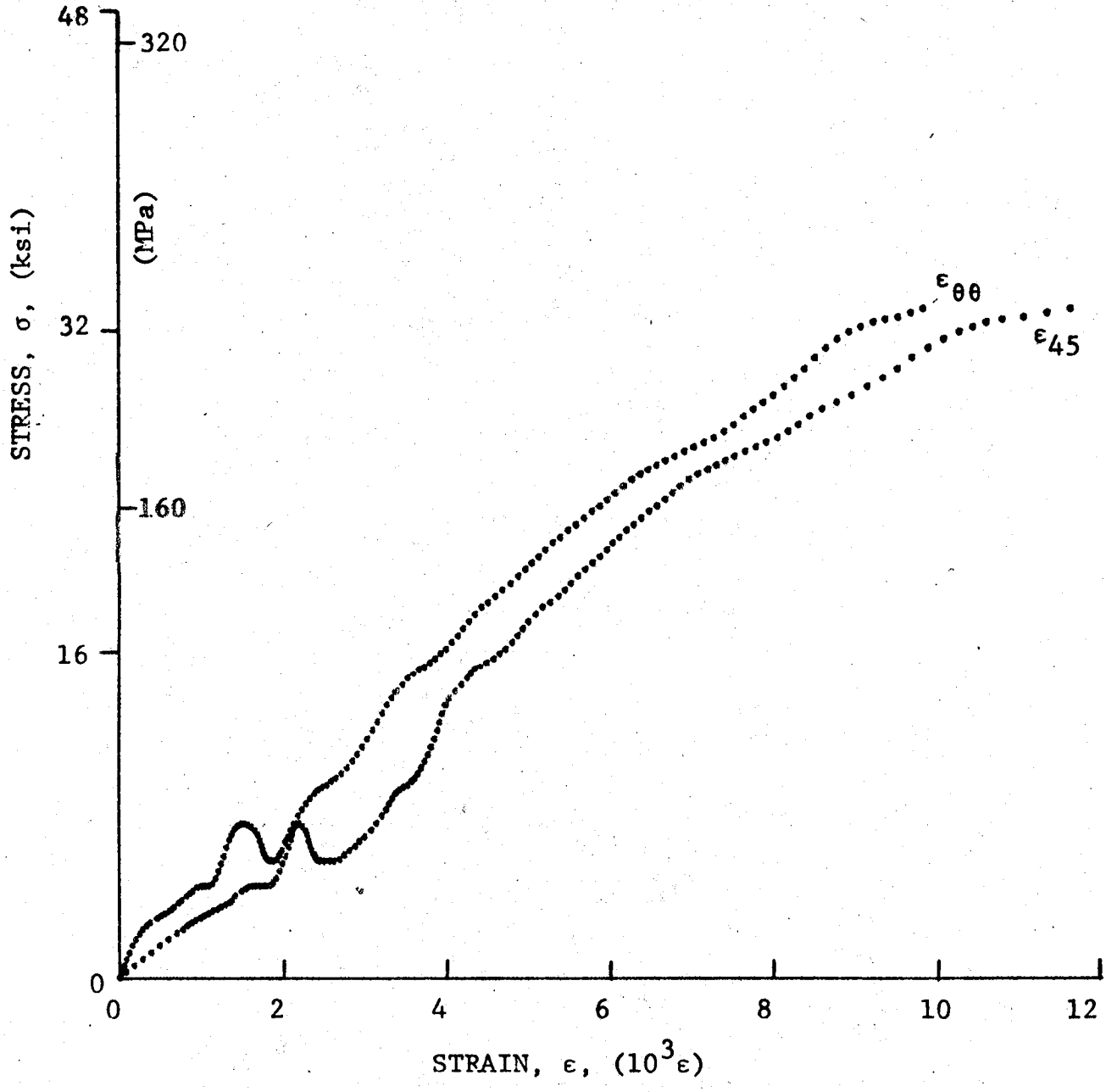

Figure 3-18. Stress-strain curves for dvnamically loaded $[30_8]$ SP288/AS graphite/epoxy ring, Specimen No. 48-9.

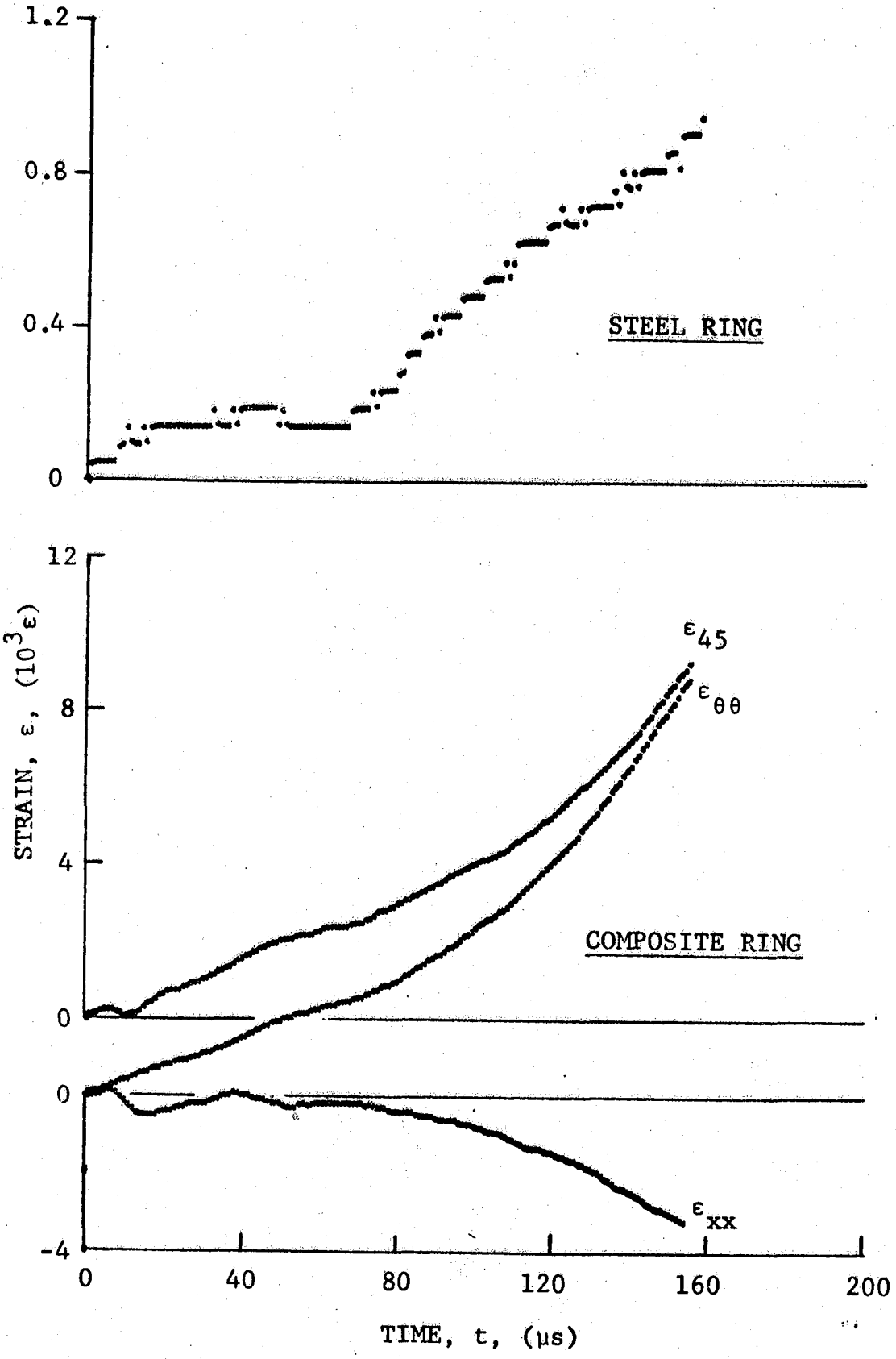

Figure 3-19. Strain records in steel ring and [30_8] 80AS/20S/PR288 graphite/S-glass/epoxy ring under dynamic loading for Specimen No. 49-8 (650 mg pistol powder).

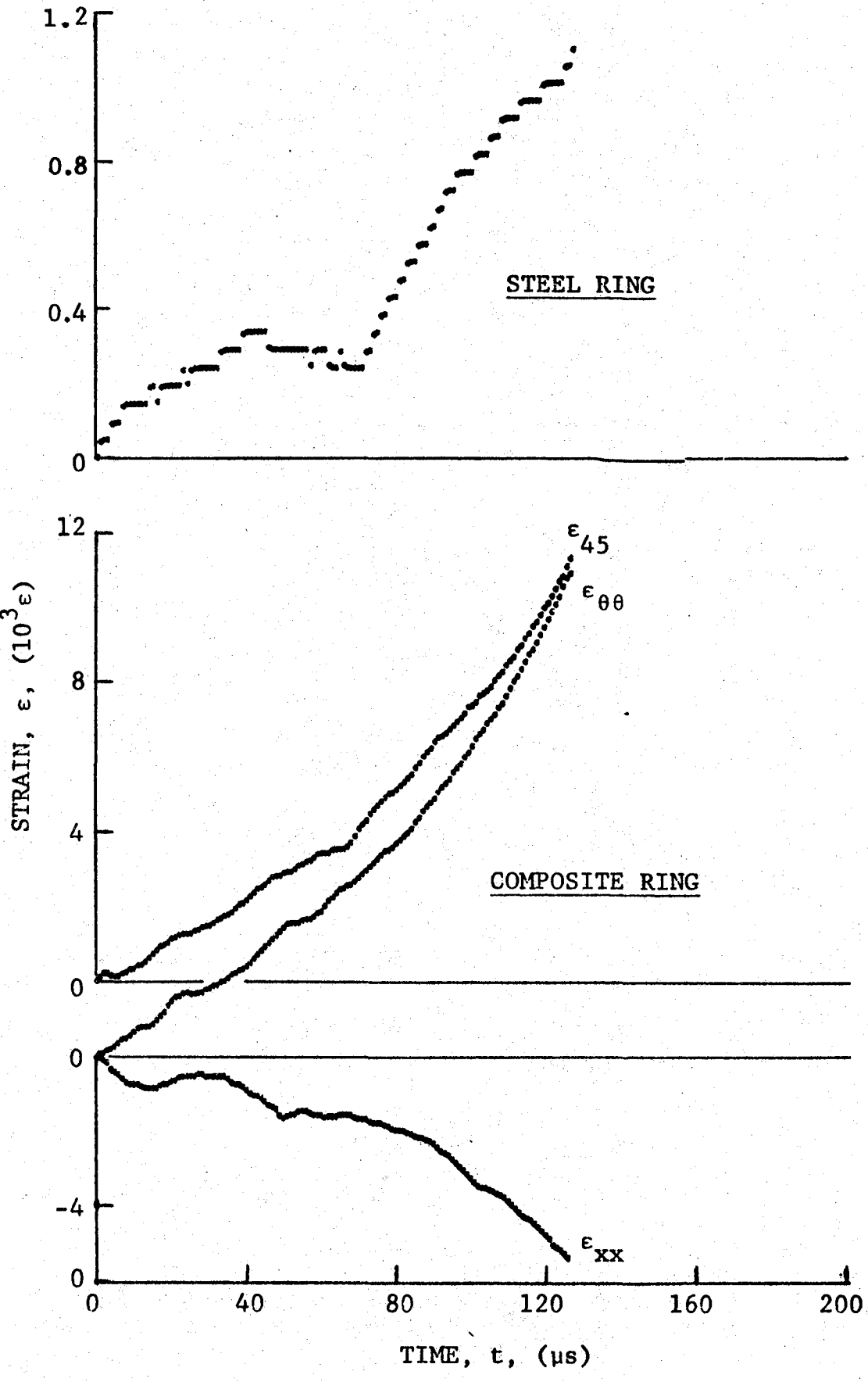

Figure 3-20. Strain records in steel ring and [30_8] 80AS/20S/PR288 graphite/S-glass/epoxy ring under dynamic loading for Specimen No. 49-9 (650 mg pistol powder).

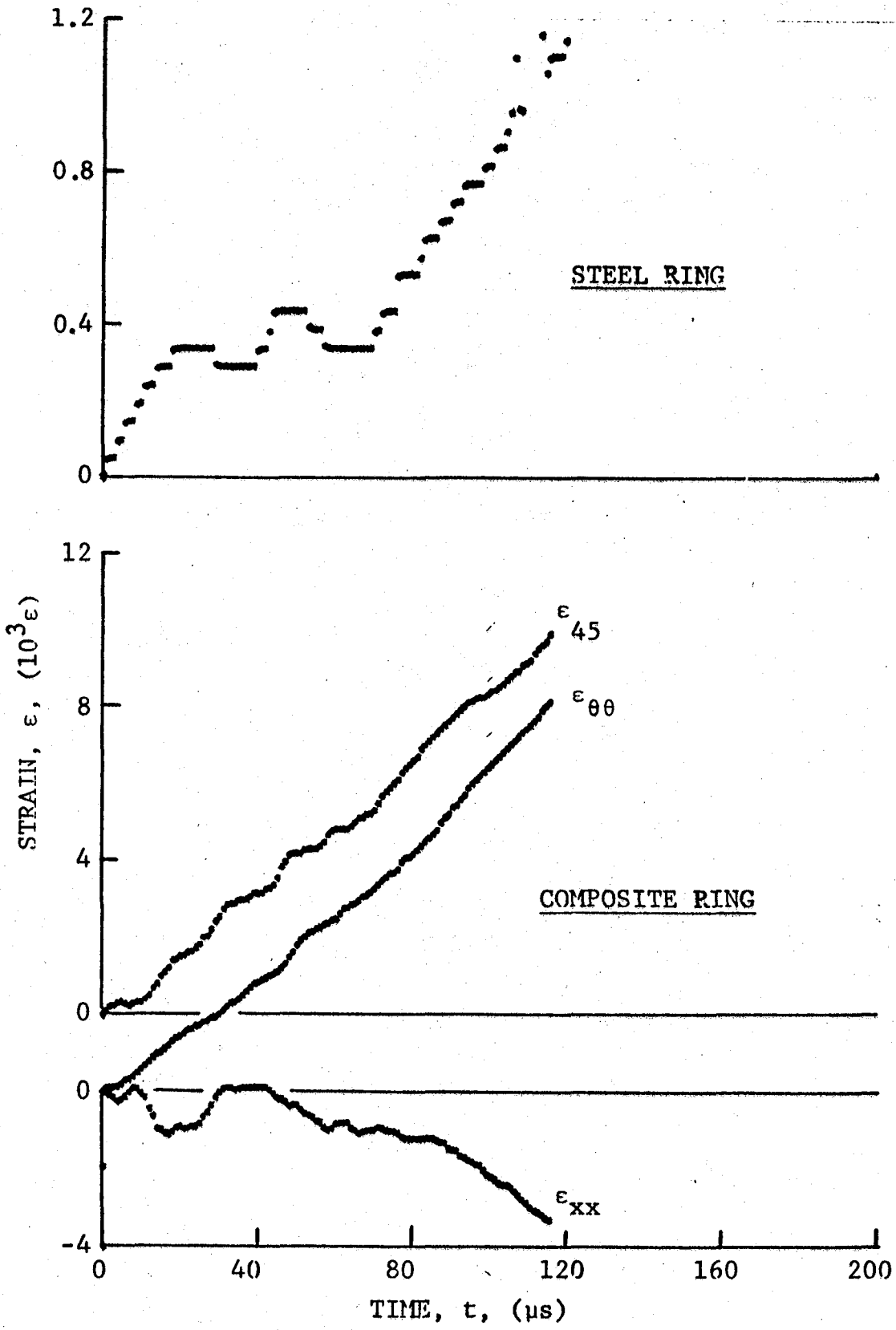

Figure 3-21. Strain records in steel ring and [30_8] 80AS/20S/PR288 graphite/S-glass/epoxy ring under dynamic loading for Specimen No. 49-10 (650 mg pistol powder).

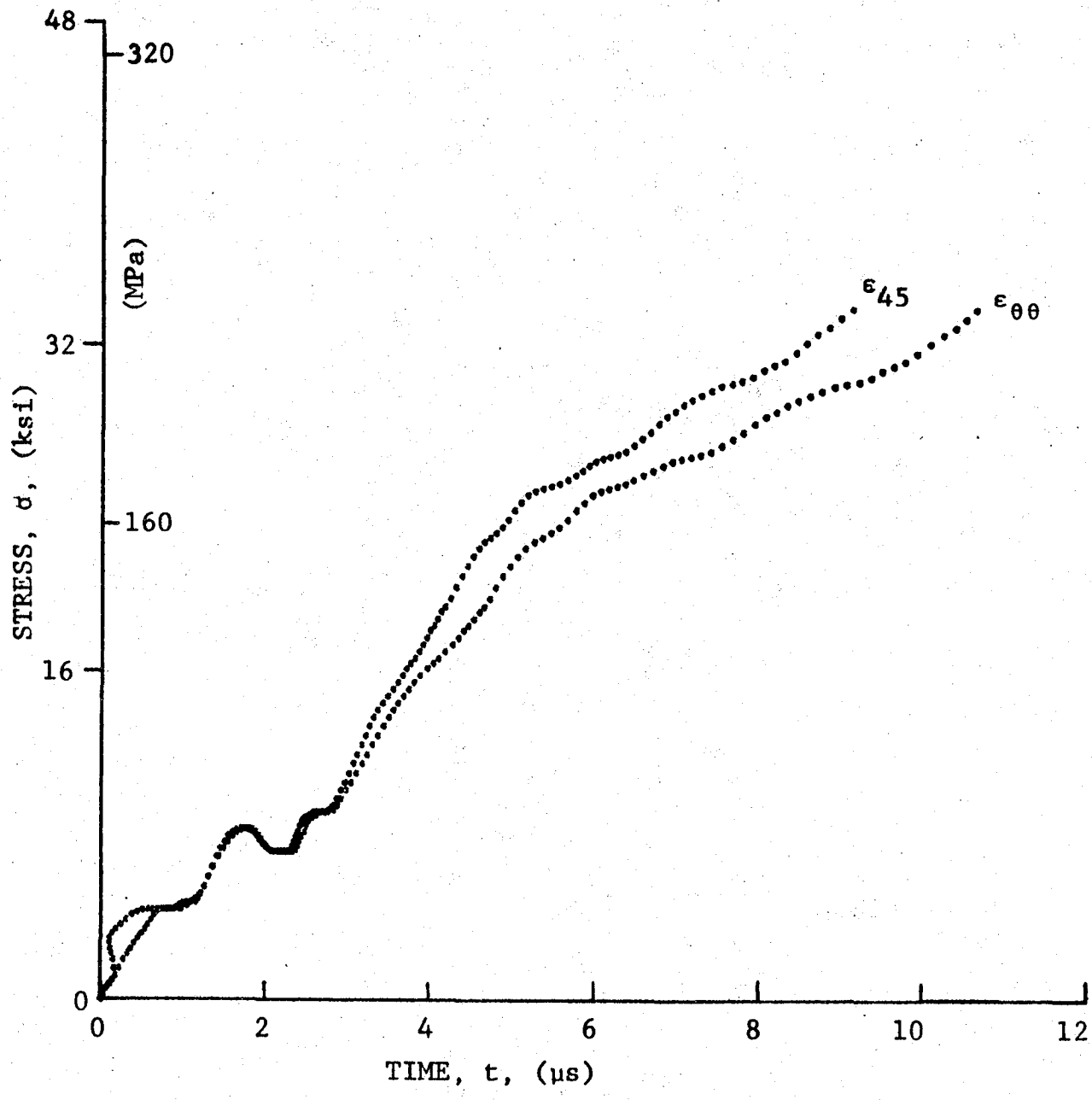

Figure 3-22. Stress-strain curves for dynamically loaded $[30_8]$ 80AS/20S/PR288 graphite/S-glass/epoxy ring, Specimen No. 49-8.

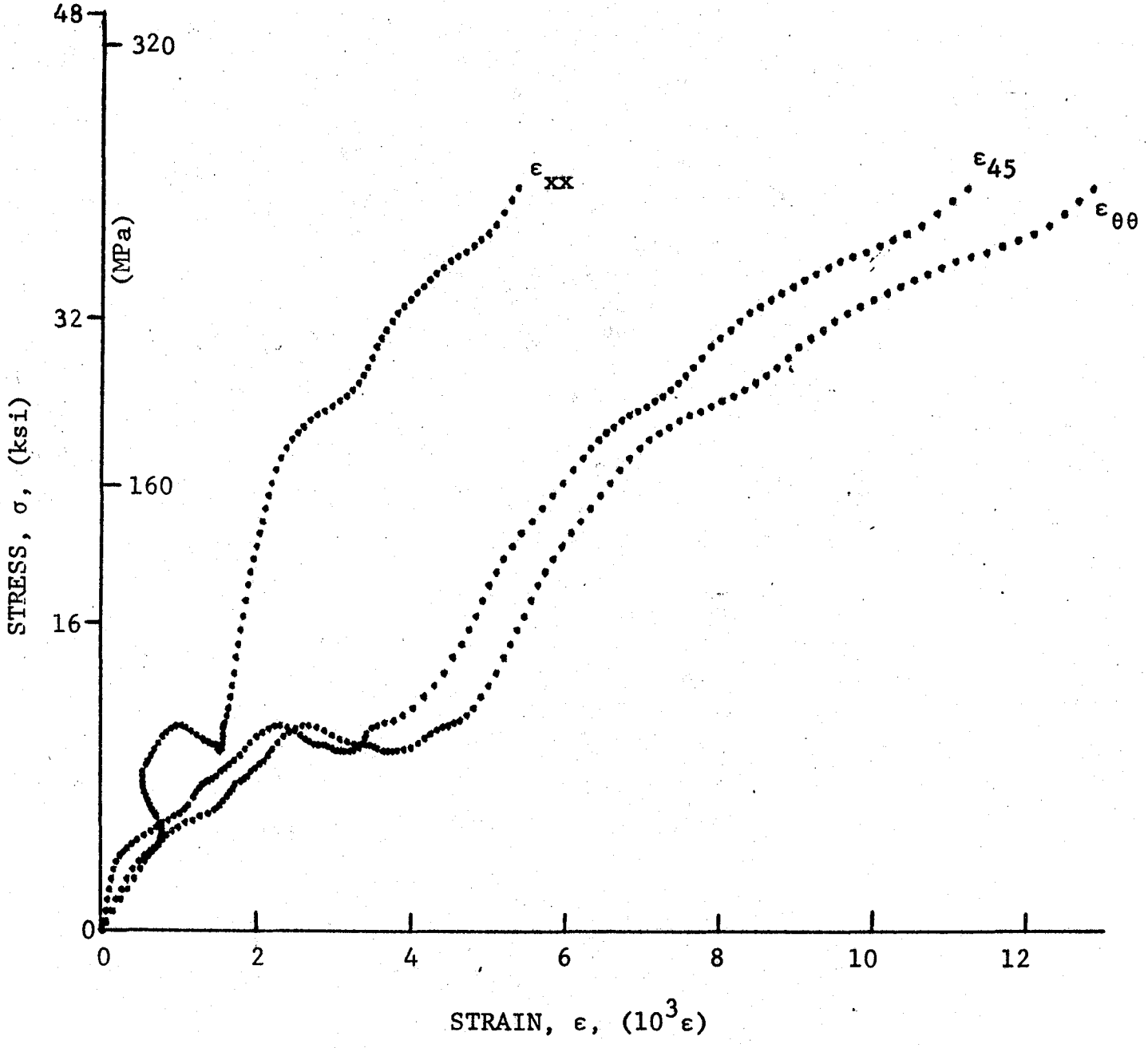

Figure 3-23. Stress-strain curves for dynamically loaded $[30_8]$ 80AS/20S/PR288 graphite/S-glass/epoxy ring for Specimen No. 49-9.

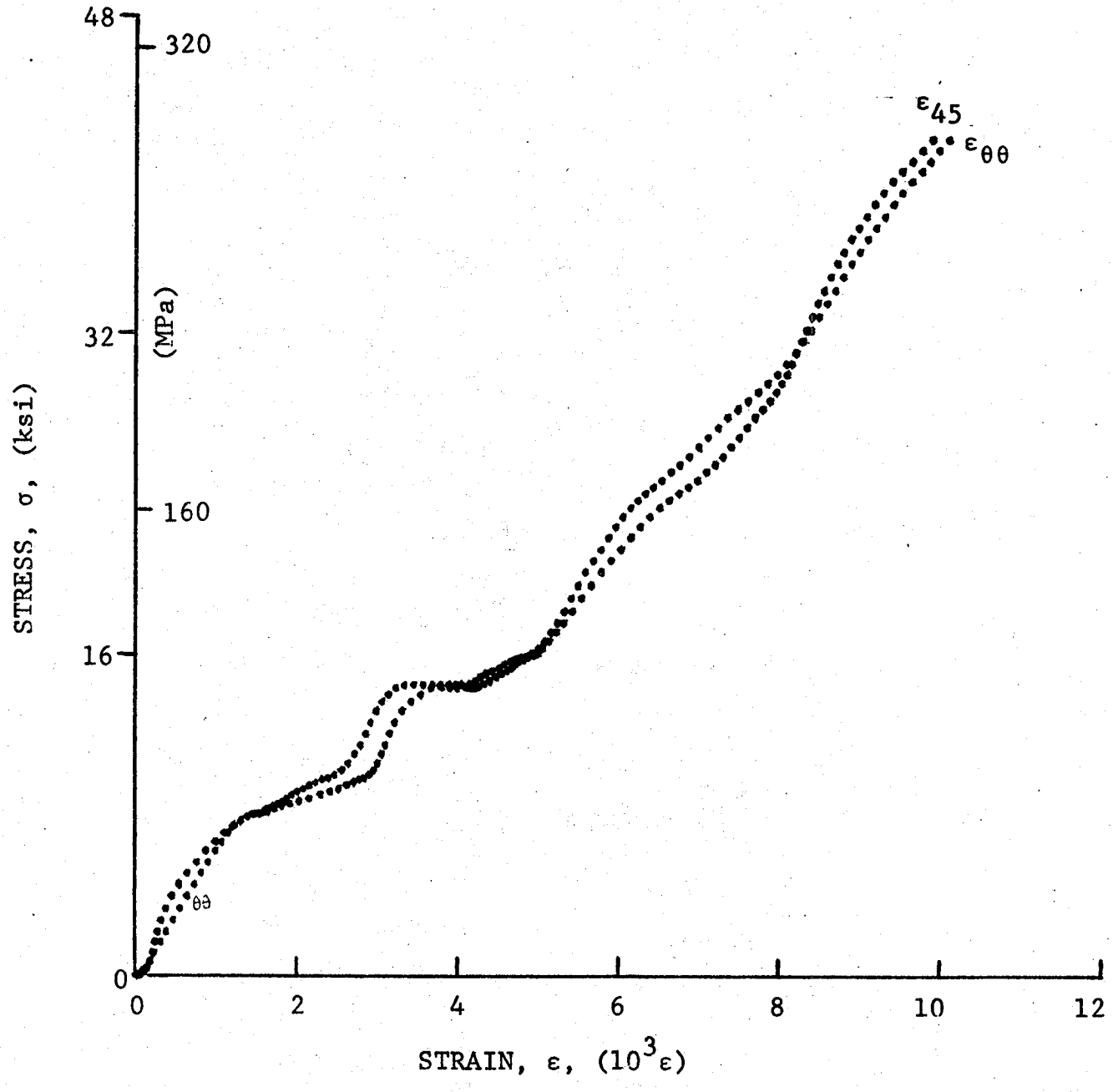

Figure 3-24. Stress-strain curves for dynamically loaded [30_8] 80AS/20S/PR288 graphite/epoxy ring for Specimen No. 49-10.

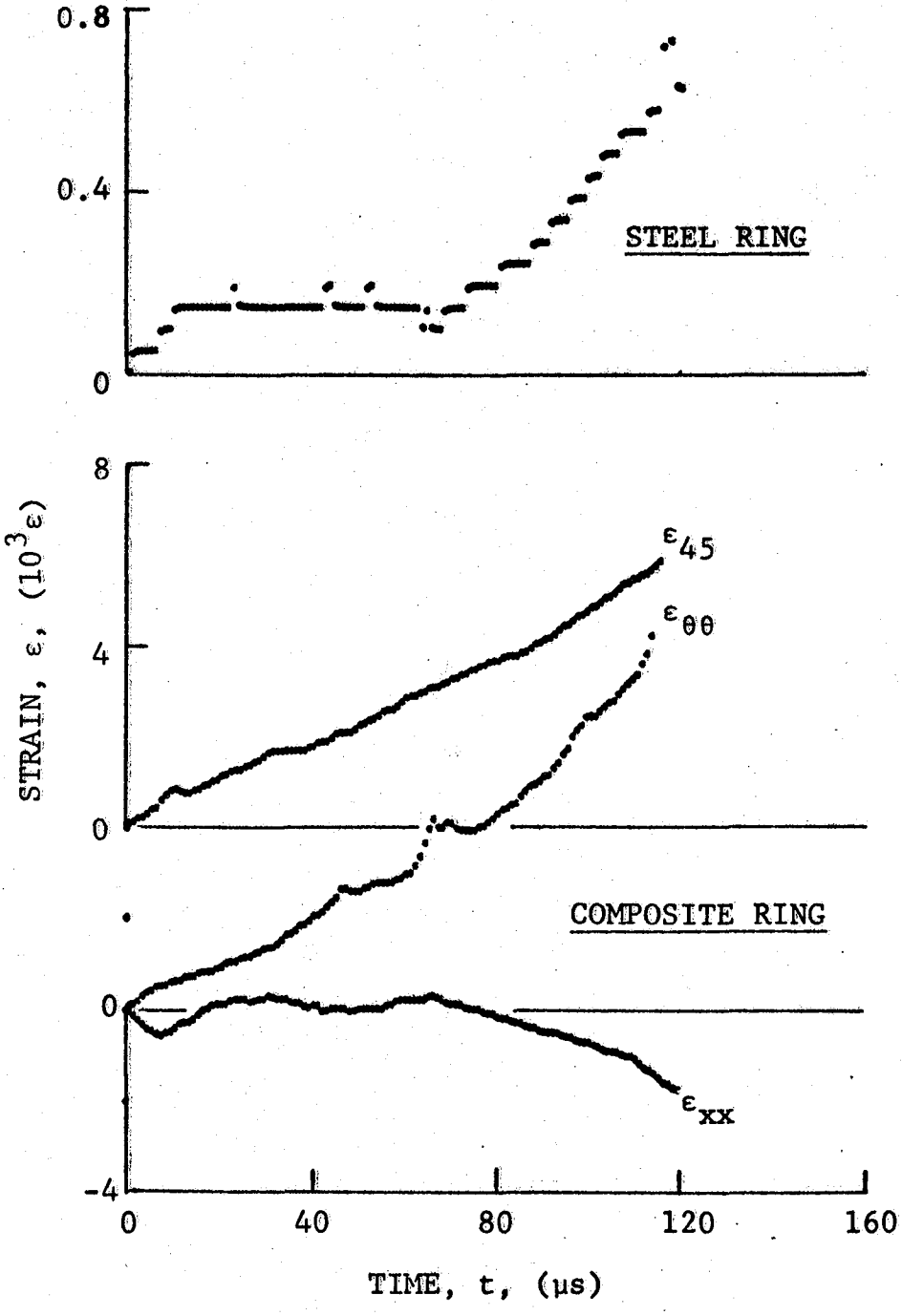

Figure 3-25. Strain records in steel ring and [45_8] SP288/AS graphite/epoxy ring under dynamic loading for Specimen No. 50-8 (650 mg pistol powder).

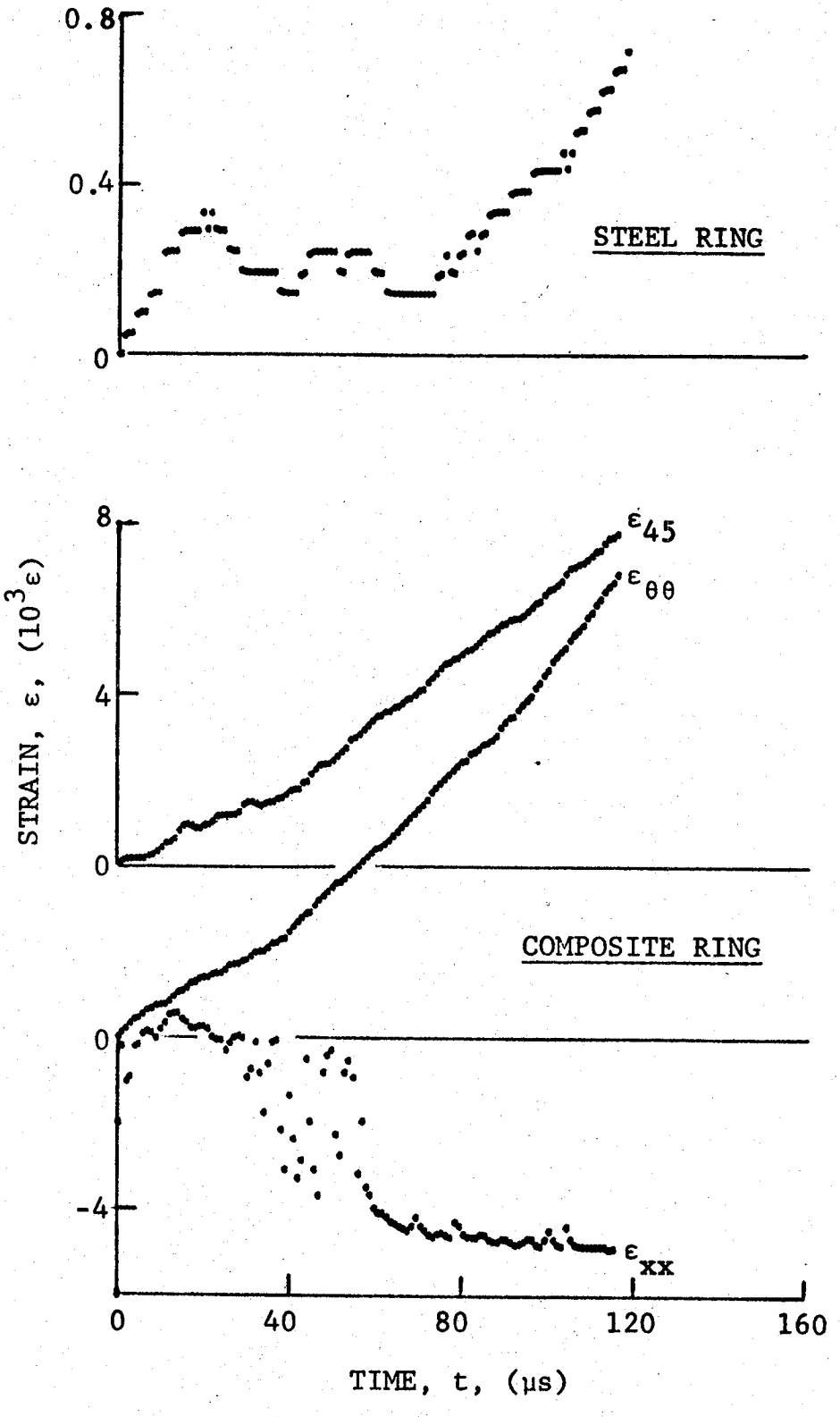

Figure 3-26. Strain records in steel ring and [45_8] SP288/AS graphite/epoxy ring under dynamic loading for Specimen No. 50-9 (650 mg pistol powder).

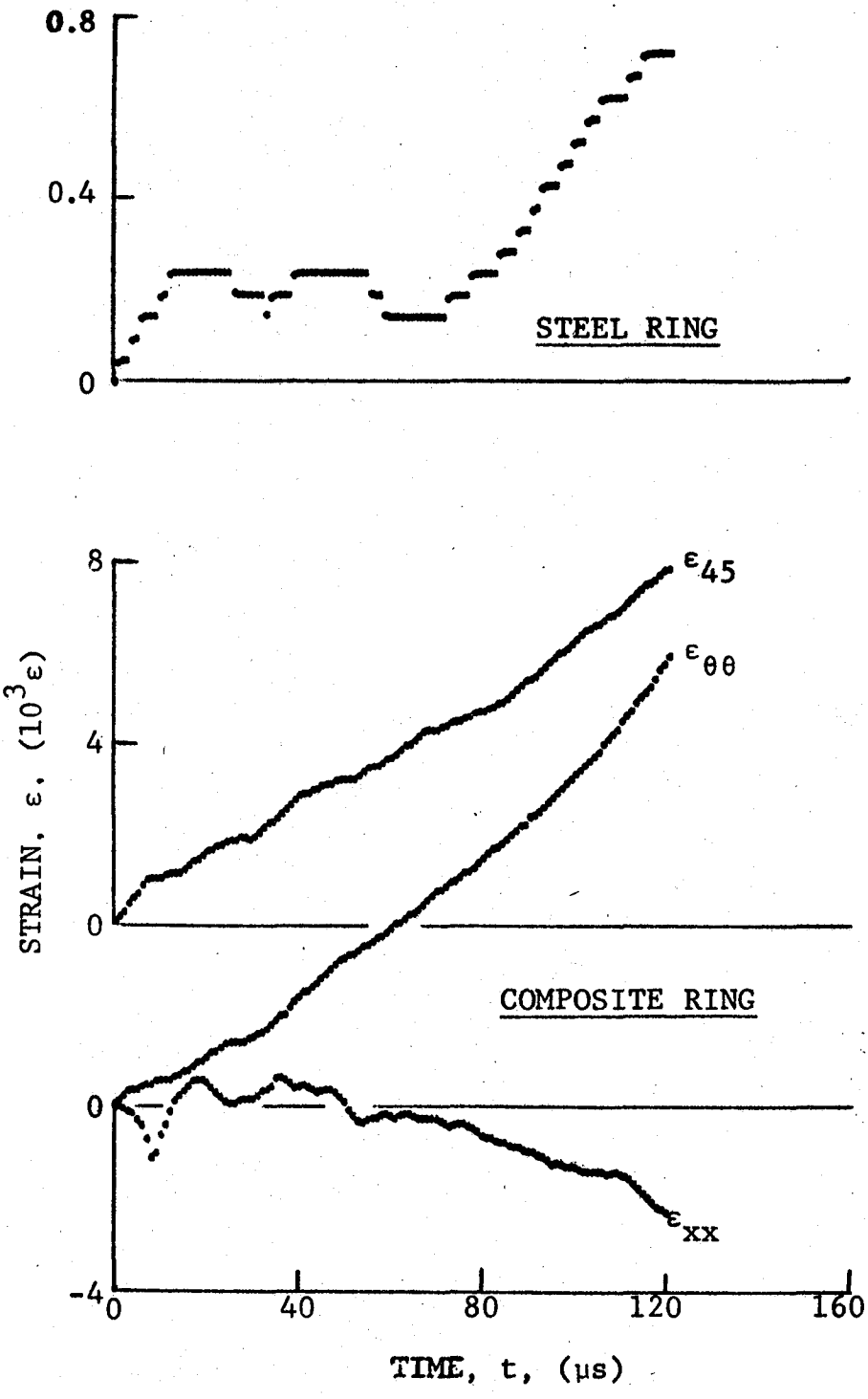

Figure 3-27. Strain records in steel ring and $[45_8]$ SP288/AS graphite/epoxy ring under dynamic loading for Specimen No. 50-10 (650 mg pistol powder).

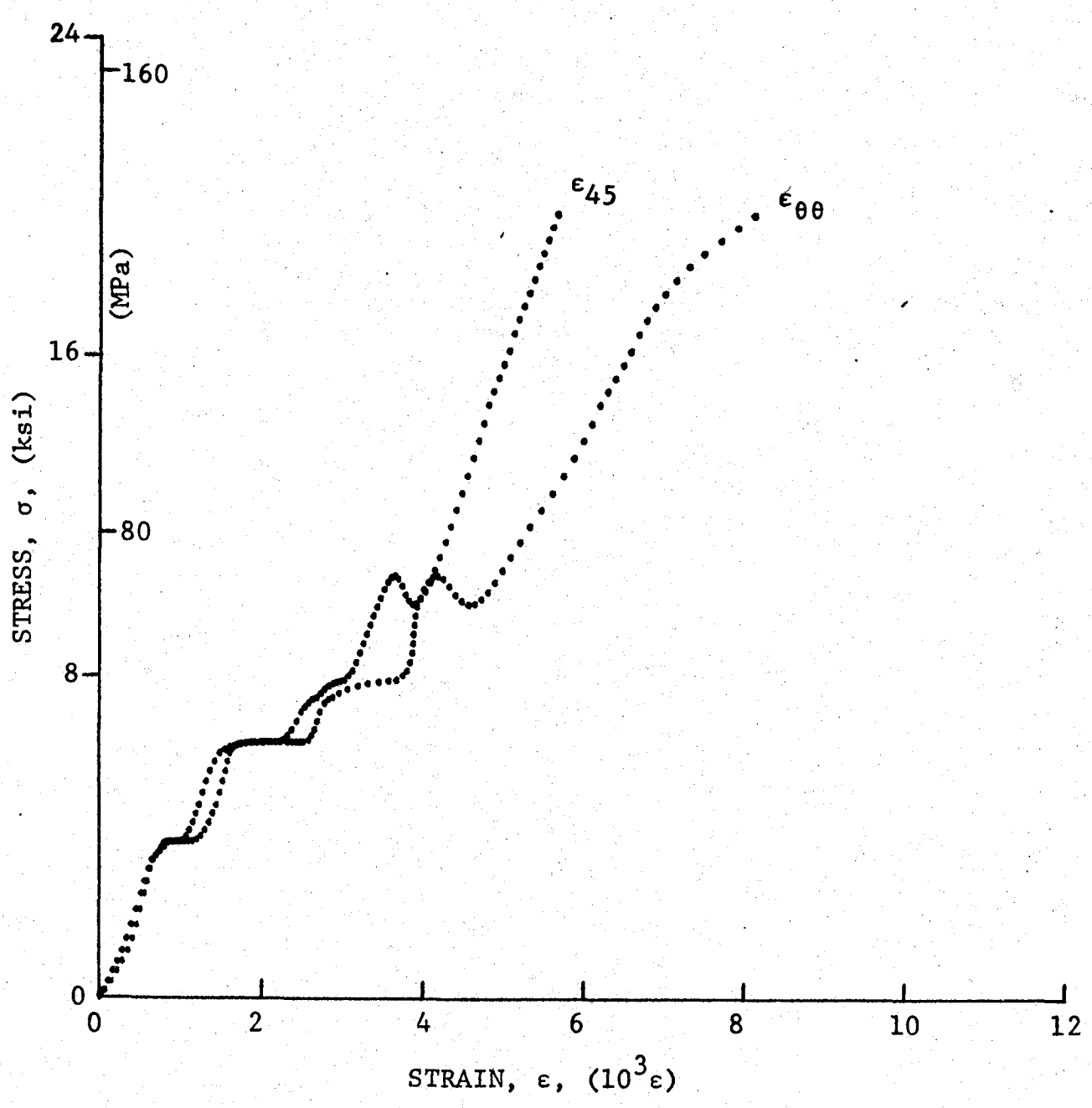

Figure 3-28. Stress-strain curves for dynamically loaded [45_8] SP288/AS graphite/epoxy ring, Specimen No. 50-8.

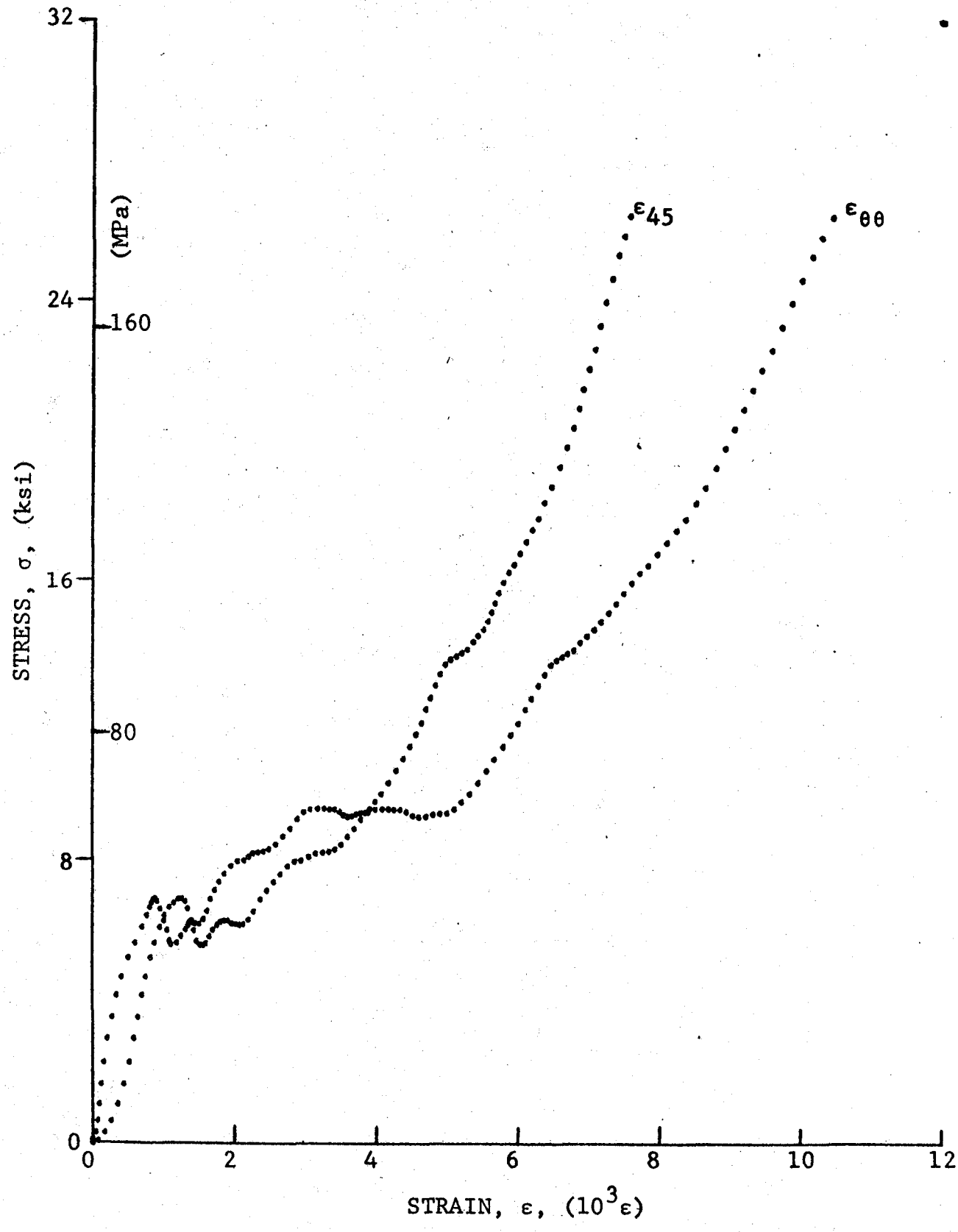

Figure 3-29. Stress-strain curves for dynamically loaded $[45_8]$ SP288/AS graphite/epoxy ring, Specimen No. 50-9.

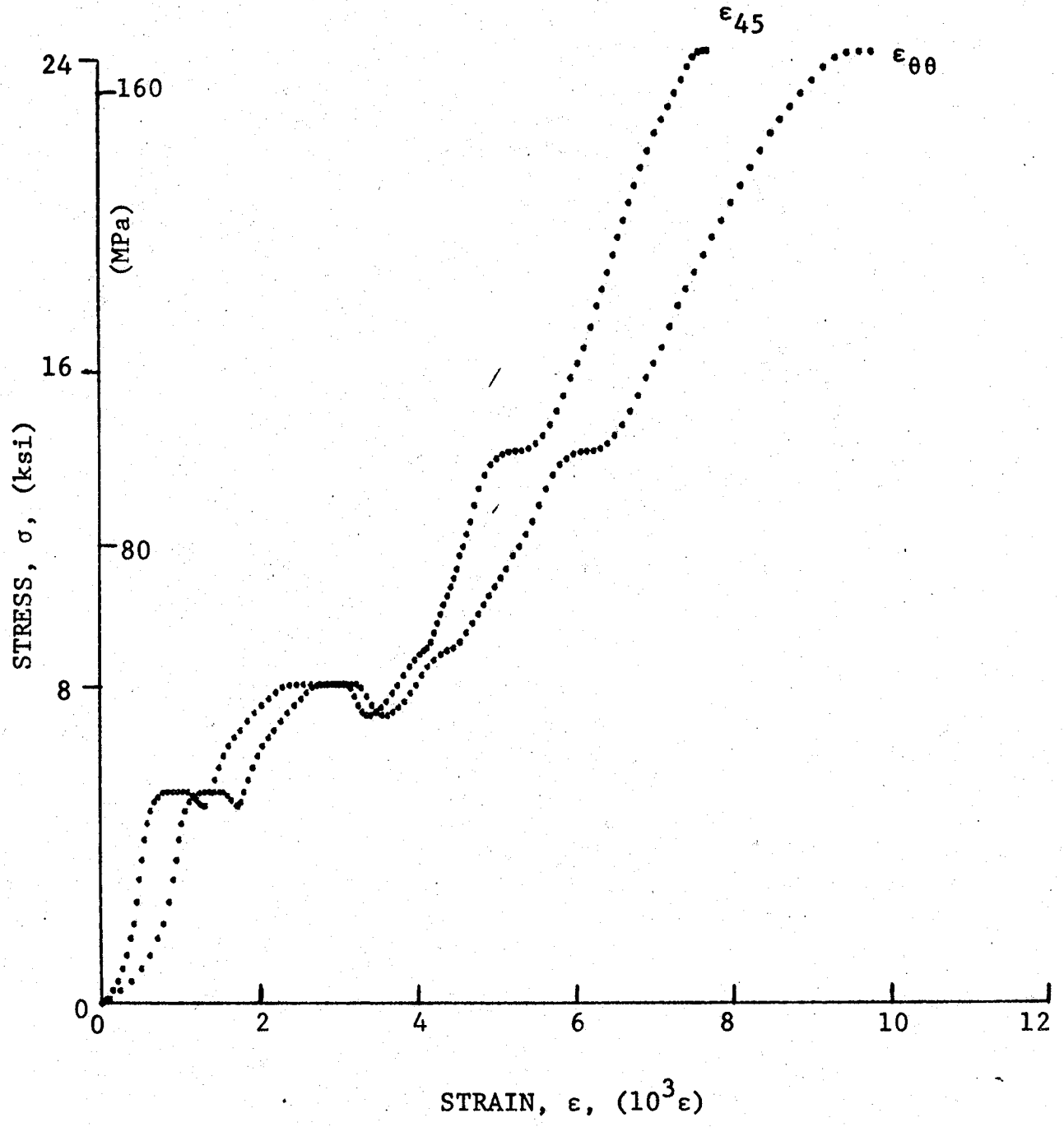

Figure 3-30. Stress-strain curves for dynamically loaded [45$_8$] SP288/AS graphite/epoxy ring, Specimen No. 50-10.

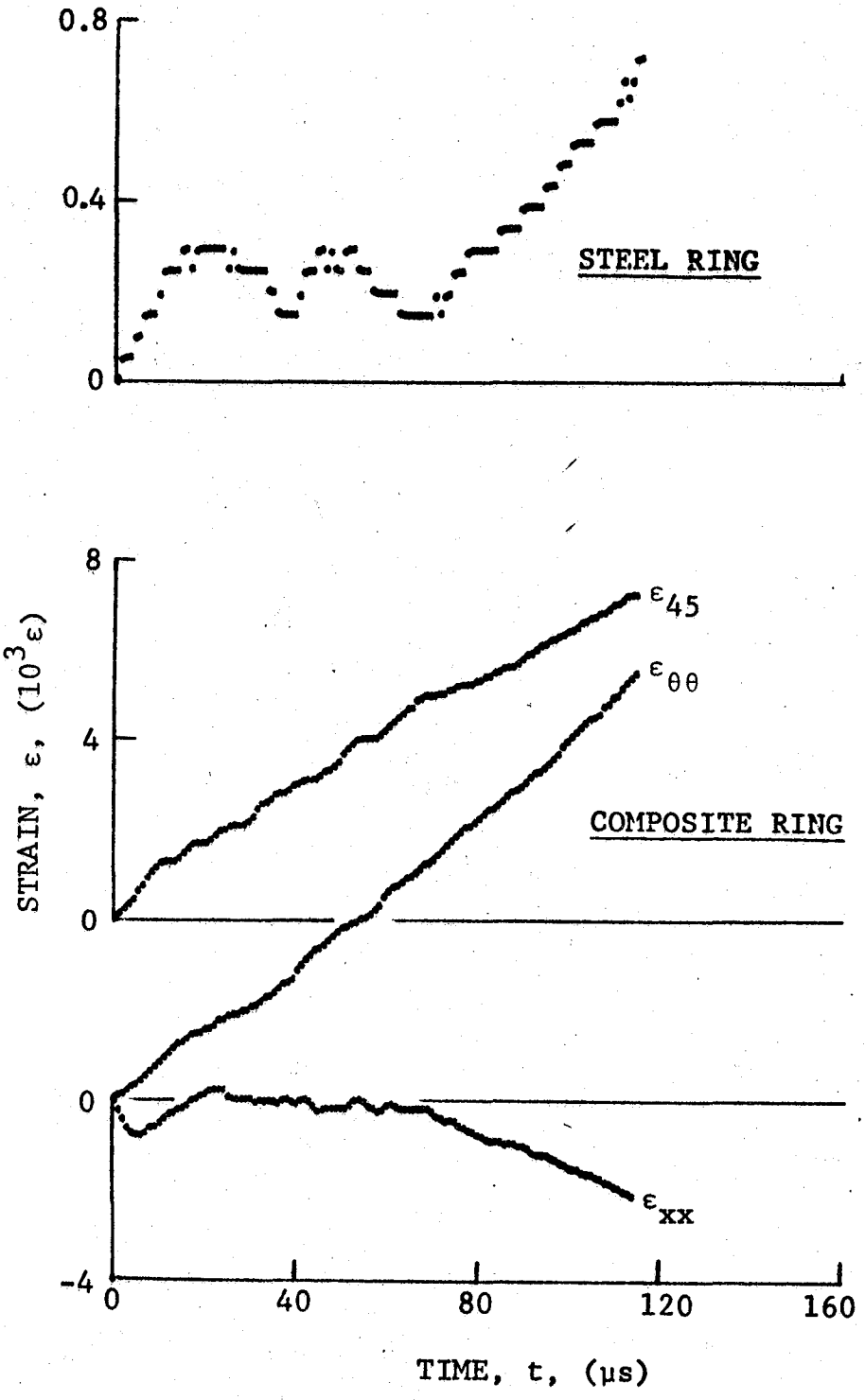

Figure 3-31. Strain records in steel ring and [45_8] 80AS/20S/PR288 graphite/S-glass/epoxy ring under dynamic loading for Specimen No. 51-7 (650 mg pistol powder).

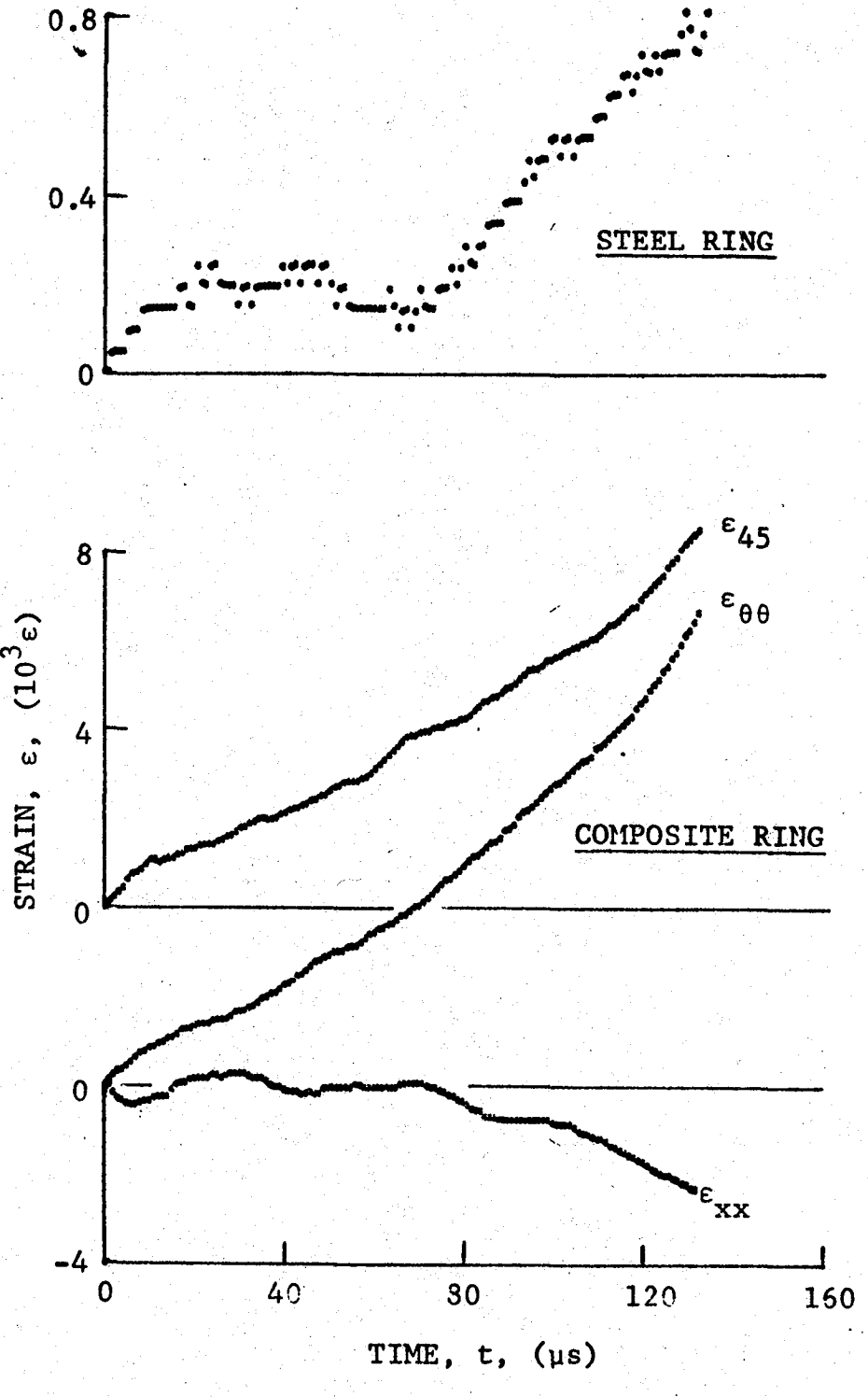

Figure 3-32. Strain records in steel ring and $[45_8]$ 80AS/20S/PR288 graphite/S-glass/epoxy ring under dynamic loading for Specimen No. 51-8 (650 mg pistol powder).

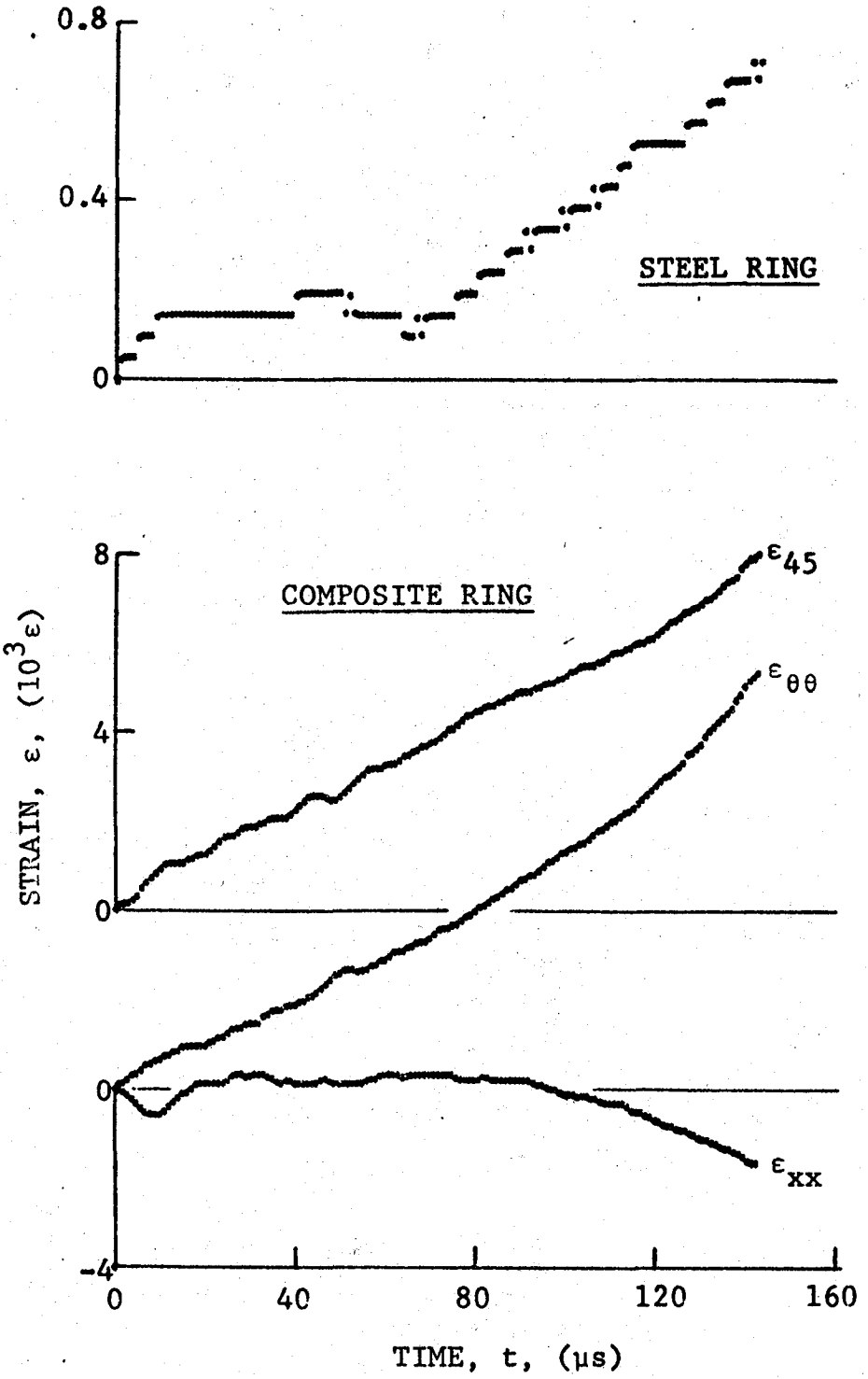

Figure 3-33. Strain records in steel ring and [45_8] 80AS/20S/PR288 graphite/S-glass/epoxy ring under dynamic loading for Specimen No. 51-9 (650 mg pistol powder).

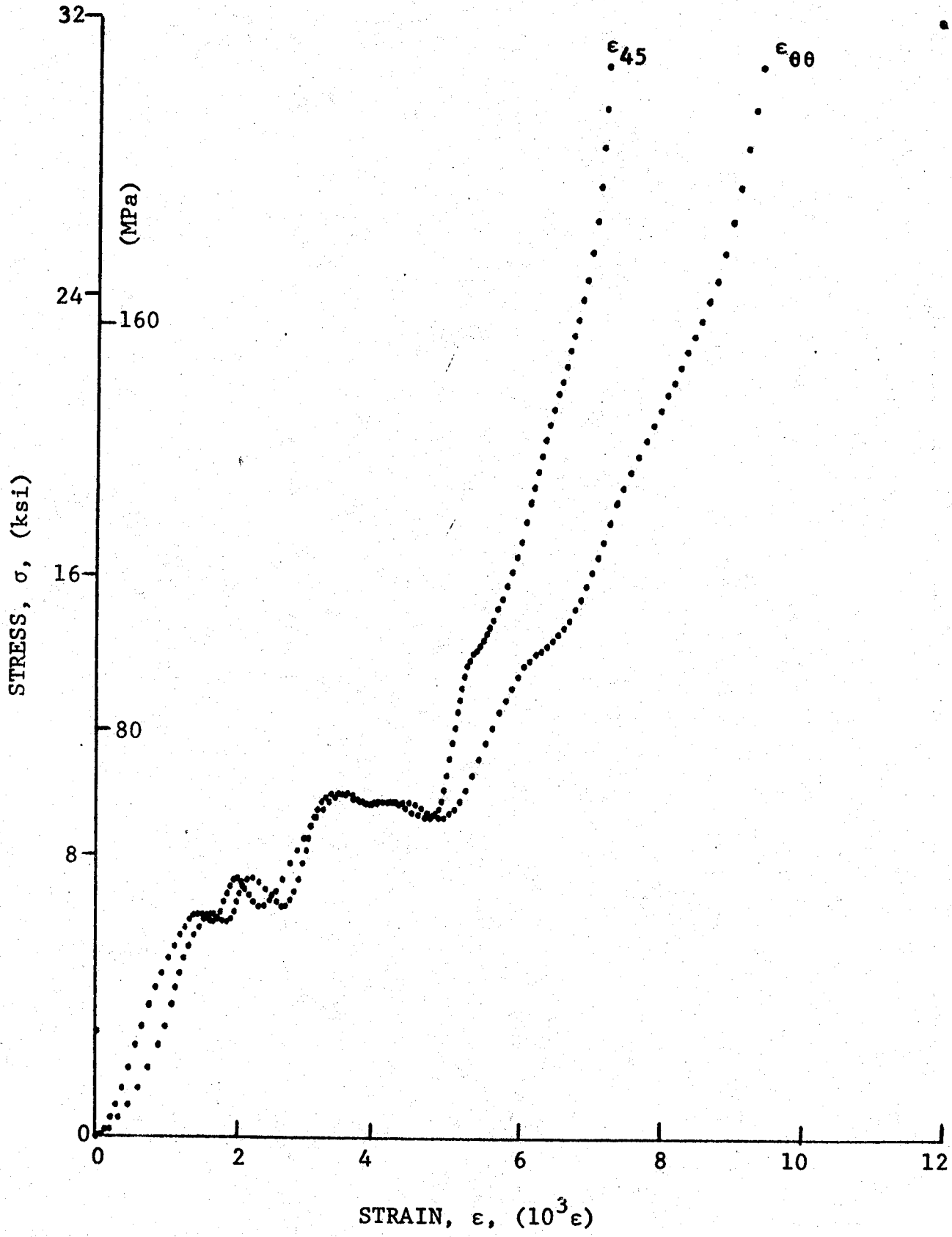

Figure 3-34. Stress-strain curves for dynamically loaded $[45_8]$ 80AS/20S/PR288 graphite/S-glass/epoxy ring, Specimen No. 51-7.

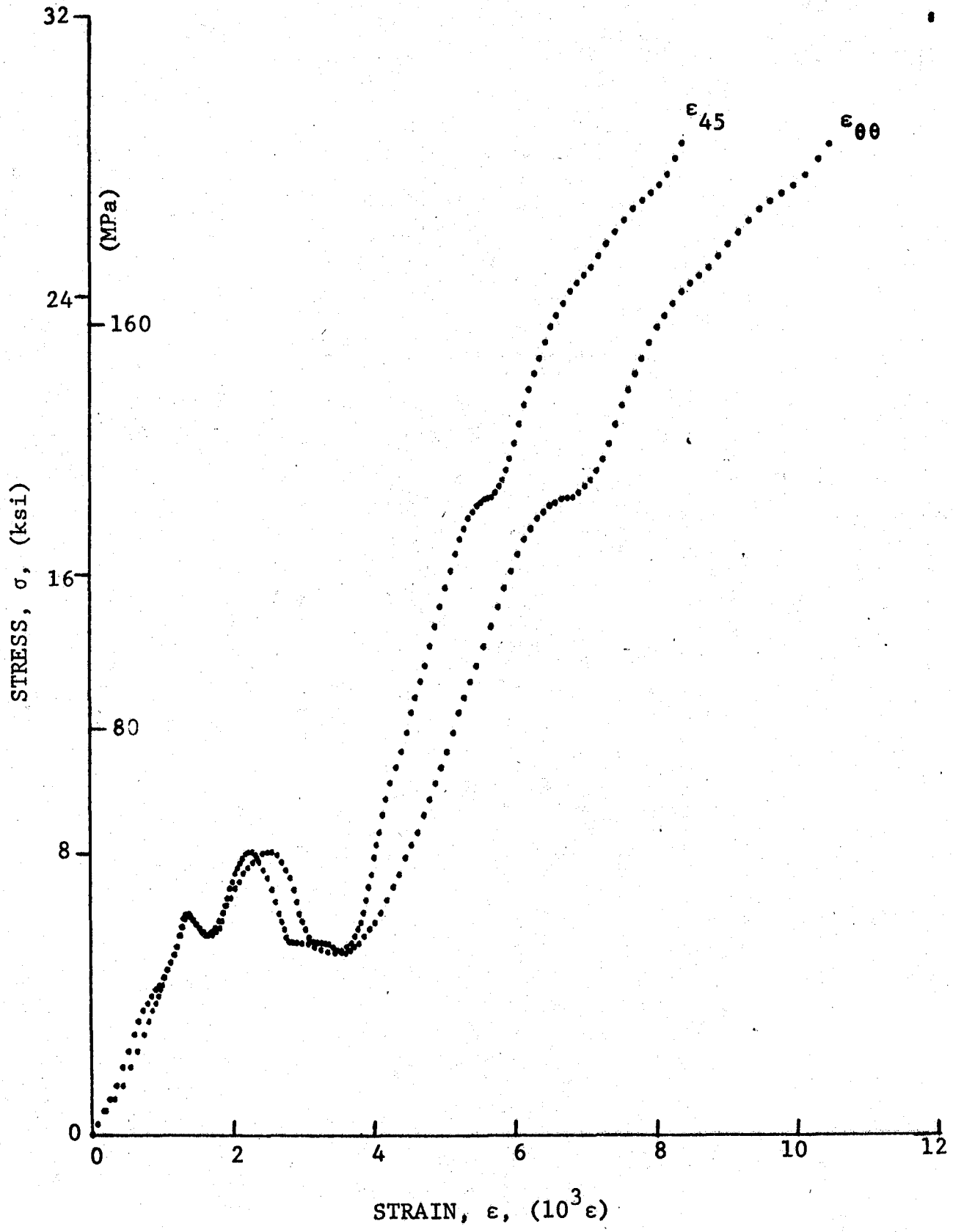

Figure 3-35. Stress-strain curves for dynamically loaded $[45_8]$ 80AS/20S/PR288 graphite/S-glass/epoxy ring, Specimen No. 51-8.

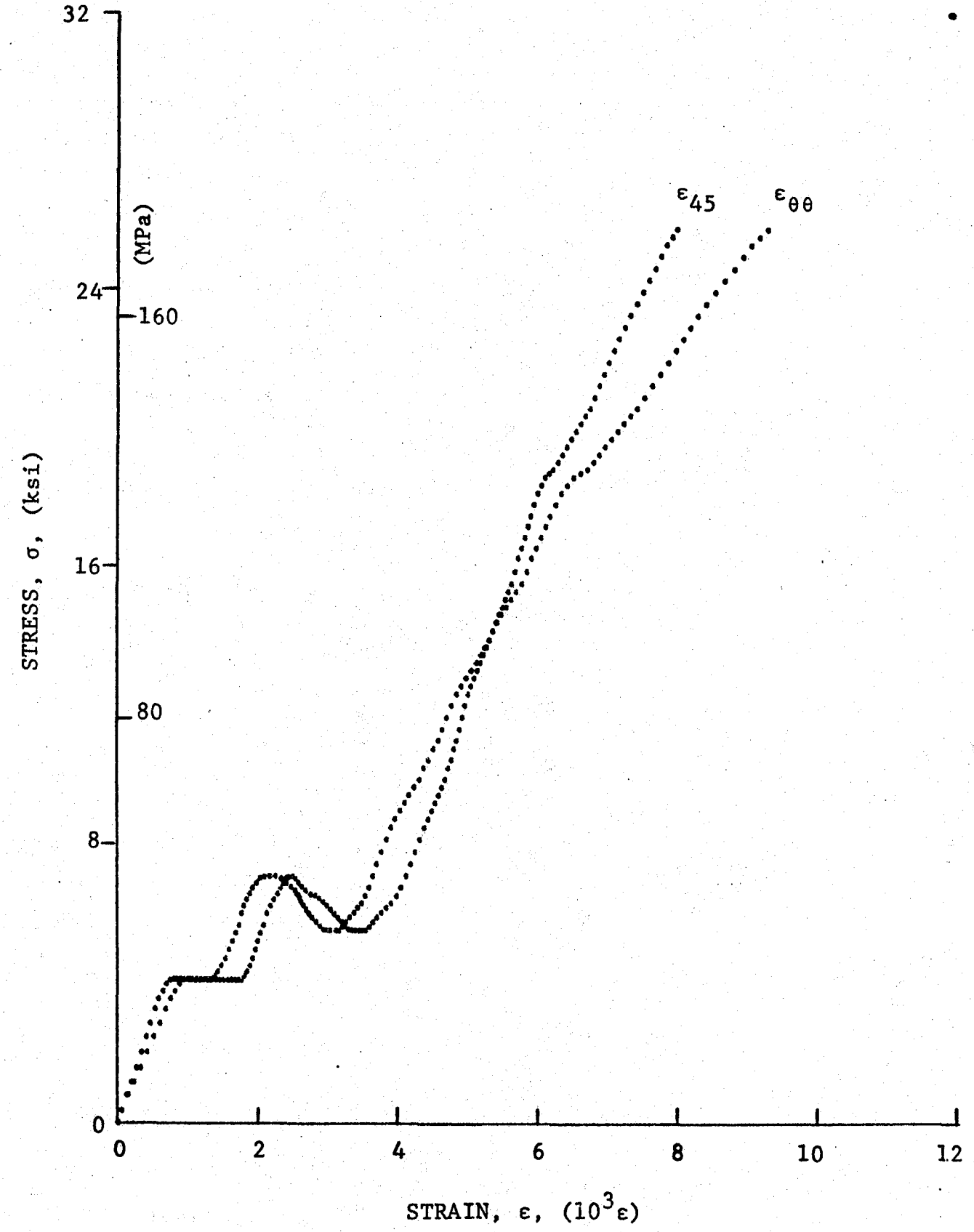

Figure 3-36. Stress-strain curves for dynamically loaded [45_8] 80AS/20S/PR288 graphite/S-glass/epoxy ring, Specimen No. 51-9.

4. HIGH STRAIN RATE TENSILE PROPERTIES OF OFF-AXIS LAMINATES

4.1 $[22.5_8]$ LAMINATES

High strain rate tensile properties of $[22.5_8]$ SP288/AS graphite/epoxy and 80AS/20S/PR288 graphite/S-glass/epoxy were obtained by testing rings under dynamic internal pressure. Three rings of each material were loaded dynamically using a 1.56 mixture of pistol powder, potassium perchlorate, and aluminum dust in the pressure chamber of the fixture. The circumferential, axial, and 45-deg strains in the composite ring and the circumferential strain in the steel calibration ring were recorded in every case.

Strain and strain derivative records for the three graphite/epoxy rings (Specimen Nos. 46-5, 46-7, and 46-8) are shown in Figures 4-1 through 4-9. These data were analyzed following the procedures described in Part I of this report. Dynamic stress-strain curves obtained by the digital processing oscilloscope are shown in Figures 4-10, 4-11, and 4-12. Results for the three rings tested are tabulated in Table 4-1. The initial strain rates range between $170s^{-1}$ and $320s^{-1}$, and the average (secant) rates between $278s^{-1}$ and $375s^{-1}$. The times to failure range between 24 μs and 32 μs. The initial and secant moduli of 62.1 GPa (9.0×10^6 psi) and 47.6 GPa (6.90×10^6 psi), respectively, are appreciably higher than the static modulus of 34.6 GPa (5.01×10^6 psi). The dynamic initial Poisson's ratio of 0.39 is higher than the static value of 0.31. The average dynamic strength of 432 MPa (62.7 ksi) is twice as high as the static strength of 218 MPa (31.6 ksi). The average dynamic ultimate strain of 0.0091 is lower than the static value of 0.0110.

Strain and strain derivative records for the three hybrid rings (Specimen Nos. 47-4, 47-5, and 47-6) are shown in Figures 4-13 through 4-21. The corresponding dynamic stress-strain curves are shown in Figures 4-22, 4-23, and 4-24. Results are tabulated in Table 4-2. The initial strain rates range between $250s^{-1}$ and $330s^{-1}$, and the average (secant) rates between $274s^{-1}$ and $420s^{-1}$. The times to failure range between 25 μs and 38 μs. The initial modulus is much higher than the secant modulus due to the characteristic shape of the stress-strain curves. The dynamic initial and secant moduli of 105.1 GPa (15.24×10^6 psi) and 52.9 GPa (7.66×10^6 psi), respectively, are much higher than the static modulus of 38.6 GPa (5.59×10^6 psi). Both dynamic and static

TABLE 4-1. HIGH STRAIN RATE TENSILE PROPERTIES OF $[22.5_8]$ SP288/AS GRAPHITE/EPOXY

Specimen Number	Strain Rate ($\dot{\varepsilon}_{\theta\theta}$), s^{-1}	Modulus ($E_{\theta\theta}$), GPa (10^6 psi)	Poisson's Ratio ($\nu_{\theta x}$)
		Initial Properties	
46-5	170	67.3 (9.70)	0.35
46-7	320	59.3 (8.60)	0.39
46-8	240	59.7 (8.70)	0.42
		Secant Properties	
46-5	278	48.5 (7.02)	0.31
46-7	375	49.1 (7.11)	0.51
46-8	306	45.4 (6.58)	0.42
		Terminal Properties	
46-5	330	34.8 (5.05)	0.53
46-7	420	36.0 (5.22)	0.57
46-8	375	28.2 (4.08)	0.30
		Ultimate Properties	
	Time to Failure (t_f), μs	Strength ($S_{\theta\theta T}$), MPa (ksi)	Strain ($\varepsilon^u_{\theta\theta T}$)
46-5	32	431 (62)	0.0089
46-7	24	442 (64)	0.0090
46-8	31	431 (62)	0.0095

TABLE 4-2. HIGH STRAIN RATE TENSILE PROPERTIES OF $[22.5_8]$ 80AS/20S/PR288 GRAPHITE/S-GLASS/EPOXY

Specimen Number	Strain Rate ($\dot{\varepsilon}_{\theta\theta}$), s^{-1}	Modulus ($E_{\theta\theta}$), GPa (10^6 psi)	Poisson's Ratio ($\nu_{\theta x}$)
		Initial Properties	
47-4	250	115.0 (16.66)	0.35
47-5	250	110.4 (16.00)	0.52
47-6	330	90.0 (13.05)	0.46
		Secant Properties	
47-4	392	52.9 (7.67)	0.46
47-5	274	66.0 (9.57)	0.37
47-6	420	39.6 (5.75)	0.44
		Terminal Properties	
47-4	520	42.6 (6.18)	0.60
47-5	325	77.6 (11.25)	0.47
47-6	550	27.3 (3.95)	0.46
		Ultimate Properties	
	Time to Failure (t_f), μs	Strength ($S_{\theta\theta T}$), MPa (ksi)	Strain ($\varepsilon^u_{\theta\theta T}$)
47-4	25	519 (75)	0.0098
47-5	38	686 (99)	0.0104
47-6	28	468 (68)	0.0118

values for the moduli of the hybrid laminate are higher than corresponding values for the graphite/epoxy laminate. The average dynamic Poisson's ratio (initial and secant) of 0.43 is higher than the static value of 0.38. The average dynamic strength of 557 MPa (81 ksi) is more than twice as high as the static strength of 204 MPa (29.6 ksi). The average dynamic ultimate strain of 0.0107 is much higher than the static value of 0.0077.

4.2 $[30_8]$ LAMINATES

High strain rate tensile properties of $[30_8]$ SP288/AS graphite/epoxy and 80AS/20S/PR288 graphite/S-glass/epoxy were obtained by testing three rings of each material as described above.

Strain and strain derivative records for the three graphite/epoxy rings above (Specimen Nos. 48-4, 48-5, and 48-6) are shown in Figures 4-25 through 4-33. These data were analyzed following previously described procedures. Dynamic stress-strain curves are shown in Figures 4-34, 4-35, and 4-36. Results are tabulated in Table 4-3. The initial strain rates range between $230s^{-1}$ and $270s^{-1}$, and the average (secant) rates between $297s^{-1}$ and $390s^{-1}$. The times to failure range between 30 μs and 39 μs. The initial and secant moduli of 66.9 GPa (9.70×10^6 psi) and 42.8 GPa (6.20×10^6 psi), respectively, are much higher than the static modulus of 25.4 GPa (3.68×10^6 psi). Values for Poisson's ratio seem to fluctuate a great deal. The average dynamic strength of 474 kPa (69 ksi) is more than three times the static strength of 149 kPa (22 ksi). The average dynamic ultimate strain of 0.0111 is higher than the static value of 0.0080.

Dynamic properties of $[30_8]$ 80AS/20S/PR288 graphite/S-glass/epoxy were obtained similarly as those for graphite/epoxy. Strain and strain derivative records for the three hybrid rings tested and the steel calibration ring are shown in Figures 4-37 through 4-45. Dynamic stress-strain curves are shown in Figures 4-46, 4-47, and 4-48. Results are tabulated in Table 4-4. The initial strain rates range between $215s^{-1}$ and $270s^{-1}$, and the average (secant) rates between $230s^{-1}$ and $325s^{-1}$. The initial and secant moduli of 52.3 GPa (7.58×10^6 psi) and 43.1 GPa (6.25×10^6 psi), respectively, are much higher than the static modulus of 24.7 GPa (3.57×10^6 psi). The overall average Poisson's ratio of 0.32 is slightly lower than the static value of 0.35. The

TABLE 4-3. HIGH STRAIN RATE TENSILE PROPERTIES OF $[30_8]$ SP288/AS GRAPHITE/EPOXY

Specimen Number	Strain Rate ($\dot{\varepsilon}_{\theta\theta}$), s^{-1}	Modulus ($E_{\theta\theta}$), GPa (10^6 psi)	Poisson's Ratio ($\nu_{\theta x}$)
		Initial Properties	
48-4	230	64.2 (9.30)	0.24
48-5	250	43.8 (6.35)	0.45
48-6	270	92.8 (13.45)	0.66
		Secant Properties	
48-4	390	36.9 (5.34)	0.39
48-5	297	54.4 (7.89)	0.33
48-6	320	37.1 (5.37)	0.54
		Terminal Properties	
48-4	510	22.2 (3.22)	0.43
48-5	400	57.6 (8.35)	-
48-6	420	41.1 (5.95)	0.78
		Ultimate Properties	
	Time to Failure (t_f), μs	Strength ($S_{\theta\theta T}$), MPa (ksi)	Strain ($\varepsilon^u_{\theta\theta T}$)
48-4	30	431 (62)	0.0117
48-5	39	631 (91)	0.0116
48-6	31	367 (53)	0.0099

TABLE 4-4. HIGH STRAIN RATE TENSILE PROPERTIES OF $[30_8]$ 80AS/20S/PR288 GRAPHITE/S-GLASS/EPOXY

Specimen Number	Strain Rate ($\dot{\varepsilon}_{\theta\theta}$), s^{-1}	Modulus ($E_{\theta\theta}$), GPa (10^6 psi)	Poisson's Ratio ($\nu_{\theta x}$)
		Initial Properties	
49-5	215	54.5 (7.90)	0.38
49-6	220	55.5 (8.05)	0.32
49-7	270	46.9 (6.80)	0.29
		Secant Properties	
49-5	260	41.8 (6.06)	0.40
49-6	230	53.2 (7.71)	0.40
49-7	325	34.4 (4.98)	0.34
		Terminal Properties	
49-5	300	26.4 (3.82)	0.20
49-6	225	45.2 (6.55)	-
49-7	410	24.8 (3.60)	0.20
		Ultimate Properties	
	Time to Failure (t_f), μs	Strength ($S_{\theta\theta T}$), MPa (ksi)	Strain ($\varepsilon^u_{\theta\theta T}$)
49-5	38	414 (60)	0.0100
49-6	38	471 (68)	0.0088
49-7	32	357 (52)	0.0104

average dynamic strength of 414 MPa (60 ksi) is much higher than the static strength of 157 MPa (23 ksi). The average dynamic ultimate strain of 0.0097 is exactly equal to the static value.

4.3 $[45_8]$ LAMINATES

High strain rate tensile properties of $[45_8]$ SP288/AS graphite/epoxy and 80AS/20S/PR288 graphite/S-glass/epoxy were obtained by testing three rings of each material as described above.

Strain and strain derivative records for the three graphite/epoxy rings (Specimen Nos. 50-4, 50-5, and 50-6) are shown in Figures 4-49 through 4-57. These data were analyzed following previously described procedures. Dynamic stress-strain curves are shown in Figures 4-58, 4-59, and 4-60. Results are tabulated in Table 4-5. The initial strain rates range between $270s^{-1}$ and $300s^{-1}$, and the average (secant) rates between $282s^{-1}$ and $285s^{-1}$. The times to failure range between 18 μs and 35 μs. The initial and secant moduli of 69.9 GPa (10.12×10^6 psi) and 36.4 GPa (5.28×10^6 psi), respectively, are much higher than the static modulus of 14.7 GPa (2.13×10^6 psi). Values of Poisson's ratio seem to fluctuate, but they are higher than the static value of 0.27. The average dynamic strength of 281 MPa (41 ksi) is more than three times the static strength of 90 MPa (13.1 ksi). The average dynamic ultimate strain of 0.0081 is a little higher than the static value of 0.0070.

Dynamic properties of $[45_8]$ 80AS/20S/PR288 graphite/S-glass/epoxy were obtained similarly as those for graphite/epoxy. Strain and strain derivative records for the three hybrid rings tested and the steel calibration ring are shown in Figures 4-61 through 4-69. Dynamic stress-strain curves are shown in Figures 4-70, 4-71, and 4-72. Results are tabulated in Table 4-6. The initial strain rates range between $210s^{-1}$ and $270s^{-1}$, and the average (secant) rates between $194s^{-1}$ and $285s^{-1}$. The initial and secant moduli of 96.4 GPa (13.97×10^6 psi) and 36.4 GPa (5.28×10^6 psi), respectively, are much higher than the static modulus of 15.3 GPa (2.22×10^6 psi). The average initial and secant Poisson's ratio is 0.27. This value becomes 0.19 if the values for Specimen No. 51-5 are ignored. The corresponding static value is 0.20. The average dynamic strength of 313 MPa (45 ksi) is approximately three times the static strength of 100 MPa (14.5 ksi). The average dynamic ultimate strain of 0.0087 is a little higher than the static value of 0.0080.

TABLE 4-5. HIGH STRAIN RATE TENSILE PROPERTIES OF $[45_8]$ SP288/AS GRAPHITE/EPOXY

Specimen Number	Strain Rate ($\dot{\varepsilon}_{\theta\theta}$), s^{-1}	Modulus ($E_{\theta\theta}$), GPa (10^6 psi)	Poisson's Ratio ($\nu_{\theta x}$)
		Initial Properties	
50-4	290	67.6 (9.80)	0.32
50-5	300	72.1 (10.45)	0.36
50-6	270	--	0.37
		Secant Properties	
50-4	285	34.9 (5.05)	0.25
50-5	283	46.0 (6.67)	0.52
50-6	282	28.4 (4.11)	0.31
		Terminal Properties	
50-4	310	14.5 (2.10)	0.16
50-5	260	41.1 (5.95)	0.53
50-6	400	20.0 (2.90)	-
		Ultimate Properties	
	Time to Failure (t_f), μs	Strength ($S_{\theta\theta T}$), MPa (ksi)	Strain ($\varepsilon^u_{\theta\theta T}$)
50-4	35	342 (50)	0.0100
50-5	18	235 (34)	0.0051
50-6	33	264 (38)	0.0093

TABLE 4-6. HIGH STRAIN RATE TENSILE PROPERTIES OF $[45_8]$ 80AS/20S/PR288 GRAPHITE/S-GLASS/EPOXY

Specimen Number	Strain Rate ($\dot{\epsilon}_{\theta\theta}$), s^{-1}	Modulus ($E_{\theta\theta}$), GPa (10^6 psi)	Poisson's Ratio ($\nu_{\theta x}$)
		Initial Properties	
51-4	210	102.1 (14.8)	0.18
51-5	210	93.1 (13.5)	0.30
51-6	270	93.8 (13.6)	0.23
		Secant Properties	
51-4	272	43.5 (6.30)	0.18
51-5	194	35.0 (5.08)	0.53
51-6	285	30.7 (4.45)	0.18
		Terminal Properties	
51-4	260	20.7 (3.00)	0.45
51-5	275	--	-
51-6	280	--	-
		Ultimate Properties	
	Time to Failure (t_f), μs	Strength ($S_{\theta\theta T}$), MPa (ksi)	Strain ($\epsilon^u_{\theta\theta T}$)
51-4	36	417 (60)	0.0098
51-5	33	224 (33)	0.0064
51-6	35	298 (43)	0.0100

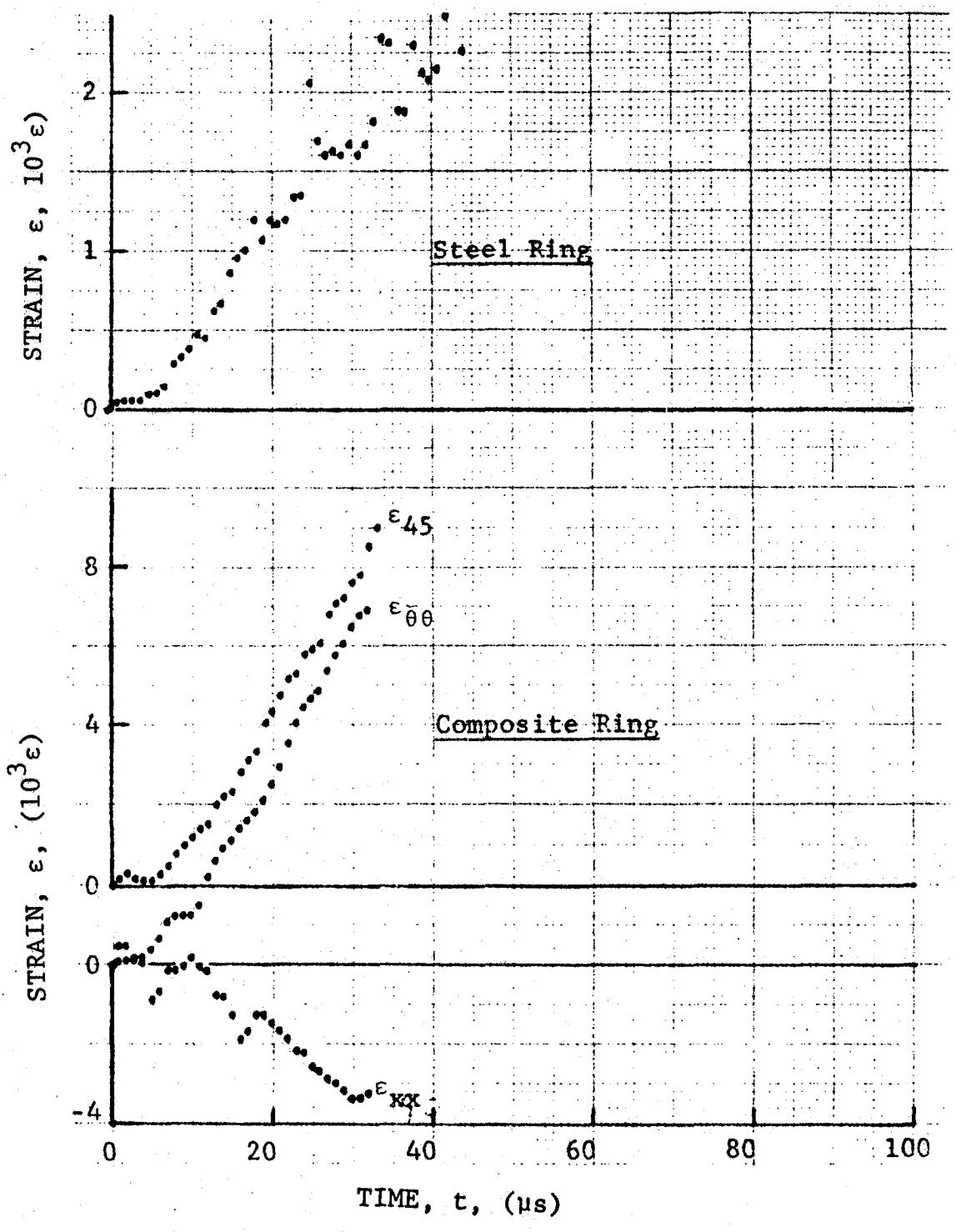

Figure 4-1. Strain records in steel ring and SP288/AS $[22.5_8]$ graphite/epoxy ring under dynamic loading for Specimen No. 46-5 (1.56 g pistol powder, $KC\ell O_4$, and aluminum dust).

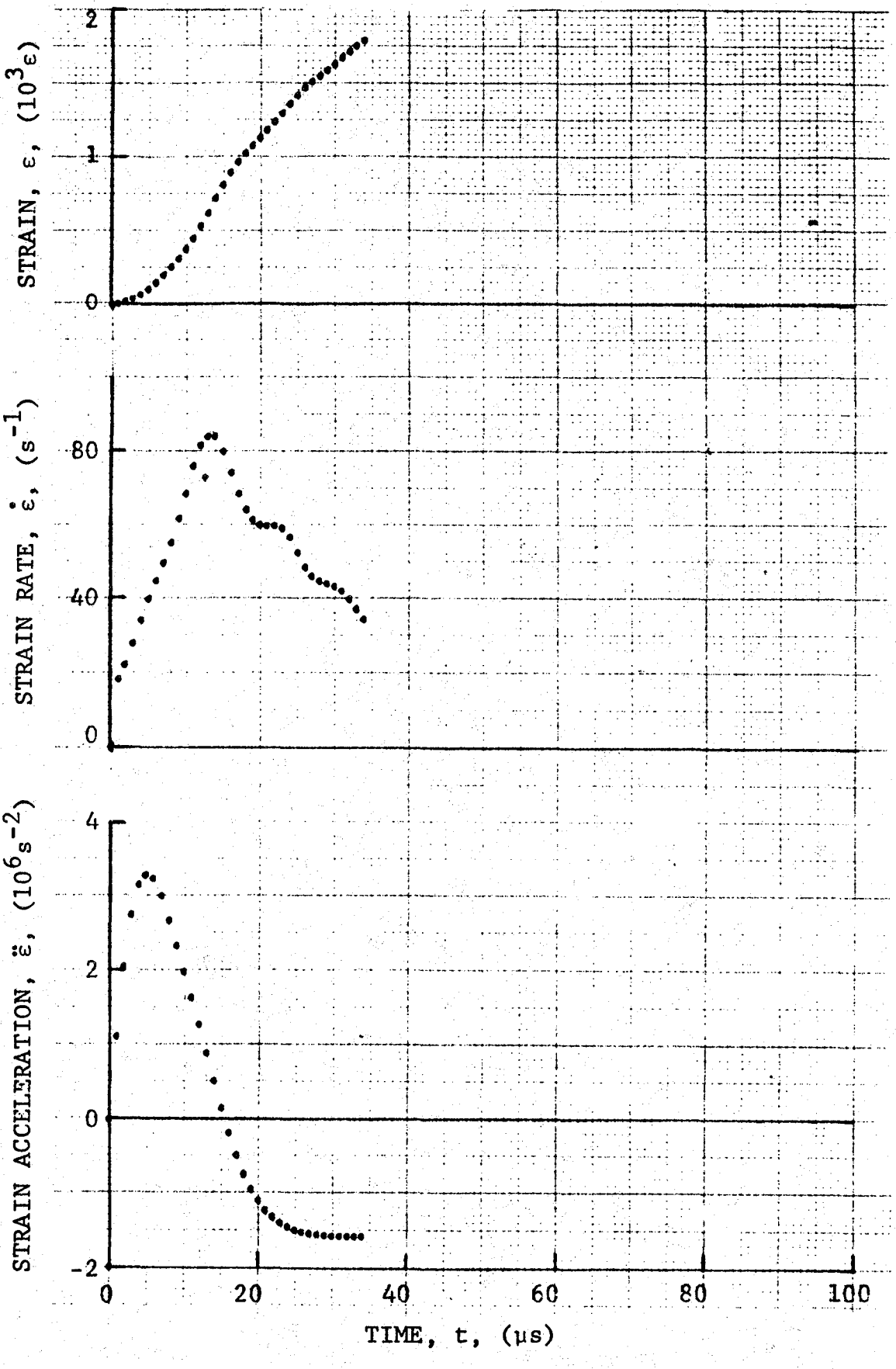

Figure 4-2. Strain and its derivatives in steel ring for Specimen No. 46-5.

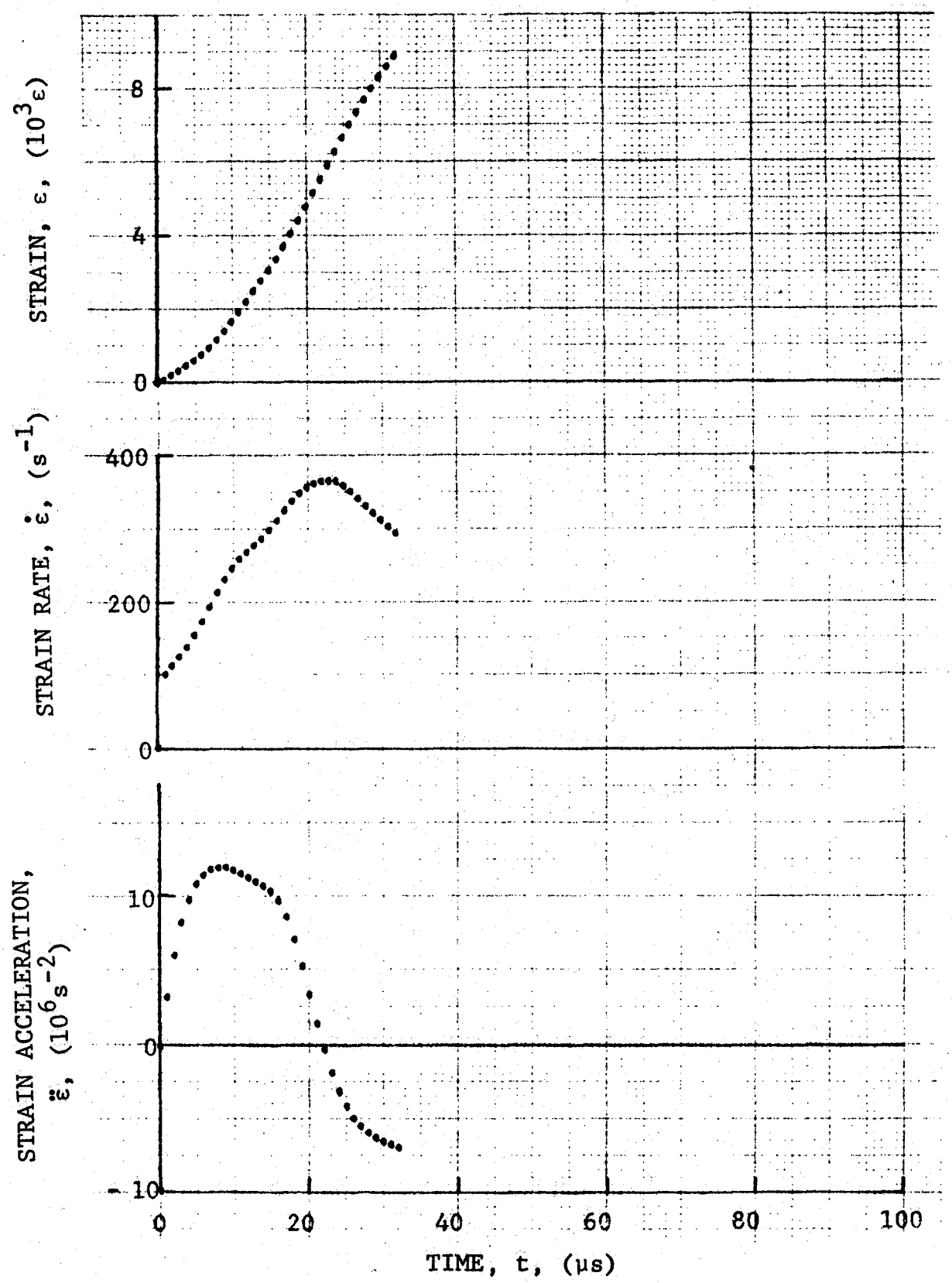

Figure 4-3. Circumferential strain and its derivatives in $[22.5_8]$ SP288/AS graphite/epoxy ring under dynamic loading for Specimen No. 46-5 (1.56 g pistol powder, $KC\ell O_4$, and aluminum dust).

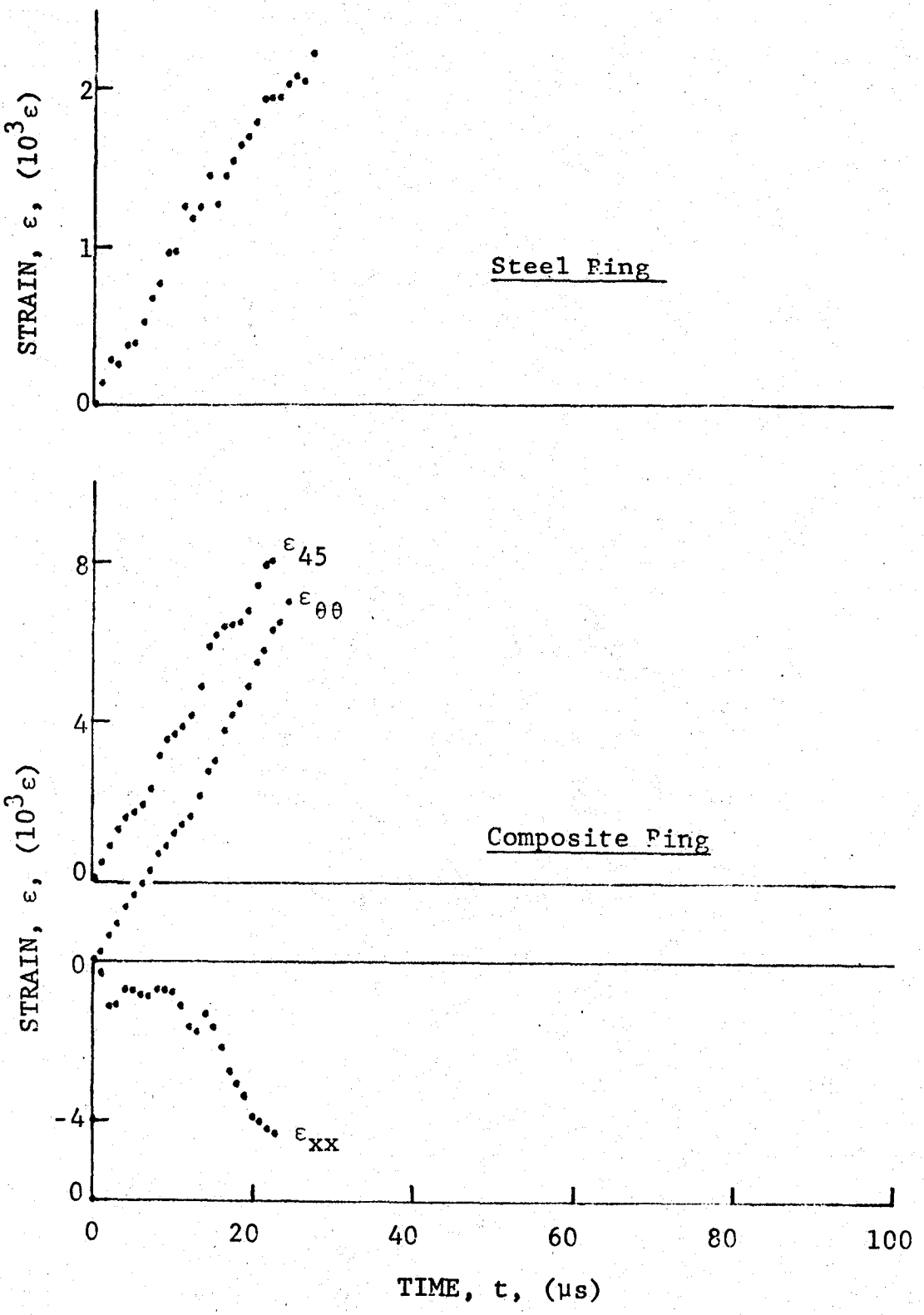

Figure 4-4. Strain records in steel ring and [22.5$_8$] SP288/AS graphite/epoxy ring under dynamic loading for Specimen No. 46-7 (1.56 g pistol powder, $KC\ell O_4$, and aluminum dust).

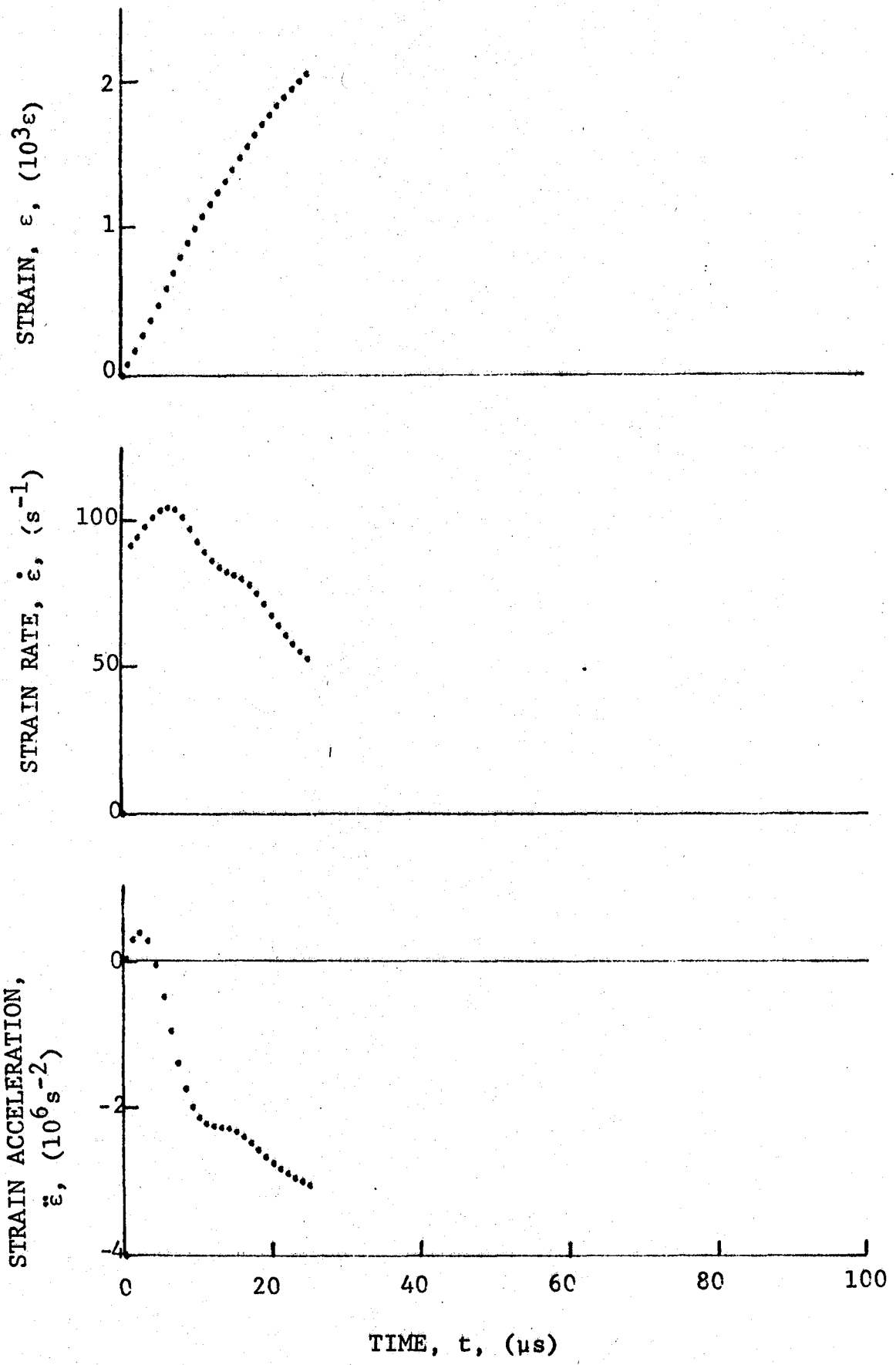

Figure 4-5. Strain and its derivatives in steel ring for Specimen No. 46-7.

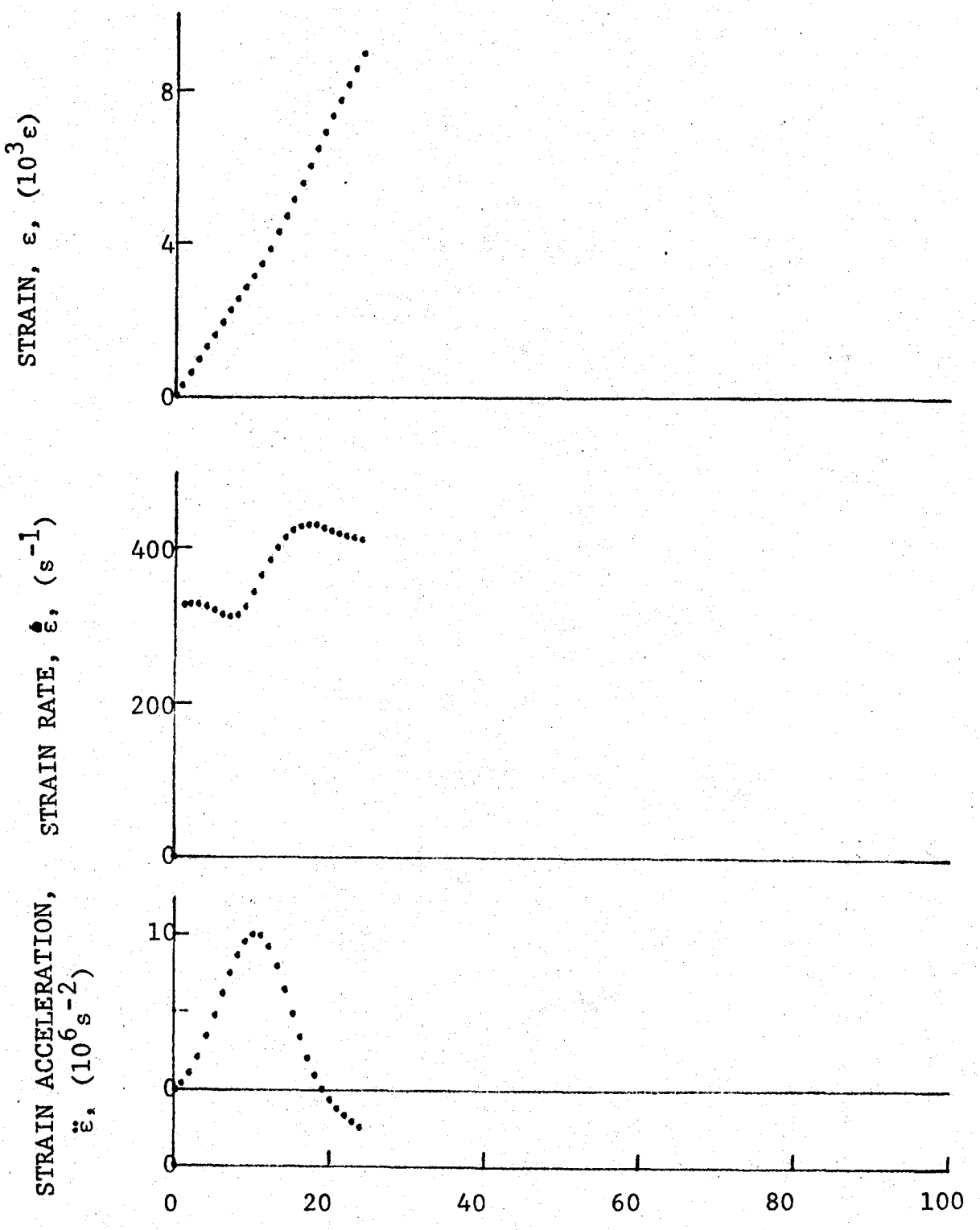

Figure 4-6. Circumferential strain and its derivatives in $[22.5_8]$ SP288/AS graphite/epoxy ring under dynamic loading for Specimen No. 46-7 (1.56 g pistol powder, $KC\ell O_4$, and aluminum dust).

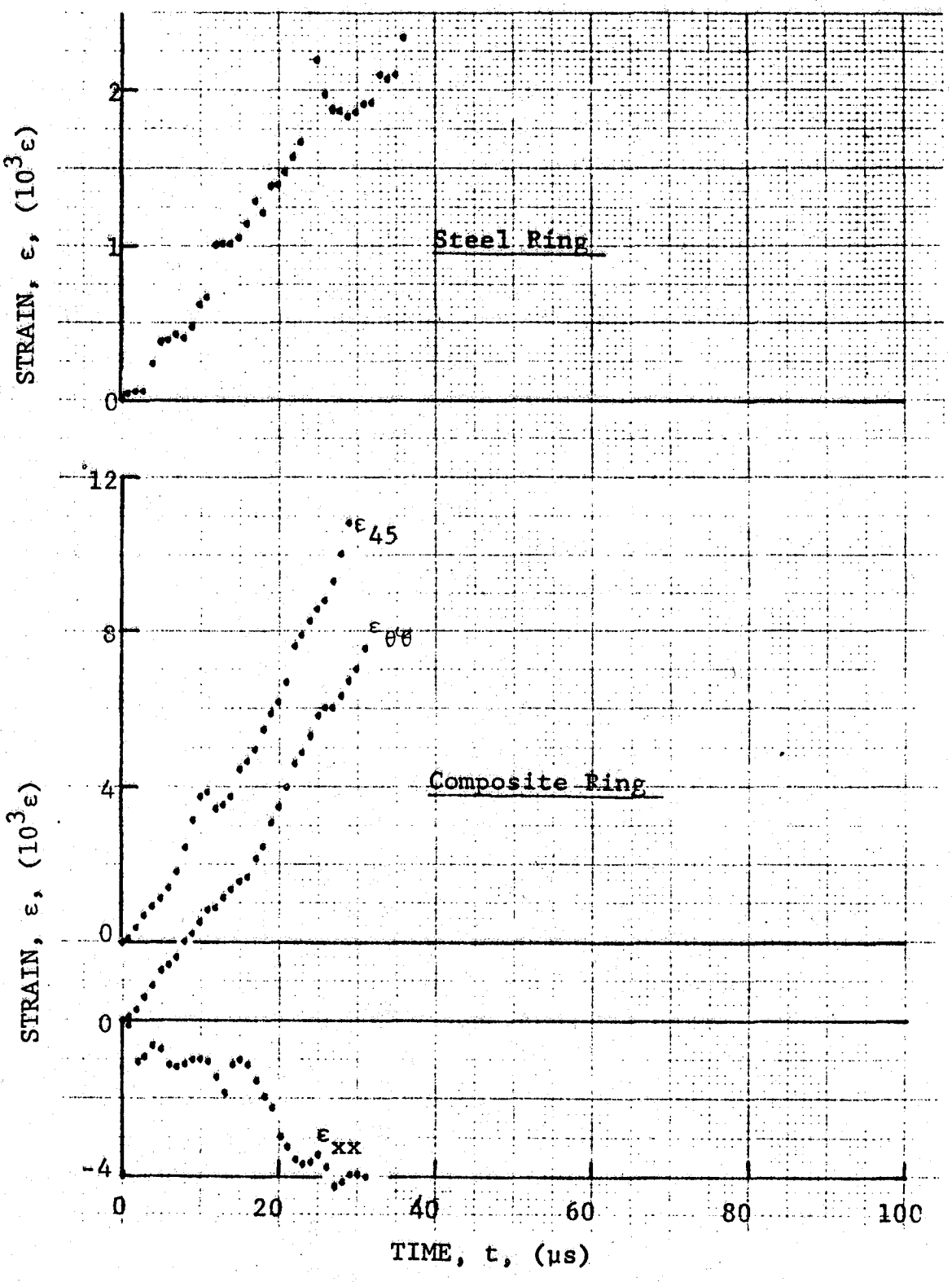

Figure 4-7. Strain records in steel ring and SP288/AS [22.5$_8$] graphite/epoxy ring under dynamic loading for Specimen No. 46-8 (1.56 g pistol powder, $KC\ell O_4$, and aluminum dust).

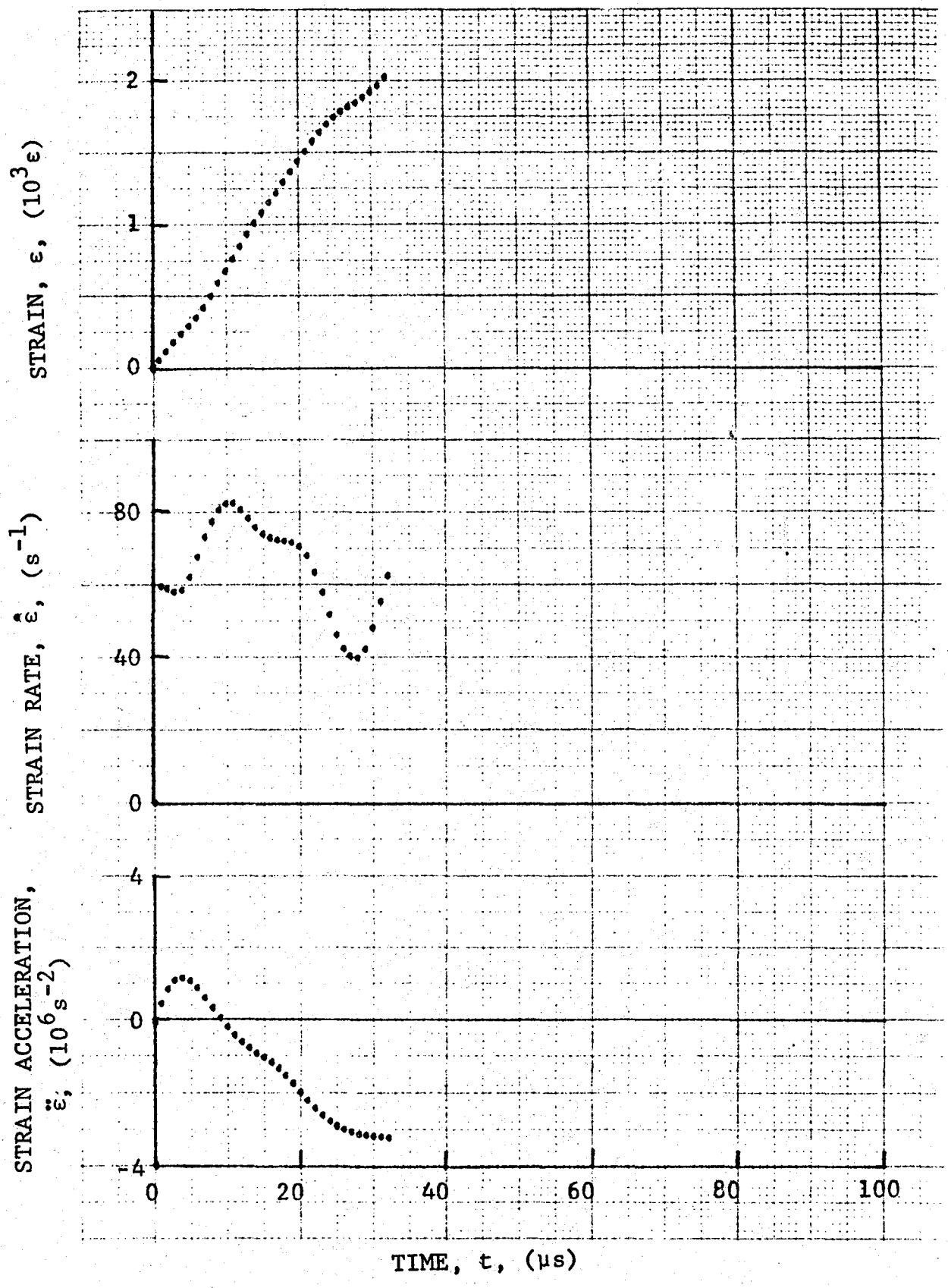

Figure 4-8. Strain and its derivatives in steel ring for Specimen No. 46-8.

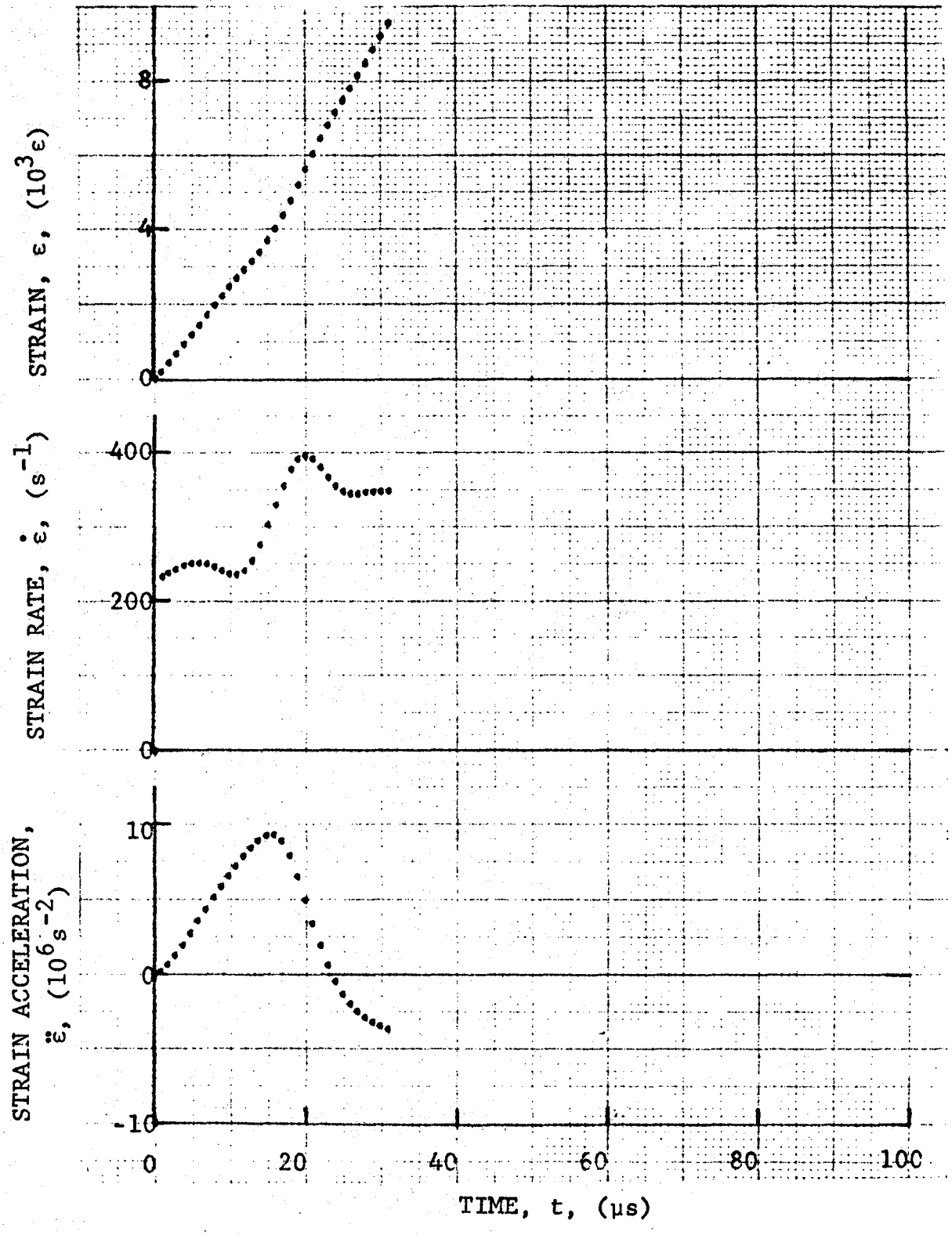

Figure 4-9. Circumferential strain and its derivatives in $[22.5_8]$ SP288/AS graphite/epoxy ring under dynamic loading for Specimen No. 46-8 (1.56 g pistol powder, $KC\ell O_4$, and aluminum dust).

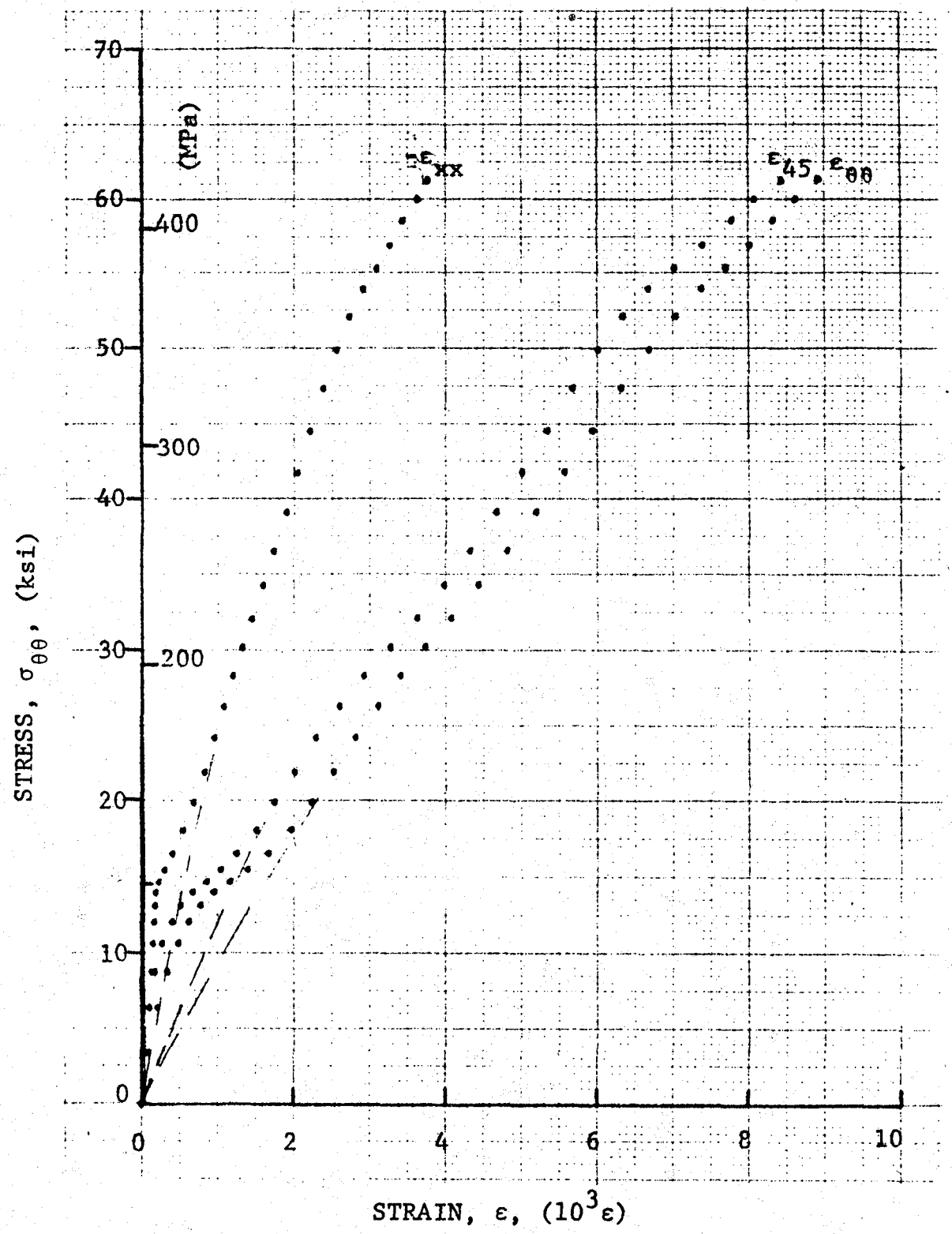

Figure 4-10. Stress-strain curve for dynamically loaded $[22.5_8]$ SP288/S graphite/epoxy ring, Specimen No. 46-5 (1.56 g pistol powder, $KC\ell O_4$, and aluminum dust).

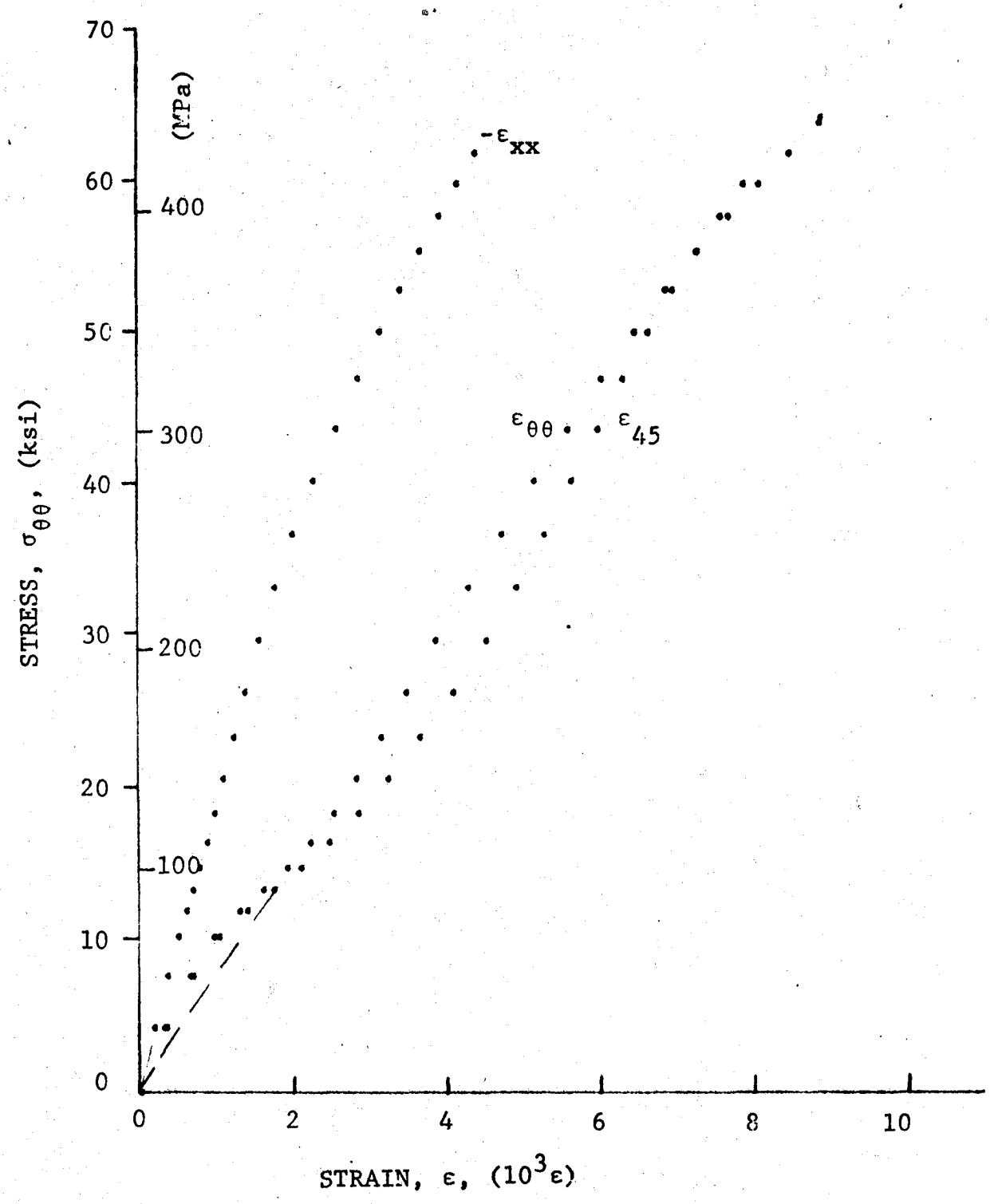

Figure 4-11. Stress-strain curve for dynamically loaded $[22.5_8]$ SP288/AS graphite/epoxy ring, Specimen No. 46-7 (1.56 g pistol powder, $KC\ell O_4$, and aluminum dust).

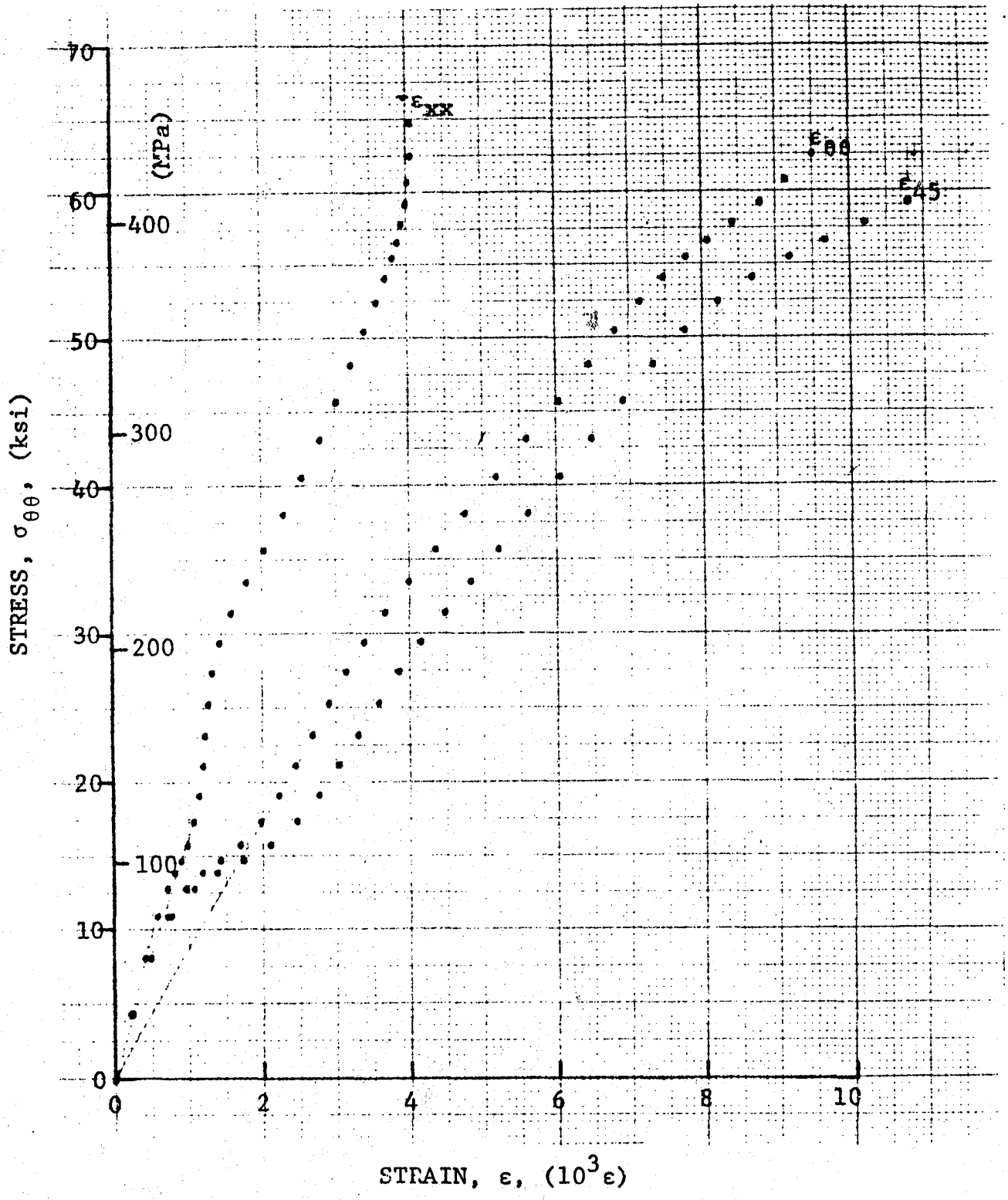

Figure 4-12. Stress-strain curve for dynamically loaded $[22.5_8]$ SP288/AS graphite/epoxy ring, Specimen No. 46-8 (1.56 g pistol powder, $KC\ell O_4$, and aluminum dust).

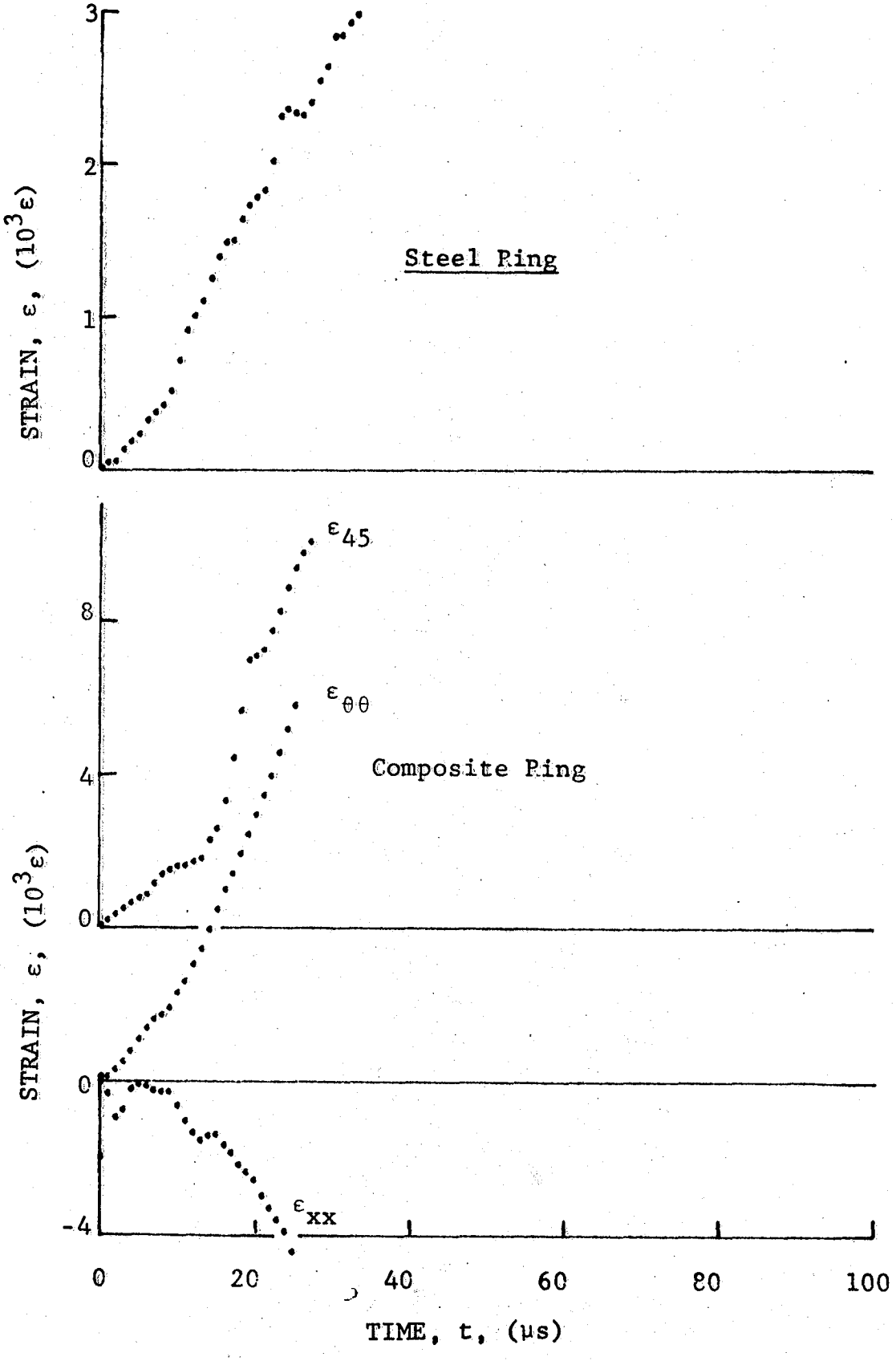

Figure 4-13. Strain records in steel ring and [22.5_8] 80AS/20S/PR288 graphite/S-glass/epoxy ring under dynamic loading for Specimen No. 47-4 (1.56 g pistol powder, $KC\&O_4$, and aluminum dust).

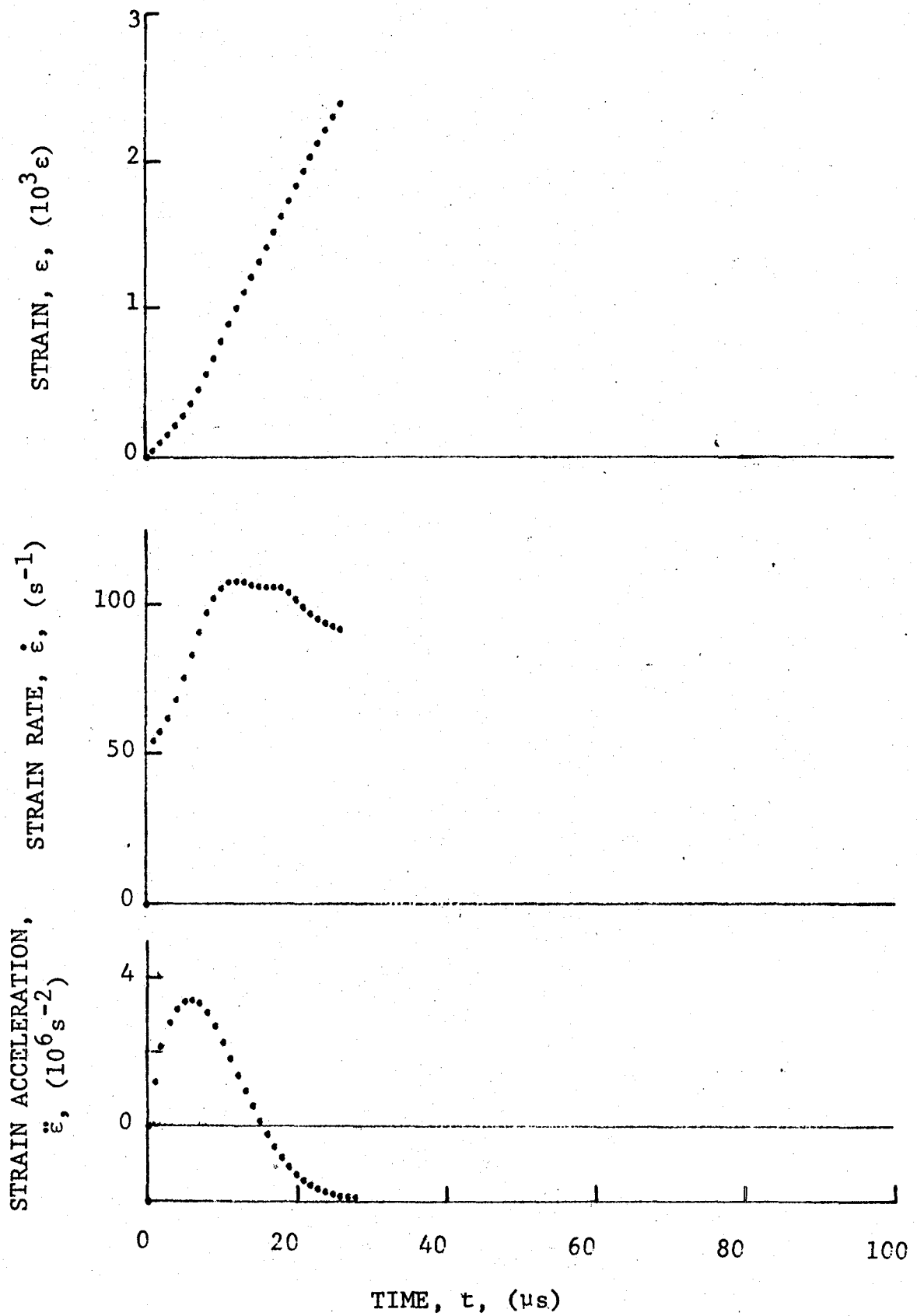

Figure 4-14. Strain and its derivatives in steel ring for Specimen No. 47-4.

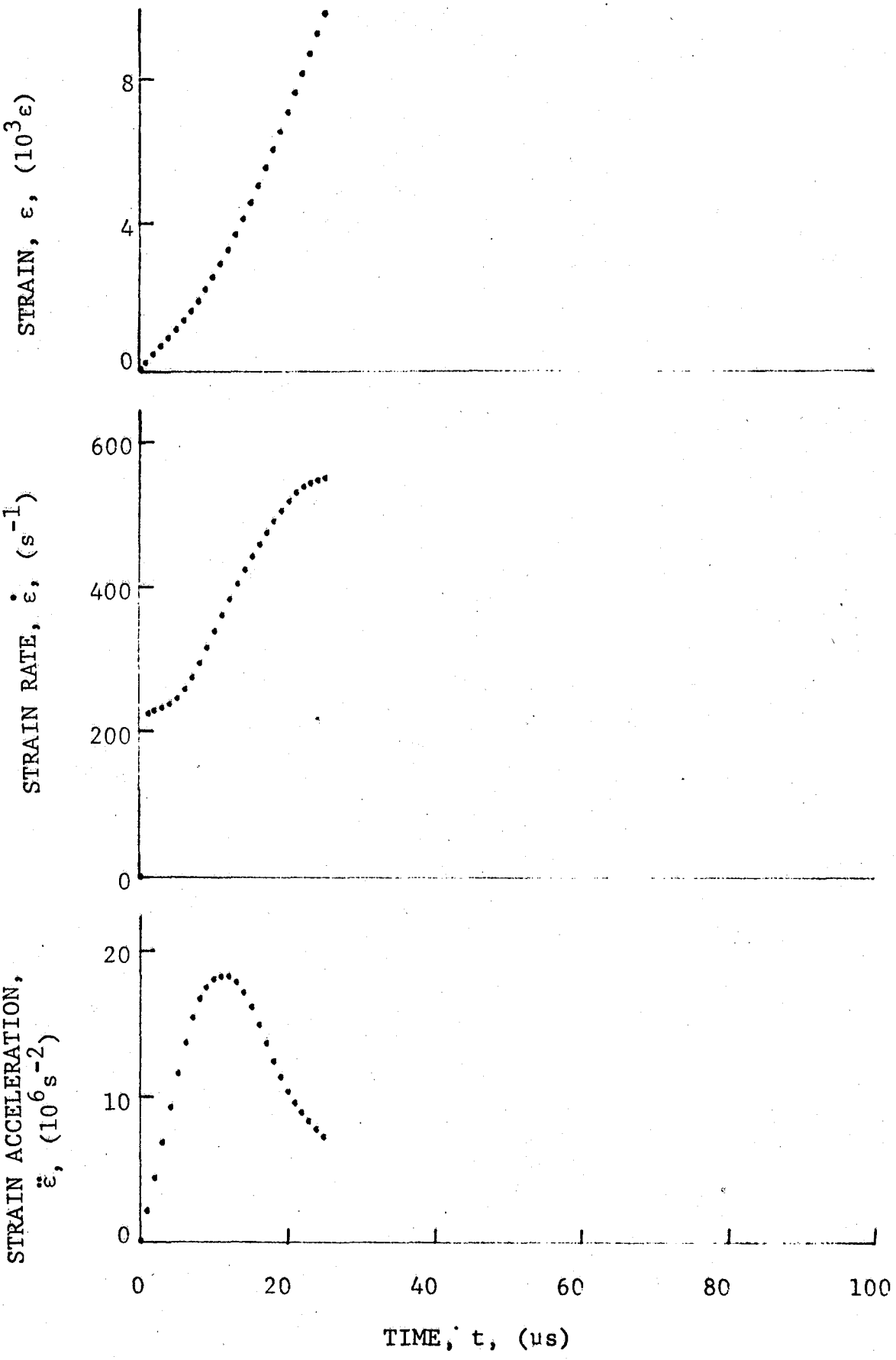

Figure 4-15. Circumferential strain and its derivatives in $[22.5_8]$ 80AS/20S/PR288 graphite/S-glass/epoxy ring under dynamic loading for Specimen No. 47-4 (1.56 pistol powder, $KC\ell O_4$, and aluminum dust).

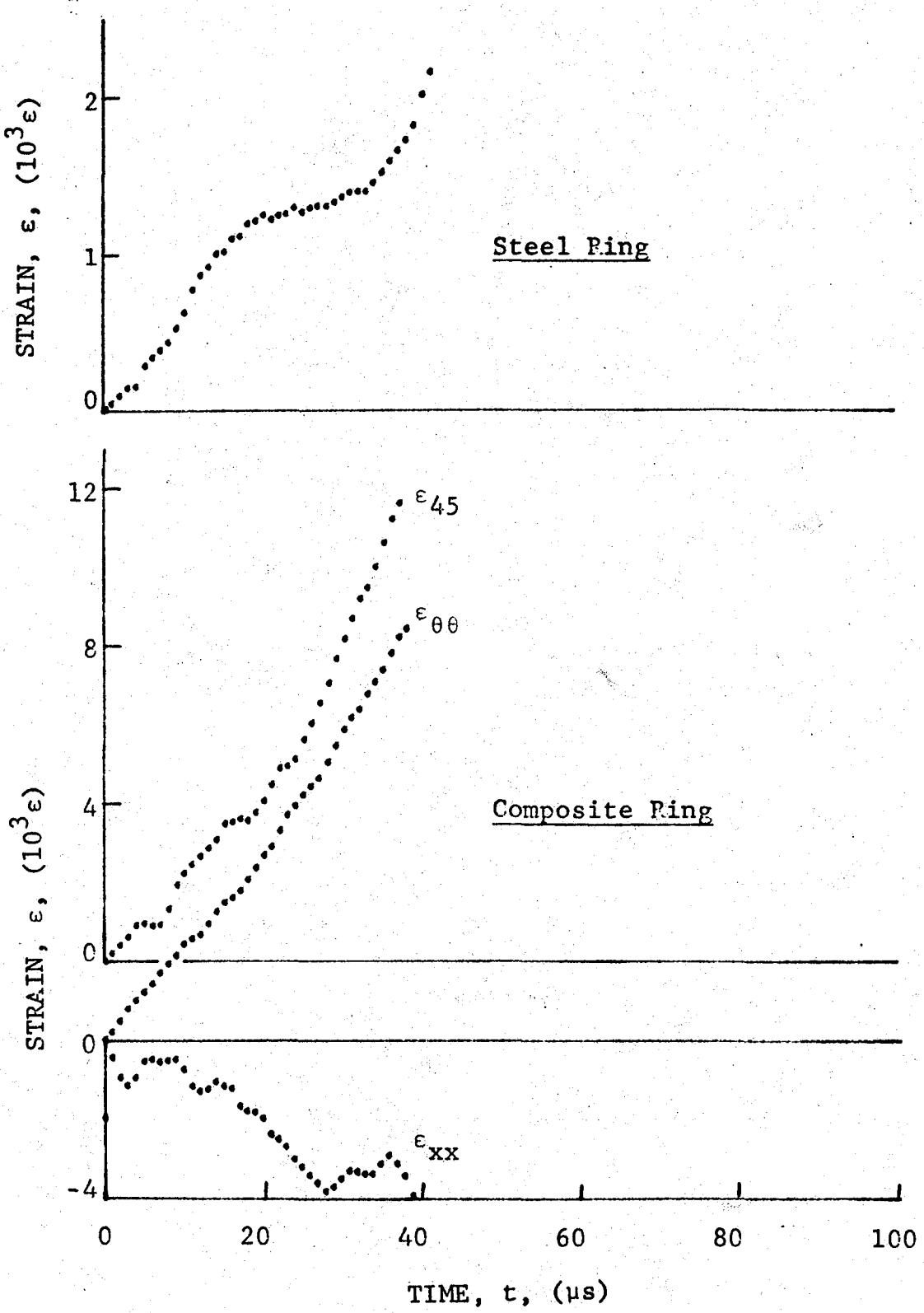

Figure 4-16. Strain records in steel ring and [22.5_8] 80AS/20S/PR288 graphite/S-glass/epoxy ring under dynamic loading for Specimen No. 47-5 (1.56 g pistol powder, $KC\ell O_4$, and aluminum dust).

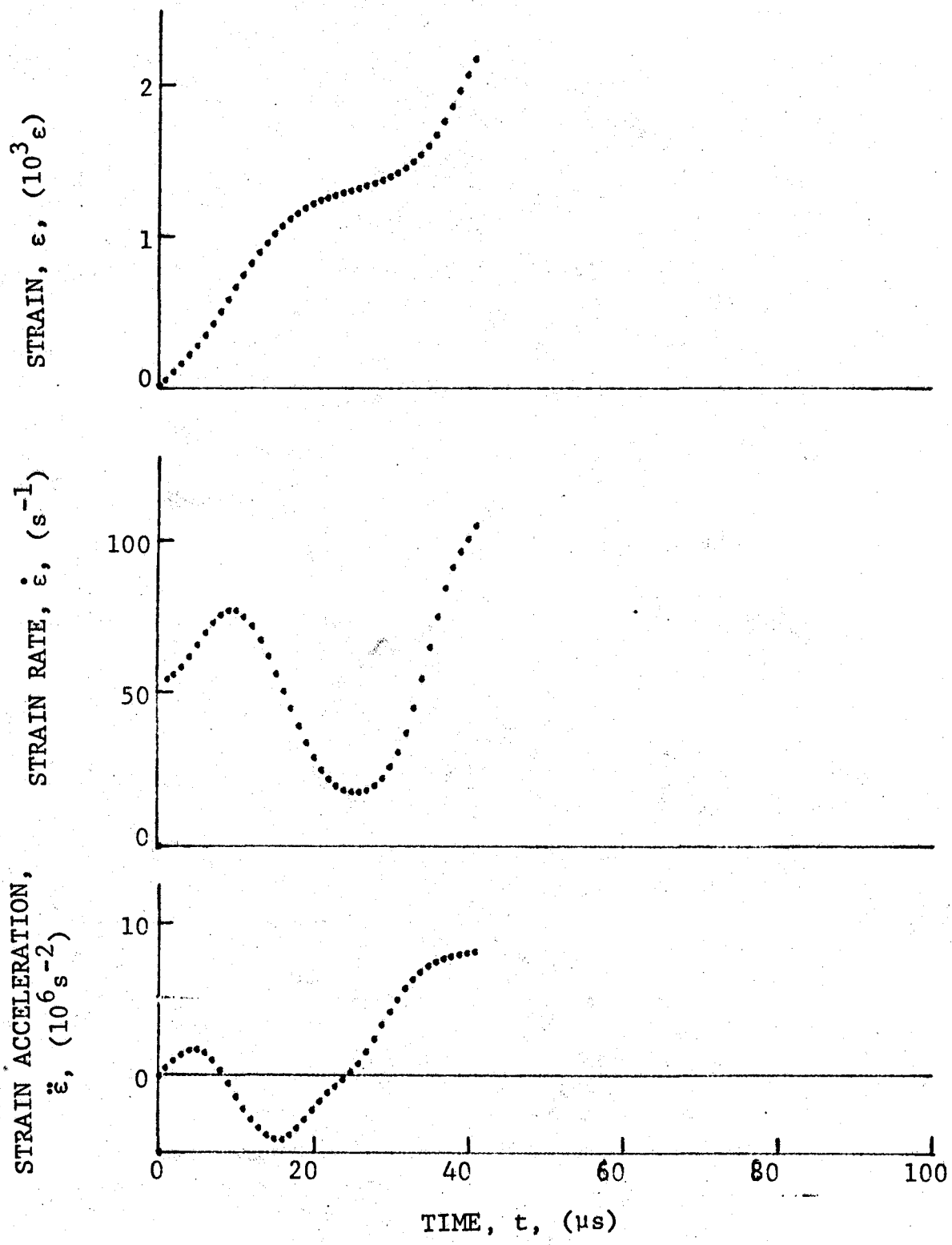

Figure 4-17. Strain and its derivatives in steel ring for Specimen No. 47-5.

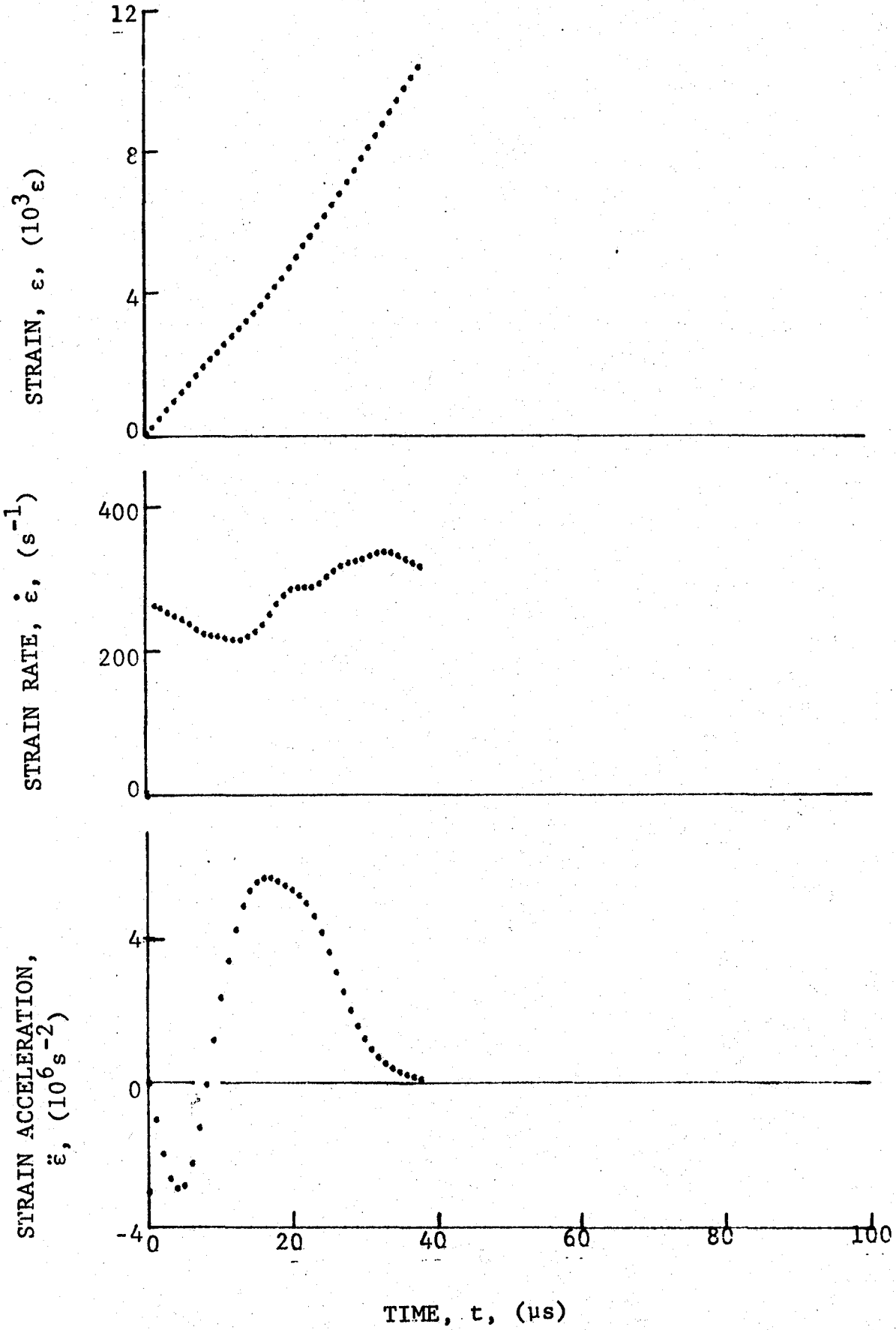

Figure 4-18. Circumferential strain and its derivatives in $[22.5_8]$ 80AS/20S/PR288 graphite/S-glass/epoxy ring under dynamic loading for Specimen No. 47-5 (1.56 g pistol powder, $KC\ell O_4$, and aluminum dust).

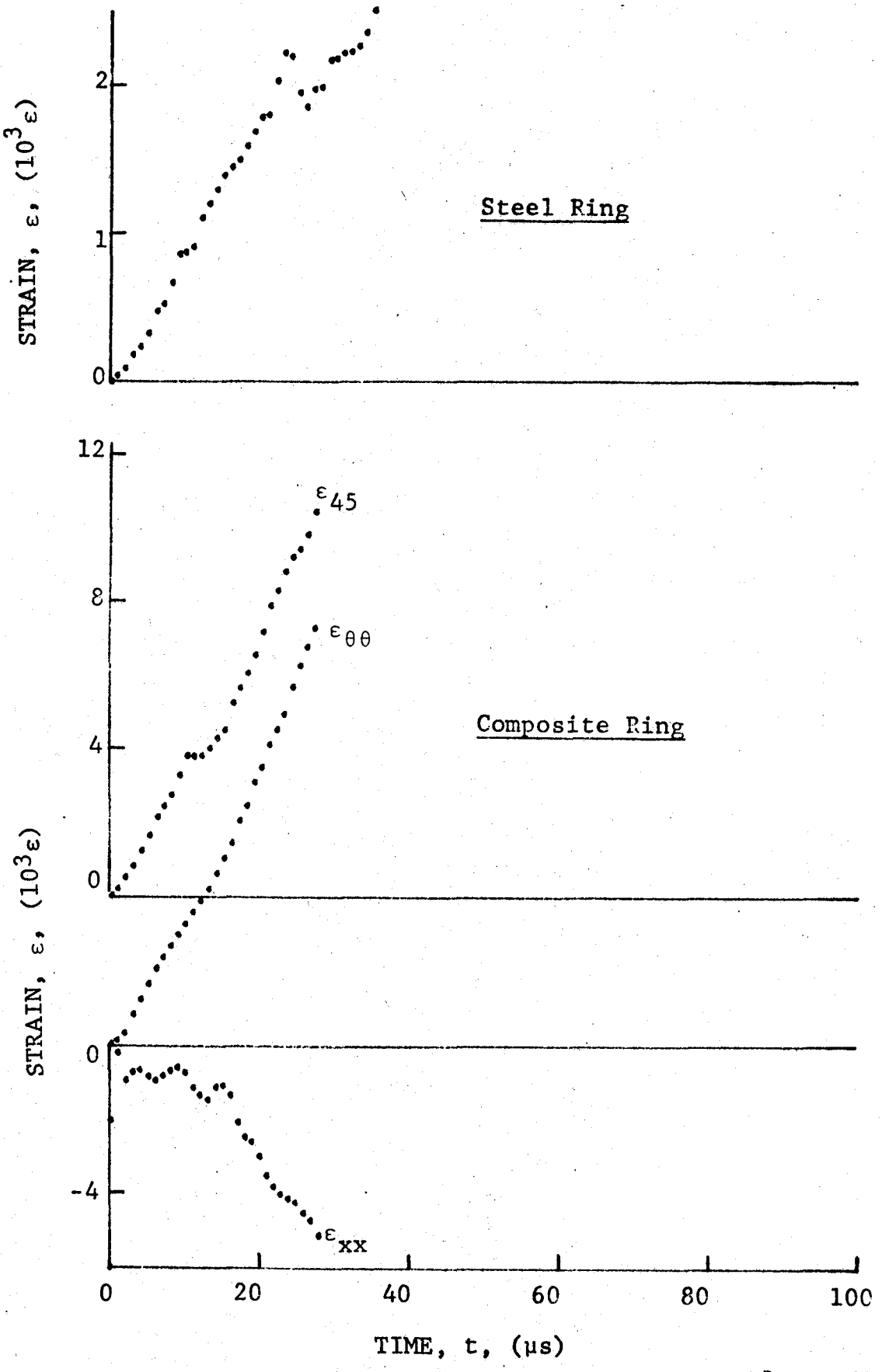

Figure 4-19. Strain records in steel ring and [22.5$_8$] 80AS/20S/PR288 graphite/S-glass/epoxy ring under dynamic loading for Specimen No. 47-6 (1.56 g pistol powder, $KC\ell O_4$, and aluminum dust).

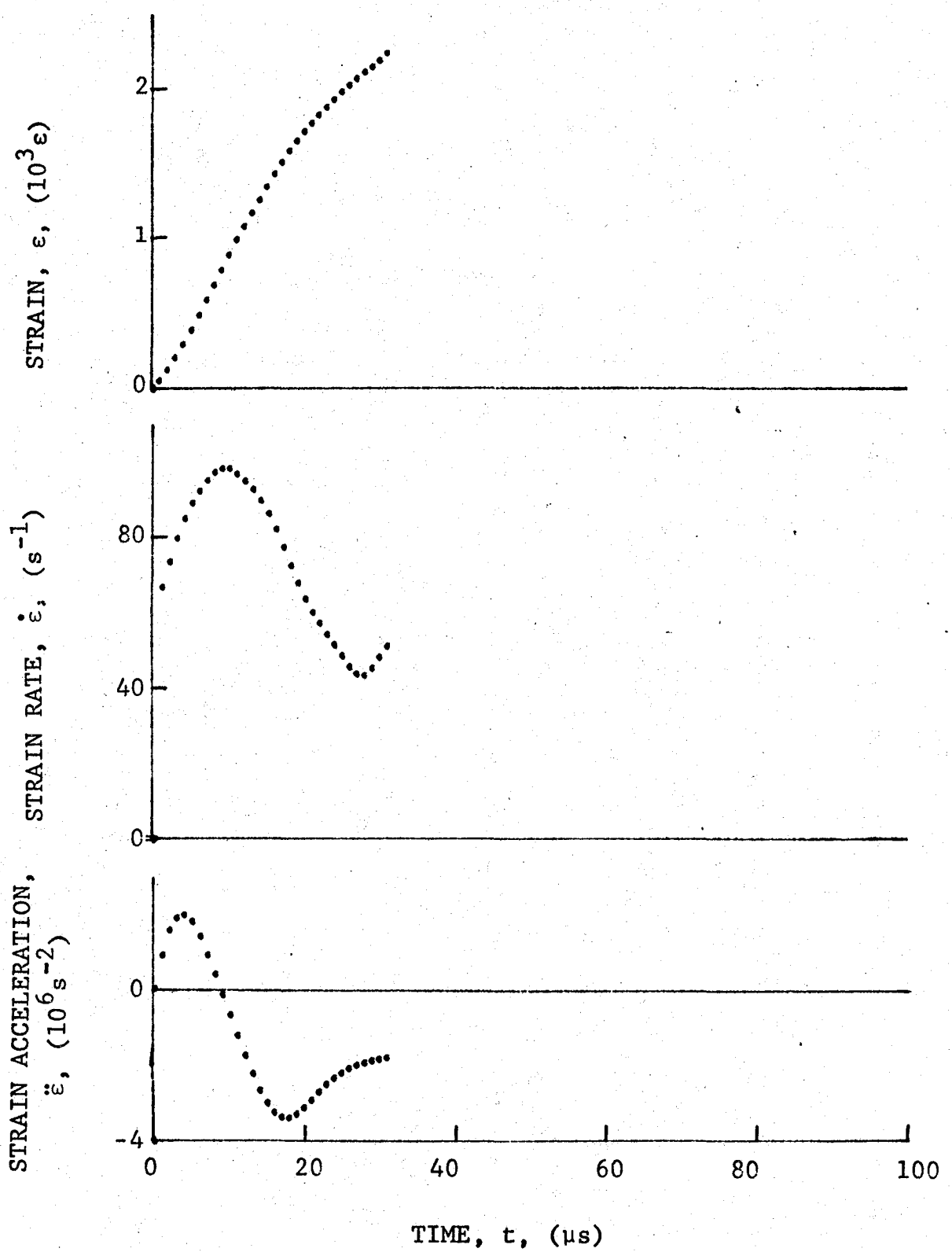

Figure 4-20. Strain and its derivatives in steel ring for Specimen No. 47-6.

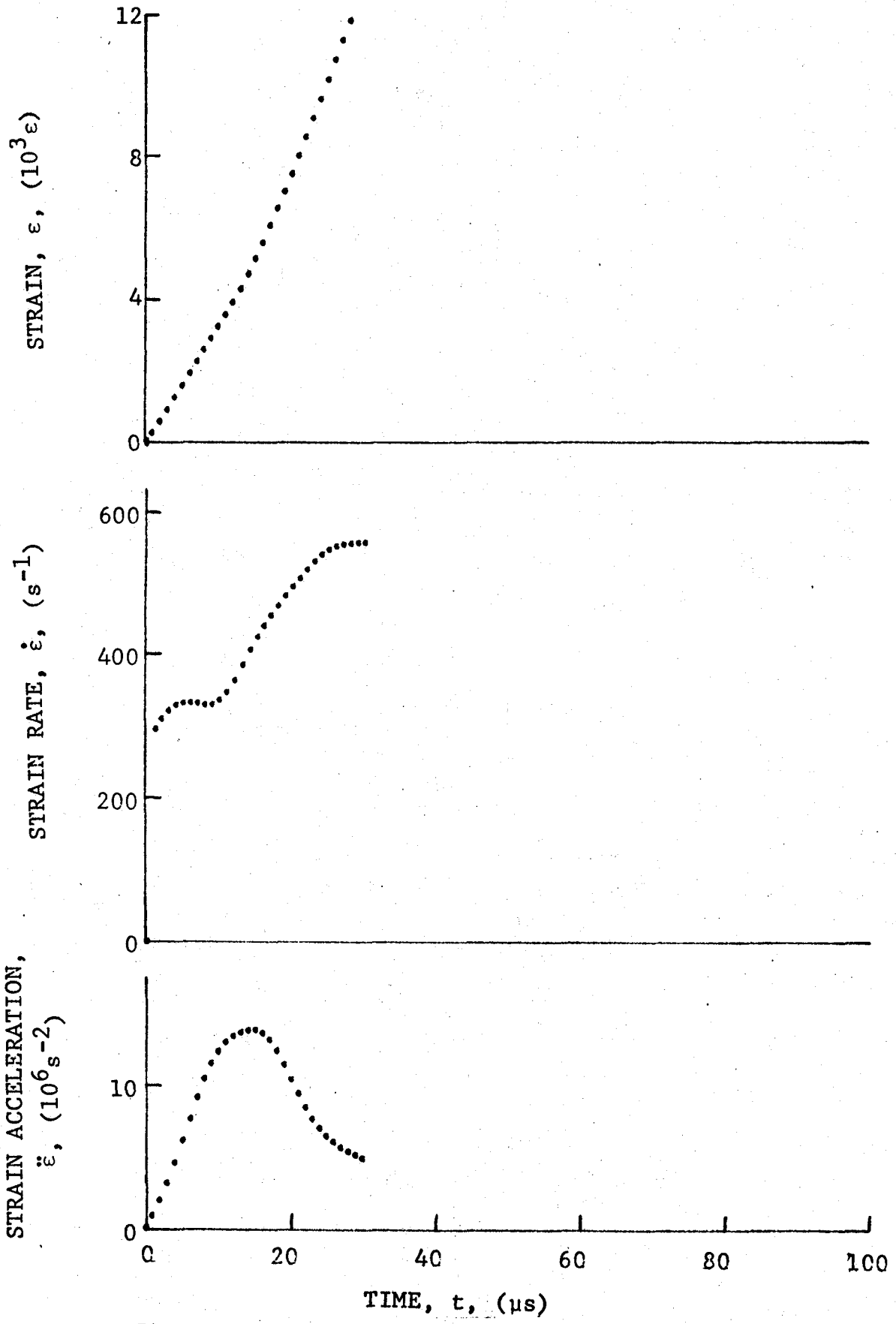

Figure 4-21. Circumferential strain and its derivatives in $[22.5_8]$ 80AS/20S/PR288 graphite/S-glass/epoxy ring under dynamic loading for Specimen No. 47-6 (1.56 g pistol powder, $KC\ell O_4$, and aluminum dust).

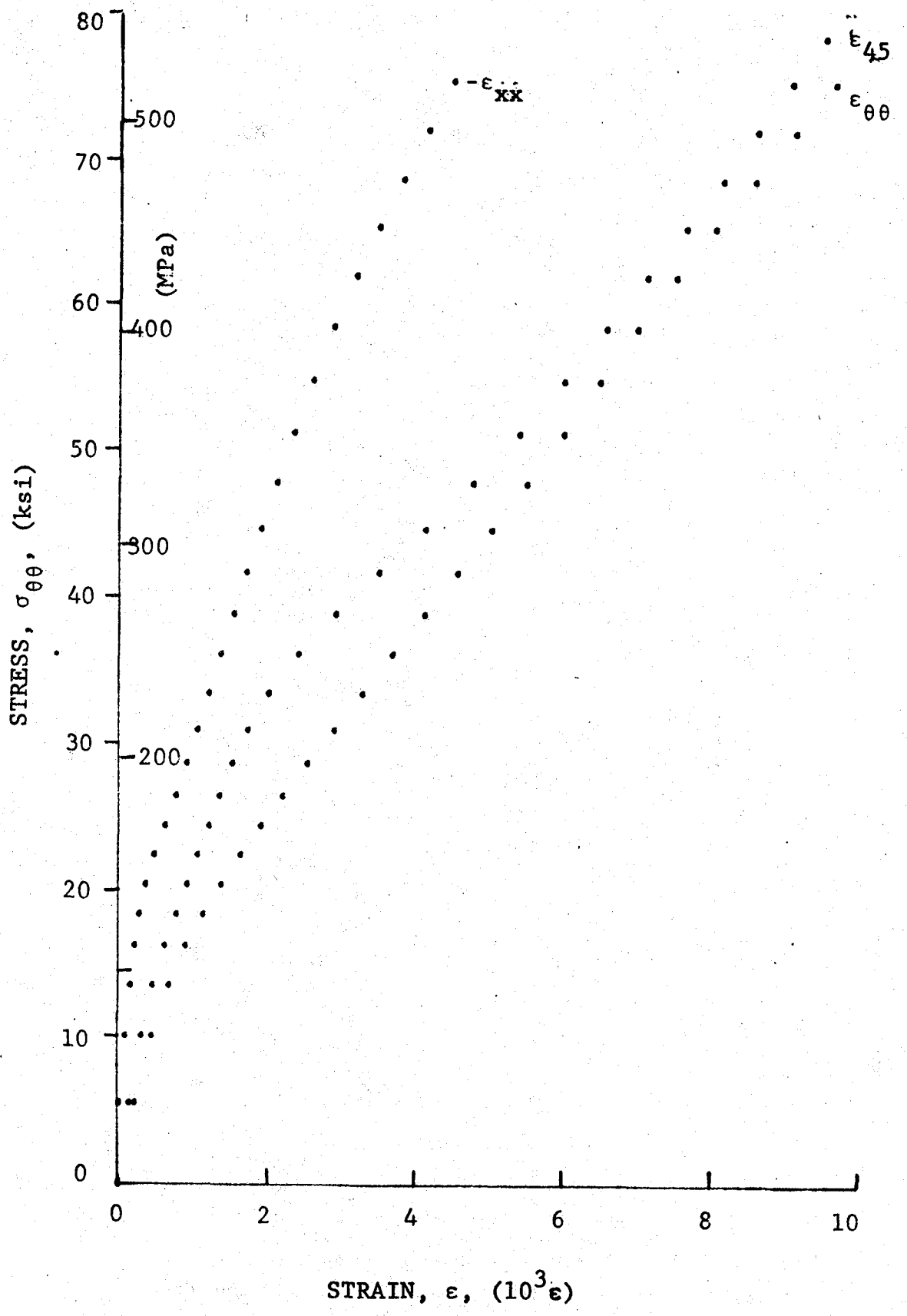

Figure 4-22. Stress-strain curve for dynamically loaded $[22.5_8]$ 80AS/20S/PR288 graphite/S-glass/epoxy ring, for Specimen No. 47-4 (1.56 g pistol powder, $KC\ell O_4$, and aluminum dust).

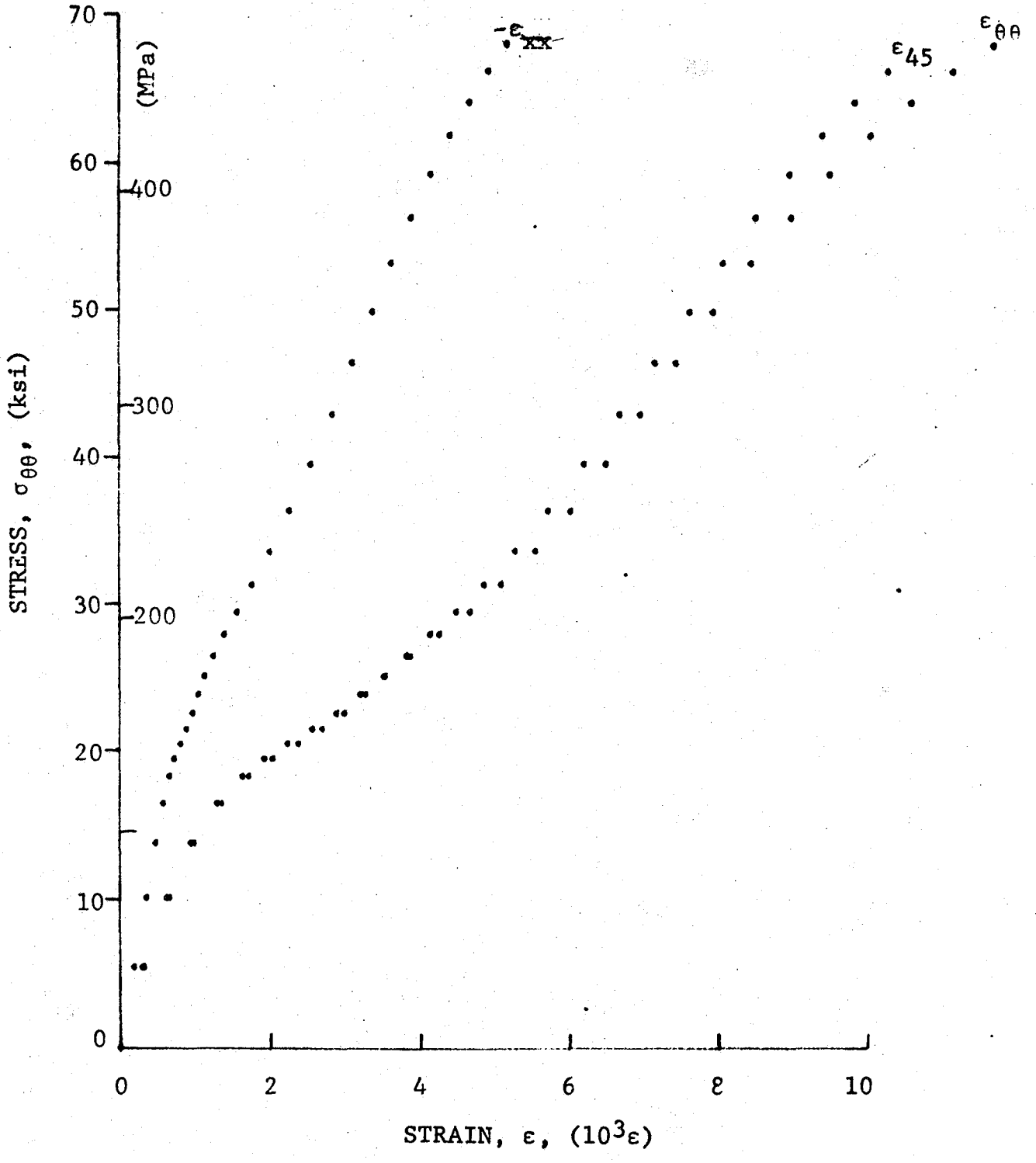

Figure 4-23. Stress-strain curve for dynamically loaded $[22.5_8]$ 80AS/20S/PR288 graphite/S-glass/epoxy ring, Specimen No. 47-5 (1.56 g pistol powder, $KC\ell O_4$, and aluminum dust).

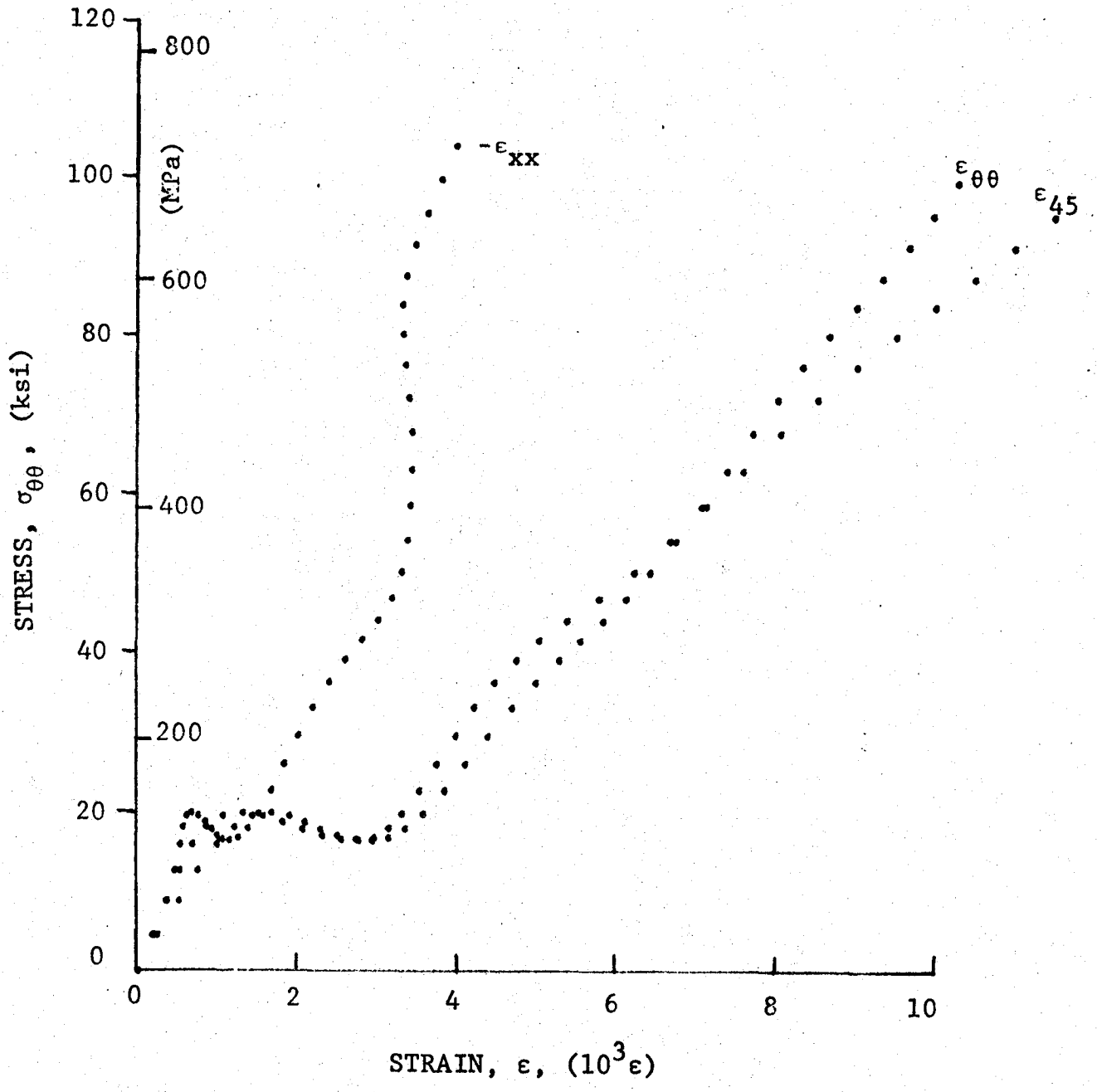

Figure 4-24. Stress-strain curve for dynamically loaded $[22.5_8]$ 80AS/20S/PR288 graphite/S-glass/epoxy ring, Specimen No. 47-6 (1.56 g pistol powder, $KC\ell O_4$, and aluminum dust).

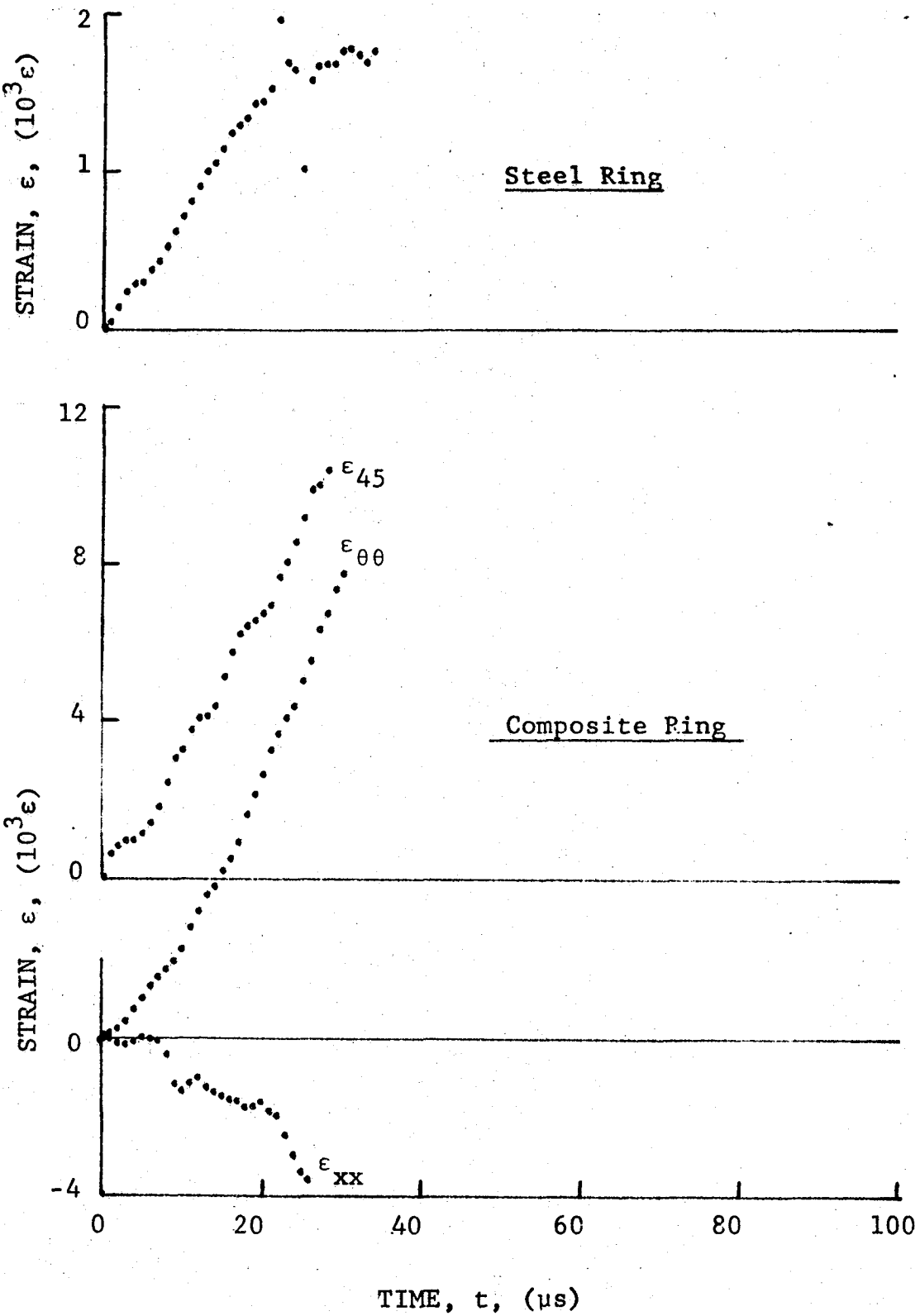

Figure 4-25. Strain records in steel ring and $[30_8]$ SP288/AS graphite/epoxy ring under dynamic loading for Specimen No. 48-4 (1.56 g pistol powder, $KC\ell O_4$, and aluminum dust).

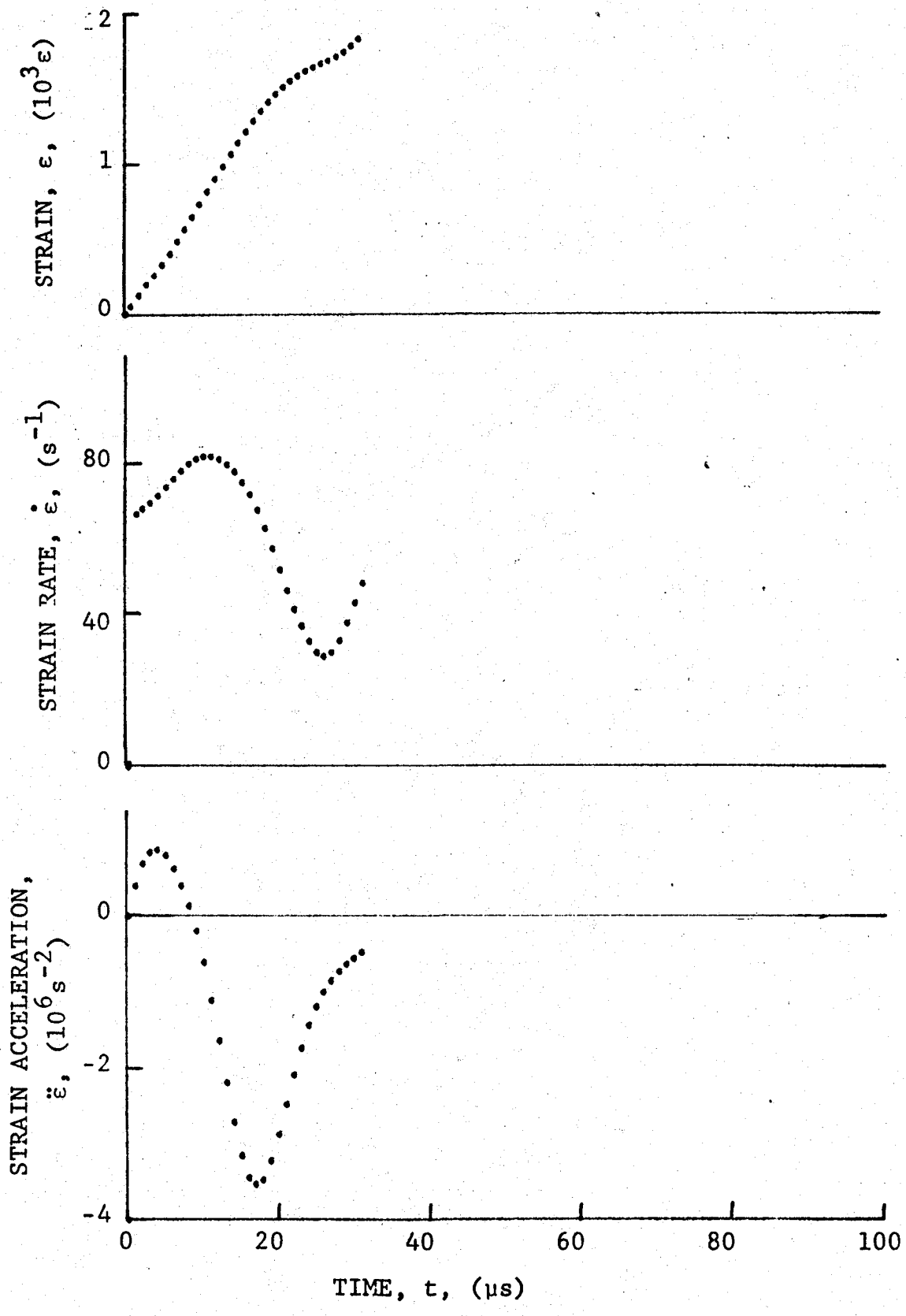

Figure 4-26. Strain and its derivatives in steel ring for Specimen No. 48-4.

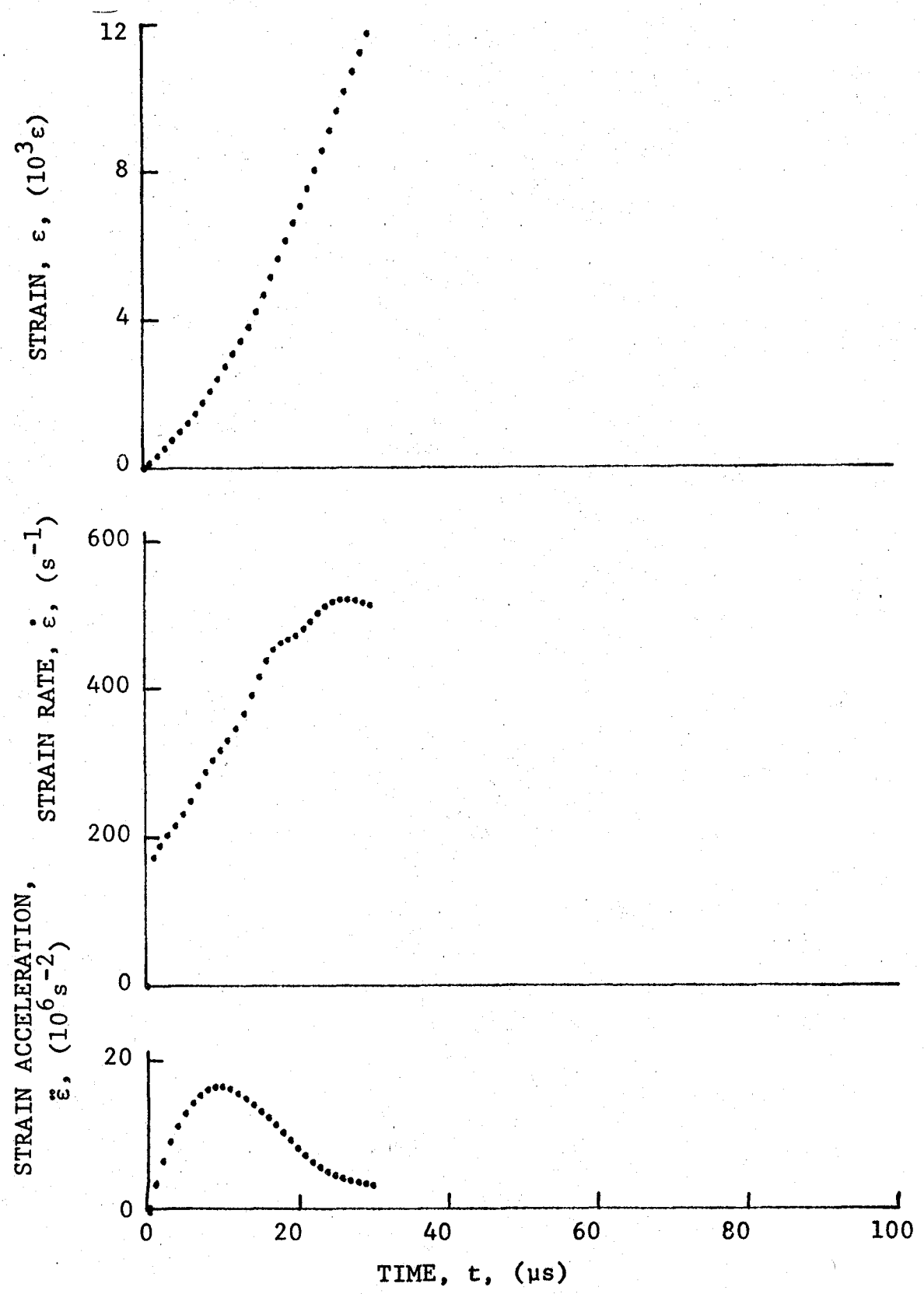

Figure 4-27. Circumferential strain and its derivatives in $[30_8]$ SP288/AS graphite/epoxy ring under dynamic loading for Specimen No. 48-4 (1.56 g pistol powder, $KC\ell O_4$, and aluminum dust).

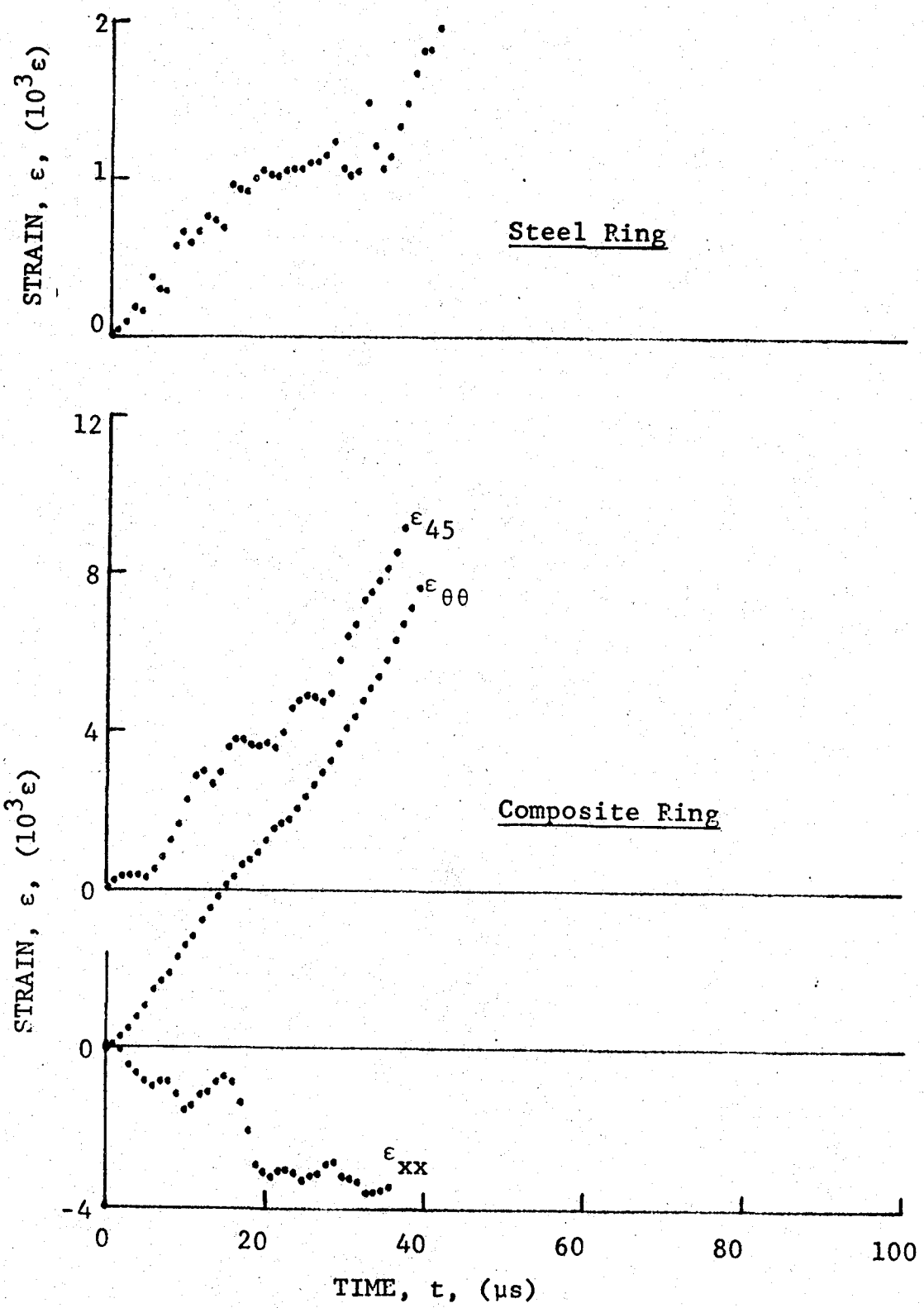

Figure 4-28. Strain records in steel ring and $[30_8]$ SP288/AS graphite/epoxy ring under dynamic loading for Specimen No. 48-5 (1.56 g pistol powder, $KC\ell O_4$, and aluminum dust).

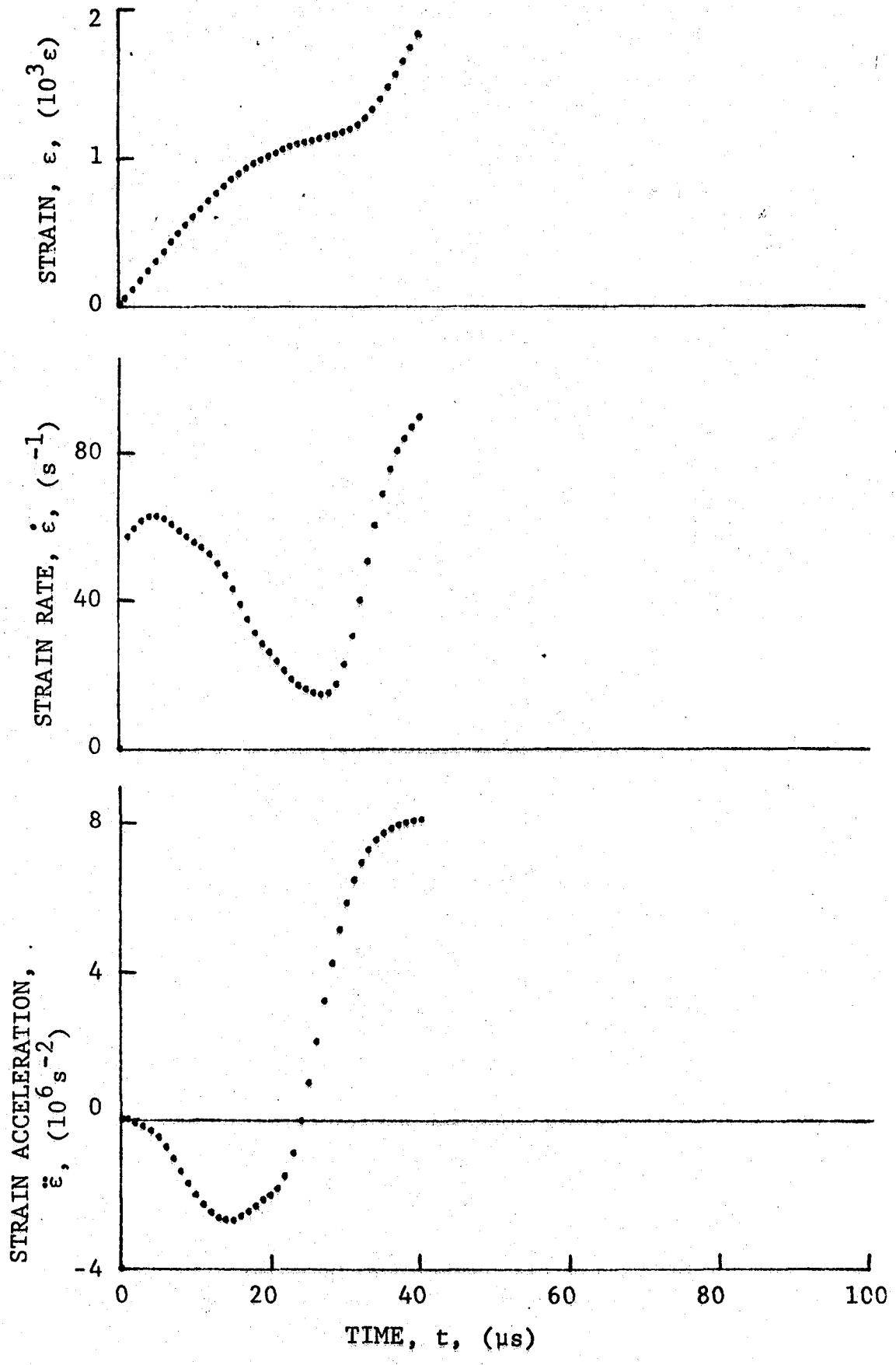

Figure 4-29. Strain and its derivatives in steel ring for Specimen No. 48-5.

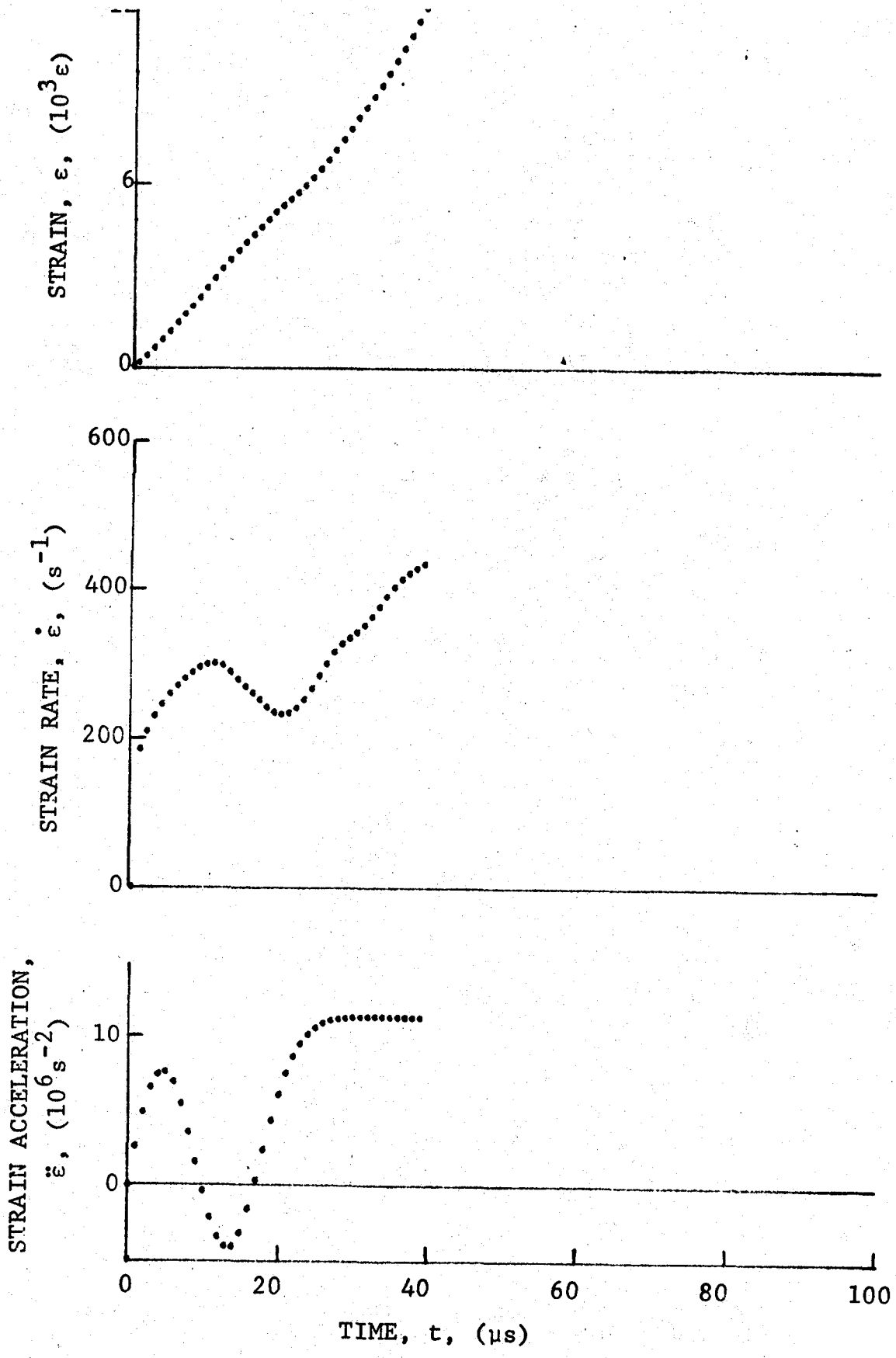

Figure 4-30. Circumferential strain and its derivatives in [30_8] SP288/AS graphite/epoxy ring under dynamic loading for Specimen No. 48-5 (1.56 g pistol powder, $KC\ell O_4$, and aluminum dust).

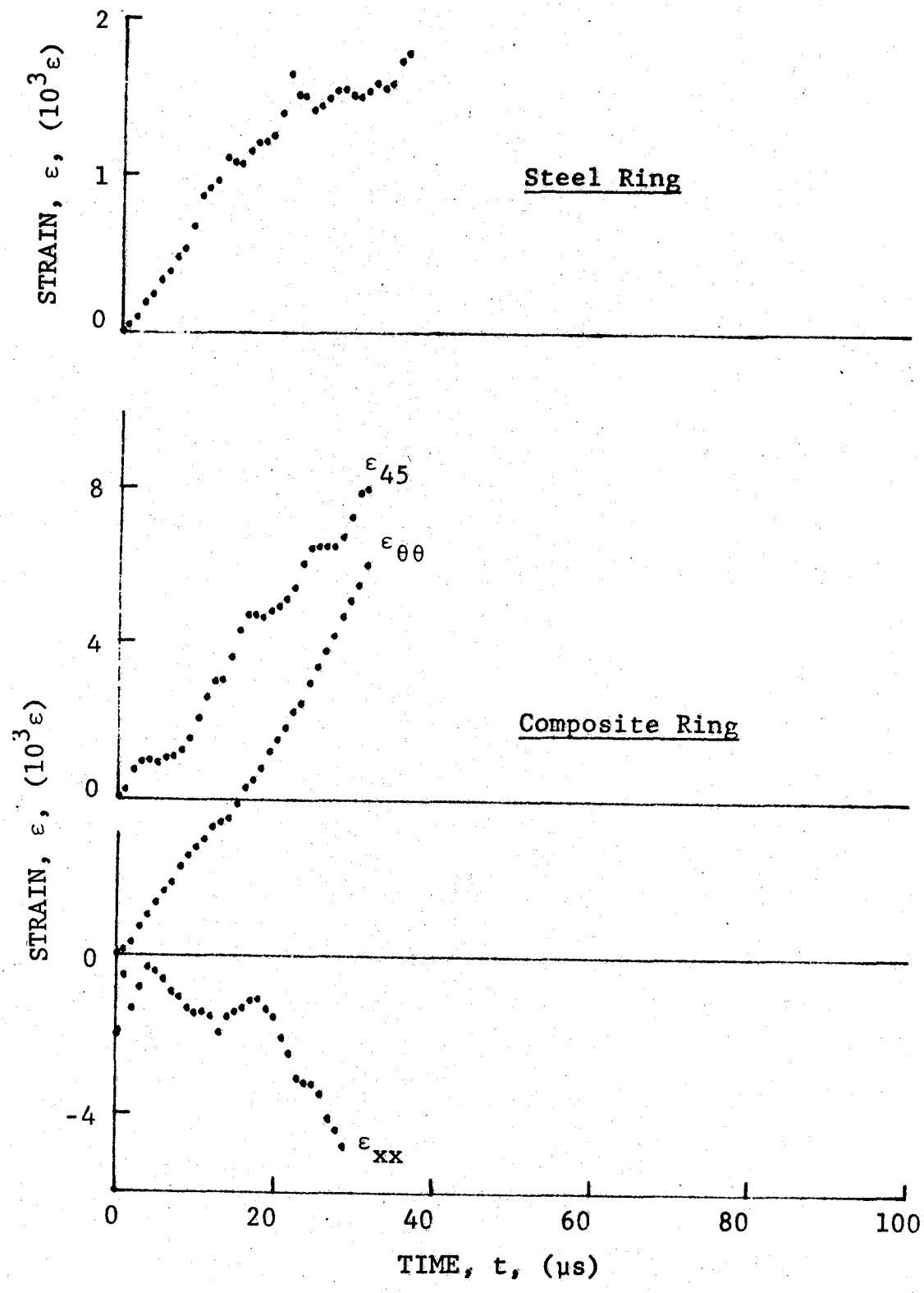

Figure 4-31. Strain records in steel ring and [30_8] SP288/AS graphite/epoxy ring under dynamic loading for Specimen No. 48-6 (1.56 g pistol powder, $KC\ell O_4$, and aluminum dust).

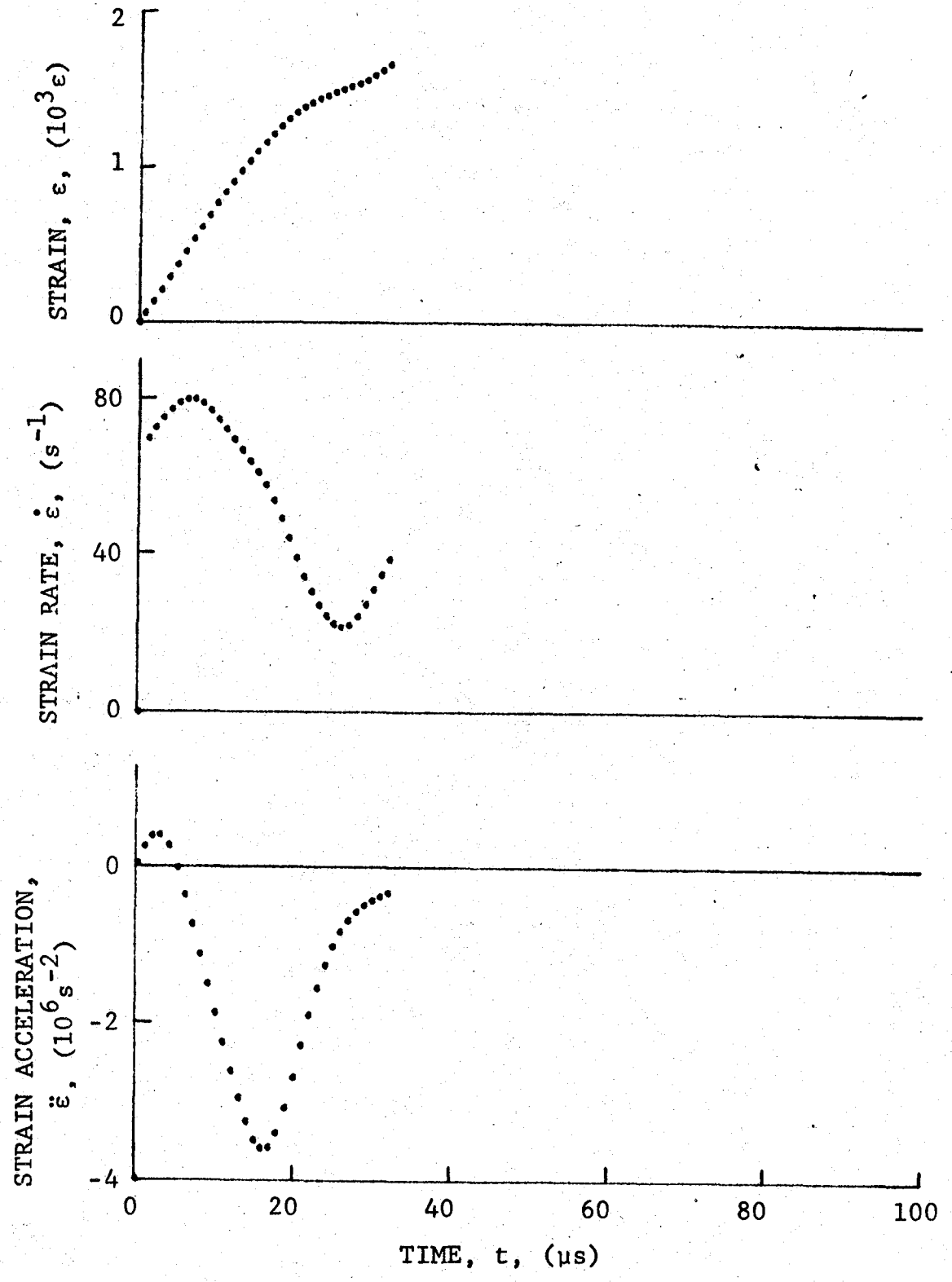

Figure 4-32. Strain and its derivatives in steel ring for Specimen No. 48-6.

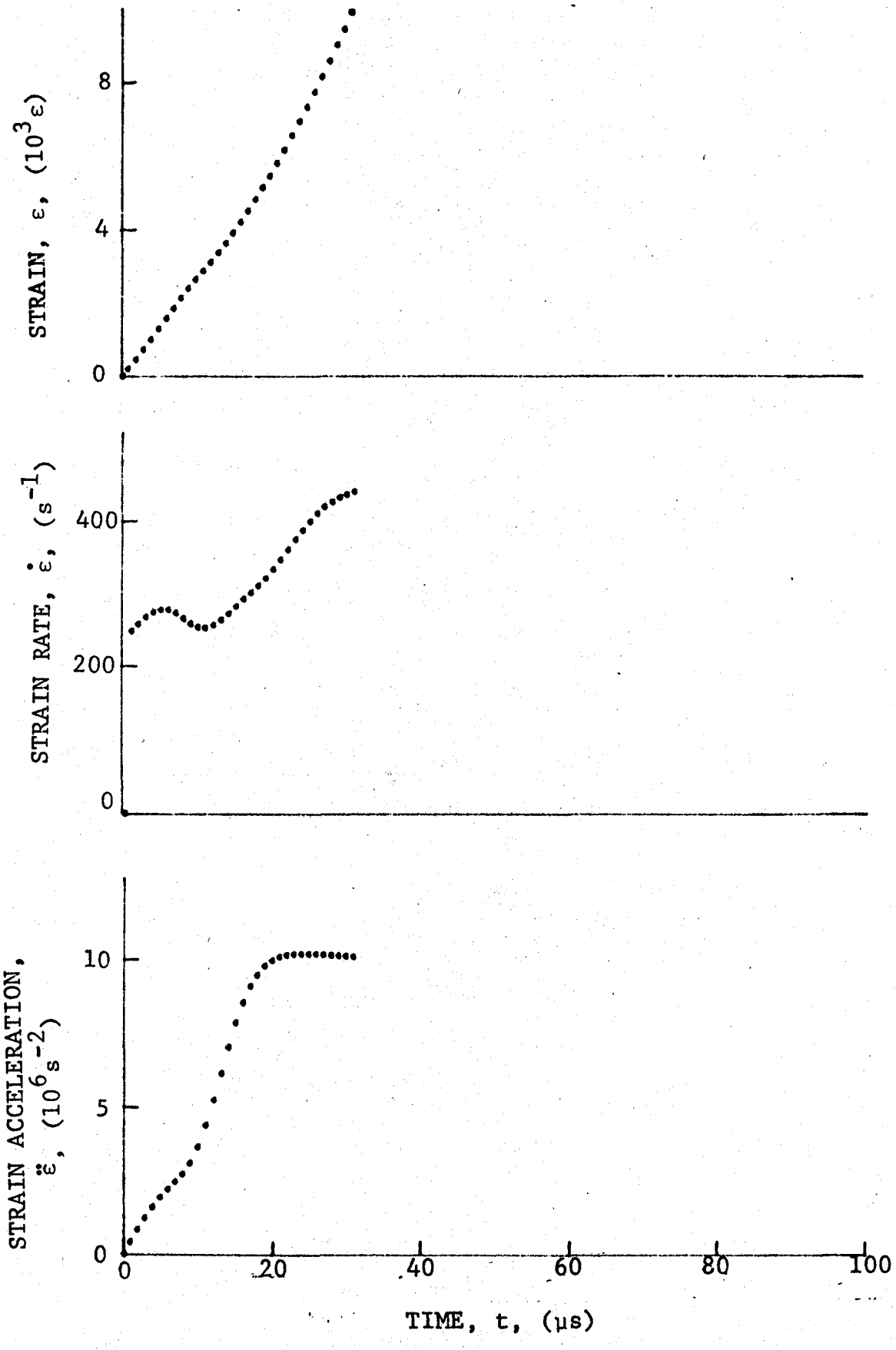

Figure 4-33. Circumferential strain and its derivatives in $[30_8]$ SP288/AS graphite/epoxy ring under dynamic loading for Specimen No. 48-6 (1.56 g pistol powder, $KC\ell O_4$, and aluminum dust).

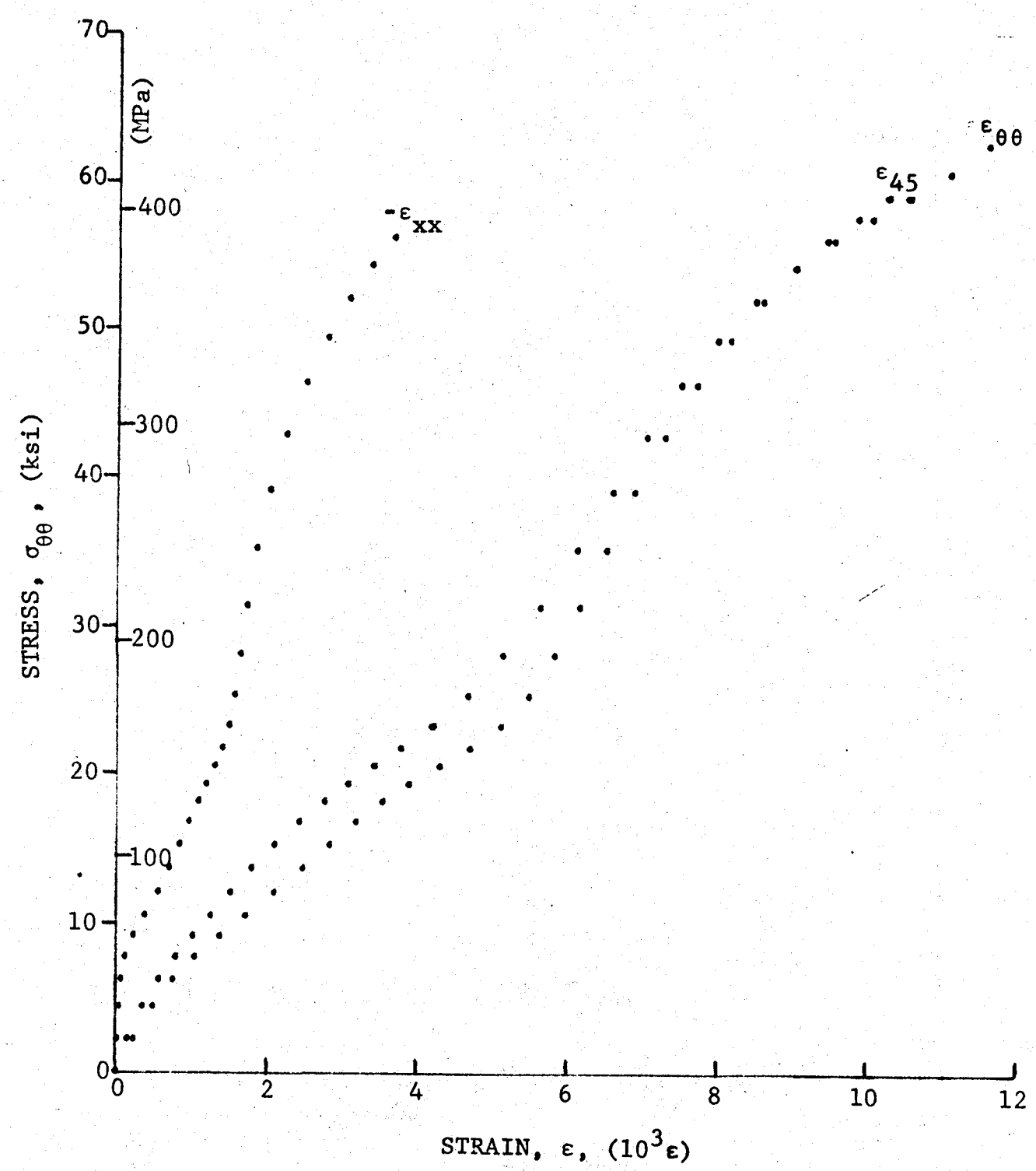

Figure 4-34. Stress-strain curve for dynamically loaded $[30_8]$ SP288/AS graphite/epoxy ring, Specimen No. 48-4 (1.56 g pistol powder, $KC\ell O_4$, and aluminum dust).

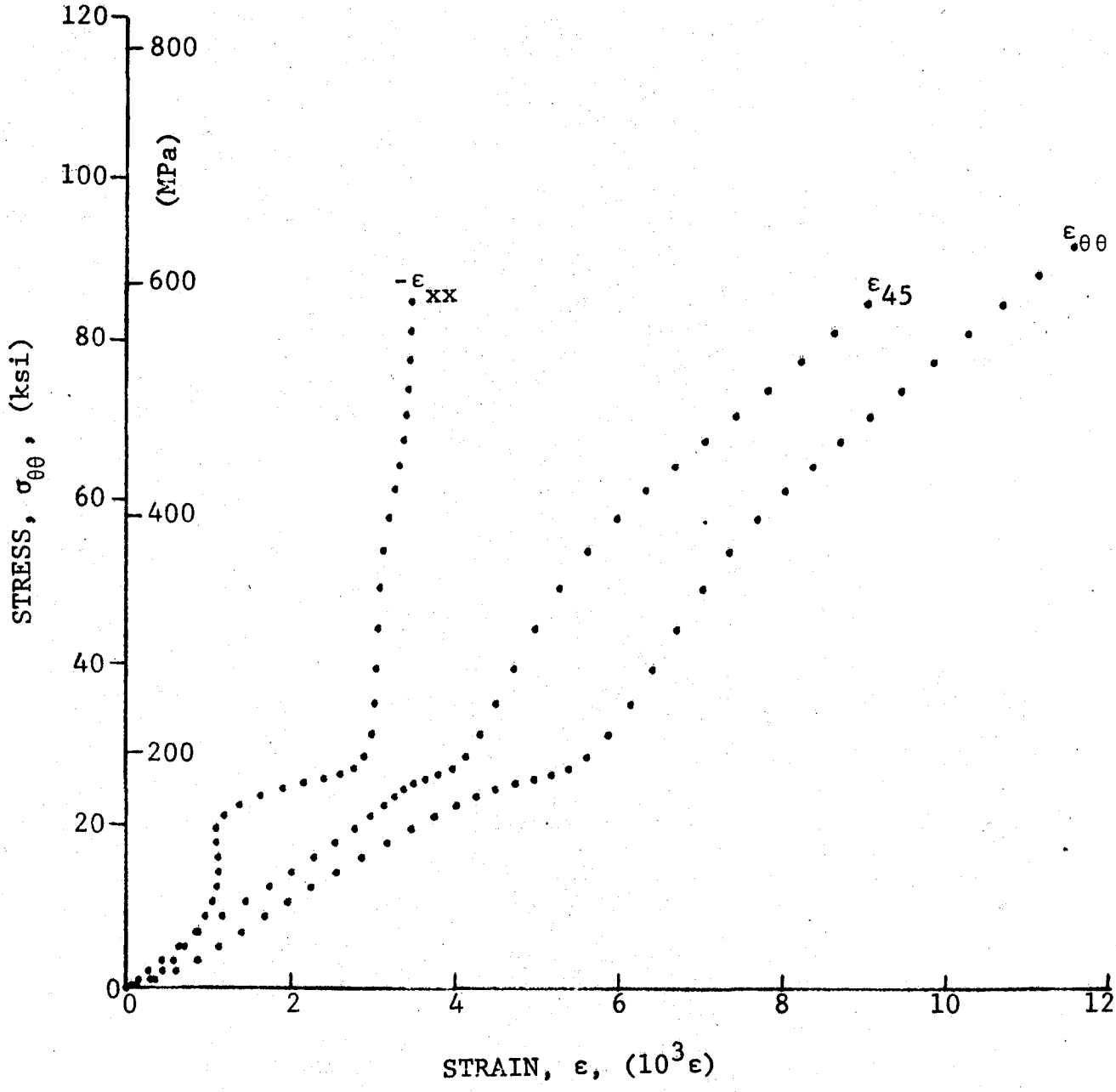

Figure 4-35. Stress-strain curve for dynamically loaded $[30_8]$ SP288/AS graphite/epoxy ring, Specimen No. 48-5 (1.56 g pistol powder, $KC\ell O_4$, and aluminum dust).

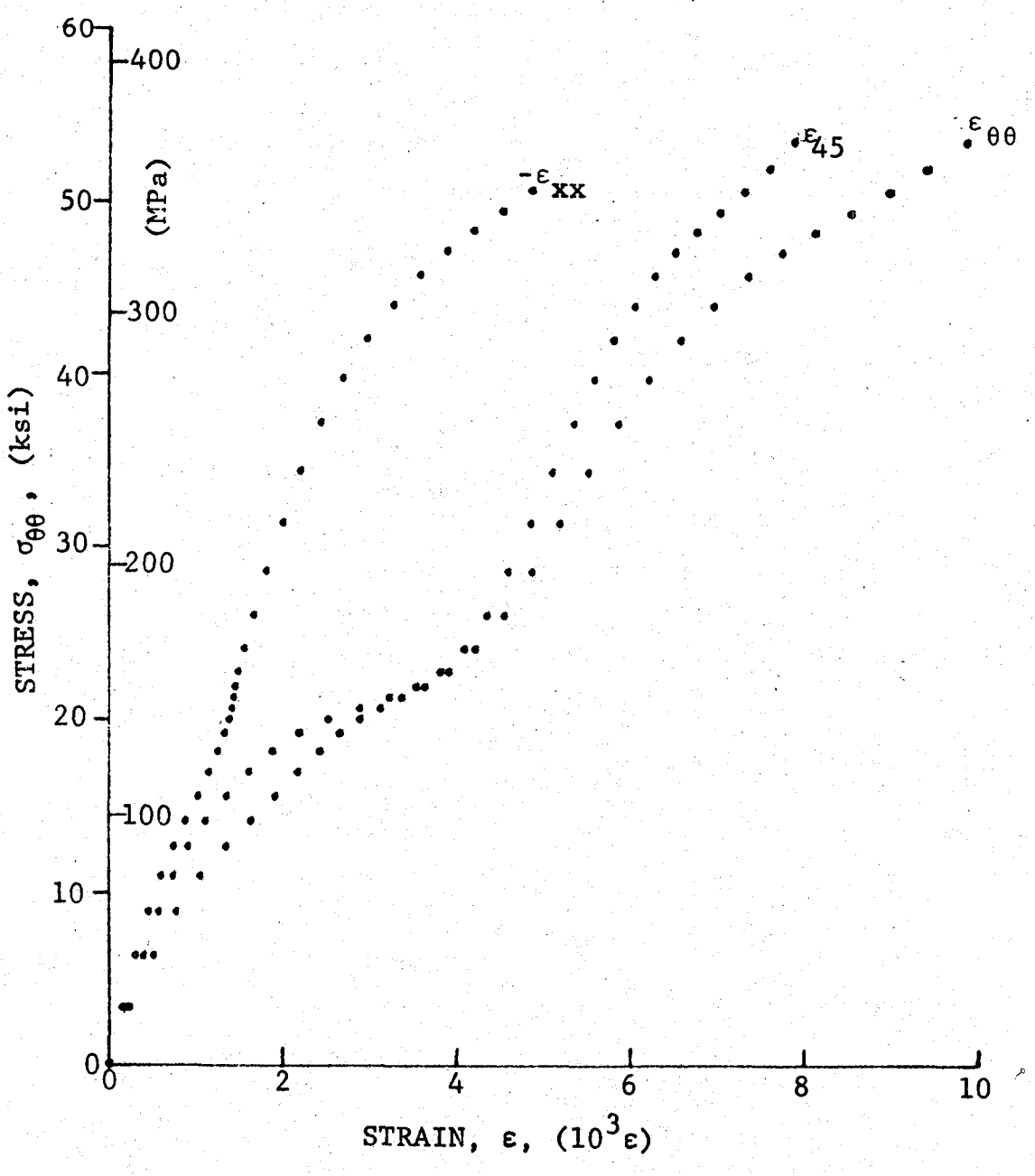

Figure 4-36. Stress-strain curve for dynamically loaded $[30_8]$ SP288/AS graphite/epoxy ring, Specimen No. 48-6 (1.56 g pistol powder, $KC\ell O_4$, and aluminum dust).

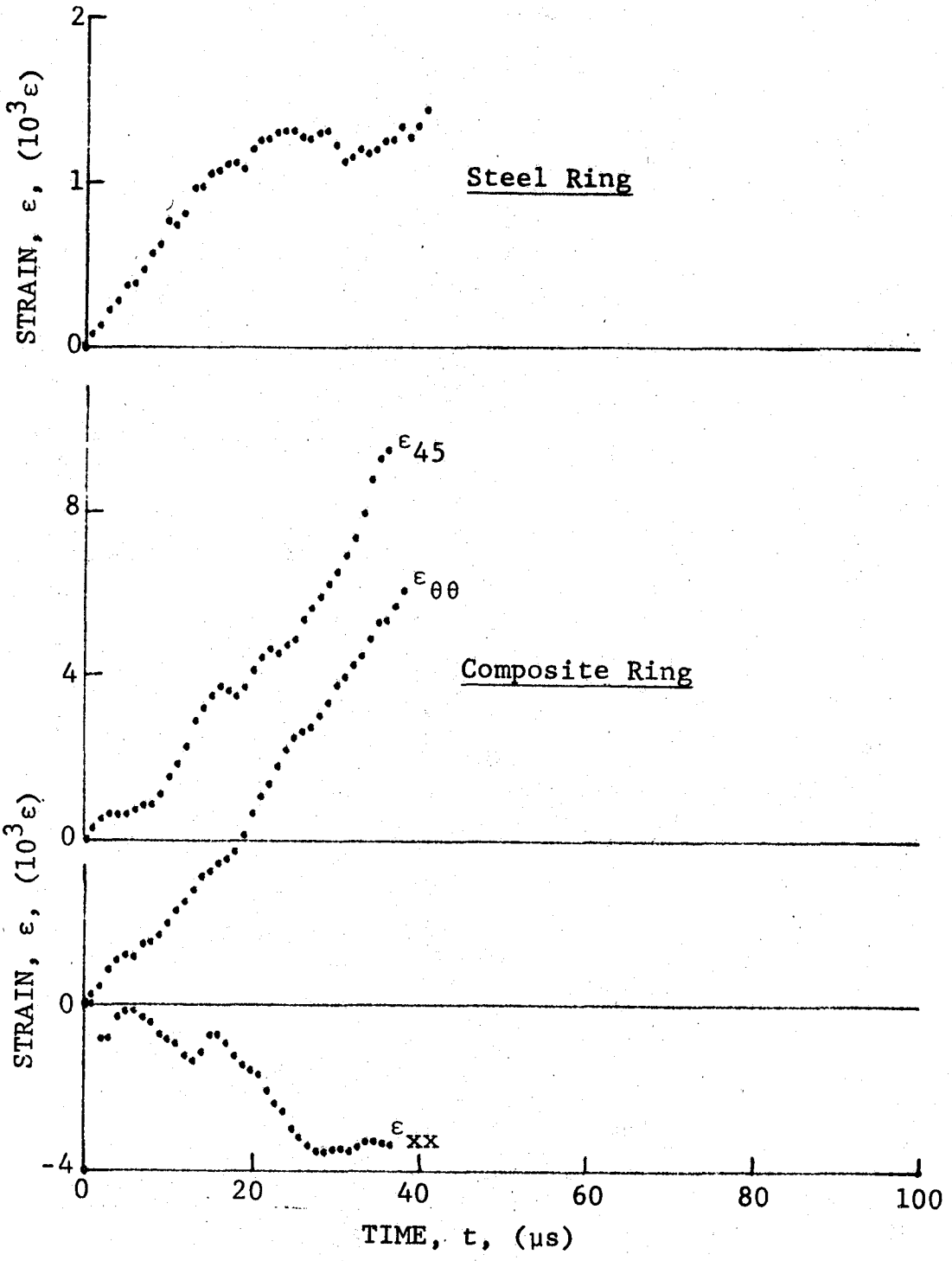

Figure 4-37. Strain records in steel ring and 80AS/20S/PR288 [30_8] graphite/S-glass/epoxy ring under dynamic loading for Specimen No. 49-5 (1.56 g pistol powder, $KC\ell O_4$, and aluminum dust).

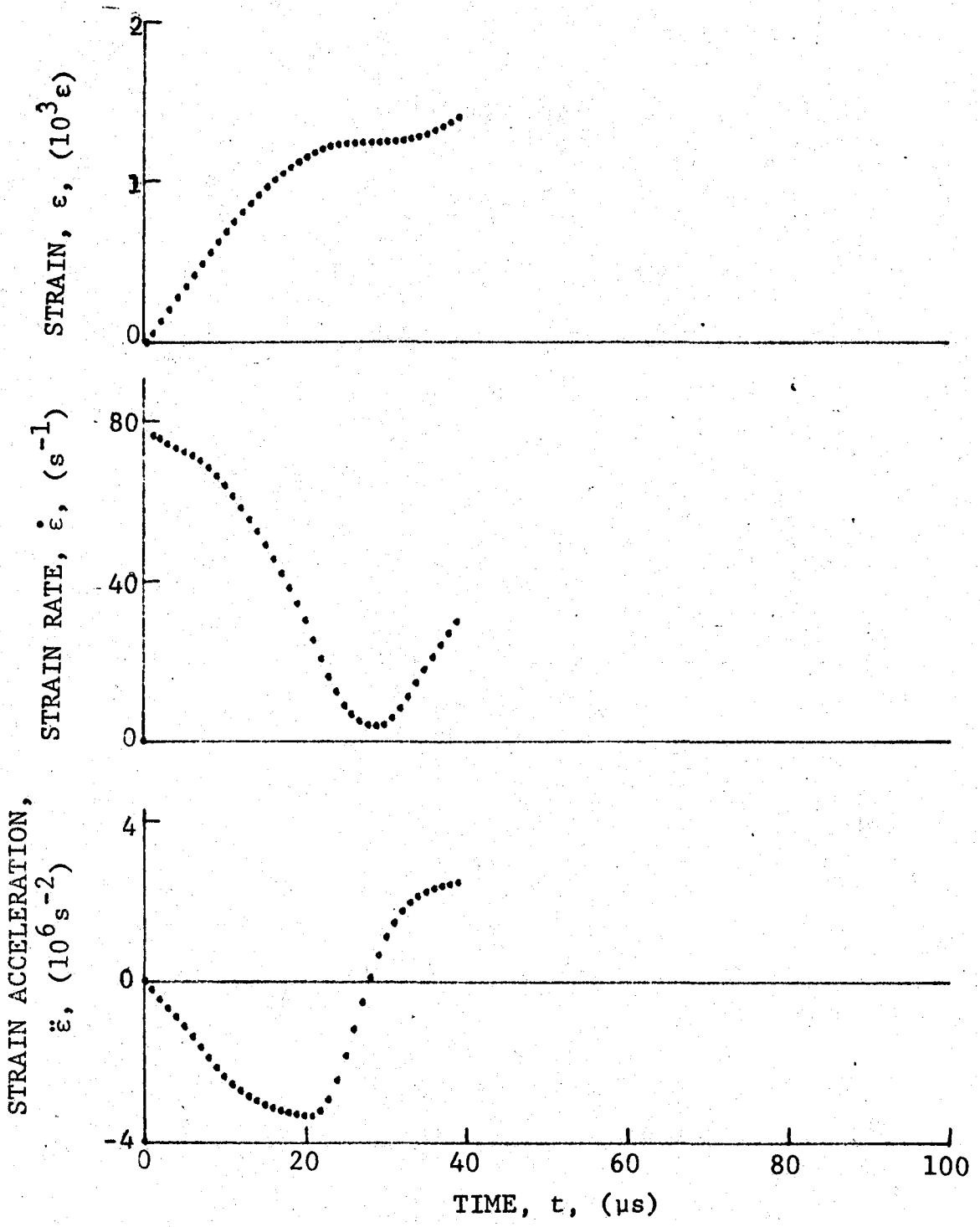

Figure 4-38. Strain and its derivatives in steel ring for Specimen No. 49-5.

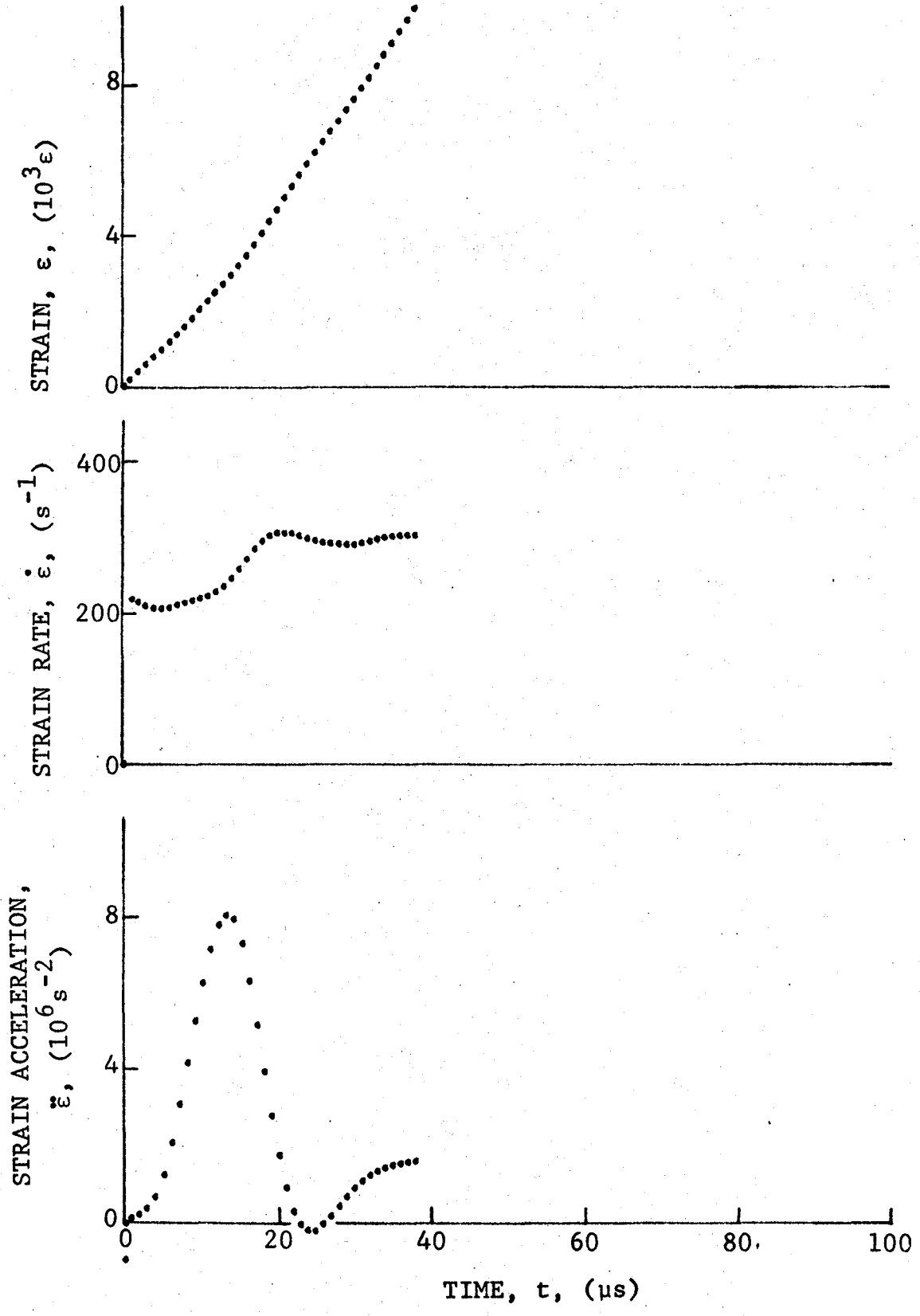

Figure 4-39. Circumferential strain and its derivatives in 80AS/20S/PR288 [30_8] graphite/S-glass/epoxy ring under dynamic loading for Specimen No. 49-5 (1.56 g pistol powder, $KC\ell O_4$, and aluminum dust).

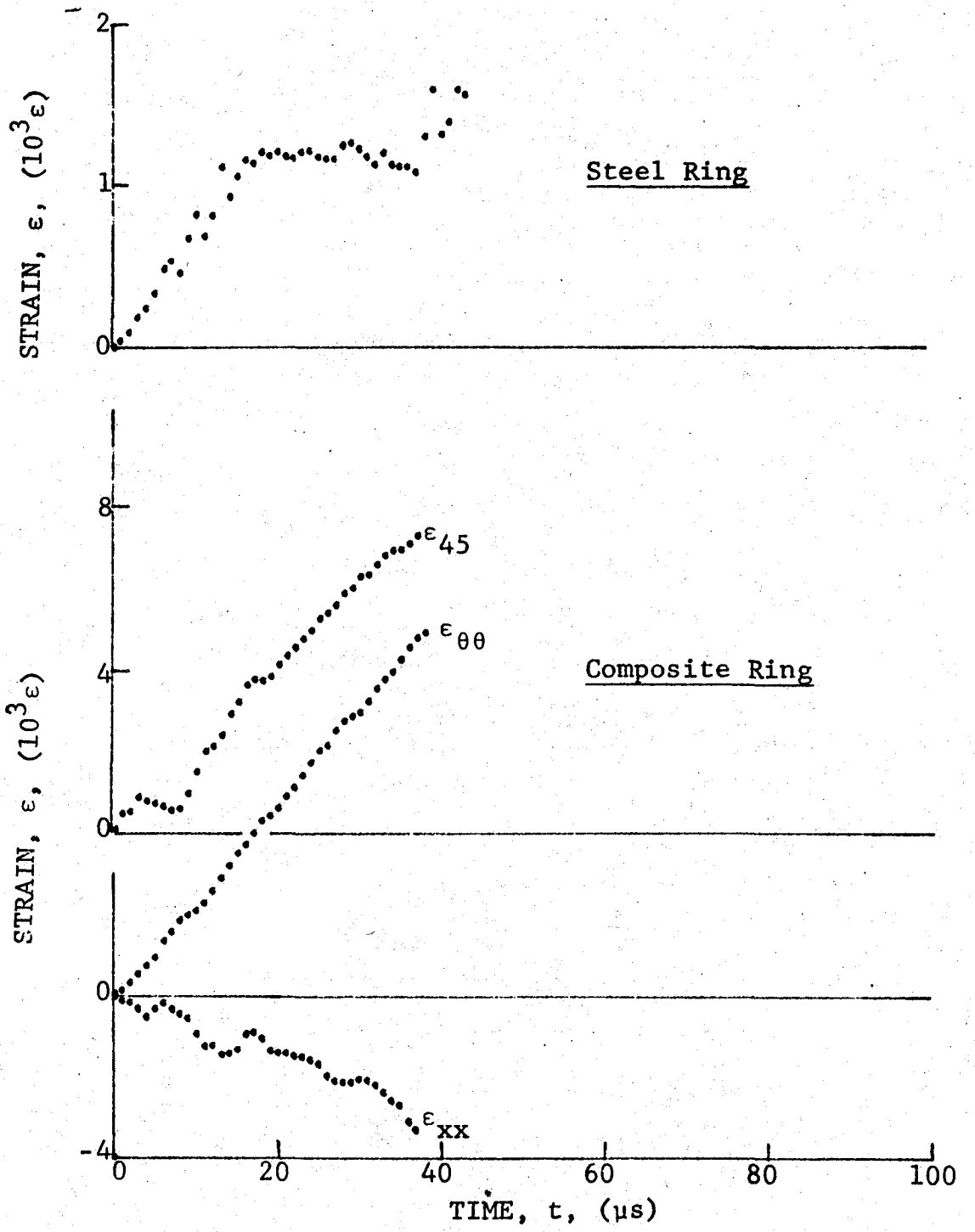

Figure 4-40. Strain records in steel ring and 80AS/20S/PR288 [30_8] graphite/S-glass/epoxy ring under dynamic loading for Specimen No. 49-6 (1.56 g pistol powder, $KC\ell O_4$, and aluminum dust).

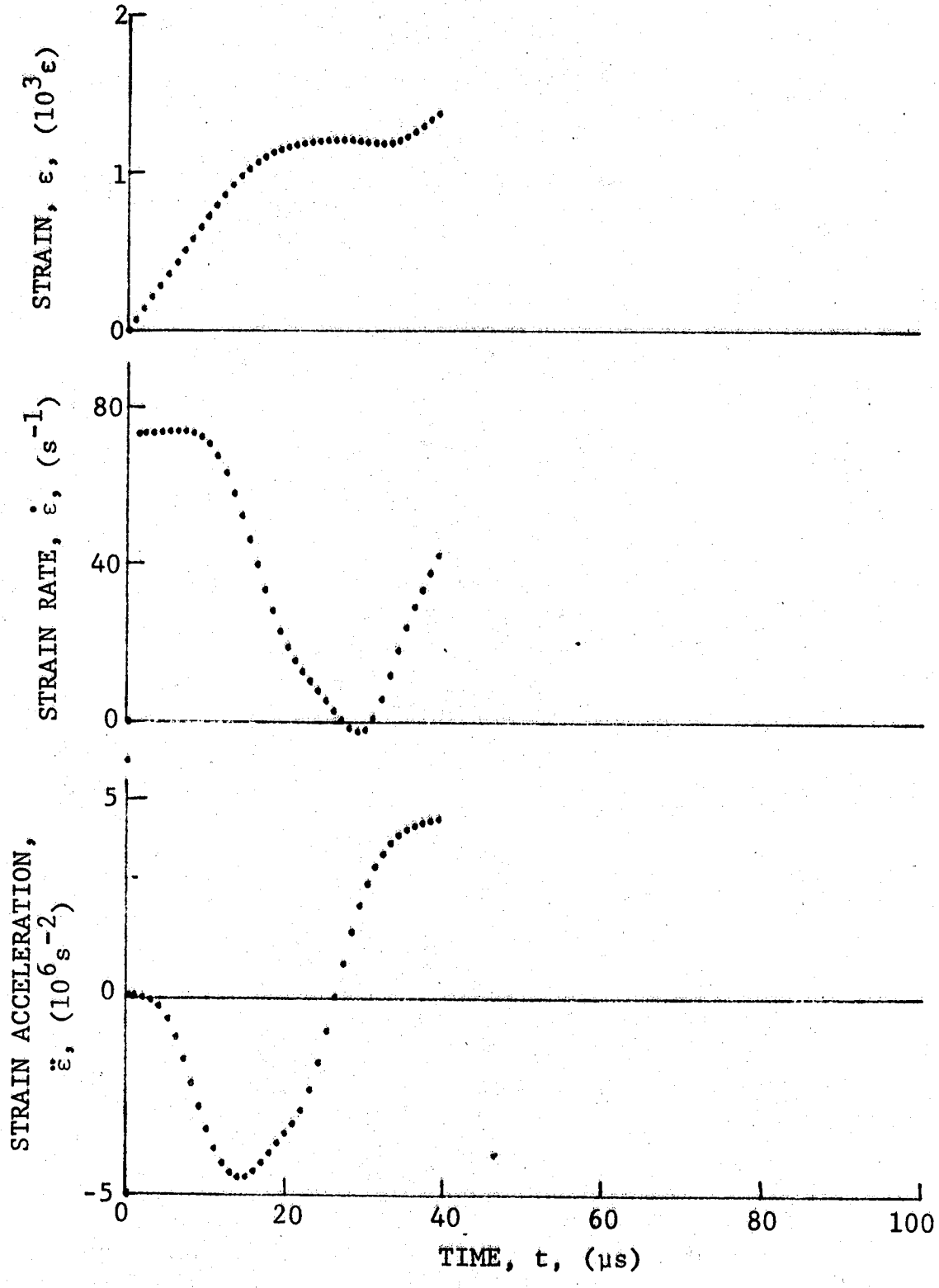

Figure 4-41. Strain and its derivatives in steel ring for Specimen No. 49-6.

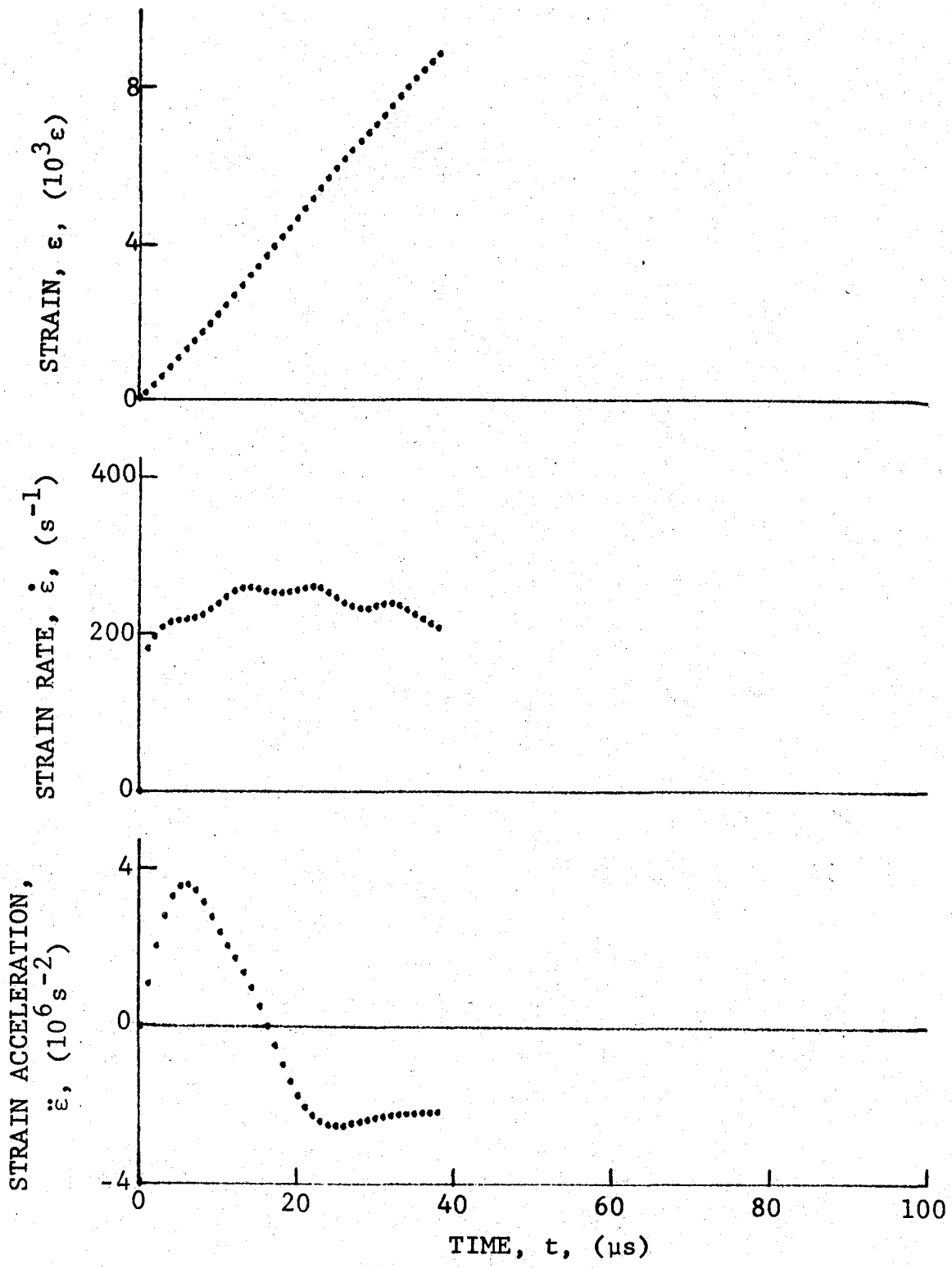

Figure 4-42. Circumferential strain and its derivatives in 80AS/20S/PR288 [30_8] graphite/S-glass/epoxy ring under dynamic loading for Specimen No. 49-6 (1.56 g pistol powder, $KC\ell O_4$, and aluminum dust).

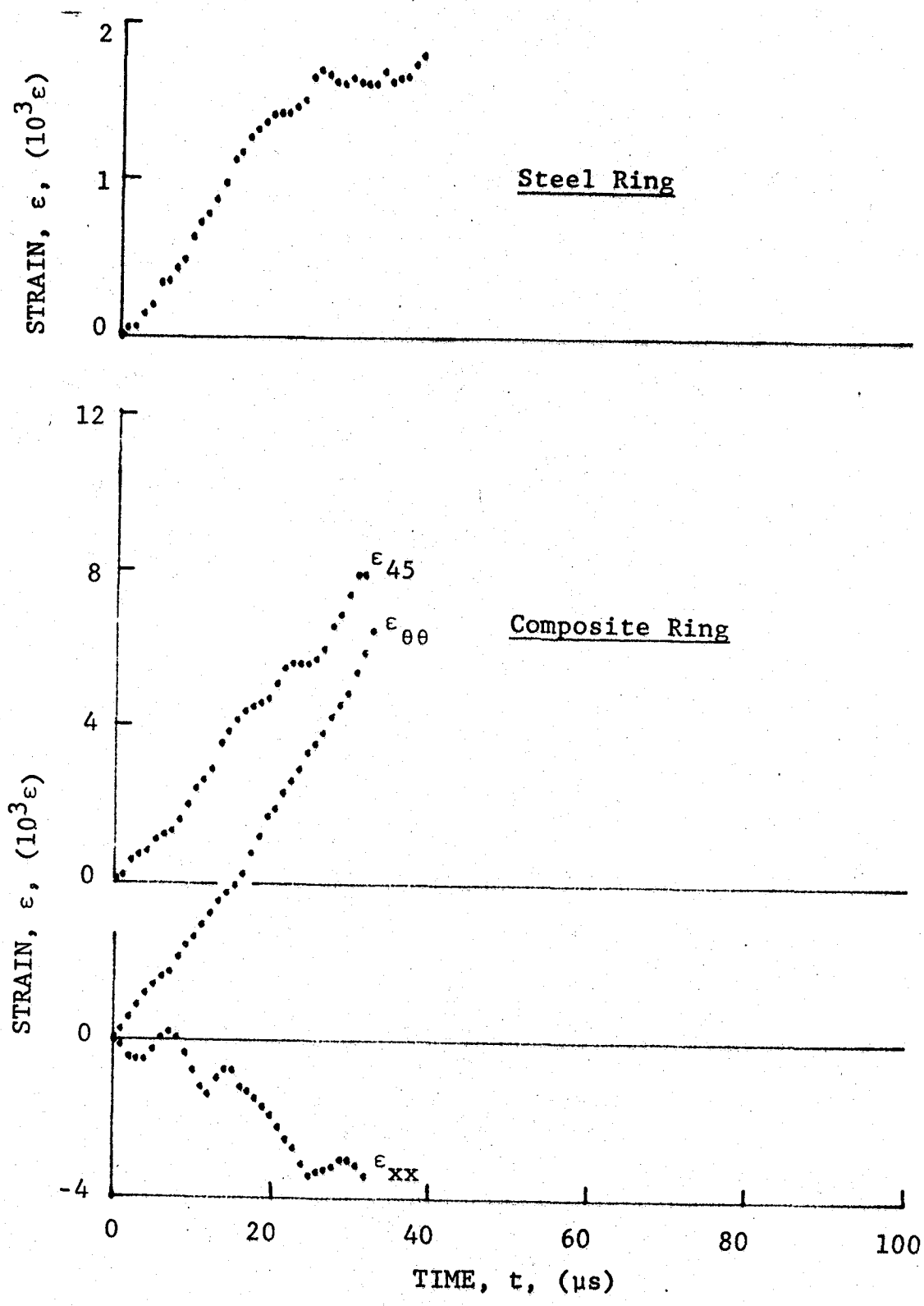

Figure 4-43. Strain records in steel ring and 80AS/20S/PR288 [30_8] graphite-S-glass/epoxy ring under dynamic loading for Specimen No. 49-7 (1.56 g pistol powder, $KC\ell O_4$, and aluminum dust).

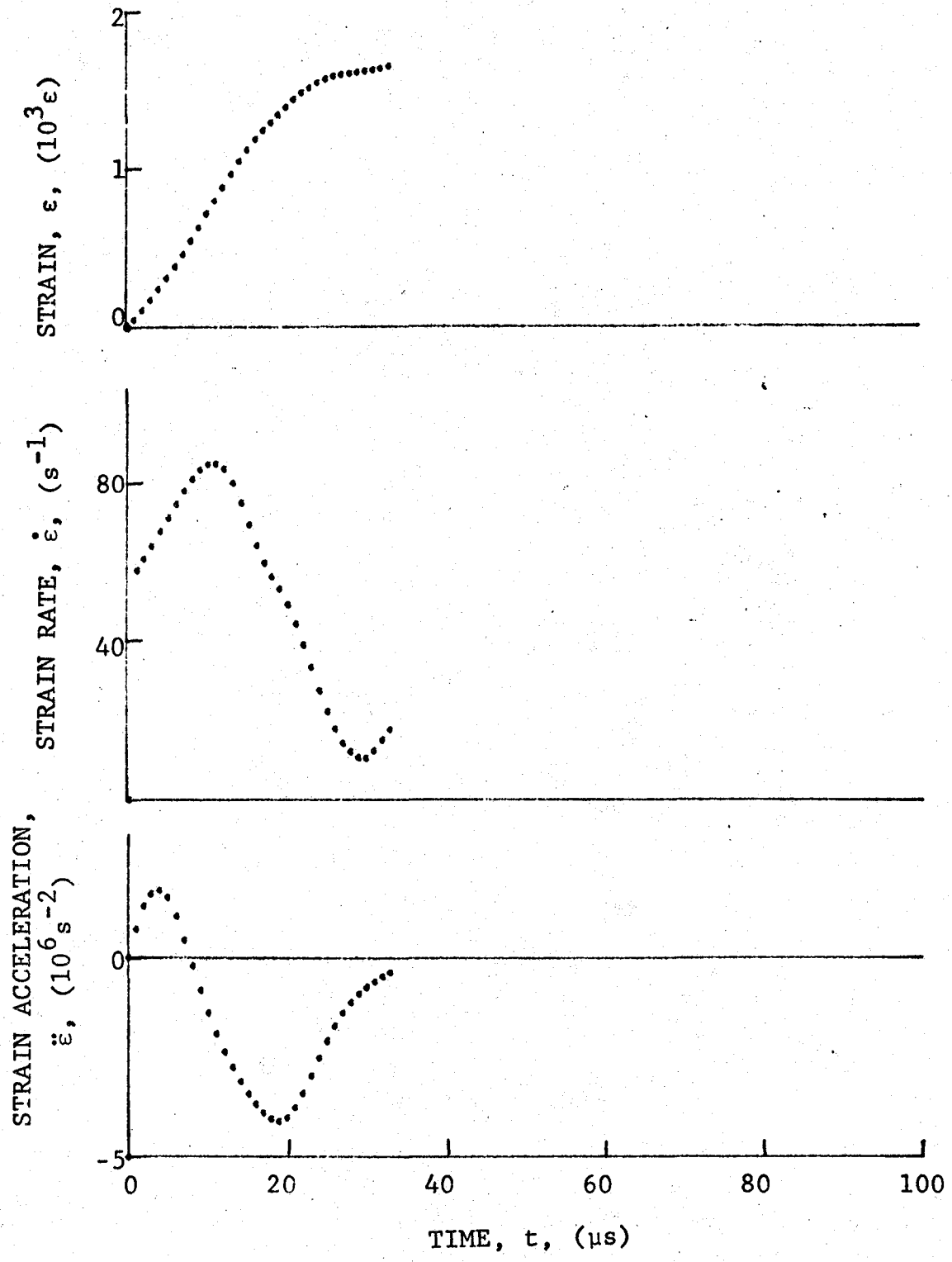

Figure 4-44. Strain and its derivatives in steel ring for Specimen No. 49-7.

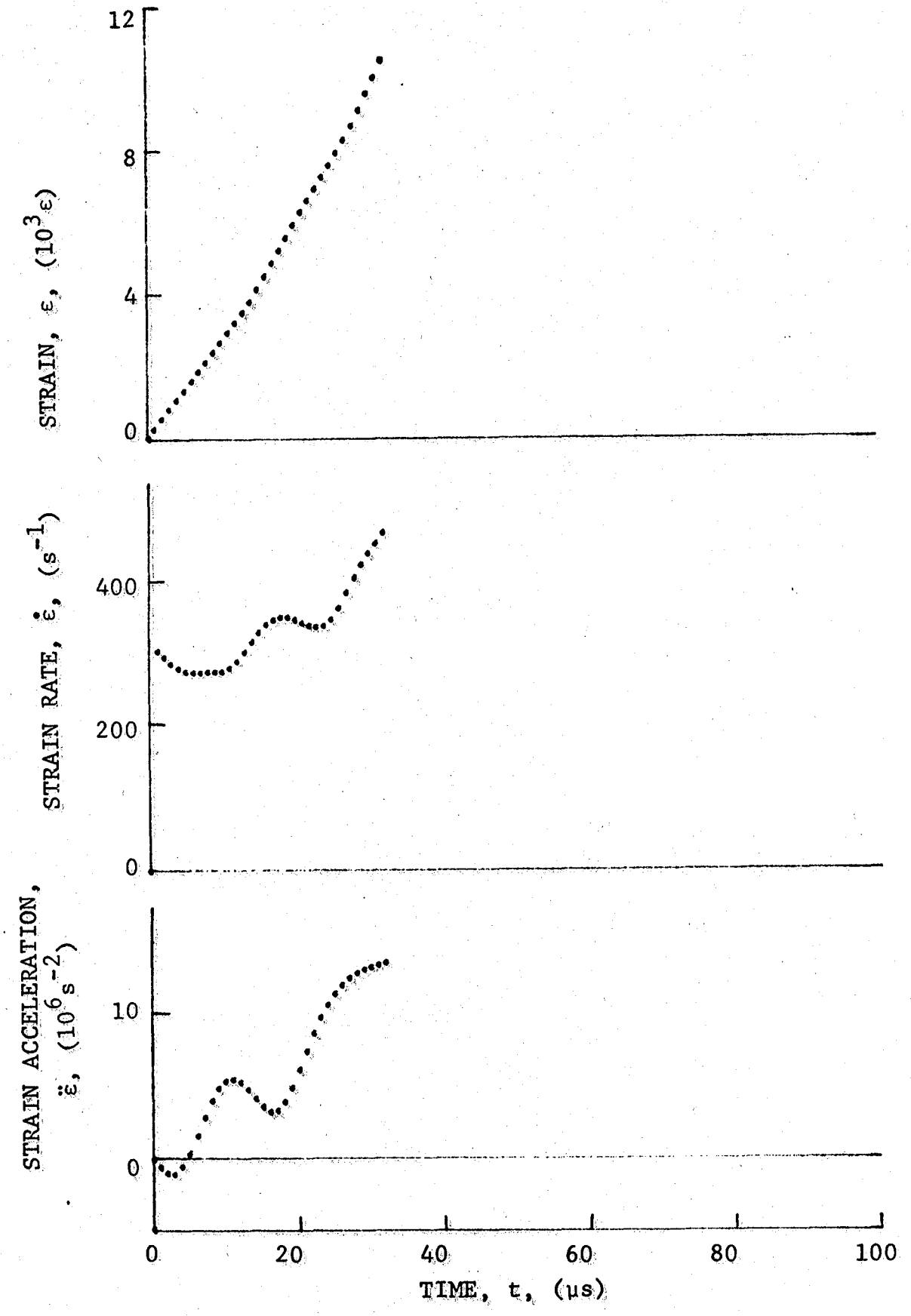

Figure 4-45. Circumferential strain and its derivatives in 80AS/20S/PR288 [30_8] graphite/S-glass/epoxy ring under dynamic loading for Specimen No. 49-7 (1.56 g pistol powder, $KC\ell O_4$, and aluminum dust).

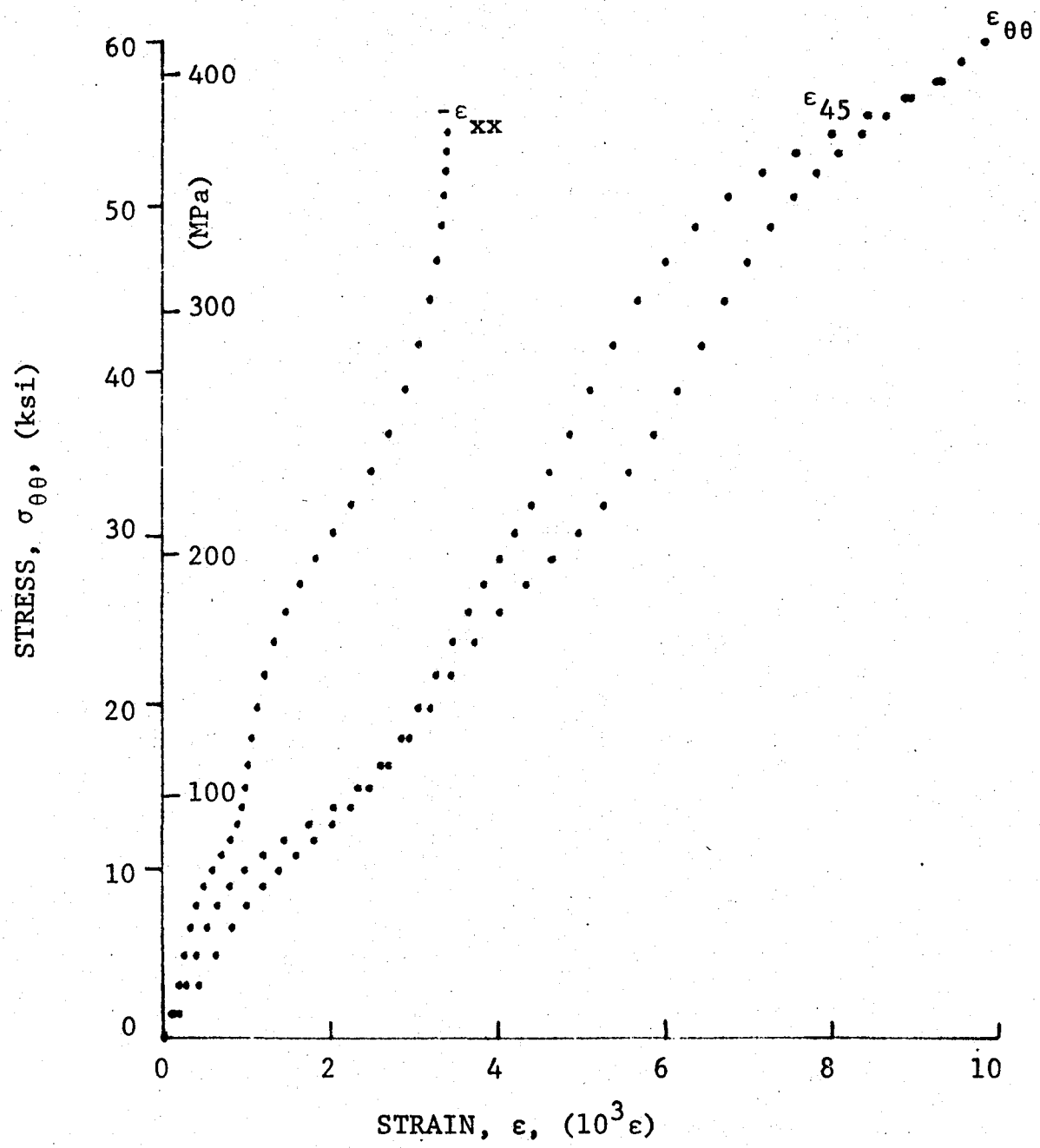

Figure 4-46. Stress-strain curve for dynamically loaded 80AS/20S/PR288 $[30_8]$ graphite/S-glass/epoxy ring, Specimen No. 49-5 (1.56 g pistol powder, $KC\ell O_4$, and aluminum dust).

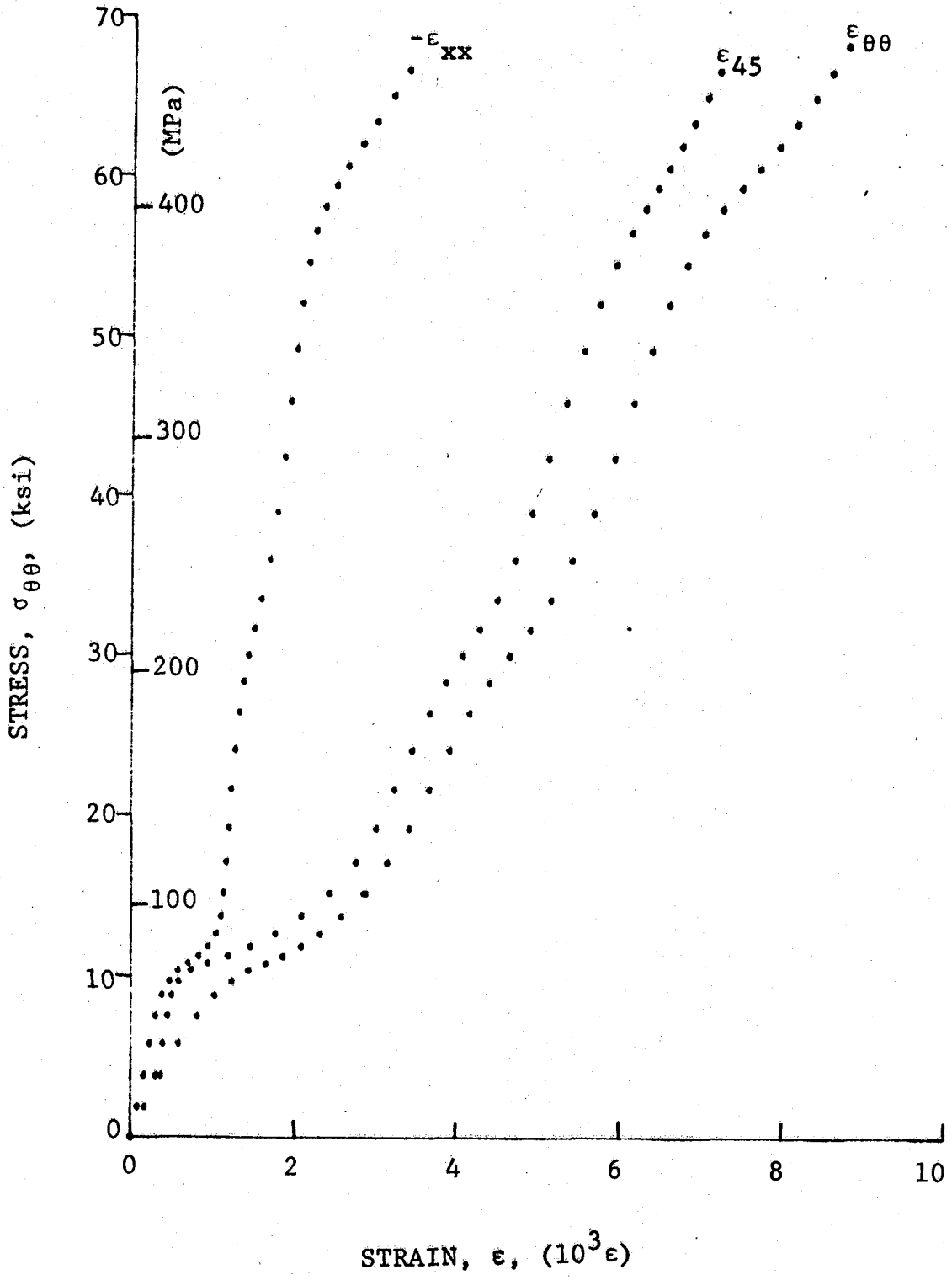

Figure 4-47. Stress-strain curve for dynamically loaded 80AS/20S/PR288 [30_8] graphite/S-glass/epoxy ring, Specimen No. 49-6 (1.56 g pistol powder, $KC\ell O_4$, and aluminum dust).

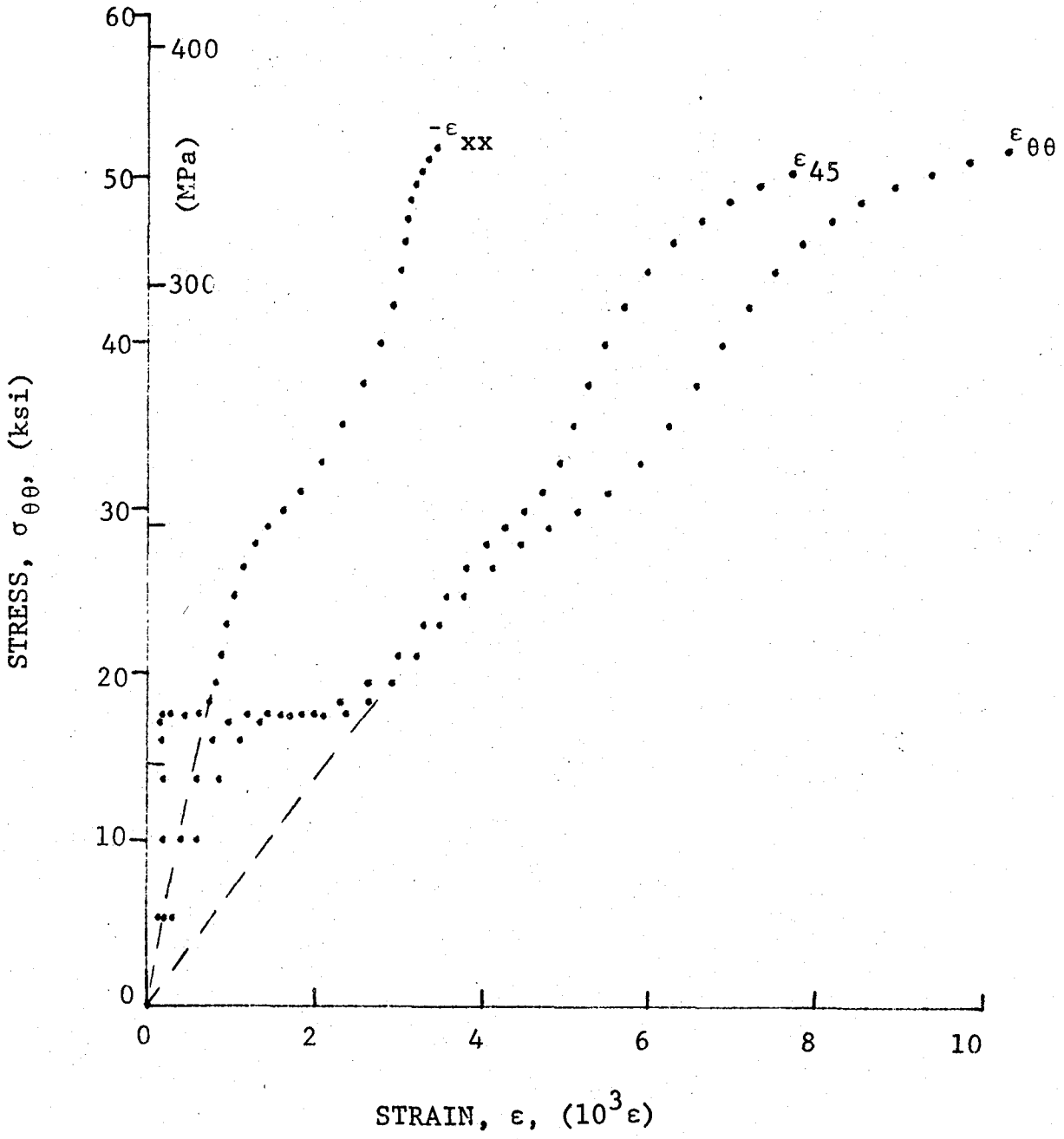

Figure 4-48. Stress-strain curve for dynamically loaded 80AS/20S/PR288 [30_8] graphite/S-glass/epoxy ring, Specimen No. 49-7 (1.56 g pistol powder, $KC\ell O_4$, and aluminum dust).

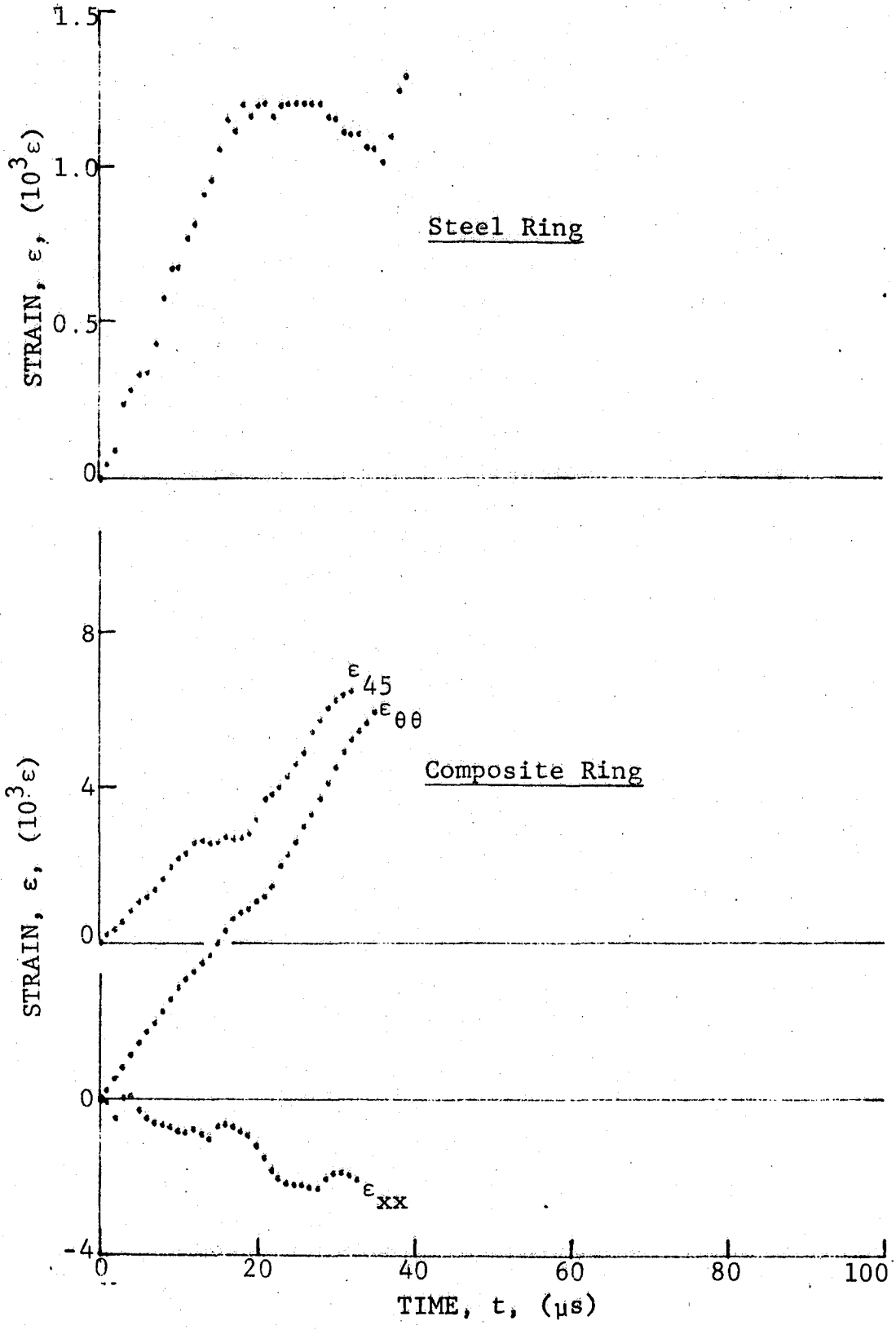

Figure 4-49. Strain records in steel ring and $[45_8]$ SP288/AS graphite/epoxy ring under dynamic loading for Specimen No. 50-4 (1.56 g pistol powder, $KClO_4$, and aluminum dust).

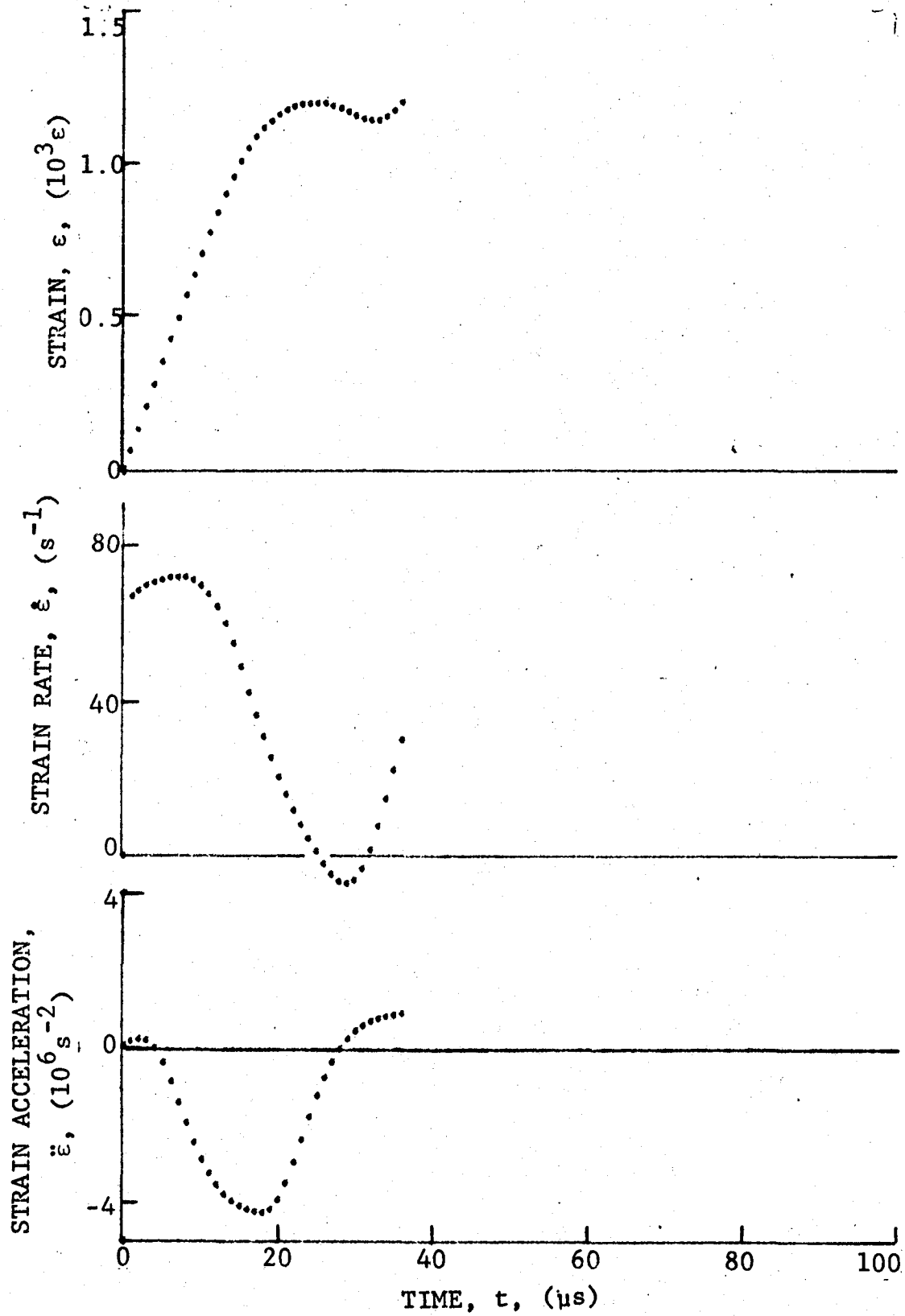

Figure 4-50. Strain and its derivatives in steel ring for Specimen No. 50-4.

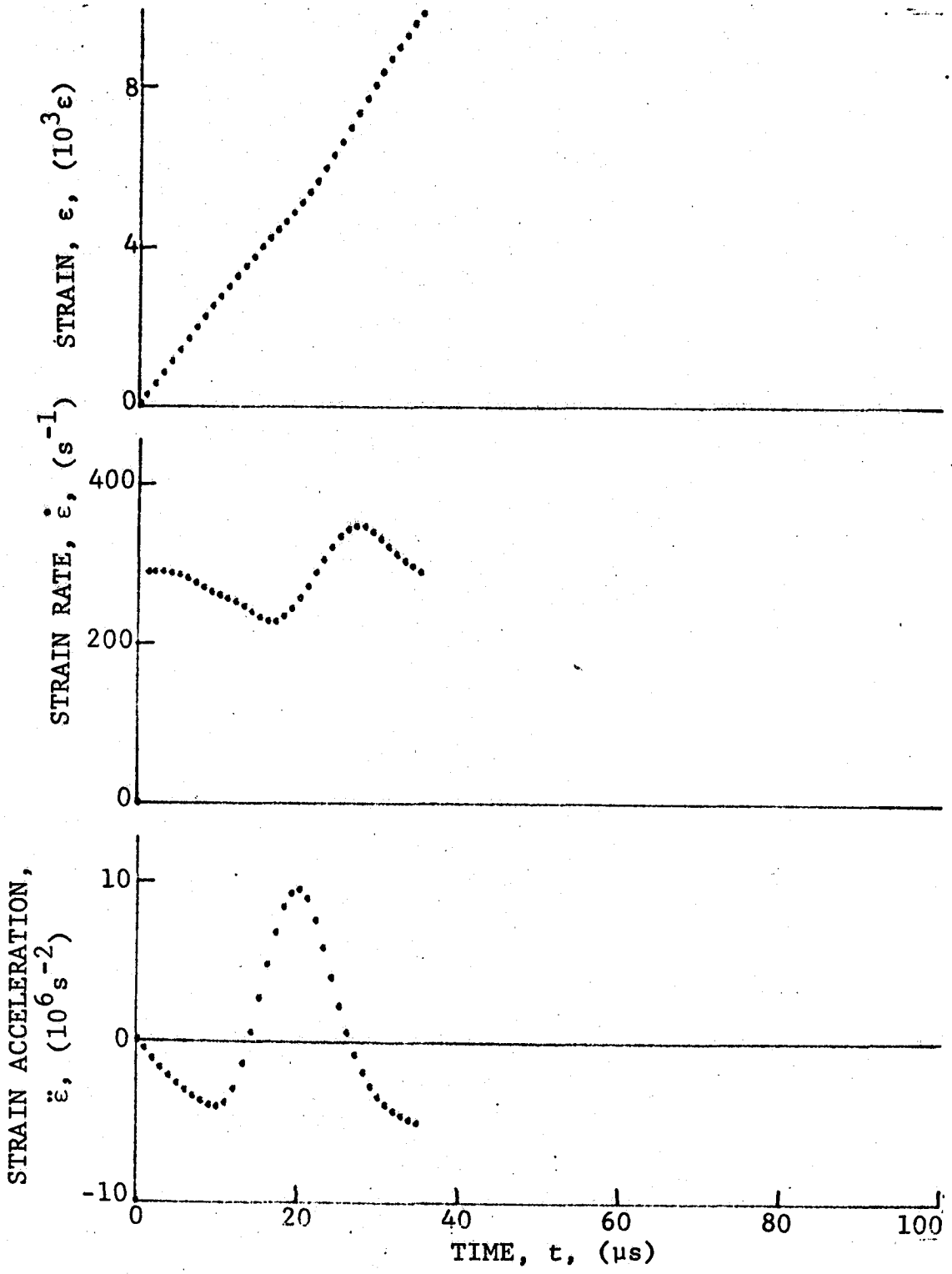

Figure 4-51. Circumferential strain and its derivatives in [45_8] SP288/AS graphite/epoxy ring under dynamic loading for Specimen No. 50-4 (1.56 g pistol powder, $KC\ell O_4$, and aluminum dust).

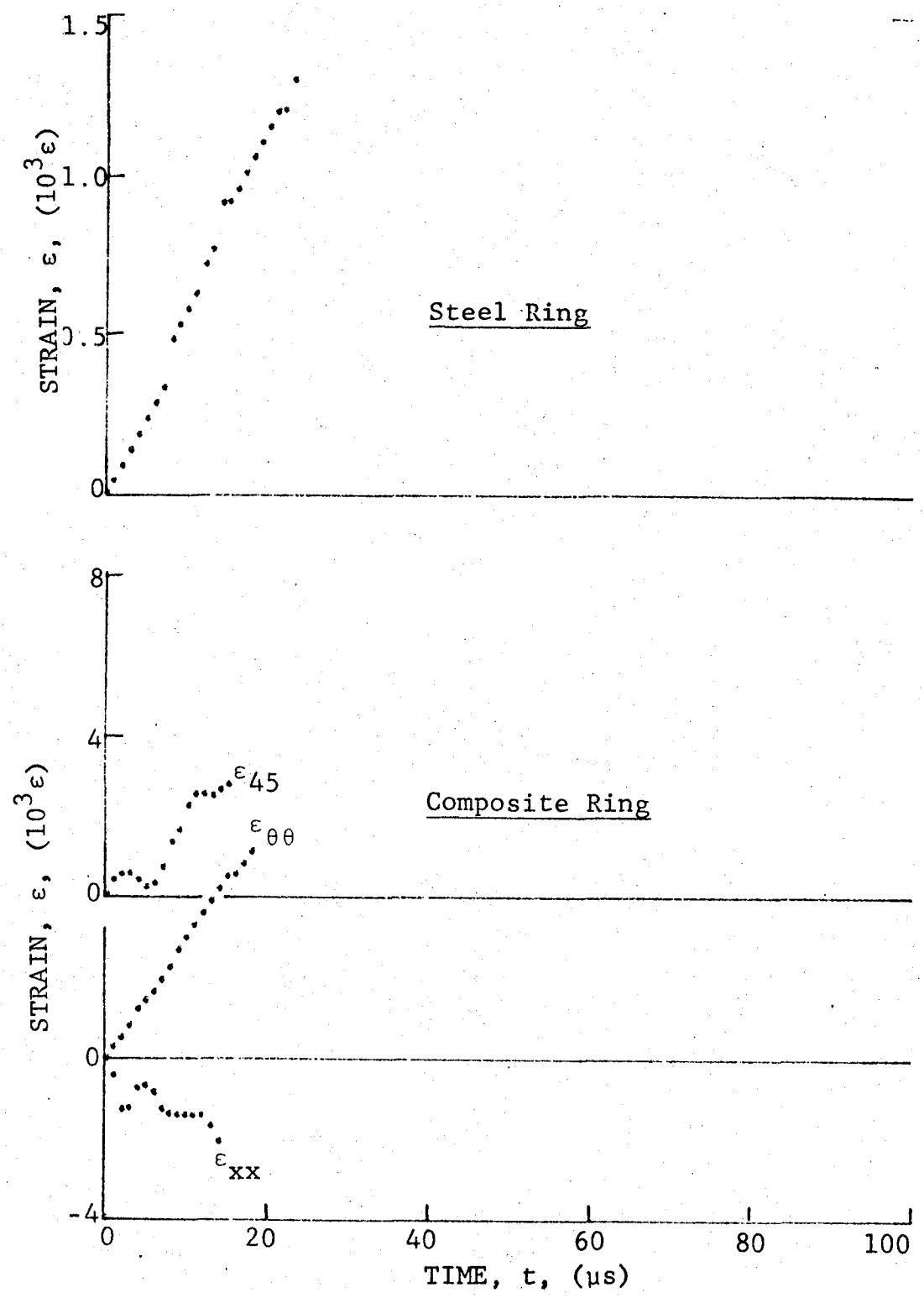

Figure 4-52. Strain records in steel ring and $[45_8]$ SP288/AS graphite/epoxy ring under dynamic loading for Specimen No. 50-5 (1.56 g pistol powder, $KC\ell O_4$, and aluminum dust).

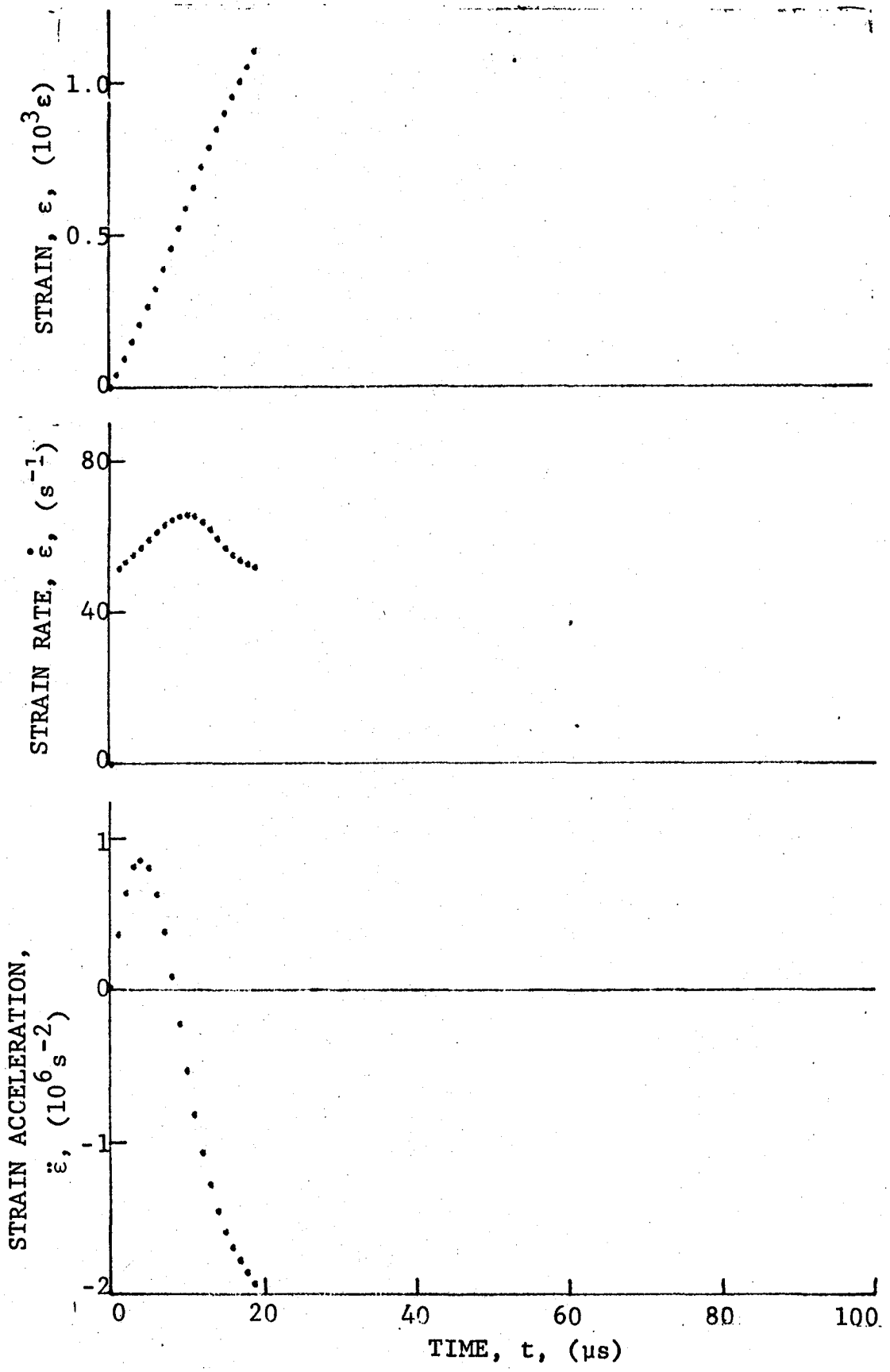

Figure 4-53. Strain and its derivatives in steel ring for Specimen No. 50-5.

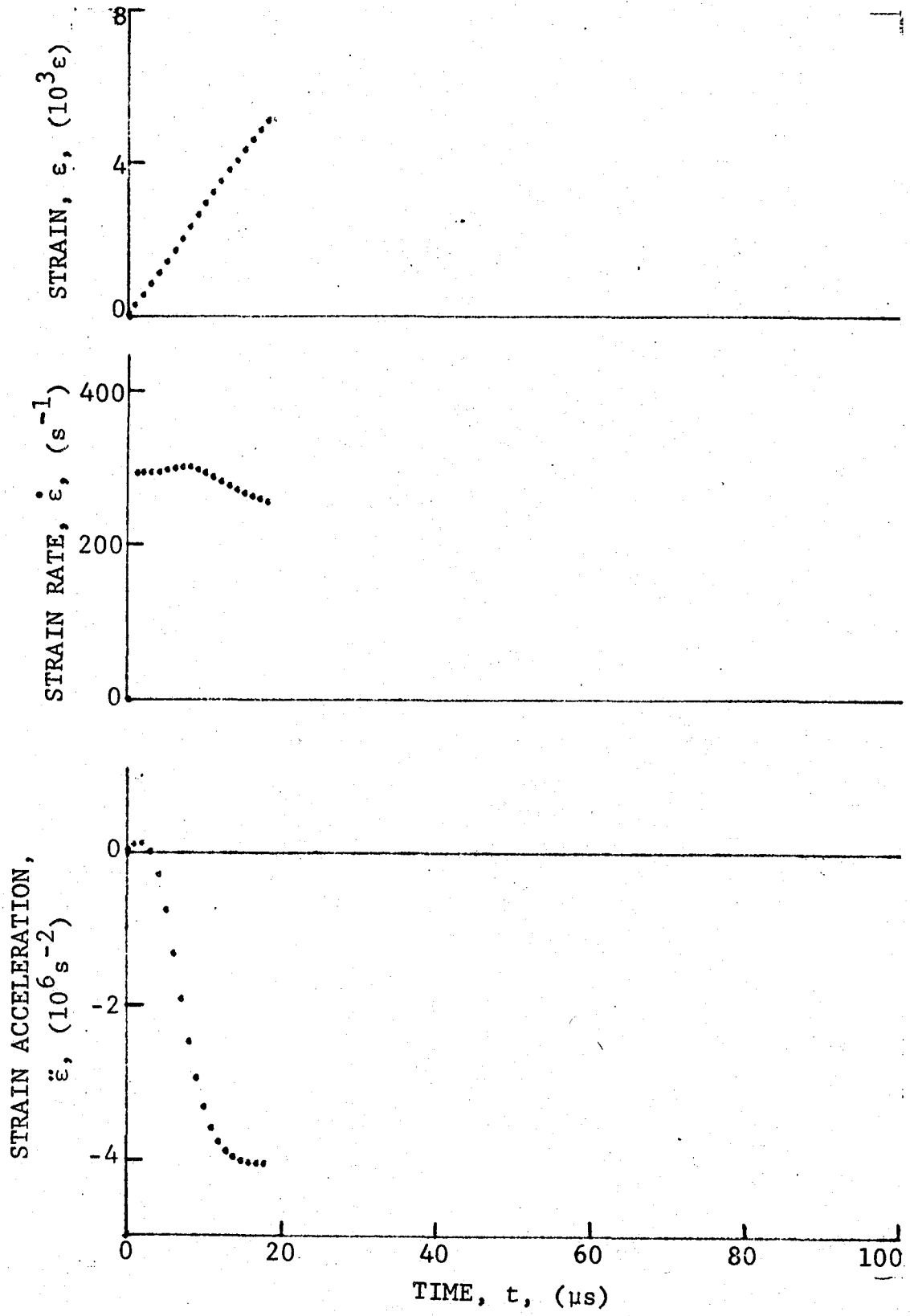

Figure 4-54. Circumferential strain and its derivatives in [45_8] SP288/AS graphite/epoxy ring under dynamic loading for Specimen No. 50-5 (1.56 g pistol powder, $KC\ell O_4$, and aluminum dust).

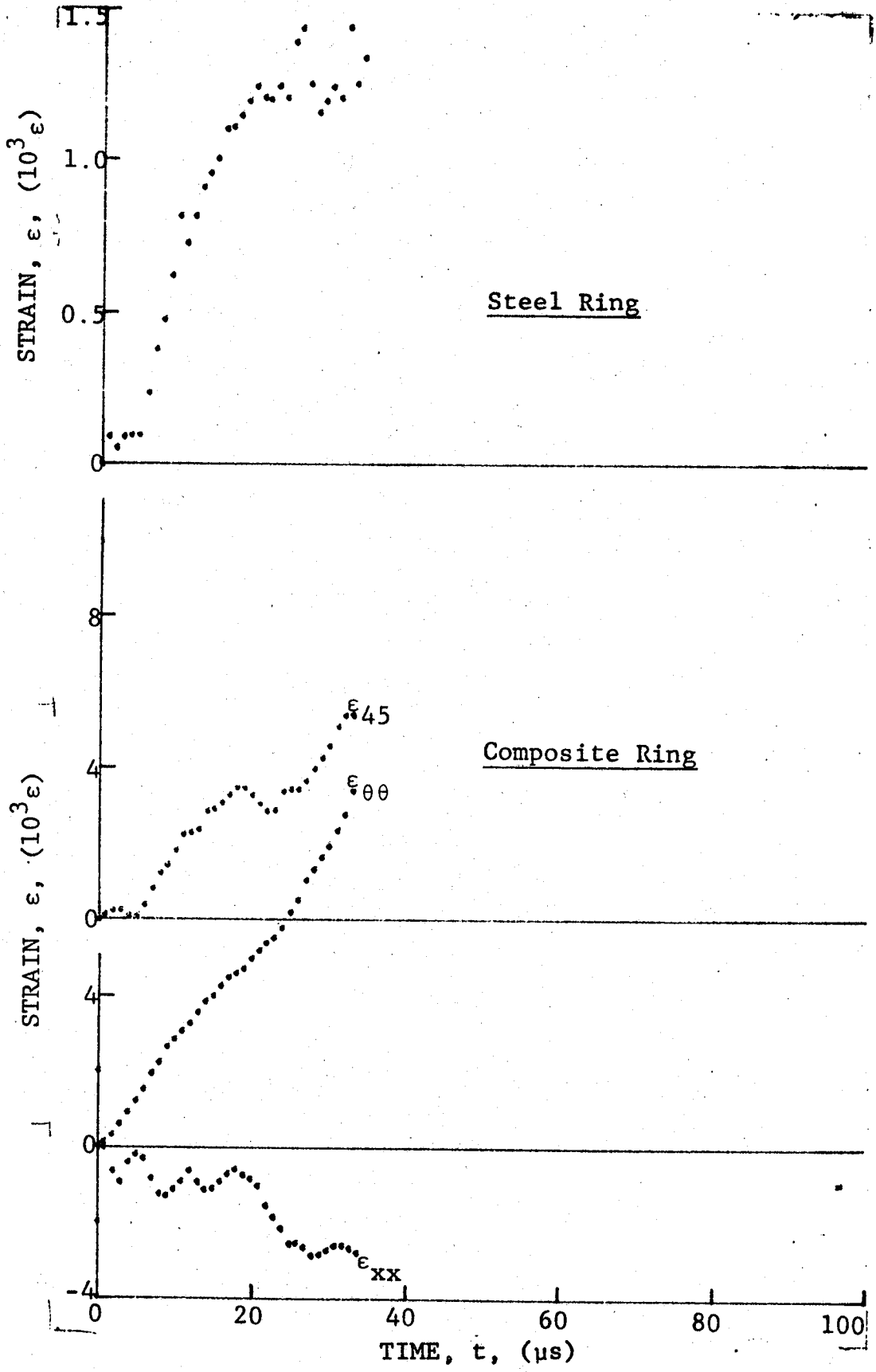

Figure 4-55. Strain records in steel ring and $[45_8]$ SP288/AS graphite/epoxy ring under dynamic loading for Specimen No. 50-6 (1.56 g pistol powder, $KC\ell O_4$, and aluminum dust).

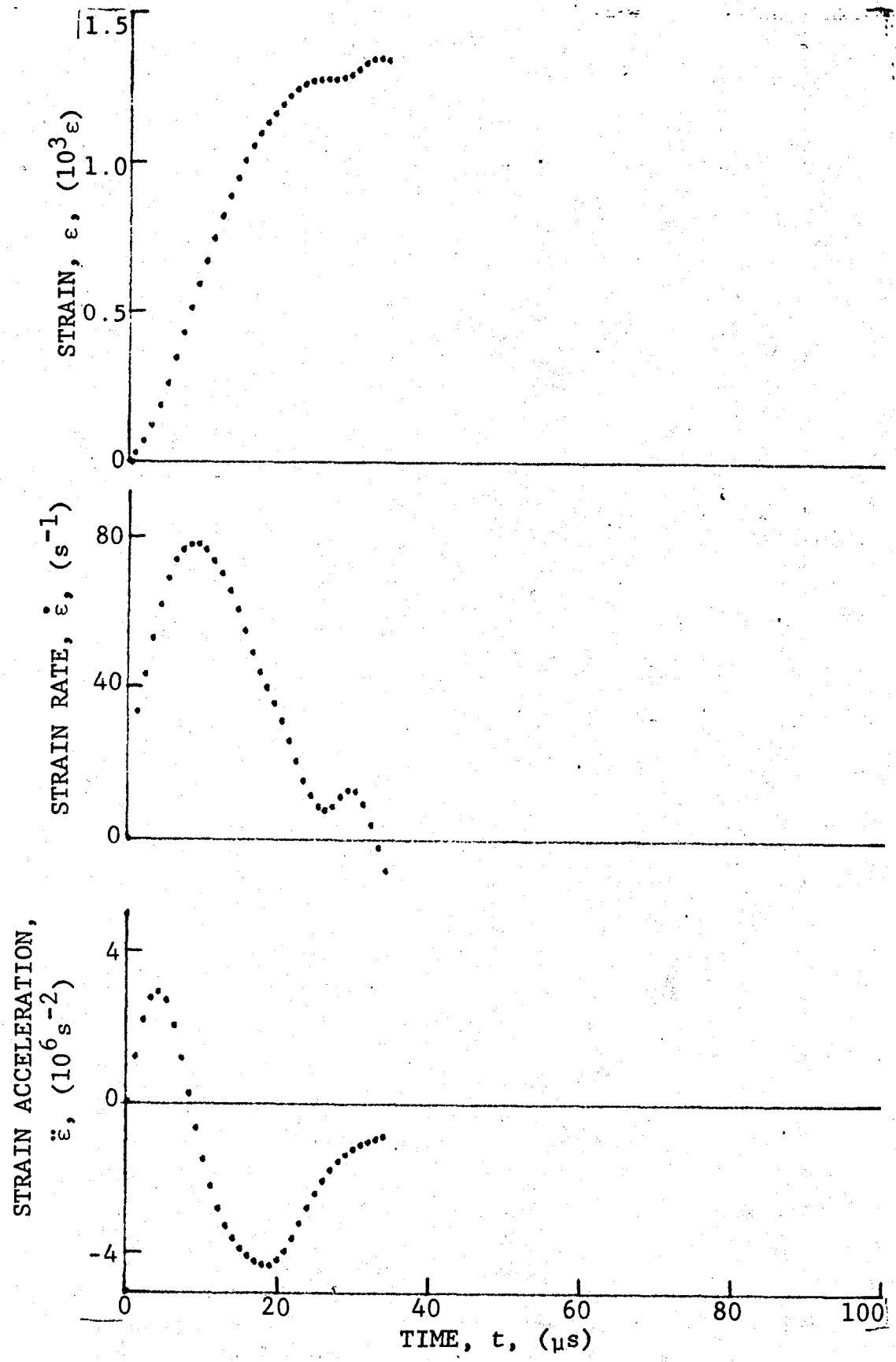

Figure 4-56. Strain and its derivatives in steel ring for Specimen No. 50-6.

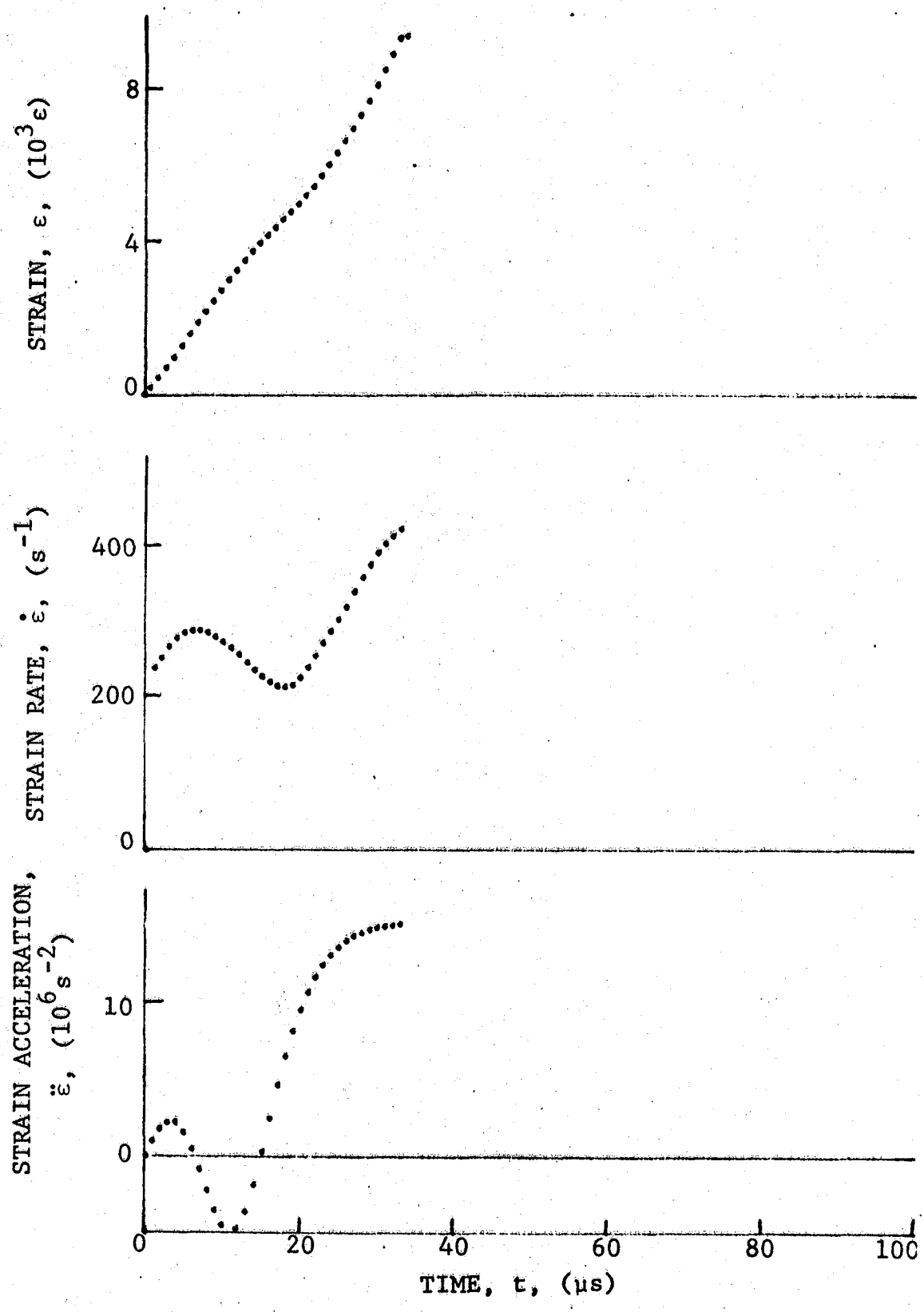

Figure 4-57. Circumferential strain and its derivatives in $[45_8]$ SP288/AS graphite/epoxy ring under dynamic loading for Specimen No. 50-6 (1.56 g pistol powder, $KC\ell O_4$, and aluminum dust).

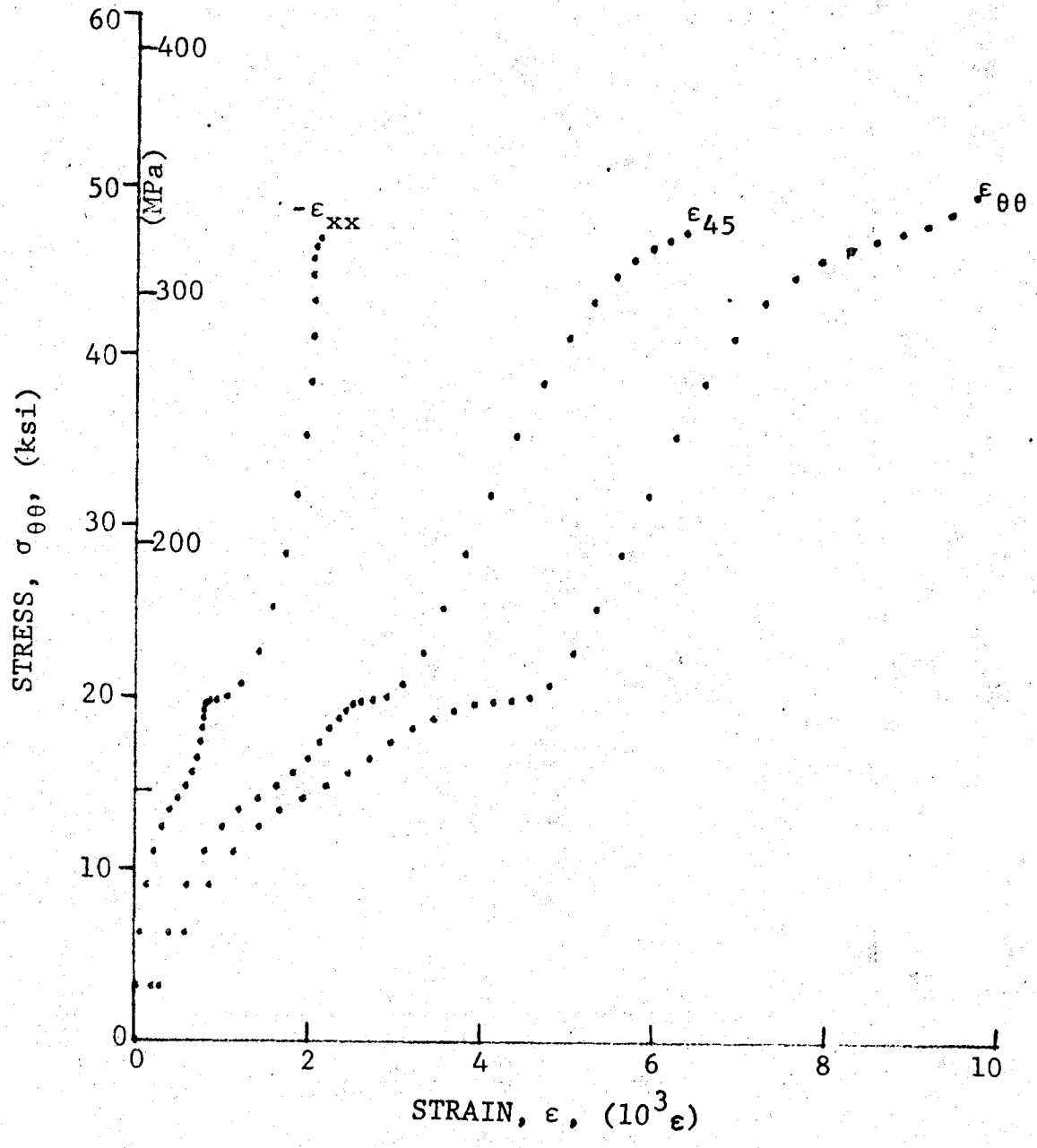

Figure 4-58. Stress-strain curve for dynamically loaded $[45_8]$ SP288/AS graphite/epoxy ring, Specimen No. 50-4 (1.56 g pistol powder, $KC\ell O_4$, and aluminum dust).

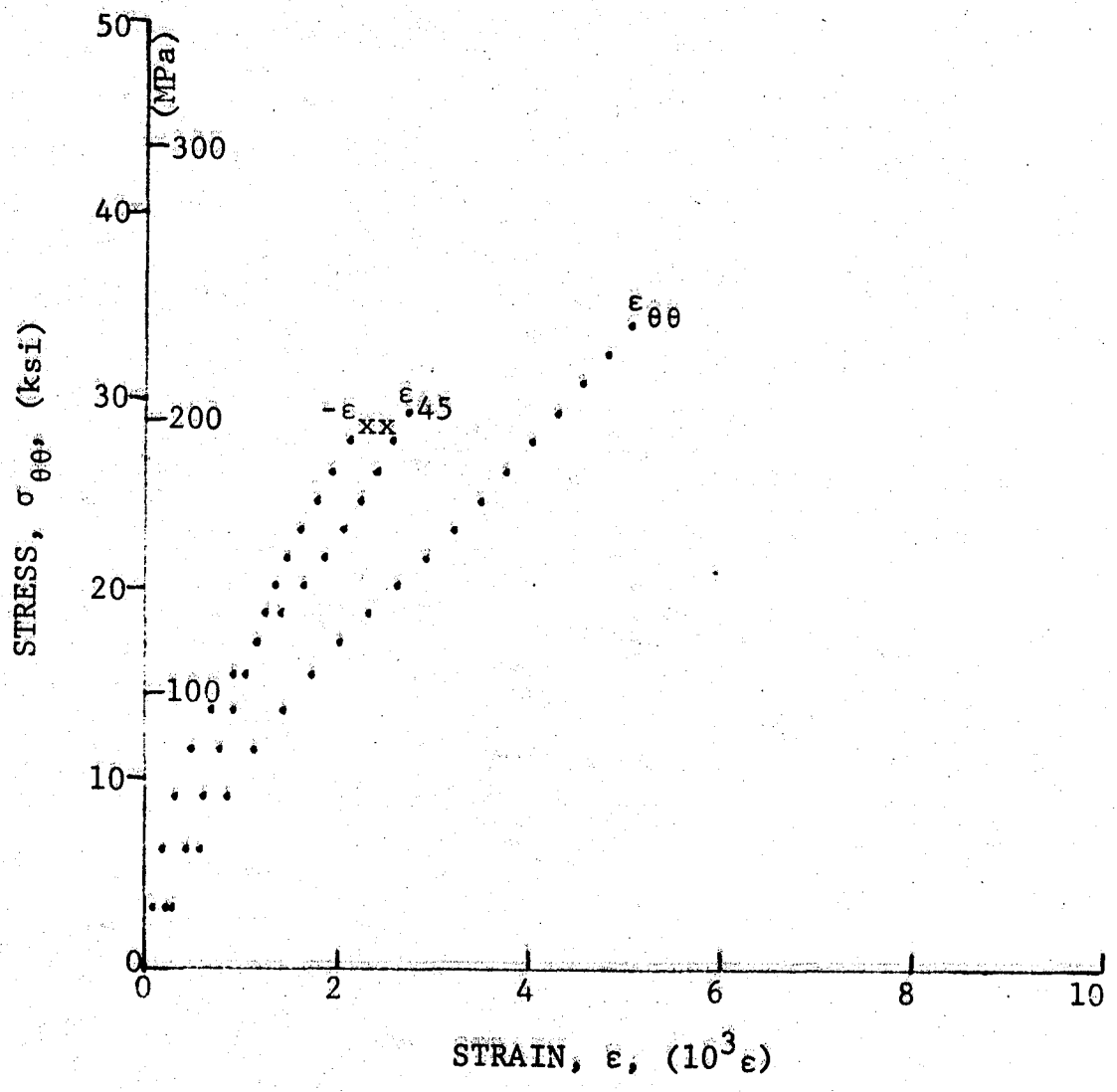

Figure 4-59. Stress-strain curve for dynamically loaded $[45_8]$ SP288/AS graphite/epoxy ring, Specimen No. 50-5 (1.56 g pistol powder, $KC\ell O_4$, and aluminum dust).

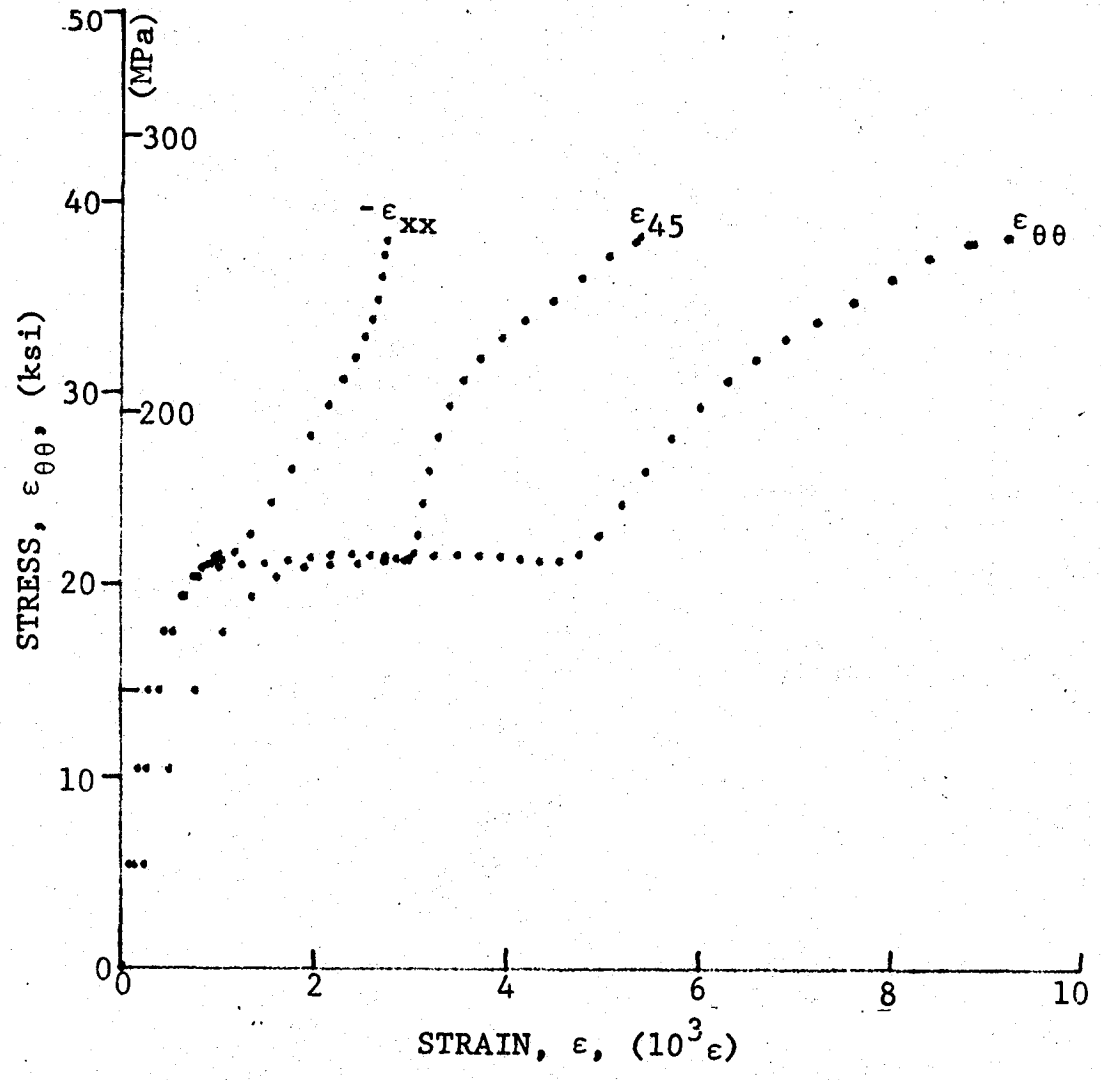

Figure 4-60. Stress-strain curve for dynamically loaded [45_8] SP288/AS graphite/epoxy ring, Specimen No. 50-6 (1.56 g pistol powder, $KC\ell O_4$, and aluminum dust).

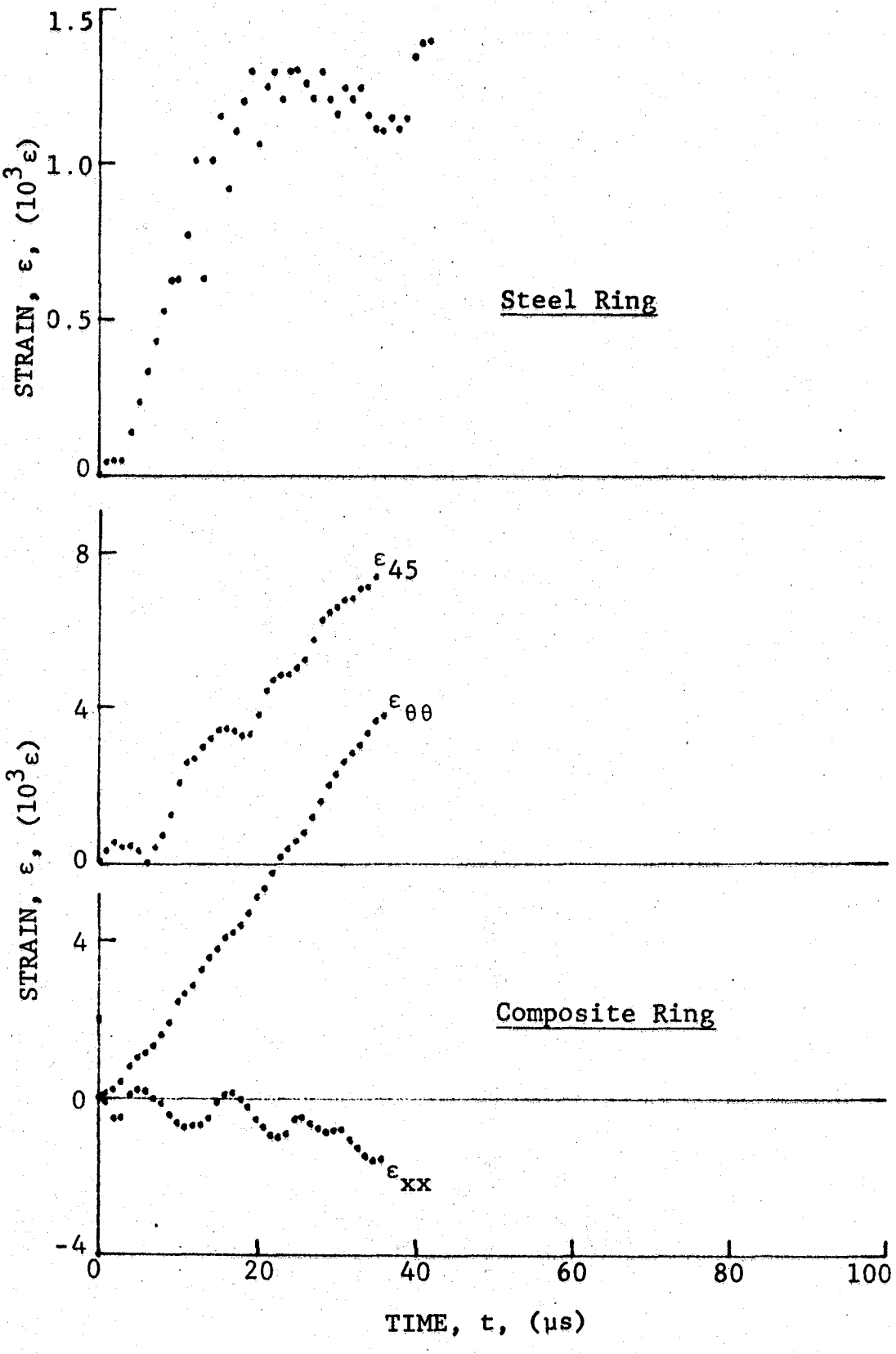

Figure 4-61. Strain records in steel ring and [45$_8$] 80AS/20S/PR288 graphite/S-glass/epoxy ring under dynamic loading for Specimen No. 51-4 (1.56 g pistol powder, $KC\ell O_4$, and aluminum dust).

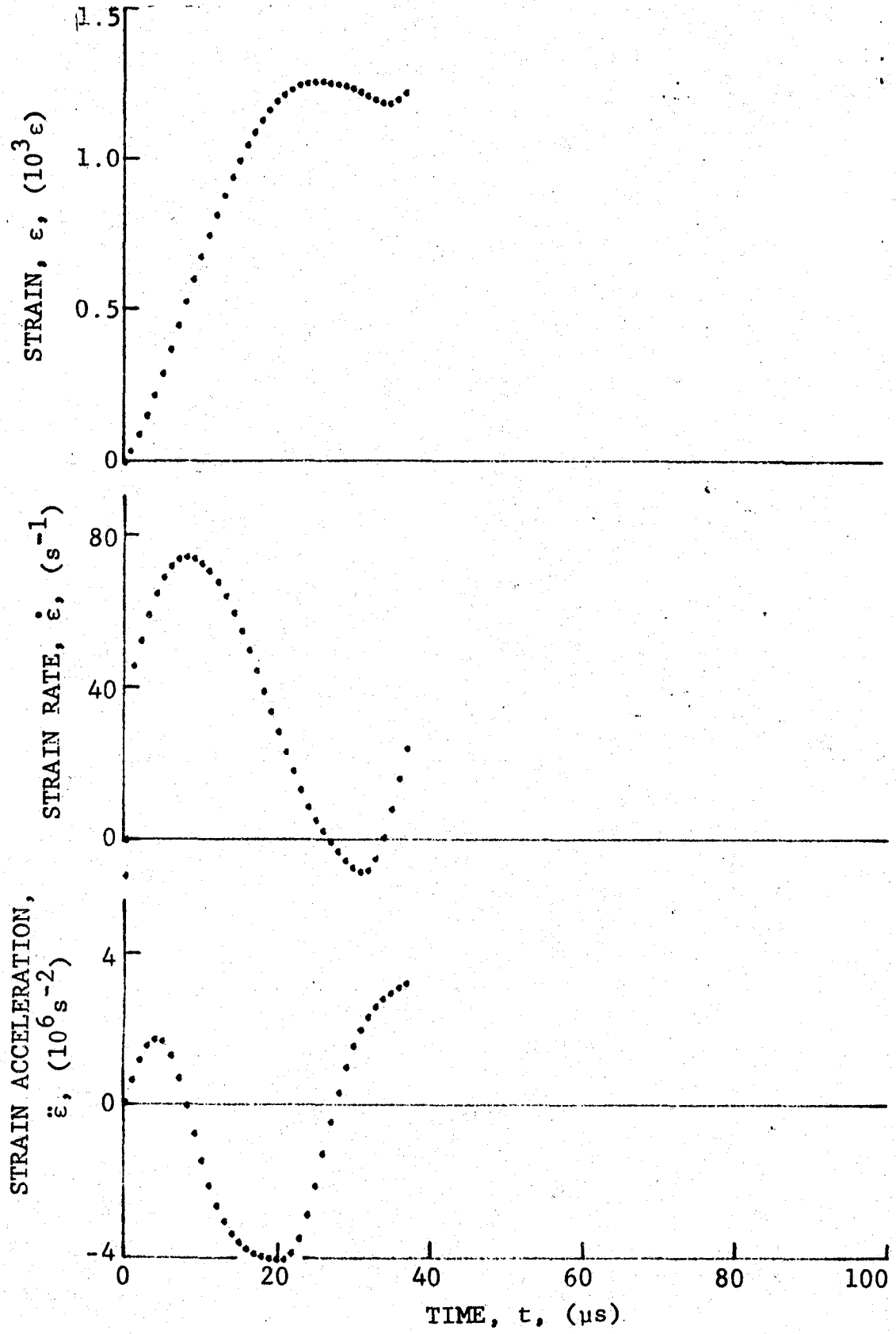

Figure 4-62. Strain and its derivatives in steel ring for Specimen No. 51-4.

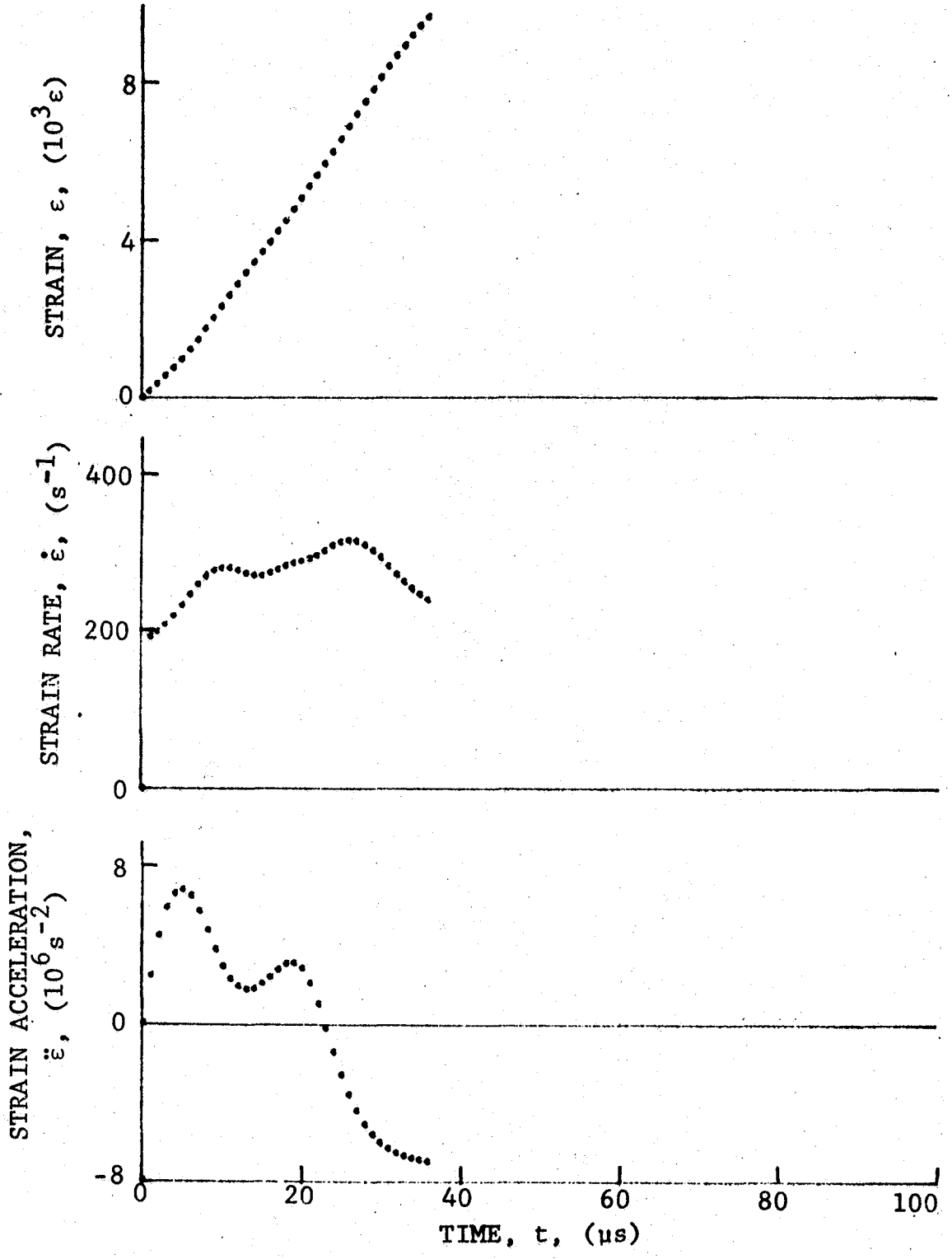

Figure 4-63. Circumferential strain and its derivatives in $[45_8]$ 80AS/20S/PR288 graphite/S-glass/epoxy ring under dynamic loading for Specimen No. 51-4 (1.56 g pistol powder, $KC\ell O_4$, and aluminum dust).

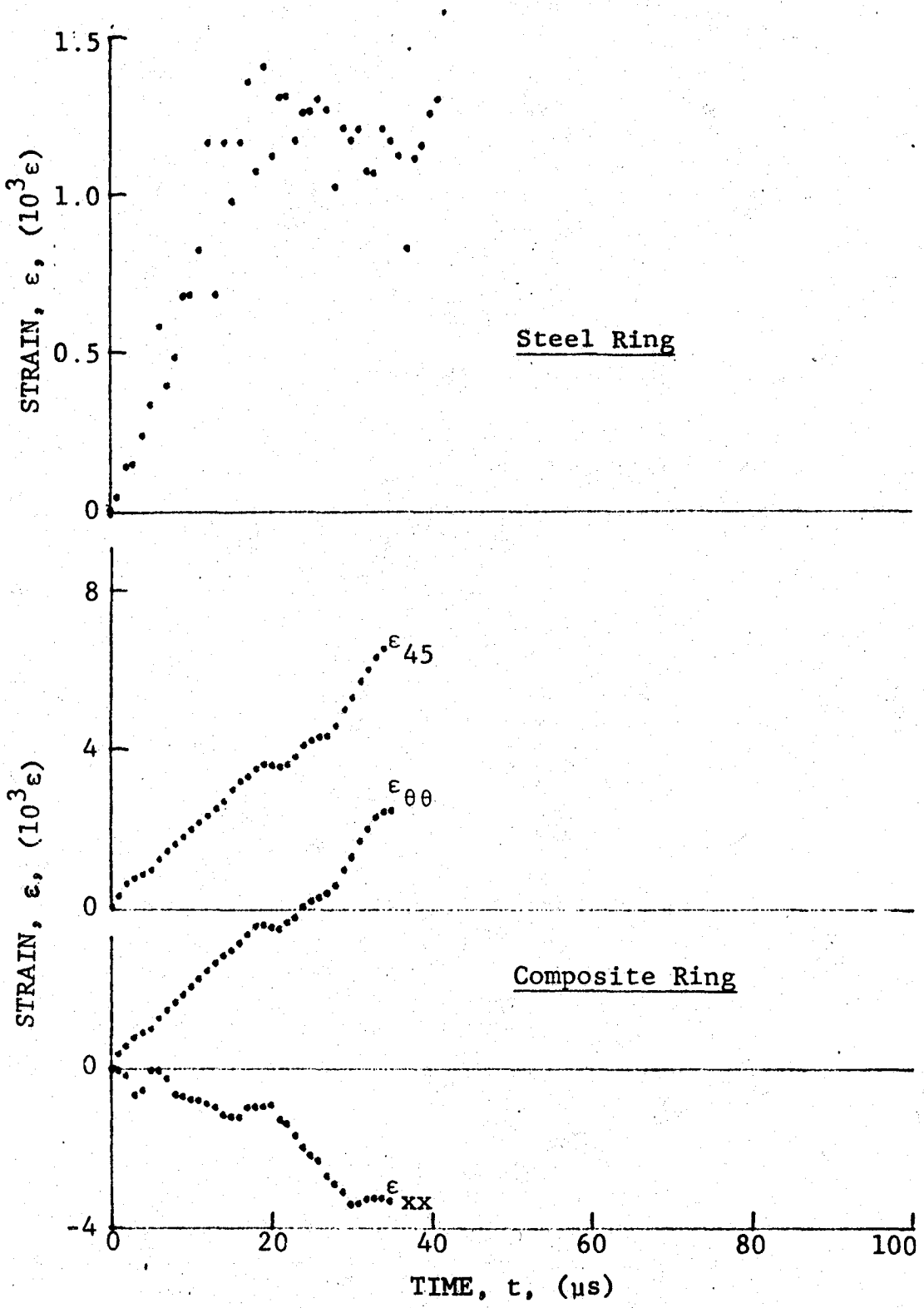

Figure 4-64. Strain records in steel ring and [45_8] 80AS/20S/PR288 graphite/S-glass/epoxy ring under dynamic loading for Specimen No. 51-5 (1.56 g pistol powder, $KC\ell O_4$, and aluminum dust).

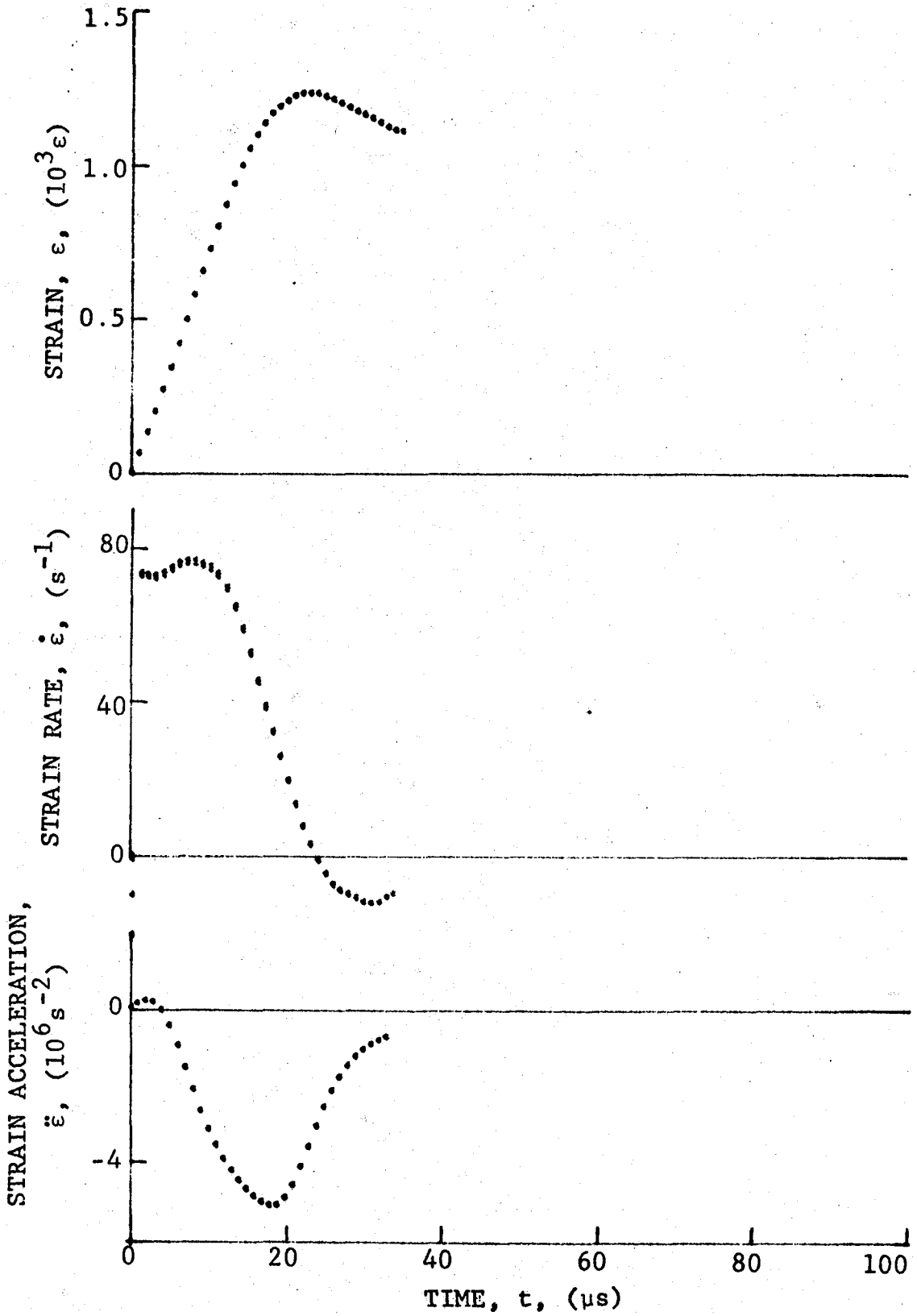

Figure 4-65. Strain and its derivatives in steel ring for Specimen No. 51-5.

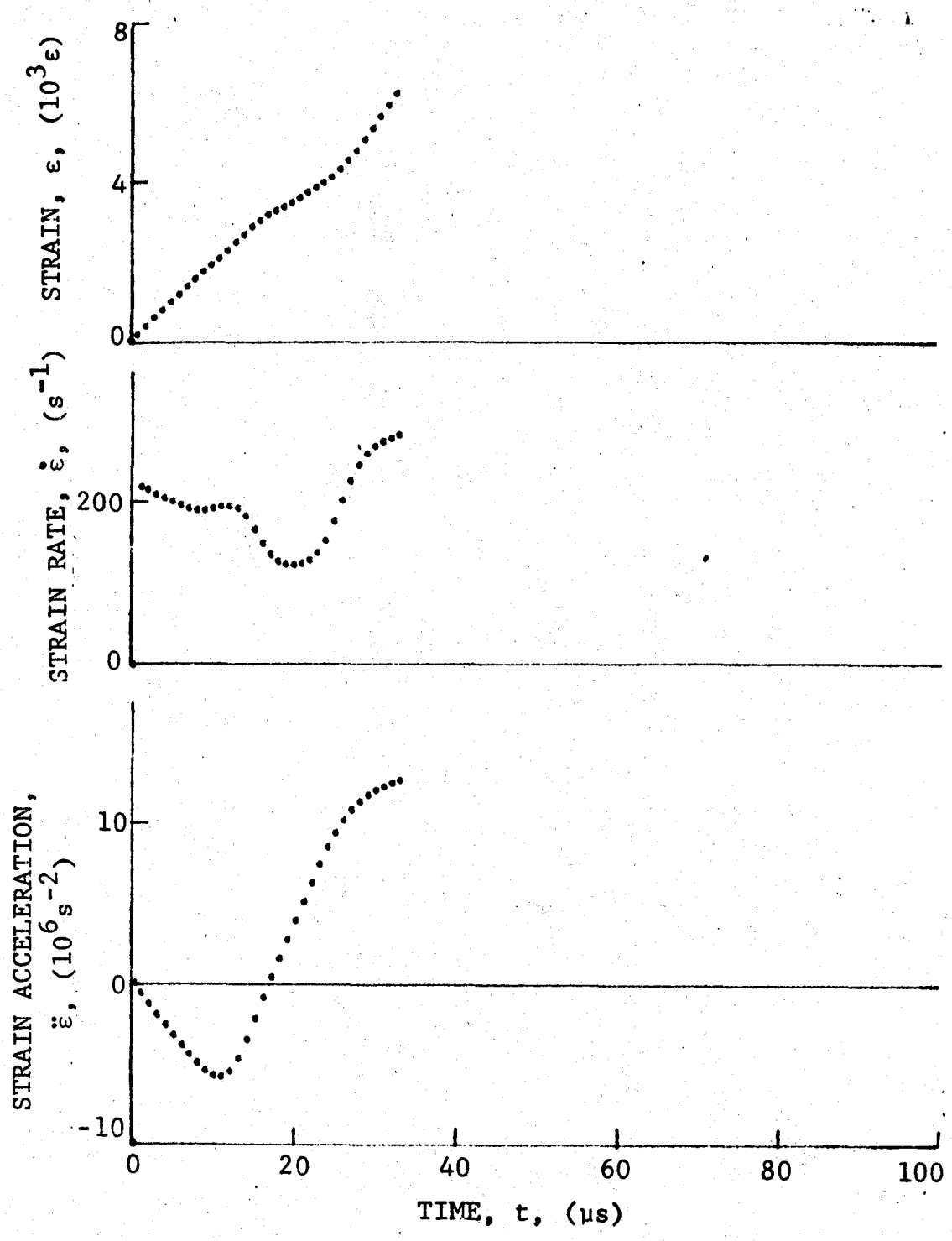

Figure 4-66. Circumferential strain and its derivatives in [45_8] 80AS/20S/PR288 graphite/S-glass/epoxy ring under dynamic loading for Specimen No. 51-5 (1.56 g pistol powder, $KC\ell O_4$, and aluminum dust).

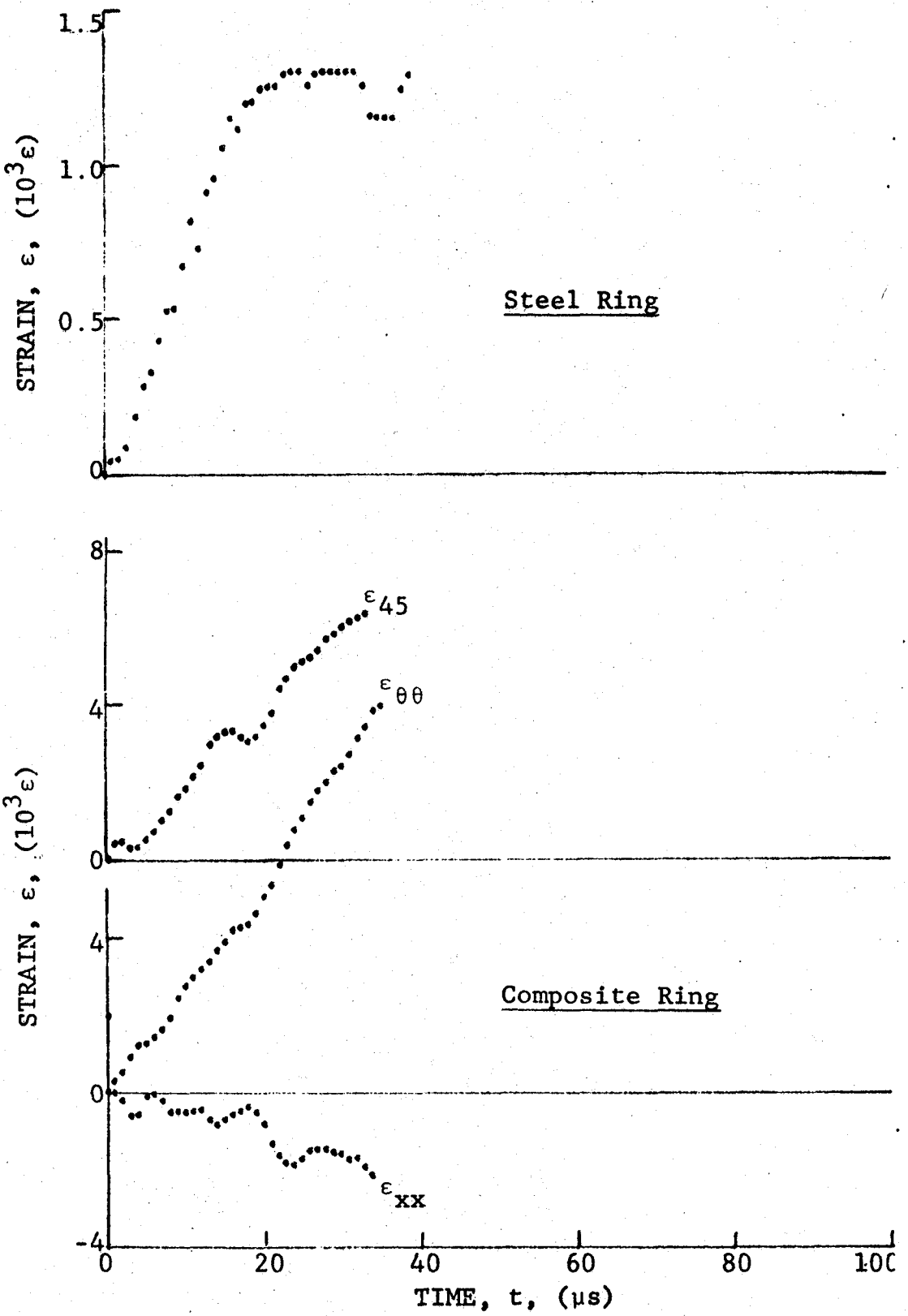

Figure 4-67. Strain records in steel ring and [45_8] 80AS/20S/PR288 graphite/S-glass/epoxy ring under dynamic loading for Specimen No. 51-6 (1.56 g pistol powder, $KC\ell O_4$, and aluminum dust).

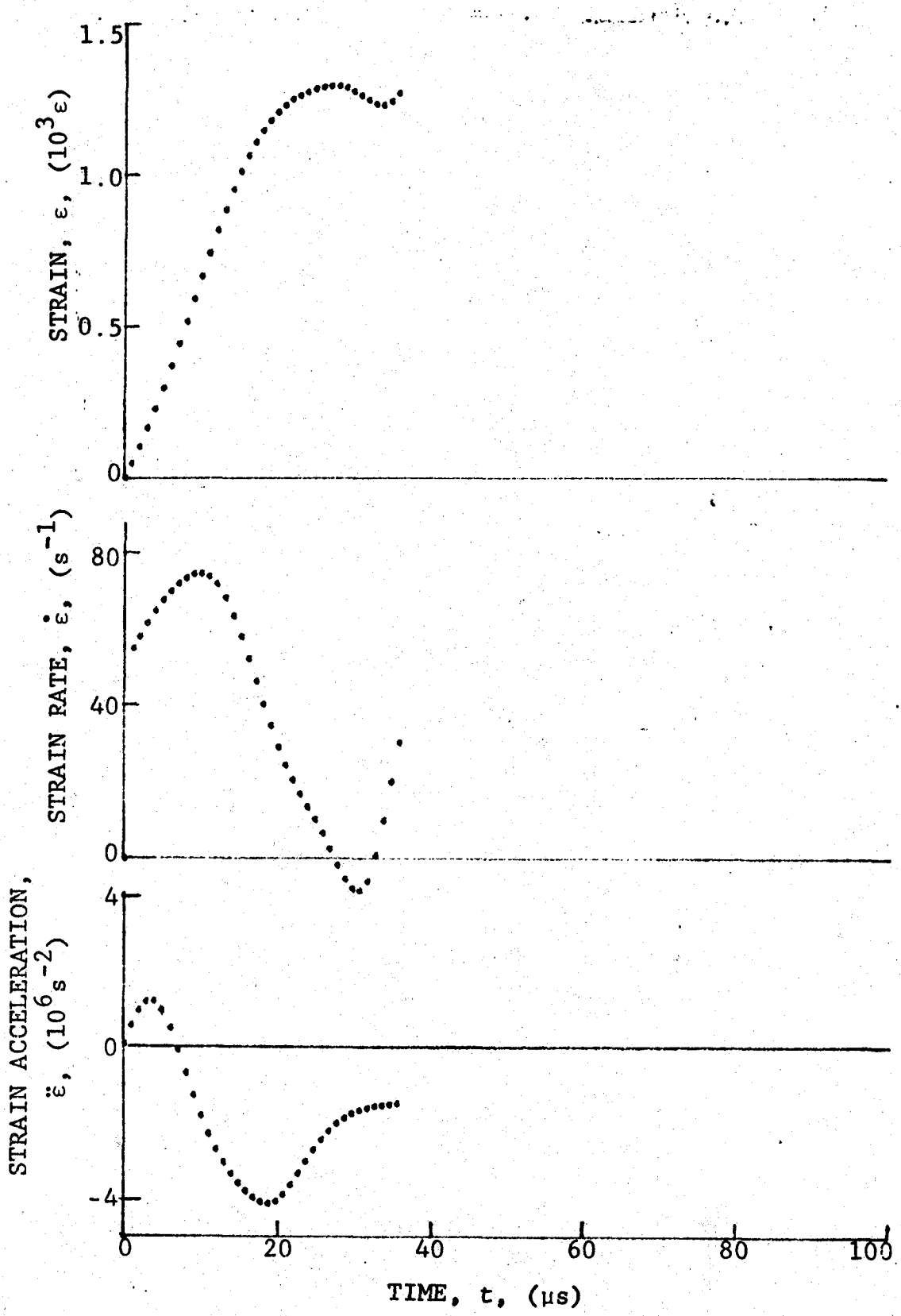

Figure 4-68. Strain and its derivatives in steel ring for Specimen No. 51-6.

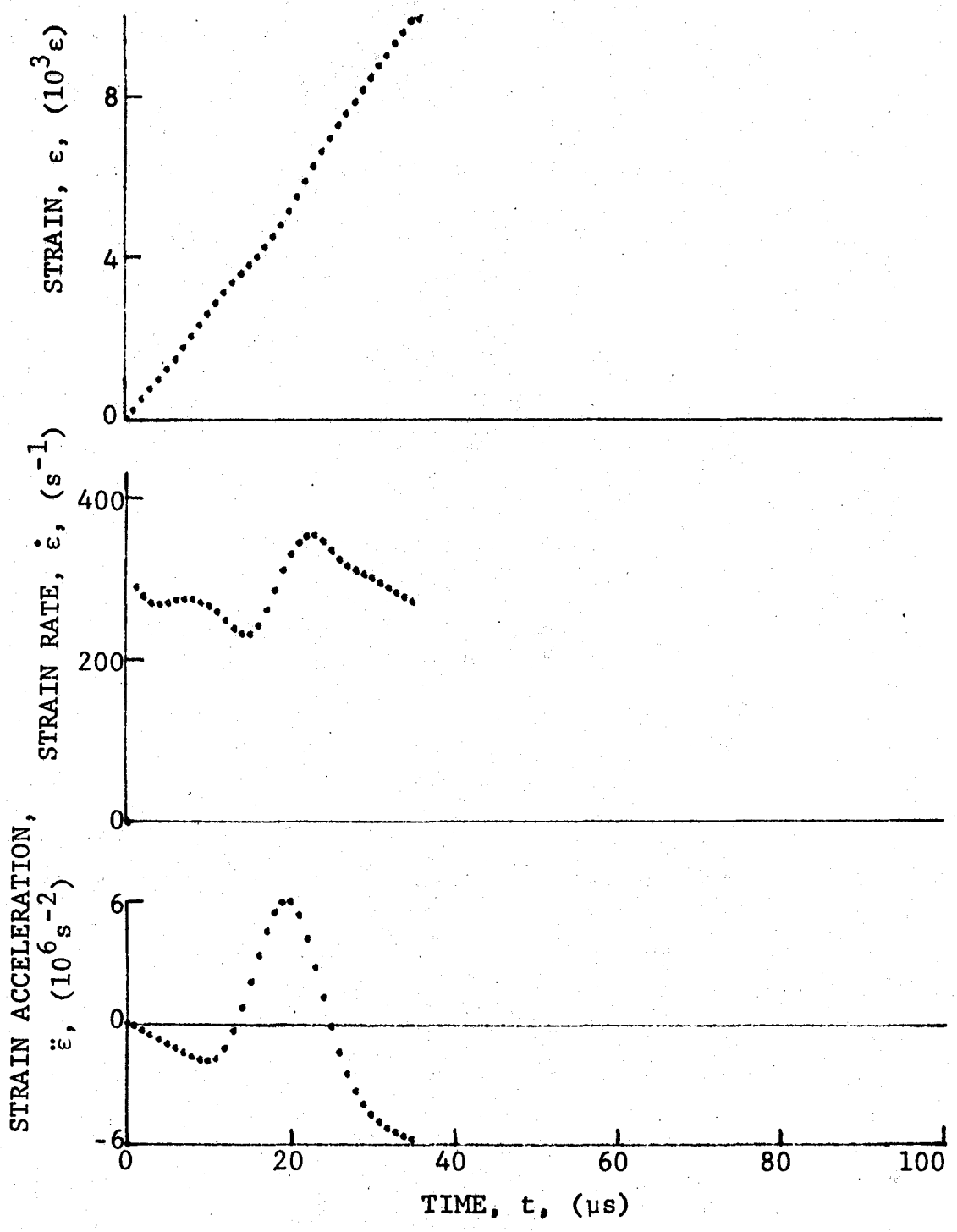

Figure 4-69. Circumferential strain and its derivatives in $[45_8]$ 80AS/20S/PR288 graphite/S-glass/epoxy ring under dynamic loading for Specimen No. 51-6 (1.56 g pistol powder, $KC\ell O_4$, and aluminum dust).

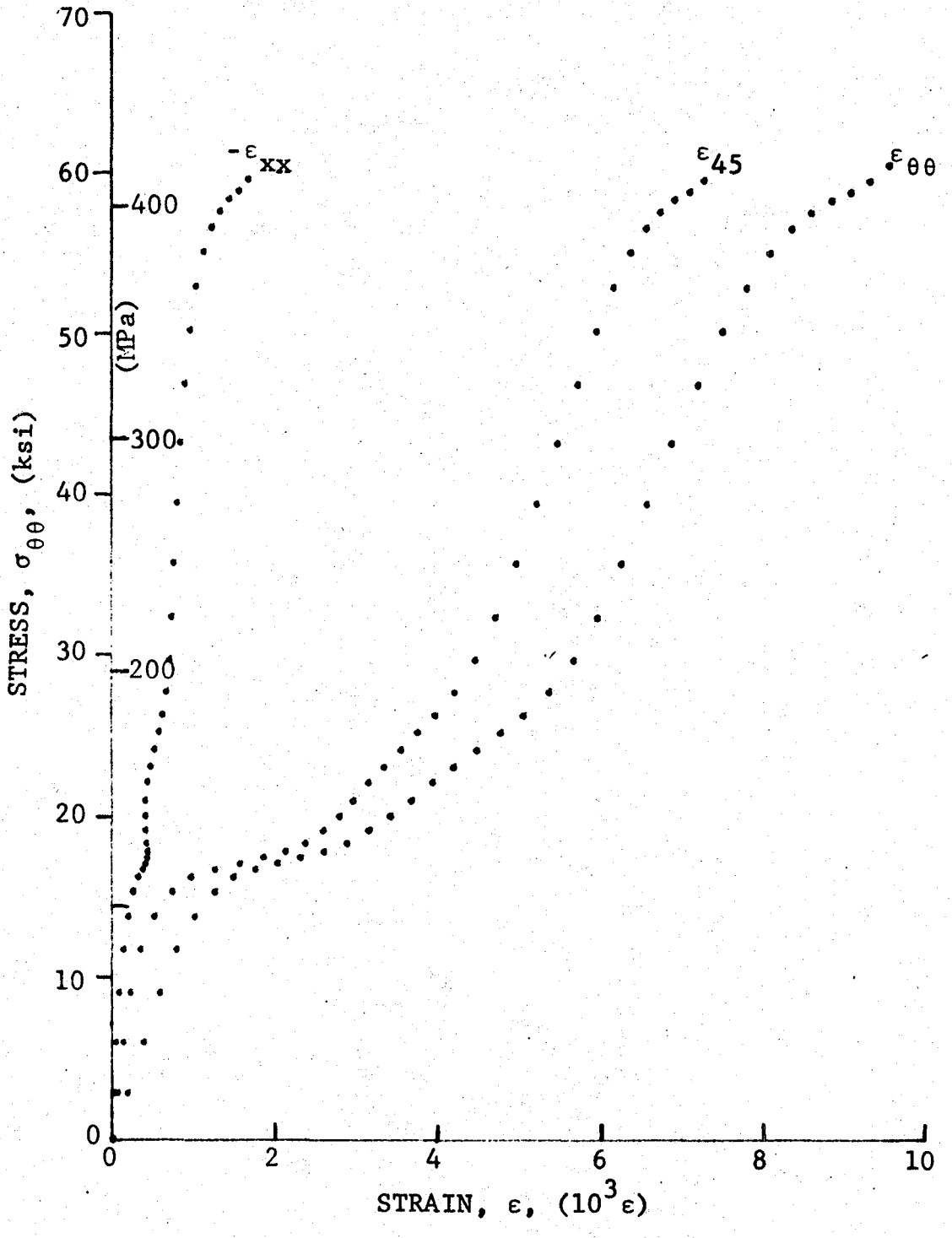

Figure 4-70. Stress-strain curve for dynamically loaded $[45_8]$ 80AS/20S/PR288 graphite/S-glass/epoxy ring, Specimen No. 51-4 (1.56 g pistol powder, $KC\ell O_4$, and aluminum dust).

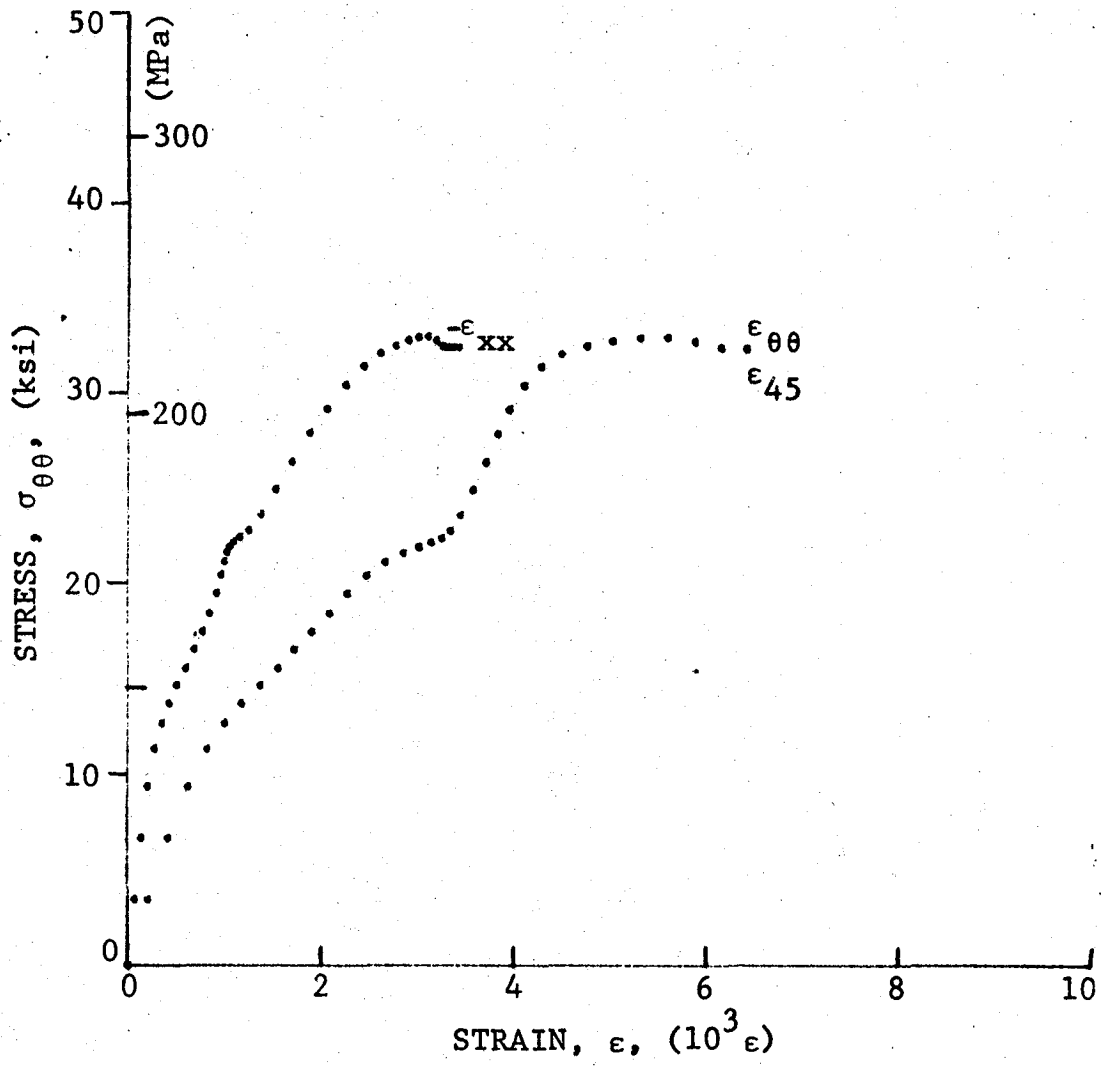

Figure 4-72. Stress-strain curve for dynamically loaded $[45_8]$ 80AS/20S/PR288 graphite/S-glass/epoxy ring, Specimen No. 51-5 (1.56 g pistol powder, $KC\ell O_4$, and aluminum dust).

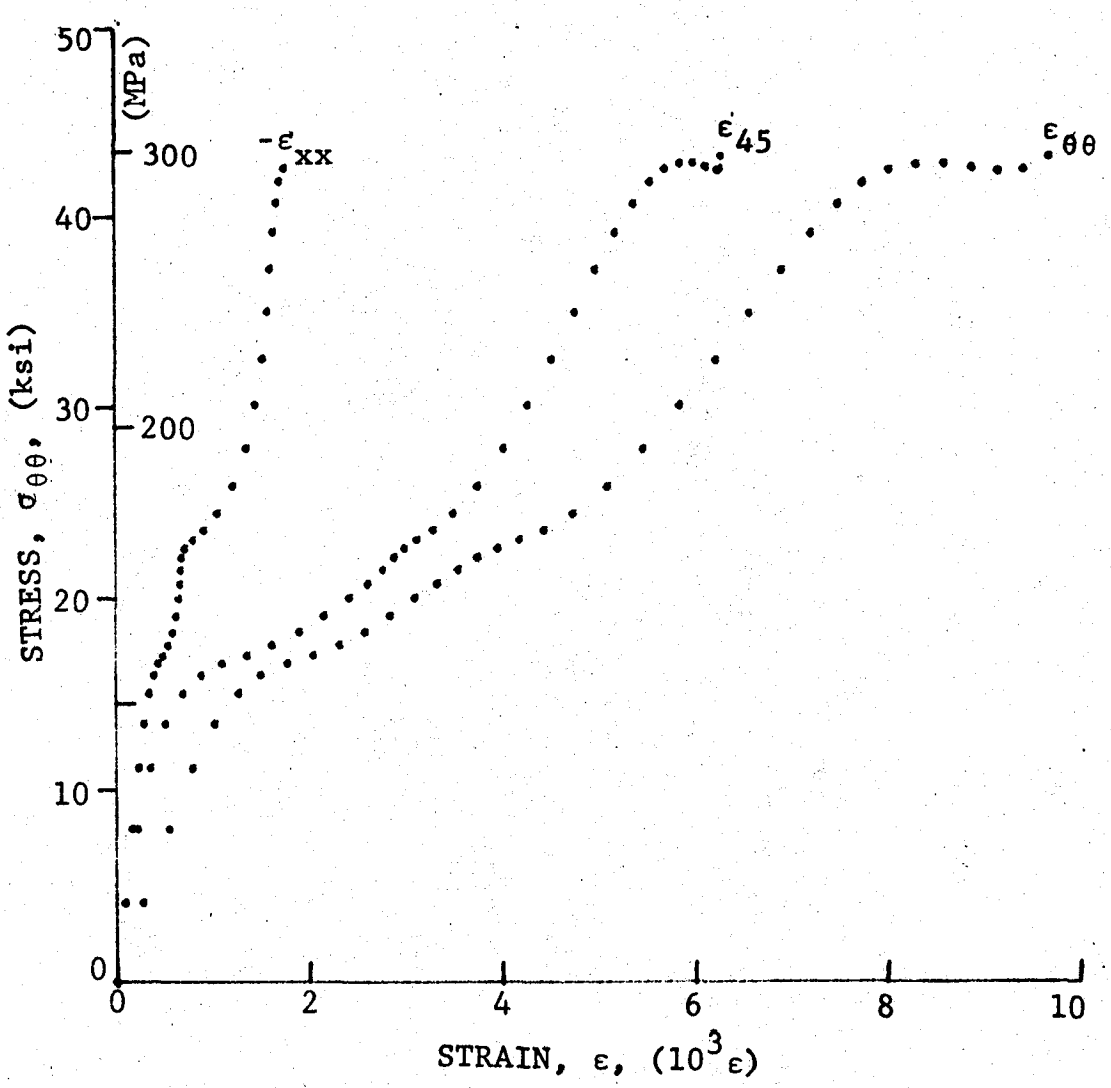

Figure 4-71. Stress-strain curve for dynamically loaded $[45_8]$ 80AS/20S/PR288 graphite/S-glass/epoxy ring, Specimen No. 51-6 (1.56 g pistol powder, $KC\ell O_4$, and aluminum dust).

5. SUMMARY AND CONCLUSIONS

Methods developed and described in Part I of this report were applied to the characterization of unidirectional off-axis laminates. Two material systems, SP288/AS graphite/epoxy and 80AS/20S/PR288 graphite/S-glass/epoxy, were characterized in uniaxial tension at 22.5°, 30°, and 45° with the fiber direction at three strain rates. The three strain rates investigated were quasi-static, intermediate, and high rates ranging from $10^{-4}s^{-1}$ to over $500s^{-1}$. Results were obtained and presented in the form of stress-strain curves to failure. Properties determined included moduli, Poisson's ratios, strength, and ultimate strain.

Average results for the $[22.5_8]$ laminates are tabulated in Tables 5-1 and 5-2 for the graphite/epoxy and hybrid materials, respectively. The initial and secant moduli increase with strain rate by 80 to 100% at the highest rate, except in the case of the initial modulus of the hybrid laminate which shows an even higher increase. The strength of the graphite/epoxy is nearly doubled at the high rate of loading, that of the hybrid laminate is even higher. The ultimate strains show opposite trends for the two materials, decreasing with strain rate for the graphite/epoxy and increasing with strain rate for the hybrid material.

Average results for the $[30_8]$ laminates are tabulated in Tables 5-3 and 5-4 for the graphite/epoxy and hybrid materials, respectively. Initial and secant moduli increase sharply for both materials, reaching values between 2.1 and 2.6 times the static values. The strengths increase even more sharply reaching values up to three times the static strength. In the case of the graphite/epoxy laminate the ultimate strain increases steadily with strain rate, whereas in the hybrid laminate it tends to fluctuate without any definite trend.

Average results for the $[45_8]$ laminates are tabulated in Tables 5-5 and 5-6 for the graphite/epoxy and hybrid materials, respectively. Initial moduli reach values approximately five times the static; secant moduli reach values a little less than three times the static values. Strengths increase sharply with strain rate reaching values more than three times the static strength. No significant variations or trends can be discerned in the ultimate strain values.

TABLE 5-1. TENSILE PROPERTIES OF [22.5$_8$] SP288/AS GRAPHITE/EPOXY

Specimen Numbers	Strain Rate ($\dot{\varepsilon}_{\theta\theta}$), s^{-1}	Modulus ($E_{\theta\theta}$), GPa (10^6 psi)	Poisson's Ratio ($\nu_{\theta x}$)
		Initial Properties	
46-1,2,3	1×10^{-4}	34.6 (5.01)	0.31
46-9,10,11	33	45.3 (6.57)	0.25
46-5,7,8	243	62.1 (9.00)	0.39
		Secant Properties	
46-1,2,3	1×10^{-4}	23.3 (3.38)	0.34
46-9,10,11	54	37.6 (5.45)	0.39
46-5,7,8	320	47.6 (6.90)	0.41
		Terminal Properties	
46-1,2,3	1×10^{-4}	11.5 (1.66)	0.31
46-9,10,11	126	30.6 (4.44)	0.39
46-5,7,8	375	33.0 (4.78)	0.47
		Ultimate Properties	
	Time to Failure (t_f), μs	Strength ($S_{\theta\theta T}$), MPa (ksi)	Strain ($\varepsilon^u_{\theta\theta T}$)
46-1,2,3	1×10^8	218 (31.6)	0.0110
46-9,10,11	175	339 (49.0)	0.0092
46-5,7,8	29	432 (62.7)	0.0091

TABLE 5-2. TENSILE PROPERTIES OF $[22.5_8]$ 80AS/20S/PR288 GRAPHITE/S-GLASS/EPOXY

Specimen Numbers	Strain Rate ($\dot{\varepsilon}_{\theta\theta}$), s^{-1}	Modulus ($E_{\theta\theta}$), GPa (10^6 psi)	Poisson's Ratio ($\nu_{\theta x}$)
		Initial Properties	
47-1,2,3	1×10^{-4}	38.6 (5.59)	0.38
47-7,8,9	36	43.6 (6.31)	0.23
47-4,5,6	277	105.1 (15.24)	0.44
		Secant Properties	
47-1,2,3	1×10^{-4}	26.7 (3.87)	0.53
47-7,8,9	62	31.7 (4.60)	0.34
47-4,5,6	362	52.9 (7.66)	0.42
		Terminal Properties	
47-1,2,3	1×10^{-4}	15.9 (2.30)	0.68
47-7,8,9	142	26.7 (3.87)	0.38
47-4,5,6	465	49.2 (7.13)	0.51
		Ultimate Properties	
	Time to Failure (t_f), μs	Strength ($S_{\theta\theta T}$), MPa (ksi)	Strain ($\varepsilon^u_{\theta\theta T}$)
47-1,2,3	1×10^8	204 (29.6)	0.0077
47-7,8,9	159	306 (44.3)	0.0098
47-4,5,6	30	557 (80.7)	0.0107

TABLE 5-3. TENSILE PROPERTIES OF $[30_8]$ SP288/AS GRAPHITE/EPOXY

Specimen Numbers	Strain Rate ($\dot{\varepsilon}_{\theta\theta}$), s^{-1}	Modulus ($E_{\theta\theta}$), GPa (10^6 psi)	Poisson's Ratio ($\nu_{\theta x}$)
		Initial Properties	
48-1,2,3	1×10^{-4}	25.4 (3.68)	0.33
48-7,8,9	60	27.5 (3.98)	0.26
48-4,5,6	250	66.9 (9.70)	0.45
		Secant Properties	
48-1,2,3	1×10^{-4}	18.6 (2.69)	0.43
48-7,8,9	76	24.9 (3.61)	0.35
48-4,5,6	336	42.8 (6.20)	0.42
		Terminal Properties	
48-1,2,3	1×10^{-4}	11.1 (1.61)	0.55
48-7,8,9	142	20.8 (3.01)	0.45
48-4,5,6	443	40.3 (5.84)	0.60
		Ultimate Properties	
	Time to Failure (t_f), μs	Strength ($S_{\theta\theta T}$), MPa (ksi)	Strain ($\varepsilon^u_{\theta\theta T}$)
48-1,2,3	1×10^8	149 (21.6)	0.0080
48-7,8,9	139	254 (36.8)	0.0105
48-4,5,6	33	474 (68.7)	0.0111

TABLE 5-4. TENSILE PROPERTIES OF $[30_8]$ 80AS/20S/PR288 GRAPHITE/S-GLASS/EPOXY

Specimen Numbers	Strain Rate ($\dot{\varepsilon}_{\theta\theta}$), s^{-1}	Modulus ($E_{\theta\theta}$), GPa (10^6 psi)	Poisson's Ratio ($\nu_{\theta x}$)
		Initial Properties	
49-1,2,3	1×10^{-4}	24.7 (3.57)	0.35
49-8,9,10	62	28.1 (4.07)	0.31
49-5,6,7	235	52.3 (7.58)	0.33
		Secant Properties	
49-1,2,3	1×10^{-4}	16.6 (2.41)	0.48
49-8,9,10	86	23.8 (3.45)	0.36
49-5,6,7	272	43.1 (6.25)	0.38
		Terminal Properties	
49-1,2,3	1×10^{-4}	9.4 (1.37)	0.58
49-8,9,10	149	22.5 (3.27)	0.50
49-5,6,7	312	32.1 (4.66)	0.20
		Ultimate Properties	
	Time to Failure (t_f), μs	Strength ($S_{\theta\theta T}$), MPa (ksi)	Strain ($\varepsilon^u_{\theta\theta T}$)
49-1,2,3	1×10^8	157 (22.8)	0.0097
49-8,9,10	133	264 (38.3)	0.0113
49-5,6,7	36	414 (60.0)	0.0097

TABLE 5-5. TENSILE PROPERTIES OF $[45_8]$ SP288/AS GRAPHITE/EPOXY

Specimen Numbers	Strain Rate ($\dot{\varepsilon}_{\theta\theta}$), s^{-1}	Modulus ($E_{\theta\theta}$), GPa (10^6 psi)	Poisson's Ratio ($\nu_{\theta x}$)
		Initial Properties	
50-1,2,3	1×10^{-4}	14.7 (2.13)	0.27
50-8,9,10	57	25.5 (3.70)	0.20
50-4,5,6	287	69.9 (10.12)	0.35
		Secant Properties	
50-1,2,3	1×10^{-4}	13.0 (1.88)	0.32
50-8,9,10	82	17.0 (2.46)	0.29
50-4,5,6	283	36.4 (5.28)	0.36
		Terminal Properties	
50-1,2,3	1×10^{-4}	10.7 (1.56)	0.39
50-8,9,10	127	20.0 (2.90)	0.32
50-4,5,6	323	25.2 (3.65)	0.35
		Ultimate Properties	
	Time to Failure (t_f), μs	Strength ($S_{\theta\theta T}$), MPa (ksi)	Strain ($\varepsilon^u_{\theta\theta T}$)
50-1,2,3	1×10^8	90 (13.1)	0.0070
50-8,9,10	117	161 (23.4)	0.0096
50-4,5,6	29	281 (40.7)	0.0081

TABLE 5-6. TENSILE PROPERTIES OF $[45_8]$ 80AS/20S/PR288 GRAPHITE/S-GLASS/EPOXY

Specimen Numbers	Strain Rate ($\dot{\varepsilon}_{\theta\theta}$), s^{-1}	Modulus ($E_{\theta\theta}$), GPa (10^6 psi)	Poisson's Ratio ($\nu_{\theta x}$)
	Initial Properties		
51-1,2,3	1×10^{-4}	15.3 (2.22)	0.20
51-7,8,9	72	24.3 (3.53)	--
51-4,5,6	230	96.4 (13.97)	0.24
	Secant Properties		
51-1,2,3	1×10^{-4}	12.5 (1.82)	0.33
51-7,8,9	76	19.9 (2.89)	0.21
51-4,5,6	250	36.4 (5.28)	0.30
	Terminal Properties		
51-1,2,3	1×10^{-4}	8.1 (1.17)	0.47
51-7,8,9	125	21.1 (3.05)	0.38
51-4,5,6	272	20.7 (3.00)	0.45
	Ultimate Properties		
	Time to Failure (t_f), μs	Strength ($S_{\theta\theta T}$), MPa (ksi)	Strain ($\varepsilon^u_{\theta\theta T}$)
51-1,2,3	1×10^8	100 (14.5)	0.0080
51-7,8,9	130	195 (28.2)	0.0098
51-4,5,6	35	313 (45.3)	0.0087

Comparison of all the results above shows that the dependence of modulus and strength on strain rate increases with the off-axis angle of the laminate. The average increases of modulus and strength at the high strain rate are approximately 100%, 150%, and 200% for the $[22.5_8]$, $[30_8]$, and $[45_8]$ laminates, respectively.

REPORT DOCUMENTATION PAGE

Form Approved
OMB No. 0704-0188

1. AGENCY USE ONLY (*Leave blank*)	2. REPORT DATE	3. REPORT TYPE AND DATES COVERED
	December 1991	Final Contractor Report

4. TITLE AND SUBTITLE

High Strain Rate Properties of Off-Axis Composite Laminates
Final Report—Part II

5. FUNDING NUMBERS

WU-505-63-5B
C-NAS3-21016

6. AUTHOR(S)

I.M. Daniel

7. PERFORMING ORGANIZATION NAME(S) AND ADDRESS(ES)

IIT Research Institute
10 West 35th Street
Chicago, Illinois 60616

8. PERFORMING ORGANIZATION REPORT NUMBER

None

9. SPONSORING/MONITORING AGENCY NAMES(S) AND ADDRESS(ES)

National Aeronautics and Space Administration
Lewis Research Center
Cleveland, Ohio 44135-3191

10. SPONSORING/MONITORING AGENCY REPORT NUMBER

NASA CR-189084

11. SUPPLEMENTARY NOTES

Project Manager, C.C. Chamis, Structures Division, NASA Lewis Research Center, (216) 433-3252.

12a. DISTRIBUTION/AVAILABILITY STATEMENT

Unclassified - Unlimited
Subject Category 24

12b. DISTRIBUTION CODE

13. ABSTRACT ***(Maximum 200 words)***

Unidirectional off-axis graphite/epoxy and graphite/S-glass/epoxy laminates were characterized in uniaxial tension at strain rates ranging from quasi-static to over $500s^{-1}$. Laminate ring specimens were loaded by internal pressure with the tensile stress at 22.5°, 30°, and 45° with the fiber direction. Results were presented in the form of stress-strain curves to failure. Properties determined included moduli, Poisson's ratios, strength, and ultimate strain. In all three laminates of both materials the modulus and strength increase sharply with strain rate, reaching values roughly 100%, 150%, and 200% higher than corresponding static values for the $[22.5_8]$, $[30_8]$, and $[45_8]$ laminates, respectively. In the case of ultimate strain no definite trends could be established, but the maximum deviation from the average of any value for any strain rate was less than 18%.

14. SUBJECT TERMS

Graphite fibers; Glass-fibers; Epoxy; Ring specimens; Off-axis tests; Properties; Strength; Data; Curves; Tables; Time histories; Initial; Secant terminal; Ultimate

15. NUMBER OF PAGES
172

16. PRICE CODE
A08

17. SECURITY CLASSIFICATION OF REPORT	18. SECURITY CLASSIFICATION OF THIS PAGE	19. SECURITY CLASSIFICATION OF ABSTRACT	20. LIMITATION OF ABSTRACT
Unclassified	Unclassified	Unclassified	

National Aeronautics and
Space Administration

Lewis Research Center
Cleveland, Ohio 44135

NASA-Langley Research C.
Attn: Library
Hampton, VA 23665

185

NASA